UNIVERSITAT POLITÈCNICA DE VALÈNCIA

DOCTORAL THESIS

A precise, general, non-invasive and automatic speed estimation method for MCSA steady-state diagnosis and efficiency estimation of induction motors in the 4.0 Industry.

Author:
Jorge Bonet Jara

Supervisors:
Dr. Joan Pons Llinares
Dr. Alfredo Quijano López

A thesis submitted in fulfillment of the requirements for the degree of Doctor of Philosophy

in the

Instituto Tecnológico de la Energía
Departamento de Ingeniería Eléctrica

May 9, 2023

UNIVERSITAT POLITÈCNICA DE VALÈNCIA

Abstract

A precise, general, non-invasive and automatic speed estimation method for MCSA steady-state diagnosis and efficiency estimation of induction motors in the 4.0 Industry.

by Jorge Bonet Jara

There are two crucial aspects when operating induction motors in industry: efficiency estimation (to minimize energy consumption) and diagnosis (to avoid untimely outages and reduce maintenance costs). To estimate the motor's efficiency, it is necessary to measure voltages and currents. Hence, it is convenient and very useful using the same current to also diagnose the motor (Motor Current Signature Analysis: MCSA). In this regard, the most suitable MCSA technique is that based on locating fault harmonics in the spectrum of the stator line current under steady-state, as this is the operating condition of most induction motors in industry. Since the frequency of these harmonics depends on the speed, it becomes essential to be able to know this magnitude with precision, as the accurate knowledge of the operating speed makes it possible to correctly locate the fault harmonics, and therefore, reduce the chances of false positives/negatives. In turn, an accurate speed information also allows to calculate the mechanical power with precision, which results in a more accurate estimation of the motor performance. Finally, to adapt to the needs of 4.0 Industry, where large numbers of motors are continuously monitored, the speed must not only be obtained very accurately, but also non-invasively, automatically (without the need for an expert) and for any induction motor. In this regard, since precise speed measurement through a shaft sensor is invasive and expensive, Sensorless Speed Estimation (SSE) techniques become the best option.

The first part of this thesis conducts a thorough analysis of all the families of SSE techniques present in the technical literature. As demonstrated therein, those techniques based on Slotting and Rotational Frequency Sideband Harmonics are the most promising, as they can potentially meet all the aforementioned requirements. However, as also proved in this part, and up to this thesis, there had always been a trade-off between accuracy and general applicability. On the one hand, the use of Rotor Slot Harmonics (RSH) provides a much better precision to estimate speed than the Rotational Frequency Sideband Harmonics (RFSH), whose imprecision usually leads to wrong diagnosis. On the other hand, RSHs-based methods are difficult to implement in industrial devices, since they require parameters that are usually unknown, such as the number of rotor slots, unlike RFSHs-based methods, which only require the number of pole pairs.

The second part, and core of this thesis, presents a methodology that ends with this trade-off between accuracy and general applicability, thus providing the first precise, general, noninvasive and automatic speed estimation method for MCSA steady-state diagnosis and efficiency estimation of induction motors that operate in a 4.0 Industry context. This is achieved by developing a novel RSH-based technique that, for the first time in technical literature, eliminates the need to know/estimate the number of rotor slots, which had so far prevented these techniques to be generally applicable. This technique also provides a reliable and automatic procedure to, from among the high number of significant harmonics present in the spectrum of the line current of an induction motor, locate the RSHs family. Also automatically and without the help of an expert, the technique is able to determine the parameters needed to estimate speed from RSHs, using only measurements taken during the motor normal operation at steady-state. The methodology is validated using motors with different characteristics, designs and working conditions (directly fed, frequency converter fed, different loads, etc.), by simulations, lab tests

and with 105 industrial motors. Furthermore, a real industrial case of application is shown as well, where the speed estimation algorithm is implemented in a continuous motor condition monitoring system via MCSA, which eventually leads to the discovery of a new fault in deep-well submersible motors: the wear of end-rings. Finally, a second direct application derived from the reliable and automatic procedure to detect RSHs is presented: the use of these harmonics to diagnose early-stage inter-turn faults in induction motors of deep-well submersible pumps.

UNIVERSITAT POLITÈCNICA DE VALÈNCIA

Resumen

A precise, general, non-invasive and automatic speed estimation method for MCSA steady-state diagnosis and efficiency estimation of induction motors in the 4.0 Industry.

by Jorge Bonet Jara

Hay dos aspectos cruciales a la hora de operar motores de inducción en la industria: la estimación de su eficiencia (para minimizar el consumo de energía) y su diagnóstico (para evitar paradas intempestivas y reducir los costes de mantenimiento). Para estimar la eficiencia del motor es necesario medir tensiones y corrientes. Por ello, resulta conveniente y muy útil utilizar la misma corriente para diagnosticar también el motor (Motor Current Signature Analysis: MCSA). En este sentido, la técnica MCSA más adecuada es aquella basada en la localización de armónicos de fallo en el espectro de la corriente de línea del estator en régimen permanente, puesto que esta es la condición de funcionamiento de la mayoría de los motores de inducción de la industria. Por otro lado, dado que la frecuencia de estos armónicos depende de la velocidad, resulta imprescindible conocer esta magnitud con precisión, ya que el conocimiento preciso de la velocidad de funcionamiento permite localizar correctamente los armónicos de fallo, y, por tanto, reducir las posibilidades de falsos positivos/negativos. A su vez, una medida precisa de la velocidad también permite calcular con precisión la potencia mecánica, lo que se traduce en una estimación más exacta del rendimiento del motor. Por último, para adaptarse a las necesidades de la Industria 4.0, en la que se monitoriza continuamente un gran número de motores, la velocidad no solo debe ser obtenida con gran precisión, sino también de manera no invasiva, automática (sin necesidad de un experto) y para cualquier motor de inducción. A este respecto, dado que la medición precisa de la velocidad a través de un sensor de eje (encóder) es invasiva y costosa, las técnicas de estimación de velocidad sin sensores (SSE en inglés) se convierten en la mejor opción.

En la primera parte de esta tesis se realiza un análisis exhaustivo de todas las familias de técnicas SSE presentes en la literatura técnica. Como se demuestra en ella, aquellos métodos basados en armónicos de ranura y armónicos laterales de frecuencia rotacional son los más prometedores, pues potencialmente pueden satisfacer todos los requisitos mencionados anteriormente. Sin embargo, como también se demuestra en esta parte, y hasta esta tesis, siempre había existido un compromiso entre la precisión y la aplicabilidad general del método. Por un lado, el uso de armónicos de ranura de rotor (RSH en inglés) proporciona una precisión mucho mayor para estimar la velocidad que los armónicos de banda lateral de frecuencia de rotación (RFSH en inglés), cuya imprecisión suele conducir a diagnósticos erróneos. Por otro lado, los métodos basados en RSHs son difíciles de implementar en dispositivos industriales, ya que requieren parámetros que suelen ser desconocidos, como el número de ranuras del rotor, a diferencia de los métodos basados en RFSHs, que sólo requieren el número de pares de polos.

En la segunda parte, y núcleo de esta tesis, se presenta una metodología que acaba con este compromiso entre precisión y aplicabilidad general, proporcionando así el primer método de estimación de velocidad preciso, general, no invasivo y automático para el diagnóstico en estado estacionario MCSA y la estimación de eficiencia de motores de inducción que operan en un contexto de Industria 4.0. Esto se consigue desarrollando una novedosa técnica basada en RSHs que, por primera vez en la literatura técnica, elimina la necesidad de conocer/estimar

el número de ranuras del rotor, lo que, como se ha mencionado anteriormente, había impedido hasta la fecha que estos métodos fueran de aplicación general. Esta técnica proporciona además un procedimiento fiable y automático para, de entre el elevado número de armónicos significativos presentes en el espectro de la corriente de línea de un motor de inducción, localizar la familia de RSHs. También de manera automática y sin la ayuda de un experto, la técnica es capaz de determinar los parámetros necesarios para estimar la velocidad a partir de los RSHs, utilizando únicamente medidas tomadas durante el funcionamiento normal del motor en régimen estacionario. La metodología es validada utilizando motores con diferentes características, diseños y condiciones de trabajo (alimentados directamente, alimentados por convertidor de frecuencia, diferentes niveles de carga, etc.), empleando para ello simulaciones, pruebas de laboratorio y 105 motores industriales. Además, se muestra un caso real de aplicación industrial en el que el algoritmo de estimación de velocidad es implementado en un sistema de monitorización continua del estado del motor mediante MCSA, lo que acaba conduciendo al descubrimiento de un nuevo fallo en motores sumergibles de pozo profundo: el desgaste de los anillos de cortocircuito. Por último, se presenta una segunda aplicación directa derivada del procedimiento fiable y automático de detección de RSHs: el uso de estos armónicos para diagnosticar, en fase temprana, cortocircuitos entre espiras en motores de inducción de bombas sumergibles de pozo profundo.

UNIVERSITAT POLITÈCNICA DE VALÈNCIA

Resum

A precise, general, non-invasive and automatic speed estimation method for MCSA steady-state diagnosis and efficiency estimation of induction motors in the 4.0 Industry.

by Jorge Bonet Jara

Hi ha dos aspectes crucials a l'hora d'operar motors d'inducció en la indústria: l'estimació de la seua eficiència (per a minimitzar el consum d'energia) i el seu diagnòstic (per a evitar parades intempestives i reduir els costos de manteniment). Per a estimar l'eficiència del motor és necessari mesurar tensions i corrents. Per això, resulta convenient i molt útil utilitzar el mateix corrent per a diagnosticar també el motor (Motor Current Signature Analysis: MCSA). En aquest sentit, la tècnica MCSA més adequada és aquella basada en la localització d'harmònics de fallada en l'espectre del corrent de línia de l'estator en règim permanent, ja que aquesta és la condició de funcionament de la majoria dels motors d'inducció de la indústria. D'altra banda, atés que la freqüència d'aquests harmònics depén de la velocitat, resulta imprescindible conéixer aquesta magnitud amb precisió, puix el coneixement precís de la velocitat de funcionament permet localitzar correctament els harmònics de fallada i, per tant, reduir les possibilitats de falsos positius/negatius. Al seu torn, una mesura precisa de la velocitat també permet calcular amb precisió la potència mecànica, la qual cosa es tradueix en una estimació més exacta del rendiment del motor. Finalment, per a adaptar-se a les necessitats de la Indústria 4.0, en la qual es monitora contínuament un gran nombre de motors, la velocitat no sols ha de ser obtinguda amb gran precisió, sinó també de manera no invasiva, automàtica (sense necessitat d'un expert) i per a qualsevol motor d'inducció. En aquest sentit, atès que el mesurament precís de la velocitat a través d'un sensor d'eix (encóder) és invasiva i costosa, les tècniques d'estimació de velocitat sense sensors (SSE en anglés) es converteixen en la millor opció.

En la primera part d'aquesta tesi es realitza una anàlisi exhaustiva de totes les famílies de tècniques SSE presents en la literatura tècnica. Com es demostra en ella, aquells mètodes basats en harmònics de ranura i harmònics laterals de freqüència rotacional són els més prometedors, ja que potencialment poden satisfer tots els requisits esmentats anteriorment. No obstant això, com també es demostra en aquesta part, i fins a aquesta tesi, sempre havia existit un compromís entre la precisió i l'aplicabilitat general del mètode. D'una banda, l'ús d'harmònics de ranura de rotor (RSH en anglès) proporciona una precisió molt major per a estimar la velocitat que els harmònics de banda lateral de freqüència de rotació (RFSH en anglès), la imprecisió dels quals sol conduir a diagnòstics erronis. D'altra banda, els mètodes basats en RSHs són difícils d'implementar en dispositius industrials, ja que requereixen paràmetres que solen ser desconeguts, com el nombre de ranures del rotor, a diferència dels mètodes basats en RFSHs, que només requereixen el nombre de parells de pols.

En la segona part, i nucli d'aquesta tesi, es presenta una metodologia que acaba amb aquest compromís entre precisió i aplicabilitat general, proporcionant així el primer mètode d'estimació de velocitat precís, general, no invasiu i automàtic per al diagnòstic en estat estacionari MCSA i l'estimació d'eficiència de motors d'inducció que operen en un context d'Indústria 4.0. Això s'aconsegueix desenvolupant una nova tècnica basada en RSHs que, per primera vegada en la literatura tècnica, elimina la necessitat de conéixer/estimar el nombre de ranures del rotor, la qual cosa, com s'ha esmentat anteriorment, havia impedit fins avui que aquests mètodes foren d'aplicació general. Aquesta tècnica proporciona a més un procediment fiable i automàtic per a, d'entre l'elevat nombre d'harmònics significatius presents en l'espectre del corrent de línia d'un

motor d'inducció, localitzar la família de RSHs. També de manera automàtica i sense l'ajuda d'un expert, la tècnica és capaç de determinar els paràmetres necessaris per a estimar la velocitat a partir dels RSHs, utilitzant únicament mesures preses durant el funcionament normal del motor en règim estacionari. La metodologia és validada utilitzant motors amb diferents característiques, dissenys i condicions de treball (alimentats directament, alimentats per convertidor de freqüència, diferents nivells de càrrega, etc.), emprant per a això simulacions, proves de laboratori i 105 motors industrials. A més, es mostra un cas real d'aplicació industrial en el qual l'algoritme d'estimació de velocitat és implementat en un sistema de monitoratge continu de l'estat del motor mitjançant MCSA, la qual cosa acaba conduint al descobriment d'una nova fallada en motors submergibles de pou profund: el desgast dels anells de curtcircuit. Finalment, es presenta una segona aplicació directa derivada del procediment fiable i automàtic de detecció de RSHs: l'ús d'aquests harmònics per a diagnosticar, en fase primerenca, curtcircuits entre espires en motors d'inducció de bombes submergibles de pou profund.

Acknowledgements

The completion of the thesis represents the culmination of an long stage in my academic career. From now on, I put an end to my supervised training stage and, in turn, I begin a new chapter in which I am supposed to be sufficiently qualified to decide and direct my own line of research. However, before embarking on this new path, I consider it extremely important to look back and remember all those people who left an indelible mark on my training, since the fact that I am here today writing these lines is undoubtedly thanks to them. In addition, this retrospection, which I am summarizing here, is also useful to keep in mind everything that these people contributed to me in their day, because in the future it will be of great use to me when I have to train someone else.

First of all, I would like to begin by remembering my primary school teacher Rosa Mussons, who already during this early stage was able to sow in me the main element on which any research is based, the curiosity to know more about what one does not know. Next, I would like to continue with my teachers Alfredo Pérez and Miguel Ángel Oliver, who, during the last years of my secondary school education, awakened in me an interest in science, and prepared me in an exceptional way for the university stage. Finally, I would like to conclude this paragraph by remembering the university professor Don Luis Serrano Iribarnegaray. You were, without any doubt, responsible for awakening in me the passion for electric machines and research. I will always be grateful to you for having placed all your trust in me when you chose me as your student for the Master's Final Project and, later, as your co-worker and friend.

Thanks to this solid academic background, I was able to begin my doctoral studies. Throughout it, I have been fortunate to meet extraordinary people, not only in the scientific field, but also in the human field. In this regard, I would like to begin by remembering and thanking my colleagues in the department, who, from the very first moment, were always willing to help me achieve my goal. I would also like to thank Professors Daniel Moríñigo, Oscar Duque and Vanesa Fernández of the University of Valladolid, whom I must thank for their support, wise advice and the fact that they welcomed me into their home during the last months of my doctoral studies. And finally, to Professor Konstantinos N. Gyftakis, from whom I learned so much about the modeling and diagnostics of electrical machines, and whom I also thank for his selfless efforts to host me in Crete.

Finally, I would like to end this brief reminder of all those people who have marked me throughout my academic training, remembering and thanking my thesis supervisors, Professors Alfredo Quijano López and Joan Pons Llinares. Thank you Alfredo for having always made things so easy for me, for your advice, for assisting me during my first classes of Electrical Machines, for having listened to me at all times, and above all, for having helped me whenever I needed it. Thank you Joan for having guided me throughout this stage in such an honest, attentive and meticulous way. Thank you also for all the time you have dedicated to me, even sacrificing part of your personal time. Whenever I have needed your help to review a certain article, discuss a certain scientific question or prepare the application for a certain grant, I have always been able to count on you. And of course thank you for not only being an exceptional mentor, but also an exceptional friend. Finally, I would like to conclude this paragraph by saying that I wish every PhD student was as lucky as I have been to have had supervisors like you.

Next, I would like to reflect a little on what a doctorate is and means on a more personal level. This stage, although stimulating and satisfying, is, at the same time, a long and hard road, which can also become lonely if one does not have the right environment. In the end, it

is the academic period where for the first time one is fully immersed in a field, in which one has to identify one of many existing problems, delimit that problem, study it and ultimately propose an original solution. With all this, it is almost inevitable that you end up becoming the foremost expert on the particular subject on which your thesis is based. This means that discussing with your close circle the technical disquisitions and drawbacks that arise around it can become quite complicated, hence the fact that it can become a lonely path. However, I can say unequivocally that this has not been my case. I have had the good fortune to have always walked in the company of people who, even if they did not understand anything I said, because it was not their duty or obligation to do so, they understood everything. That is why I would like to conclude this section, remembering and thanking those people as well.

To my parents and my sister, who always accompanied me along this journey, supporting and assisting me at all times so that I could reach the final goal. Thank you for being an inexhaustible source of light and guidance, for your advice, always given with love but also with honesty, and for always being there when I needed it most.

To my grandmothers Maruja and Carmen, who through their affection, their constant calls, their understanding and interest, always gave me the necessary strength to not give up and to go ahead with all my aspirations. To my grandparents Pere and Vicente, who, although they are no longer here, I know they would have been very proud to have seen their grandson finish this thesis, and who, in addition, would have read it from beginning to end before submitting it, in order to have alerted me to any small mistakes.

To my friends, who, from the purest honesty and humility, have always shown me their support and admiration for my projects and, especially, for embarking on this journey towards the PhD. Thank you for helping me to face each new week of work through the laughter and moments shared during the weekend.

And last but by no means least, to Bea, who has become a fundamental pillar for me during this last year, as well as a mirror to look at myself when my strength weakened the most. Thank you for being a permanent example of struggle, sacrifice and love, for having supported me unconditionally in all my decisions and, also, thank you for having taken an interest in this work as if it were your own.

I dedicate this thesis to each and every one of the people mentioned above.

Agradecimientos

La culminación de la tesis representa el primer punto y aparte de mi carrera académica, pues por un lado pongo punto y final a mi etapa formativa supervisada y, por otro lado, doy comienzo a un nuevo capítulo donde ya se me supone lo suficientemente capacitado como para decidir y dirigir mi propia línea de investigación. No obstante, antes de iniciar esta nueva senda, considero que es sumamente importante volver la mirada atrás y recordar a todas aquellas personas que en su día dejaron una huella imborrable en mi formación, pues el hecho de que hoy esté aquí escribiendo estas líneas es, sin duda alguna, gracias a ellos. Además, sirva también esta retrospección, de la cual dejo aquí constancia de manera resumida, para tener siempre en mente todo lo que estas personas en su día me aportaron, pues en un futuro me será de gran utilidad cuando sea yo quien tenga que formar a otra persona.

En primer lugar, me gustaría empezar por recordar a mi maestra de primaria Rosa Mussons, quien ya durante esta temprana etapa fue capaz de sembrar en mí el elemento principal sobre el cual se fundamenta cualquier investigación, la curiosidad por saber más sobre aquello que uno desconoce. A continuación, quisiera seguir con mis profesores Alfredo Pérez y Miguel Ángel Oliver, quienes durante los últimos años de mi educación secundaria avivaron en mí el interés por las ciencias, preparándome además de manera excepcional para la etapa universitaria. Finalmente, me gustaría concluir este párrafo, recordando al profesor y catedrático de universidad Don Luís Serrano Iribarnegaray. Usted fue, sin ningún tipo de dudas, el responsable de despertar en mí la pasión por las máquinas eléctricas y la investigación. Siempre le estaré agradecido por haber depositado en mí toda su confianza a la hora de elegirme como su tutorando para el Trabajo Final de Master y, posteriormente, como su compañero de trabajo y amigo.

Gracias a esta sólida formación académica pude dar comienzo mi etapa doctoral. A lo largo de ella he tenido la suerte de conocer a personas extraordinarias, no solo en el ámbito científico, sino también en el humano. A este respecto, quiero empezar por recordar y agradecer a mis compañeros de departamento, quienes, desde el primer momento, siempre estuvieron dispuestos a echarme una mano para conseguir mi objetivo. También a los profesores Daniel Moríñigo, Oscar Duque y Vanesa Fernández de la Universidad de Valladolid, a quienes he de agradecerles su apoyo, sabios consejos y el hecho de que me acogieran en su casa durante los últimos meses de doctorado. Y finalmente, al profesor Konstantinos N. Gyftakis, de quien tanto aprendí sobre el modelado y diagnóstico de máquinas eléctricas, y a quien además agradezco que, de manera totalmente desinteresada, hiciera todo el esfuerzo posible por acogerme en Creta.

Por último, me gustaría acabar este breve recordatorio sobre todas aquellas personas que me han marcado a lo largo de mi formación académica, recordando y agradeciendo a mis directores de tesis, los profesores Alfredo Quijano López y Joan Pons Llinares. Gracias Alfredo por haberme facilitado siempre tanto las cosas, por tus consejos, por asistirme durante mis primeras clases de Máquinas Eléctricas, por haberme escuchado en todo momento, y sobre todo, por haberme ayudado siempre que lo he necesitado. Gracias Joan por haberme guiado a lo largo de esta etapa de forma tan honesta, atenta y meticulosa. Gracias también por todo el tiempo que me has dedicado, incluso llegando a sacrificar parte del tuyo personal. Siempre que he necesitado tu ayuda para revisar un determinado artículo, discutir una determinada cuestión científica o preparar la solicitud para conseguir una determinada ayuda, he podido contar contigo. Y por supuesto gracias por no solo haber sido un excepcional mentor, sino también un excepcional amigo. Finalmente, quisiera concluir este párrafo diciendo que ojalá todo doctorando tuviera la suerte que yo he tenido teniendo unos directores como vosotros.

A continuación, quisiera reflexionar un poco sobre lo que supone y significa el doctorado desde un plano más personal. Esta etapa, aunque estimulante y satisfactoria, es a su vez un camino largo y duro, el cual puede llegar también a convertirse en solitario si uno no tiene el entorno adecuado. Al final, es el periodo académico donde por primera vez uno se sumerge de lleno en un campo, en el cual ha de identificar uno de tantos problemas existentes, acotar dicho problema, estudiarlo y en última instancia proponer una solución original. Con todo esto, es casi inevitable que uno acabe convirtiéndose en el mayor experto en el tema concreto sobre el que versa su tesis. Esto significa que discutir con tu círculo cercano las disquisiciones técnicas e inconvenientes que surgen a su alrededor pueda volverse hartamente complicado, de ahí el hecho de que pueda convertirse en una senda solitaria. No obstante, puedo decir sin ambages, que ese no ha sido mi caso. Que he tenido la suerte de haber caminado siempre en compañía de personas que, aun no entendiendo nada de lo que decía, pues no era su deber ni obligación hacerlo, lo entendían todo. Es por ello que quisiera concluir esta sección, recordando y agradeciendo también a dichas personas.

A mis padres y mi hermana, quienes siempre me acompañaron a lo largo de este trayecto, apoyándome y asistiéndome en todo momento para que pudiese llegar a la meta final. Gracias por ser esa fuente inagotable de luz y guía, por vuestros consejos, dados siempre desde el cariño pero también desde la honestidad, y en definitiva, por haber siempre estado ahí cuando más lo he necesitado.

A mis abuelas Maruja y Carmen, quienes a través de su cariño, sus constantes llamadas, su comprensión e interés, siempre me dieron las fuerzas necesarias para no rendirme y seguir adelante con todas mis aspiraciones. A mis abuelos Pere y Vicente, quienes, a pesar de ya no estar aquí, sé que hubieran estado muy orgullosos de haber visto a su nieto finalizar esta tesis, y que, además, la hubiesen leído de principio a fin antes de entregarla, con el objetivo de haberme alertado sobre cualquier pequeño fallo.

A mis amigos y amigas, quienes, desde la más pura honestidad y humildad, siempre me han mostrado su apoyo y admiración por mis proyectos y, en especial, por embarcarme en este viaje hacia el doctorado. Gracias por haberme ayudado a afrontar cada nueva semana de trabajo a través de las risas y momentos compartidos durante el fin de semana.

Y finalmente, y en absoluto por ello menos importante, a Bea, quien se ha convertido en un pilar fundamental para mí durante este último año, así como en un espejo donde mirarme cuando las fuerzas más me flaqueaban. Gracias por ser ese ejemplo permanente de lucha, sacrificio y cariño, por haberme apoyado incondicionalmente en todas mis decisiones y, también, gracias por haberte interesado por este trabajo como si del tuyo mismo se tratase.

Dedico esta tesis a todas y cada una las personas mencionadas anteriormente.

Contents

List of Figures

List of Tables

List of Abbreviations

1BB	**1** **B**roken **B**ar
2BB	**2** **B**roken **B**ars
AGT	**A**ir **G**ap **T**orque
AI	**A**rtificial **I**ntelligence
ANN	**A**rtificial **N**eural **N**etworks
BBH	**B**roken **B**ar **H**armonic
CUI	**C**urrent **U**nbalance **I**ndex
DE	**D**ynamic **E**ccentricity
DT	**D**emodulation **T**est
DEH	**D**ynamic **E**ccentricity **H**armonic
EKF	**E**xtended **K**alman **F**ilter
ET	**E**ccentricity **T**est
FEA	**F**inite **E**lements **A**nalysis
FFT	**F**ast **F**ourier **T**ransform
FMB	**F**undamental **M**odel **B**ased
FL	**F**uzzy **L**ogic
GA	**G**enetic **A**lgorithms
IA	**I**ncipient **A**symmetry
IF	**I**ncipient **F**ault
IM	**I**nduction **M**otor
LRFSH [1]	**L**ower **R**otational **F**requency **S**ideband **H**armonic
LMEH	**L**ower **M**ixed **E**ccentricity **H**armonic
LSH	**L**ower **S**ideband **H**armonic
MAB	**M**agnetic **A**nisotropy **B**ased
MCSA	**M**otor **C**urrent **S**ignature **A**nalysis
MEH	**M**ixed **E**ccentricity **H**armonic
MRAS	**M**odel **R**eference **A**daptive **S**ystem
PSH	**P**rincipal **S**lot **H**armonic
PWM	**P**ulse **W**idth **M**odulation
RET	**R**otor **E**valuation **T**est
RF	**R**otor **F**ault
RFSH	**R**otational **F**requency **S**ideband **H**armonic
RMS	**R**oot **M**ean **S**quare
RSH	**R**otor **S**lot **H**armonic
SaEHB	**S**lotting **a**nd **E**ccentricity **H**armonics **B**ased
SE	**S**tatic **E**ccentricity
SEH	**S**tatic **E**ccentricity **H**armonic

[1] Rotational Frequency Sideband Harmonics are also known in literature as Mixed Eccentricity Harmonics. The first nomenclature is used throughout the thesis except in Chapter 2, Chapter 4, and Chapter 5, where the second one is used instead. This is because a reviewer of the publication of Chapter 3 suggested this change of nomenclature, and as a result, the entire thesis was adapted to it, with the exception of these three chapters, since they must reflect their associated publications as they appear in the accepted version of the manuscripts. Therefore, in this thesis, RFSH is equivalent to MEH, LRFSH to LMEH, URFSH to UMEH, and SRFSHB to SaEHB.

SIB	**S**ignal **I**njection **B**ased
SIH	**S**peed **I**ndependent **H**armonic
SRFSHB	**S**lotting (and) **R**otational **F**requency **S**ideband **H**armonics **B**ased
SSE	**S**ensorless **S**peed **E**stimation
UMEH	**U**pper **M**ixed **E**ccentricity **H**armonic
URFSH	**U**pper **R**otational **F**requency **S**ideband **H**armonic
USH	**U**pper **S**ideband **H**armonic
VU	**V**oltage **U**nbalance
VUI	**V**oltage **U**nbalance **I**ndex

List of Symbols

Chapter 1 [2]

f_{RSH}	Rotor Slot Harmonics frequency in the spectrum of the stator current	Hz
k	Natural number (1, 2, 3,...)	(-)
s	Slip	dimensionless
R	Number of rotor slots/bars	Slots/Bars
p	Number of pole pairs	Pole pairs
ν	Order of the time harmonic present in the stator current (1, 3, 5...)	(-)
f_0	Fundamental supply frequency in the spectrum of the stator current	Hz
f_{RFSH}	Rotational Frequency Sideband Harmonics frequency in the spectrum of the stator current	Hz

Chapter 2

n	Speed	rpm
n_{sync}	Synchronous speed	rpm
n_N	Rated speed	rpm
f_{MEH}	Mixed Eccentricity Harmonics frequency in the spectrum of the stator current	Hz
f^*_{LMEH}	Lower Mixed Eccentricity Harmonic frequency in the spectrum of quantities other than the stator current (EXP4000)	Hz
f^{Demod}_{MEH}	Mixed Eccentricity Harmonic frequency in the spectrum of the demodulated stator current (MCEMAX)	Hz
f_{BBH}	Broken Bar Harmonics frequency in the spectrum of the stator current	Hz
f^{Demod}_{BBH}	Broken Bar Harmonic frequency in the spectrum of the demodulated stator current (MCEMAX)	Hz
f_{LSH}	Lower Sideband Harmonic frequency in the spectrum of the stator current	Hz
f_{RSH}	Rotor Slot Harmonics frequency in the spectrum of the stator current	Hz
f_{res}	Frequency resolution	Hz
I_N	Rated current	A
I_0	No-load current	A
I_L	Operating current	A

[2] Given the idiosyncrasy of the *Thesis as a Collection of Articles*, it has been decided to present the list of symbols by chapter, as some of them may mean different things depending on the publication.

k_{exp}	Experimental factor to correct slip estimation in MCEMAX alike algorithm	dimensionless
f_h	Generic harmonic frequency in the spectrum of the stator current	Hz
f_0	Fundamental supply frequency in the spectrum of the stator current	Hz
p	Number of pole pairs	Pole pairs
s	Slip	dimensionless
R	Number of rotor slots/bars	Slots/Bars
k	Natural number (1, 2, 3...)	(-)
n_d	Positive integer number (0, 1, 2,..)	(-)
ν	Order of the time harmonic present in the stator current (1, 3, 5...)	(-)

Chapter 3

f_{RSH}	Rotor Slot Harmonics frequency in the spectrum of the stator current	Hz
k	Natural number (1, 2, 3,...)	(-)
s	Slip	dimensionless
R	Number of rotor slots/bars	Slots/Bars
p	Number of pole pairs	Pole pairs
ν	Order of the time harmonic present in the stator current (1, 3, 5...)	(-)
f_0	Fundamental supply frequency in the spectrum of the stator current	Hz
$f_{RSH}\|_{s=0}$	Rotor Slot Harmonics frequency at no-load in the spectrum of the stator current	Hz
O_ν	quotient between $f_{RSH}\|_{s=0}$ and f_0	dimensionless
n	Positive integer number starting at 4	(-)
f_{BBH_1}	First family of Broken Bar Harmonics frequency in the spectrum of the stator current	Hz
f_{BBH_2}	Second family of Broken Bar Harmonics frequency in the spectrum of the stator current	Hz
k/p	Odd positive integer number (1, 3, 5,...)	(-)
$f_{BBH_{Hilb}}$	Broken Bar Harmonics frequency in the spectrum of the Hilbert modulus	Hz
f_{RFSH}	Rotational Frequency Sideband Harmonics frequency in the spectrum of the stator current	Hz
f_{DEH}	Dynamic Eccentricity Harmonics frequency in the spectrum of the stator current	Hz
n_D	Positive integer number (1, 2, 3,...)	(-)
k_1	Experimental factor to compensate rated slip tolerance	dimensionless
k_2	Experimental factor to avoid detecting an odd multiple of f_0	Hz
s_N	Rated slip	dimensionless

Chapter 4

A_1	Amplitude of the LSH under single end-ring fault	dB

A_{1-x}	Amplitude of the LSH under double end-ring fault (segment 1 and segment x)	dB
$i_{l(n)}$	Current of the Nth rotor loop	A
i_{er}	End-ring current	A
$\Psi_{l(n)}$	Total flux linkages of the Nth rotor loop	$Wb - turns$
$R_{b(n)}$	Resistance of the Nth bar	Ω
$R_{uers(n)}$	Resistance of the Nth upper end-ring segment	Ω
$R_{lers(n)}$	Resistance of the Nth lower end-ring segment	Ω
$L_{\sigma lers(n)}$	Leakage inductance of the Nth lower end-ring segment	H
f	fundamental supply frequency in the spectrum of the stator current	Hz
s	Slip	dimensionless
k	Natural number (1, 2, 3,...)	(-)
n	Positive integer number (1, 2, 3,...)	(-)
p	Number of pole pairs	Pole pairs
V	Rated voltage	V
N_{bars}	Number of rotor bars	(bars)
h	Relative order of the maximum field harmonic considered	(-)
T	Rated torque	$N \cdot m$
J	Rated inertia	$kg \cdot m^2$
R_{est}	Stator phase resistance	Ω
$L_{\sigma,est}$	Stator leakage inductance	H
$L_{\mu,est}$	Stator magnetizing inductance	H
R_b	Rotor bar resistance	Ω
$L_{\sigma,b}$	Rotor bar leakage inductance	H
$L_{\mu,rot}$	Rotor magnetizing inductance	H
R_{ring}	Rotor end-ring resistance	Ω
$L_{\sigma,ring}$	Rotor end-ring leakage inductance	H

Chapter 5

f_{RSH}	Rotor Slot Harmonics frequency in the spectrum of the stator current	Hz
k	Natural number (1, 2, 3,...)	(-)
s	Slip	dimensionless
R	Number of rotor slots/bars	Slots/Bars
p	Number of pole pairs	Pole pairs
ν	Order of the time harmonic present in the stator current (1, 3, 5...)	(-)
f_0	Fundamental supply frequency in the spectrum of the stator current	Hz
h_{rot}	Relative order of the rotor spatial flux harmonic wave that induces the RSHs in the stator windings	(-)
h_{st}	Relative order of the stator spatial flux harmonic wave through which the time harmonic νf_0 interacts with the rotor system	(-)
$I_{l,A}$	Stator line A current	A
I_A	Stator phase A current	A

I_{sc}	Short circuit current	A
I_{cr}	Contact resistance current	A
$I_{l,A,h}$	Healthy stator line A current	A
$I_{A,h}$	Healthy stator phase A current	A

Power units equivalence

Page(s) 13, 100, 110, 112, 123, 127, and 135	230 HP	169.16 kW
Page(s) 71	100 HP	73.55 kW
Page(s) 103	340 HP	250.07 kW

Chapter 1

General introduction

In this first chapter, the background of the present doctoral thesis is introduced, its main and partial objectives are defined, and its structure is described, which is in the form of *Thesis as a Collection of Articles*. As the articles share some references that do not necessarily appear in the same order in each of them, it has been arranged that all chapters where other works are cited have their own bibliography section, in order to facilitate reading. Furthermore, keeping the objective of facilitate reading, in the PDF version of this document, each time a chapter, section, subsection, equation, figure, table or citation is mentioned, a hyperlink to that chapter, section, subsection, equation, figure, table or reference is provided. In the bibliography, a hyperlink has also been added to the DOI, if available, that leads directly to the web page hosting the work (in case the work does not have a DOI but is available in a repository or bookstore on the Internet, a link to that website has also been added). Finally, like this chapter, each of the following ones has a brief introduction below its title.

1.1 Background

The current industrial trend is to develop a set of intelligent sensors that determine the state of a given industry and help make decisions in order to optimize its operation. In this sense, the development of devices that, by capturing different signals from electric motors, are capable of diagnosing them and determining their efficiency, is of paramount importance. This makes it possible to make decisions regarding optimal maintenance and to minimize the energy consumption of the industry. The diagnosis through Motor Current Signature Analysis (MCSA) in induction machines (IM) needs accurate speed information in order to correctly locate the fault harmonics[1] (as further explained below). In the same way, when determining the efficiency of an IM, either by estimating the equivalent circuit parameters or the mechanical torque, it is necessary to know the speed with precision. In industry, motors are usually not equipped with speed sensors, so it is necessary to estimate this magnitude. Nevertheless, the methods present in the technical literature have a number of shortcomings that prevent their application to real industrial contexts.

Thus, the present thesis is located within the field of Sensorless Speed Estimation (SSE) in IMs. Its objective is to develop a new speed estimation method that solves the problems of current SSE techniques when applied in real industrial environments. In particular, the method has been designed to serve as the basis of a smart sensor to meet the needs of 4.0 Industry. To this end, the algorithm must not require any motor data beyond its nameplate (thereby enabling its application to any motor), it must solve the problem automatically (without the need of an expert) and in a non-invasive way (without the need of using tests/procedures other than measurements under normal motor operation), achieve high precision (avoiding inaccurate efficiency estimation, and eliminating the appearance of false positives and false negatives when used for diagnosis purposes), be integrated into smart devices installed in-situ (enabling continuous monitoring) and work with both grid supply and any type of frequency converter. Since for both MCSA steady-state diagnosis and efficiency estimation, SSE is a first key step, these characteristics will allow the algorithm to be the basis of a device for such applications, and constitute the necessary tool to develop such functions in the context of a 4.0 Industry.

Although SSE has been studied for decades in the field of electric motor control [1], less attention has been paid to its application to efficiency estimation, and diagnosis via steady-state MCSA. It must be noted that, although the idea underlying a SSE technique is the same regardless the field of application (estimate speed without the need of a physical sensor), the restrictions and requirements imposed by each particular application affect the characteristics and suitability of the different SSE methods.

In advanced electric motor control (e.g., Field Oriented Control), the real-time estimation of certain machine magnitudes, such as speed, is a paramount requirement. This real-time response implies using short current/voltage captures. In terms of SSE, this means having to resort to methods based on the machine model, which, although their accuracy does not depend on the capture length, it depends on parameters very sensitive to the operating conditions, or having to resort to other SSE techniques, which, although insensitive to the variation of motor parameters, their accuracy depends proportionally on the capture length, hindering real-time response. Therefore, advance electric motor control impose the condition of having to find a compromise solution between response time and accuracy.

[1]The term "fault harmonics" is used in this thesis to refer to all speed-dependent harmonics that appear in the stator current as a consequence of mechanical or electrical asymmetries.

The control of IMs is useful to achieve smooth starts and stops, as well as to bring the motor and load to the desired operating point. However, in most industrial applications, once the IM is started and the desired operating speed is reached, this operating point usually does not vary. There are very few applications where the load varies (wood shredders, mixing of material for recycled paper, etc.). In most applications, the load is constant, as well as the speed: hydraulic pumps, fans, compressors, etc. At most, they have different load levels where the operator can decide to make them work, but the load does not change by itself. It is precisely under these conditions where efficiency estimation and MCSA steady-state diagnosis is performed. In terms of SSE, the fact of being performed under fixed steady-state conditions makes a very big difference with respect to the field of advanced electric motor control, as there is no longer that trade-off between accuracy and real-time response. In this case, since the operating conditions do not change, only a single speed value needs to be estimated for the whole capture interval, instead of a speed value for each instant of time. Moreover, since, on the one hand, it is not necessary to estimate efficiency every few seconds and, on the other hand, many of the faults (such as bar breakage or eccentricity problems) evolve slowly, the measurement of voltages and currents can last tens of seconds or even minutes. As mentioned before, the latter allows to greatly exploit the accuracy of those SSE methods whose precision increases with the capture length. Thus, since the SSE technique here presented has been developed for efficiency estimation and diagnosis, it is in steady-state with long capture times where the research of the present thesis is focused: this enables a high precision in certain type of SSE techniques, which, in turn, becomes decisive in order to have reliable efficiency estimation, and MCSA steady-state diagnosis applications.

In accurate efficiency estimation methods, it is necessary to know the speed, whether it is used to obtain the mechanical power once the torque has been estimated, or whether it is used to determine the slip and solve the equivalent electrical circuit to subsequently perform the power balance [2]. Therefore, the accuracy with which the efficiency is estimated is not only linked to the method itself, but also to the accuracy with which the speed is estimated.

In MCSA steady-state diagnosis, the fault harmonics present in the stator line currents are used to diagnose the motor [3]. The frequencies of these harmonics depend on the slip or, in other words, on the speed [4]. Although some authors propose locating the fault harmonics without knowing the operating speed by calculating the maximum of the spectrum in the harmonic operating frequency band (determined by the slip varying from 0 to its rated load) [5]–[7], it has been shown that constructional characteristics, supply, load oscillations, etc., can generate significant harmonics in these search bands, and produce false positives [8]. Moreover, the fault harmonic can also be outside the defined search band due to error tolerance in the name-plate rated slip [9], [10], thus generating a false negative [11]. In this way, accurate speed estimation becomes essential to avoid false positives/negatives [4], [8].

Finally, in recent years, new requirements have started to emerge among those industries that are adopting a 4.0 Industry philosophy: collect considerable amounts of data related to different systems, process them with specific algorithms to obtain information and act through this set of interconnected systems to achieve optimal autonomous production. In terms of diagnosis and efficiency estimation this means:

- Continuous monitoring: the performance and condition of the motor must be continuously assessed to achieve an optimal operation without requiring to interrupt the production process.
- Automated process without human intervention with efficient and fast assessment of big and varied amounts of motors.

- Intelligent operation of the facility: take the proper actions based on reliable motor condition and performance assessment.
- Interoperability via the Internet of Things: information related to the state of the machines must be shared with the rest of the systems and take decisions collectively.

Hence, the selected SSE technique not only has to be accurate, but also of general application, automatic and non-invasive, being able to work with the measurements taken during normal operation of the motor, which, as explained, may consist of long steady-states.

Next, a state-of-the-art review is performed[2], with the aim of identifying those families of SSE techniques that best fit the needs of steady-state MCSA diagnosis and efficiency estimation for IMs in a 4.0 Industry context. Moreover, the following subsections also determine the important drawbacks that prevent current SSE from meeting all the aforementioned requirements, namely: accuracy, general applicability, non-invasiveness and automaticity.

For the revision, SSE methods are classified into two major families of techniques: Fundamental Model Based (FMB) and Magnetic Anisotropy Based (MAB). The latter are subdivided into: Signal Injection Based (SIB) and Slotting and Rotational Frequency Sideband Harmonics Based (SRFSHB).

1.1.1 Fundamental Model Based methods

These techniques describe the machine model assuming a sinusoidal distribution of the air-gap flux (spatial harmonics of a higher order than the fundamental are neglected) and mainly using the d-q axes as the reference system. The parameters of the model usually needs to be determined before hand with especial tests. Furthermore, they are normally presented in the form of closed-loop schemes where error signals between measured and estimated magnitudes are used to correct the response and/or the parameters of the model. Despite the variety of closed-loop schemes that exist, they can be subdivided into: Model Reference Adaptive Systems (MRASs), observer schemes and schemes that incorporate Artificial Intelligence (AI).

MRASs [12]–[19] are schemes that consist of a reference model, an adaptive model and an adjustment mechanism. Reference and adaptive models estimate the same intermediate output but from different inputs. The desired magnitude to be estimated, in this case speed, is an input of the adaptive model, but not of the reference model. Finally, speed is estimated by minimizing the error between the intermediate outputs of both models through a controller.

An observer scheme is a dynamic structure that uses a model of the system (e.g., IM) to estimate internal/no-measurable variables (e.g., flux) from measurable inputs/outputs (e.g., stator currents and voltages). For example, observers based on the Extended Kalman Filter (EKF) [20]–[27] model the machine as a non-linear 5th-order system, where the mechanical speed is regarded as an additional state variable. Using this system, the EKF applies a two-stage recursive algorithm: first stage predicts the state variables, while the second (filtering stage) corrects these predicted variables.

[2]Here is presented a summarized version of the state-of-the-art review of SSE methods. For a more detailed version of the same, the reader is referred to the publication presented in Chapter 2, which is devoted to this purpose, as well as to the introduction of the publication presented in Chapter 3.

AI techniques can be used as complementary tools for MRAS and EKF closed-loop schemes aimed to overcome three of their major problems: complexity of non-linear mathematical models, instability and parameter compensation [28]. Among them, the most used for these purposes are: Artificial Neural Networks [29]–[32] (ANNs), Fuzzy Logic [33]–[35] (FL) and Genetic Algorithms [36], [37] (GAs).

In FMB methods, the degree of accuracy depends on the degree of robustness against variations in the model parameters (e.g., the variation of stator resistance with the temperature). In this regard, there has been a considerably improvement in recent years. Some methods, such as [19], [26], can obtain maximum errors of only a few rpm when there are changes in the model parameters. However, while this degree of accuracy may be enough for sensorless control (the field for which these methods are designed for), this might not hold true for steady-state MCSA, especially at low slips and in an industrial environment. As shown in [11], only an error of 3 rpm is enough to issue a false positive.

With respect to the invasiveness of the technique, FMB methods need voltage sensing which requires the motor to be stopped in order to couple the probes without electrical hazard. While this does not increase the invasiveness of an efficiency estimation technique, as it also requires voltage sensing, it does in a MCSA technique (especially when is implemented in a portable device), since this only requires current sensing, which can be done without interrupting the process using current clamps. Moreover, another inconvenient from this point of view is that, in order to conduct the first stage of model parameter identification that these methods require, it is usually necessary to perform especial tests that require to purposely stop the motor or wait for a scheduled stop.

Finally, regarding the ability to automate the technique and to achieve general applicability, it could be achieved it only if a reliable method is provided to automatically estimate the model parameters of any IM.

1.1.2 Magnetic Anisotropy Based methods

These techniques exploit the effects of magnetic saturation and rotor slotting in IMs. Among their advantages are their total independence to machine parameter variations (stator resistance, rotor time constant, etc.), the fact that they do not require the construction of a model of the machine, and that with some of them a high degree of accuracy can be achieved. This makes them really robust and often preferable to FMB methods. However, the existence or lack of certain anisotropies, as well as the intensity with which the effects due to slotting are manifested, depend on the machine design, which may reduce the applicability. Therefore, in many cases, a preliminary study of the motor (number of rotor bars/slots, rotor type, depth of slots, etc.) is required.

Signal Injection Based methods

SIB methods were born in the late 1990s as a response to the unstable performance of FMB methods at low or zero stator frequency. At these frequencies, the voltage induced in stator by rotor currents is practically zero, which makes the model unobservable: it is not possible to obtain information on rotor dynamics from stator terminals. However, it is possible to obtain accurate information about rotor position and rotor speed if the machine magnetic anisotropies are exploited [38].

In this regard, the technique consists of adding a high frequency and low amplitude voltage to the fundamental excitation in order to exploit these anisotropies. As explained by Holtz in [39]: "The resulting high-frequency currents generate flux linkages that close through the leakage paths in the stator and the rotor, leaving the mutual flux linkage with the fundamental wave almost unaffected". This signal, called carrier, is modulated periodically by the spatial orientation of the magnetic anisotropies present in the IM. Thus, by extracting and processing the modulated signal, it is possible to obtain information about the rotor angle and the rotor speed [39].

The carrier can be of two types: a revolving signal [40] or an alternating signal [41]. On the one hand, revolving carriers provide a general view of all machine positions in order to locate the spatial orientation of a particular machine anisotropy. On the other hand, alternating carriers provide a high-sensitive view in a specific spatial direction, which is chosen based on previous knowledge [39]. As an alternative to revolving or alternating carriers, transient signals injected by PWM switches can be exploited. Finally, it is also possible to use AI methods in order to improve some of the drawbacks of the technique, such as the need of having to determine with the help of an expert the magnetic fingerprint of each machine [42].

SIB methods do not depend on time varying parameters, and therefore, they can provide more accurate speed estimations than FMB techniques. However, these methods were born to meet a very specific need for sensorless control: good performance at zero or very low speed. Outside this low-speed range, which is precisely where steady-state MCSA and efficiency estimation techniques are usually applied, the accuracy gained does not compensate the excessive complexity of implementation.

With respect to the invasiveness of the technique, SIB methods need the machine to be excited with a source other than its normal power supply to inject the carriers. Although it is not necessary to use an additional power supply if the motor is powered by a frequency converter, it is necessary if it is a grid-powered motor, which increases the invasiveness in case of being implemented in a MCSA steady-state diagnostic or efficiency estimation application.

Finally, regarding the ability to automate the technique and to achieve general applicability for any motor, the main problem with this type of techniques is that they usually need a preliminary study of the motor to determine which is the best machine anisotropy to be exploited, as well as its location, especially, if an alternating carrier is used for a better sensitivity. This makes it unfeasible to deploy the technique on a massive scale in a MCSA steady-state diagnostic or efficiency estimation system.

Slotting and Rotational Frequency Sideband Harmonics Based methods

Unlike SIB methods, SRFSHB algorithms exploit magnetic anisotropies using the machine response to the fundamental excitation and its low-order harmonics (3rd, 5th, 7th,...). Particularly, these techniques track those anisotropies that are due to slotting and constructional/-coupling imbalances such as static and dynamic eccentricity. In a simplified and brief way, the discrete nature of the squirrel cage bars causes the rotor system to generate magneto-motive force spatial harmonics, as well as a periodic variation of the air-gap permeance. By interacting, they produce air-gap flux components that induce a set of harmonics in the stator windings called Rotor Slot Harmonics (RSHs). When there are also misalignments between rotor and stator (eccentricity), the air-gap permeance is further modified, giving rise to additional air-gap flux components. If static and dynamic eccentricity coexist, these additional flux components

induce the so-called Rotational Frequency Sideband Harmonics (RFSHs). The relationship between the frequencies of these harmonics in the stator current spectrum and the machine characteristics has been extensively studied in [43] and can be given in a compact form by:

$$f_{RSH} = \left[k\frac{R}{p}(1-s) \pm \nu \right] f_0 \tag{1.1}$$

$$f_{RFSH} = \left[1 \pm k\frac{(1-s)}{p} \right] f_0 \tag{1.2}$$

where k is a natural number $1, 2, 3 \ldots$, p the number of fundamental pole pairs, s the slip, ν the order of the time harmonic present in the stator current $1, 3, 5 \ldots$, f_0 the fundamental supply frequency and R the number of rotor bars.

As can be seen, both equations contain information on motor speed through the slip. Therefore, what these techniques do is to process the line current in order to determine the frequency of one or more of these harmonics and then, using (1.1) or (1.2), calculate the slip and with it, the mechanical speed. The precision with which the speed is determined is intrinsically linked to the precision with which the frequency of the harmonic is determined, which in turn, is related to the frequency resolution (the inverse of the capturing time): the longer the capturing time, the better the frequency resolution.

RFSHs-based methods are used in both, online condition monitoring [44] and in-situ efficiency estimation [45]–[47]. Moreover, since they only require the number of pole pairs (available on the nameplate), RFSHs-based methods are preferred by industry and used in commercial diagnostic devices (MCEMAX [48], EXP4000 [49]). However, their frequencies only vary a few fractions of hertz from no to full load [50]. Therefore, a small error in their frequencies estimation implies a large error in the speed estimation. On the other hand, RSHs-based methods [51]–[64] are much more accurate due to their wider operating bandwidth [11], [65]. Nevertheless, they depend on the number of rotor bars, which is a parameter that manufacturers do not normally provide. Therefore, the most common target of these techniques are specific motors where the number of rotor bars are known.

SRFSHB methods do not depend on time varying parameters, and therefore, can provide reliable and robust speed estimations. If the harmonics used are the RSHs, the accuracy can reach values lower than 1 rpm [56], [59], [61].

With respect to the invasiveness of the technique, SRFSHB methods only require sensing line currents, which do not increase the invasiveness of the target MCSA steady-state diagnostic or efficiency estimation application, as both techniques already do so.

Finally, regarding the ability to automate the technique and to achieve general applicability, the main problem with this type of techniques is that in order to use the most accurate one (RSH-based), the number of rotor bars needs to be known (other problems related with this technique are discussed below), which dramatically reduce its implementation on a massive scale in a MCSA steady-state diagnostic or efficiency estimation system, since the number of rotor bars is a parameter rarely know by motor owners. On the contrary, with RFSHS-based methods is more feasible to achieve general applicability, as they only depend on a nameplate parameter (the number of poles), which enables an immediate definition of the operational bandwidth of these harmonics for any motor. However, they are less accurate and can encounter dectectability problems, especially in 2-pole machines [11].

1.1.3 Discussion

As determined above, the most suitable family of SSE techniques to be applied in steady-state MCSA diagnosis and efficiency estimation of IMs in an 4.0 Industry context is one that meets the following requirements: accuracy, general applicability, non-invasiveness and automaticity.

FMB methods are less robust at providing accurate speed estimations as they depend on time varying parameters (e.g., stator resistance changing with temperature). In addition, invasive procedures (special tests) are usually needed to make a preliminary estimation of the motor parameters so that the model can start running, which greatly increases the invasiveness of the technique. SIB methods introduce complexity and invasiveness as they need the machine to be excited with a source other than its normal power supply (in grid-powered motors) and, in addition, they are more difficult to be automated as they usually need a previous study of the machine to determine which is the existing anisotropy more suited to be exploited. Finally, a study of the frequency converter is also necessary, if their feeding voltages are used instead of injecting a carrier. Unlike them, SRFSHB methods are able to provide accurate estimations in a non-invasive way and can be generalized and automated. Therefore, among the three families, the last one is the best option to be used in a steady-state MCSA diagnostic or efficiency estimation application within a 4.0 Industry context. However, while the non-invasiveness characteristic is shared by both types of SRFSHB methods, high accuracy is only characteristic of RSH-based methods and general applicability only of RFSH-based methods (putting aside detectability problems in two poles machines). In this regard, the ideal scenario would be to develop a SSE technique based on RSHs (to guarantee accuracy) that did not require to know the number of rotor bars (to try reaching general applicability). However, even if this was achieved, using these harmonics would not be trivial. The first problem would be to identify which harmonics in the spectrum constitute a RSHs family (a difficult task, since the RSHs, submerged inside a very populated spectrum, have a position that changes with the motor design). Then, even assuming that they had been correctly identified, each RSH should be assigned ν index; there is an erroneous trend to assign $+1$ or -1 to the RSH with the highest amplitude.

In this regard, most of the papers assume R, the position of the RSHs in the spectrum and their ν values as known information [51]–[57]. To solve this lack of data, others propose non-automatic/invasive methods that require visual inspection and/or subject the motor to different operating conditions [58]–[61]. Finally, only three papers propose self-commission methods to ascertain this set [62]–[64]:

The method presented in [62], which relies on a preliminary slip estimation from RFSHs, has three disadvantages. First, R is constrained from 30 to 54, which leaves quite a few machines out below 30 (2-pole and small-medium 4-pole machines) and above 54 (medium-large 4-pole and 6-pole machines). Second, RFSHs are an unreliable source of information since small errors in frequency estimation mean big errors in speed. Finally, RFSHs do not often manifest themselves with sufficient intensity to be distinguished from the noise level (especially in 2-pole machines). When this happens, the paper proposes to perform a no-load test to determine the main RSH and asks the user to introduce R (increasing invasiveness and decreasing automaticity).

In [63], the method searches a RFSH and the RSH with $\nu = 1$ (not specifying how the search bands are defined). Then, using these two harmonics and the value of the fundamental frequency, R is calculated. If the decimal of R is lower than 0.1 or higher than 0.9, the number is rounded and the process ends; otherwise, the process is repeated (it is not specified how the

band for the RSH is re-defined). The drawbacks of this method are the same as in [62] with respect to RFSHs, with the added disadvantage of assuming that RSH($\nu = 1$) may always be identified automatically .

In [64], the method, which relies on a preliminary speed estimation based on nameplate data, has three disadvantages. First, as stated before, constraining the number of R to consider may leave some motors out of the algorithm's scope; although in this case the range is wider than in [62], large motors could still be left out. Another problem with this methodology is that it uses a fixed band to localize RSHs (8.609 Hz), which, to work properly, should depend on the specific motor and its load. Finally, the main problem is that the convergence criteria is based on a preliminary speed estimation from nameplate: this estimation can be quite unreliable because nameplate data, apart from being subjected to wide tolerances (especially rated slip where a maximum tolerance of ± 20 % is allowed [9], [10]), can change through time due to degradation.

Therefore, no method has yet solved the problems of RSHs-based techniques in a robust, reliable and non-invasive way.

1.1.4 Conclusion

The best suited SSE technique for steady-state MCSA diagnosis and efficiency estimation in the 4.0 Industry context would be one based on RSHs, complemented with a method to eliminate the need to know the number of rotor bars, to localize the RSHs in a reliable way and to proper assign their ν indexes. Since the state-of-the-art review (here summarized, but deeply analyzed in Chapter 2) confirms that, up to date, an RSHs-based technique with such characteristics does not exist, it will be the main object of this thesis to develop it.

1.2 Objectives

The objective of this thesis is the development of an algorithm to estimate the operating speed of an IM in a precise, general, non-invasive and automatic way. In order to guarantee accuracy, the algorithm will make use of RSHs, while in order to guarantee non-invasiveness and general applicability, the algorithm will make use of a novel method to eliminate the need to know the number of rotor bars, so it only will use as starting point the stator line current and the number of pole pairs. In this way, the aim is to overcome the problems of existing techniques, which are either not accurate enough or cannot be generalized in a non-invasive way, since they require parameters that are difficult to know, which, in turn, distances them from an automatic operation and, even more, from an online operation, so necessary today in companies working with a 4.0 Industry philosophy. The effectiveness and usefulness of this new algorithm will be tested particularly in the fields of IM fault diagnosis via steady-state MCSA and efficiency estimation, in order to have a tool to reliably analyze motors in industry on a massive scale, thanks to said characteristics of accuracy, general applicability, non-invasiveness and automaticity. The industrial approach will be essential to assess the conditioning factors and features needed to implement this algorithm in continuous condition monitoring systems of IMs operating in 4.0 Industries.

The specific objectives are:

- To conduct an exhaustive state-of-the-art review of the families of SSE techniques, also including commercial devices that make use of them in their efficiency estimation and diagnosis algorithms, with the aim of identifying: which of the families is the best suited to be implemented in steady-state MCSA diagnosis and efficiency estimation algorithms for IMs, which are the main drawbacks of said family, and how these weaknesses might be overcome.
- To develop a theoretical formula to obtain the frequency of the RSHs without knowing the number of rotor bars, thus overcoming the non-applicability of these type of techniques in IMs of unknown parameters.
- To build an algorithm to locate the RSHs, among the numerous harmonics of the current spectrum, as well as to determine their parameters (e.g., ν index), all in an automatic and reliable way, thus allowing to determine the speed with accuracy, as well as the position of the fault harmonics.
- To test the algorithm with a set of motors covering different designs, driving different loads and fed with different power supplies, achieving this by using signals from simulation, lab tests and 105 industrial motors.
- To implement the algorithm in a plug and play device that conducts the continuous condition monitoring of an IM in an automatic and online way, so that it can detect those faults present in IMs that generate speed-dependent harmonics in the stator current spectrum.
- To study the RSHs as potential indicators for early detection of inter-turn short-circuits (especially in deep-well motors).

1.3 Thesis structure

As previously mentioned, this work is provided in the form of a *Thesis as a Collection of Articles*, being each of the four publications presented therein self-sufficient, that is, they can be read independently from the other chapters of the thesis, since they contain all the information necessary for their comprehension: abstract, introduction, technical/theoretical development, analysis of results (obtained by simulation, in the laboratory and in the field), discussion of said results and conclusions. In spite of their self-sufficiency, the four papers are in turn related to each other, with a logical order of progression, forming a coherent and clearly defined line of research, the culmination of which is the present thesis.

Apart from this chapter and the four chapters corresponding to each of the publications, the thesis is completed with three more chapters where, respectively, the results as a whole are discussed, the final conclusions are drawn and the future lines of research are described.

Chapter 2: Sensorless speed estimation for the diagnosis of induction motors via MCSA. Review and commercial devices analysis

In this publication, a thorough state-of-the-art review is presented on SSE techniques to see which of them is the most suitable to be used in steady-state MCSA algorithms for the diagnosis of IMs. Moreover, the study is complemented with a detailed analysis of the SSE methods

used by two of the leading commercial diagnostic devices in their steady-state MCSA algorithms, highlighting which are their main drawbacks. Therefore, the overall contribution of this paper is to determine the lacks and weaknesses of the industry application of these methods, which helps to highlight the open problems, challenges and research prospects, showing the direction in which research efforts have to be made to have a precise, general, non-invasive and automatic SSE method to be used in IM diagnosis via steady-state MCSA.

The paper, authored by Jorge Bonet-Jara, Alfredo Quijano-Lopez, Daniel Moriñigo-Sotelo and Joan Pons-Llinares, was published in 2021 in the journal *Sensors* from the publisher house *MDPI*. According to 2021 data, the journal has the following metrics:

TABLE 1.1: Journal metrics for *Sensors*

Producer	Index	Quartile/Decile
Clarivate	3.847 JIF	Q2 (95/276) in *Electrical and Electronic Engineering*
Scopus	6.4 CiteScore	Q1 (134/708) in *Electrical and Electronic Engineering*
Scimago	0.803 SJR	Q1 (25/141) in *Instrumentation*

Chapter 3: A precise, general, non-invasive and automatic speed estimation method for MCSA diagnosis and efficiency estimation of induction motors

In this paper, a precise, general, non-invasive and automatic speed estimation method is proposed for its application to steady-state MCSA diagnosis and efficiency estimation of IMs. The presented method belongs to the family of SSE techniques based on stator current harmonics, which according to the study conducted in the present chapter, in Chapter 2 and in [65], is the best suited for these two applications. This new methodology ends with the main weakness identified in the present chapter and Chapter 2 for SSE methods in their industrial application: the trade-off between accuracy (characteristic of techniques based on RSHs) and applicability (characteristic of techniques based on Rotational Frequency Sideband harmonics). This is achieved thanks to the use of a novel RSHs-based technique, that, for the first time in technical literature, eliminates the need to know/estimate the number of rotor slots, and provides a reliable and automatic procedure to locate the RSHs family in the stator current spectrum and determine their characteristic parameters. The method is validated under all types of conditions and for different motor designs, by simulations, lab tests and with 105 industrial motors, highlighting its high accuracy (errors below 0.05 rpm), and applicability. In this way, this publication is the natural continuation of the one presented in Chapter 2: once the state-of-the-art related to the technique to be developed has been analyzed and its problems have been studied, a method to solve them is proposed (the precise, general, non-invasive and automatic speed estimation method).

The paper, authored by Jorge Bonet-Jara and Joan Pons-Llinares, was published in 2022 in the journal *IEEE Transactions on Energy Conversion* from the publisher house *IEEE*. According to 2021 data (last available), the journal has the following metrics:

TABLE 1.2: Journal metrics for *IEEE Transactions on Energy Conversion*

Producer	Index	Quartile/Decile
Clarivate	4.877 JIF	Q1 (65/276) in *Electrical and Electronic Engineering*
Scopus	9.0 CiteScore	Q1 (81/708) in *Electrical and Electronic Engineering*
Scimago	2.087 SJR	D1 (55/730) in *Electrical and Electronic Engineering*

Chapter 4: End-ring wear in deep-well submersible motor pumps

In this publication, a previously unreported failure that takes place in deep-well submersible motors is described: the wear of the rotor end-rings. The first part of the paper comprises an analysis of the peculiarities of these IMs, and especially of their unusual rotor manufacturing process, explaining how they intervene in the failure mechanism of the end-ring. In the second part, the difficulties of diagnosing this fault through conventional rotor asymmetry indicators are investigated, coming up with a new paradigm to perform condition monitoring: the ratio of change in the Lower Sideband Harmonic (LSH) amplitude must be used as an indicator of end-ring wear, even if classic LSH alarm thresholds are not reached. Conclusions are supported by simulations, laboratory tests, and the continuous monitoring of two field motors working in deep boreholes. It is precisely in this last part where the method presented in Chapter 3 plays a key role. The algorithm was implemented in a diagnostic monitoring equipment, providing a precise estimation of the speed which allowed to accurately track (during nearly a year) the rotor asymmetry harmonics, discovering new fault patterns that later were reproduced in simulation and lab tests. The non-invasiveness of the method was essential in this application, as these motors are submerged at depths of up to 500 m, and also the automation of the process, since in this way it was possible to analyze four signals per day. Thus, this publication is the natural continuation of the ones presented in Chapter 2 and Chapter 3[3]: once a method has been developed to solve the weaknesses identified in the state-of-the-art revision, it is applied to one of its target industrial problem: accurate speed estimation for IM diagnosis via steady-state MCSA.

The paper, authored by Jorge Bonet-Jara, Daniel Morinigo-Sotelo, Oscar Duque-Perez, Luis Serrano-Iribarnegaray and Joan Pons-Llinares, was published in 2022 in the journal *IEEE Transactions on Industry Applications* from the publisher house *IEEE*. According to 2021 data (last available), the journal has the following metrics:

TABLE 1.3: Journal metrics for *IEEE Transactions on Industry Applications*

Producer	Index	Quartile/Decile
Clarivate	4.079 JIF	Q1 (23/92) in *Multidisciplinary Engineering*
Scopus	9.7 CiteScore	D1 (64/708) in *Electrical and Electronic Engineering*
Scimago	1.983 SJR	D1 (61/730) in *Electrical and Electronic Engineering*

Chapter 5: Comprehensive Analysis of Principal Slot Harmonics as Reliable Indicators for Early Detection of Inter-turn Faults in Induction Motors of Deep-Well Submersible Pumps

In this publication, a comprehensive analysis of Principal Slot Harmonics (PSHs) (a particular case of RSHs) is presented in order to asses their potential as reliable indicators for early detection of inter-turn faults in IMs, one of the most challenging faults to be detected in electrical machines. In particular, the study focuses on deep-well submersible motors since, as shown in the paper, they present a series of constructional and operating characteristics that act as game changers in terms of inter-turn fault detection through PSHs. The analysis comprises up to 65 different finite element simulations that are used to asses the sensitivity and reliability of these harmonics in detecting inter-turn faults in four different fault states, both alone and coexisting with different levels of voltage unbalance, rotor asymmetry and eccentricity. The findings from this analysis are used to develop a reliable diagnostic scheme based on

[3]The article associated with Chapter 3 was published after the one associated with Chapter 4. This is because the content of the article associated with Chapter 3 is linked to a patent, which was not filed until May 2022. This is the reason why there is no mention in the article of Chapter 4 about the novel method presented in Chapter 3.

the monitoring of the most fault-sensitive PSHs along with the voltage and current unbalance indexes (VUI and CUI). The diagnostic scheme is then applied, for the first time, in the context of a continuous monitoring of a 230 HP IM, showing its efficacy. In this way, this provides a second direct application of the developed method to reliably and automatically detect RSHs within the field of IM diagnosis. Therefore, this publication is the natural continuation of the ones presented in Chapter 2, Chapter 3 and Chapter 4: once a method has been developed to solve the weaknesses identified in the state-of-the-art revision and applied to one of its target industrial problem (accurate speed estimation for IMs diagnosis via steady-state MCSA), its capabilities are extended in order to address new industrial problems: to diagnose short-circuits with the same harmonics that are used to estimate speed.

The paper, authored by Jorge Bonet-Jara, Joan Pons-Llinares and Konstantinos N. Gyftakis, was published in 2022 in the journal *IEEE Transactions on Industrial Electronics* from the publisher house *IEEE*. According to 2021 data (last available), the journal has the following metrics:

TABLE 1.4: Journal metrics for *IEEE Transactions on Industrial Electronics*

Producer	Index	Quartile/Decile
Clarivate	8.162 JIF	D1 (28/276) in *Electrical and Electronic Engineering*
Scopus	17.1 CiteScore	D1 (20/708) in *Electrical and Electronic Engineering*
Scimago	3.519 SJR	D1 (21/730) in *Electrical and Electronic Engineering*

Chapter 6: General discussion

This chapter discusses the results obtained through the different publications, linking them within the general framework of this thesis.

Chapter 7: Contributions and conclusions

This chapter presents the main contributions of this thesis and the conclusions derived from the entire research.

Chapter 8: Future works

This chapter presents the lines of future research that are the the next natural step to be taken after the work shown in this thesis.

Bibliography

[1] M. Korzonek, G. Tarchala, and T. Orlowska-Kowalska, "A review on mras-type speed estimators for reliable and efficient induction motor drives," *ISA Transactions*, vol. 93, pp. 1 – 13, 2019, doi: 10.1016/j.isatra.2019.03.022

[2] B. Lu, T. Habetler, and R. Harley, "A survey of efficiency-estimation methods for in-service induction motors," *IEEE Transactions on Industry Applications*, vol. 42, no. 4, pp. 924–933, 2006, doi: 10.1109/TIA.2006.876065

[3] W. T. Thomson and M. Fenger, "Current signature analysis to detect induction motor faults," *IEEE Industry Applications Magazine*, vol. 7, no. 4, pp. 26–34, 2001, doi: 10.1109/2943.930988

[4] P. Gangsar and R. Tiwari, "Signal based condition monitoring techniques for fault detection and diagnosis of induction motors: A state-of-the-art review," *Mechanical Systems and Signal Processing*, vol. 144, p. 106908, 2020, doi: 10.1016/j.ymssp.2020.106908

[5] R. Schoen, B. Lin, T. Habetler, J. Schlag, and S. Farag, "An unsupervised, on-line system for induction motor fault detection using stator current monitoring," *IEEE Transactions on Industry Applications*, vol. 31, no. 6, pp. 1280–1286, 1995, doi: 10.1109/28.475698

[6] S. H. Kia, H. Henao, and G.-A. Capolino, "Diagnosis of broken-bar fault in induction machines using discrete wavelet transform without slip estimation," *IEEE Transactions on Industry Applications*, vol. 45, no. 4, pp. 1395–1404, 2009, doi: 10.1109/TIA.2009.2018975

[7] H. Guesmi, S. Ben Salem, and K. Bacha, "Smart wireless sensor networks for online faults diagnosis in induction machine," *Computers and Electrical Engineering*, vol. 41, pp. 226–239, 2015, doi: 10.1016/j.compeleceng.2014.10.015

[8] S. B. Lee, D. Hyun, T.-j. Kang, C. Yang, S. Shin, H. Kim, S. Park, T.-S. Kong, and H.-D. Kim, "Identification of false rotor fault indications produced by online mcsa for medium-voltage induction machines," *IEEE Transactions on Industry Applications*, vol. 52, no. 1, pp. 729–739, 2016, doi: 10.1109/TIA.2015.2464301

[9] *UNE-EN Maquinas electricas rotativas 60034-1*, 2011. [Online]. Available: https://www.une.org/encuentra-tu-norma/busca-tu-norma/norma/?c=N0047178

[10] *NEMA Motors and Generators, MG-1-2016*, 2016. [Online]. Available: https://www.nema.org/standards/view/motors-and-generators

[11] J. Bonet-Jara, A. Quijano-Lopez, D. Morinigo-Sotelo, and J. Pons-Llinares, "Sensorless speed estimation for the diagnosis of induction motors via mcsa. review and commercial devices analysis," *Sensors*, vol. 21, no. 15, 2021, doi: 10.3390/s21155037

[12] S. Tamai, H. Sugimoto, and P. Yano, "Speed sensorless vector control of induction motor applied model reference adaptive system," in *1985 Conference Record IEEE/MS Annual Meeting 6th*, 1985, pp. 613–620.

[13] C. Schauder, "Adaptive speed identification for vector control of induction motors without rotational transducers," *IEEE Transactions on Industry Applications*, vol. 28, no. 5, pp. 1054–1061, 1992, doi: 10.1109/28.158829

[14] Fang-Zheng Peng and T. Fukao, "Robust speed identification for speed-sensorless vector control of induction motors," *IEEE Transactions on Industry Applications*, vol. 30, no. 5, pp. 1234–1240, 1994, doi: 10.1109/28.315234

[15] S. Maiti, C. Chakraborty, and S. Sengupta, "Adaptive estimation of speed and rotor time constant for the vector controlled induction motor drive using reactive power," in *IECON 2007 - 33rd Annual Conference of the IEEE Industrial Electronics Society*, 2007, pp. 286–291, doi: 10.1109/IECON.2007.4460396

[16] A. V. Ravi Teja, C. Chakraborty, S. Maiti, and Y. Hori, "A new model reference adaptive controller for four quadrant vector controlled induction motor drives," *IEEE Transactions on Industrial Electronics*, vol. 59, no. 10, pp. 3757–3767, 2012, doi: 10.1109/TIE.2011.2164769

[17] A. V. Ravi Teja, V. Verma, and C. Chakraborty, "A new formulation of reactive-power-based model reference adaptive system for sensorless induction motor drive," *IEEE Transactions on Industrial Electronics*, vol. 62, no. 11, pp. 6797–6808, 2015, doi: 10.1109/TIE.2015.2432105

[18] Y. B. Zbede, S. M. Gadoue, and D. J. Atkinson, "Model predictive mras estimator for sensorless induction motor drives," *IEEE Transactions on Industrial Electronics*, vol. 63, no. 6, pp. 3511–3521, 2016, doi: 10.1109/TIE.2016.2521721

[19] S. Das, R. Kumar, and A. Pal, "Mras-based speed estimation of induction motor drive utilizing machines' d- and q-circuit impedances," *IEEE Transactions on Industrial Electronics*, vol. 66, no. 6, pp. 4286–4295, 2019, doi: 10.1109/TIE.2018.2860530

[20] Young-Real Kim, Seung-Ki Sul, and Min-Ho Park, "Speed sensorless vector control of induction motor using extended kalman filter," *IEEE Transactions on Industry Applications*, vol. 30, no. 5, pp. 1225–1233, 1994, doi: 10.1109/28.315233

[21] K. L. Shi, T. F. Chan, Y. K. Wong, and S. L. Ho, "Speed estimation of an induction motor drive using an optimized extended kalman filter," *IEEE Transactions on Industrial Electronics*, vol. 49, no. 1, pp. 124–133, 2002, doi: 10.1109/41.982256

[22] M. Barut, S. Bogosyan, and M. Gokasan, "Speed sensorless direct torque control of ims with rotor resistance estimation," *Energy Conversion and Management*, vol. 46, no. 3, pp. 335 – 349, 2005, doi: 10.1016/j.enconman.2004.04.002

[23] B. Akin, U. Orguner, A. Ersak, and M. Ehsani, "Simple derivative-free nonlinear state observer for sensorless ac drives," *IEEE/ASME Transactions on Mechatronics*, vol. 11, no. 5, pp. 634–643, 2006, doi: 10.1109/TMECH.2006.882996

[24] P. Rokhforoz and J. Poshtan, "Rotor speed and resistance estimation using robust extended kalman filter for sensorless vector control of induction motor drives," in *The 6th Power Electronics, Drive Systems Technologies Conference (PEDSTC2015)*, 2015, pp. 304–309, doi: 10.1109/PEDSTC.2015.7093292

[25] Z. Yin, G. Li, Y. Zhang, J. Liu, X. Sun, and Y. Zhong, "A speed and flux observer of induction motor based on extended kalman filter and markov chain," *IEEE Transactions on Power Electronics*, vol. 32, no. 9, pp. 7096–7117, 2017, doi: 10.1109/TPEL.2016.2623806

[26] E. Zerdali, "Adaptive extended kalman filter for speed-sensorless control of induction motors," *IEEE Transactions on Energy Conversion*, vol. 34, no. 2, pp. 789–800, 2019, doi: 10.1109/TEC.2018.2866383

[27] R. Yildiz, M. Barut, and E. Zerdali, "A comprehensive comparison of extended and unscented kalman filters for speed-sensorless control applications of induction motors," *IEEE Transactions on Industrial Informatics*, vol. 16, no. 10, pp. 6423–6432, 2020, doi: 10.1109/TII.2020.2964876

[28] S. Rind, Y. Ren, and L. Jiang, "Traction motors and speed estimation techniques for sensorless control of electric vehicles: A review," in *2014 49th International Universities Power Engineering Conference (UPEC)*, 2014, pp. 1–6, doi: 10.1109/UPEC.2014.6934646

[29] Seong-Hwan Kim, Tae-Sik Park, Ji-Yoon Yoo, and Gwi-Tae Park, "Speed-sensorless vector control of an induction motor using neural network speed estimation," *IEEE Transactions on Industrial Electronics*, vol. 48, no. 3, pp. 609–614, 2001, doi: 10.1109/41.925588

[30] S. Maiti, V. Verma, C. Chakraborty, and Y. Hori, "An adaptive speed sensorless induction motor drive with artificial neural network for stability enhancement," *IEEE Transactions on Industrial Informatics*, vol. 8, no. 4, pp. 757–766, 2012, doi: 10.1109/TII.2012.2210229

[31] J. M. Gutierrez-Villalobos, J. Rodriguez-Resendiz, E. A. Rivas-Araiza, and M. A. Martínez-Hernández, "Sensorless foc performance improved with on-line speed and rotor resistance estimator based on an artificial neural network for an induction motor drive," *Sensors*, vol. 15, no. 7, pp. 15 311–15 325, 2015, doi: 10.3390/s150715311

[32] S. V. B. S. Reddy, B. Kumar, and D. Swaroop, "Investigations on training algorithms for neural networks based flux estimator used in speed estimation of induction motor," in *2019 6th International Conference on Signal Processing and Integrated Networks (SPIN)*, 2019, pp. 1090–1094, doi: 10.1109/SPIN.2019.8711623

[33] Y. Luo and C. Lin, "Fuzzy mras based speed estimation for sensorless stator field oriented controlled induction motor drive," in *2010 International Symposium on Computer, Communication, Control and Automation (3CA)*, vol. 2, 2010, pp. 152–155, doi: 10.1109/3CA.2010.5533625

[34] S.-Y. Wang, C.-L. Tseng, S.-C. Lin, C.-J. Chiu, and J.-H. Chou, "An adaptive supervisory sliding fuzzy cerebellar model articulation controller for sensorless vector-controlled induction motor drive systems," *Sensors*, vol. 15, no. 4, pp. 7323–7348, 2015, doi: 10.3390/s150407323

[35] S. Mohan Krishna and J. Febin Daya, "Mras speed estimator with fuzzy and pi stator resistance adaptation for sensorless induction motor drives using rt-lab," *Perspectives in Science*, vol. 8, pp. 121 – 126, 2016, doi: 10.1016/j.pisc.2016.04.013

[36] Li Cai, Yinhai Zhang, Zhongchao Zhang, Chenyang Liu, and Zhengyu Lu, "Application of genetic algorithms in ekf for speed estimation of an induction motor," in *IEEE 34th Annual Conference on Power Electronics Specialist, 2003. PESC '03.*, vol. 1, 2003, pp. 345–349 vol.1, doi: 10.1109/PESC.2003.1218317

[37] I. M. Alsofyani, N. R. N. Idris, M. Jannati, S. A. Anbaran, and Y. A. Alamri, "Using nsga ii multiobjective genetic algorithm for ekf-based estimation of speed and electrical torque in ac induction machines," in *2014 IEEE 8th International Power Engineering and Optimization Conference (PEOCO2014)*, 2014, pp. 396–401, doi: 10.1109/PEOCO.2014.6814461

[38] J. Holtz, "Sensorless position control of induction motors-an emerging technology," *IEEE Transactions on Industrial Electronics*, vol. 45, no. 6, pp. 840–851, 1998, doi: 10.1109/41.735327

[39] J. Holtz, "Sensorless control of induction machines—with or without signal injection?" *IEEE Transactions on Industrial Electronics*, vol. 53, no. 1, pp. 7–30, 2006, doi: 10.1109/TIE.2005.862324

[40] M. W. Degner and R. D. Lorenz, "Using multiple saliencies for the estimation of flux, position, and velocity in ac machines," *IEEE Transactions on Industry Applications*, vol. 34, no. 5, pp. 1097–1104, 1998, doi: 10.1109/28.720450

[41] Jung-Ik Ha and Seung-Ki Sul, "Sensorless field-orientation control of an induction machine by high-frequency signal injection," *IEEE Transactions on Industry Applications*, vol. 35, no. 1, pp. 45–51, 1999, doi: 10.1109/28.740844

[42] T. M. Wolbank, M. A. Vogelsberger, R. Stumberger, S. Mohagheghi, T. G. Habetler, and R. G. Harley, "Autonomous self-commissioning method for speed-sensorless-controlled induction machines," *IEEE Transactions on Industry Applications*, vol. 46, no. 3, pp. 946–954, 2010, doi: 10.1109/TIA.2010.2046288

[43] P. Vas, *Parameter Estimation, Condition Monitoring, and Diagnosis of Electrical Machines*. Oxford Science Publications, 1993, [Online]. Available: https://global.oup.com.

[44] A. K. Samanta, A. Naha, A. Routray, and A. K. Deb, "Fast and accurate spectral estimation for online detection of partial broken bar in induction motors," *Mechanical Systems and Signal Processing*, vol. 98, pp. 63–77, 2018, doi: 10.1016/j.ymssp.2017.04.035

[45] P. Phumiphak and C. Chat-uthai, "Non-intrusive method for induction motor field efficiency estimation using on-site measurement and modified equivalent circuit," in *2012 15th International Conference on Electrical Machines and Systems (ICEMS)*, 2012, pp. 1–5. [Online]. Available: https://ieeexplore.ieee.org/document/6401991

[46] A. G. Siraki and P. Pillay, "An in situ efficiency estimation technique for induction machines working with unbalanced supplies," *IEEE Transactions on Energy Conversion*, vol. 27, no. 1, pp. 85–95, 2012, doi: 10.1109/TEC.2011.2168563

[47] M. Al-Badri, P. Pillay, and P. Angers, "A novel in situ efficiency estimation algorithm for three-phase induction motors operating with distorted unbalanced voltages," *IEEE Transactions on Industry Applications*, vol. 53, no. 6, pp. 5338–5347, 2017, doi: 10.1109/TIA.2017.2728786

[48] PDMA, *Introduction to MCEMAX*. [Online]. Available: https://www.pdma.com/PdMA-intro-mcemax.php

[49] Megger, *Instantaneous torque as a predictive maintenance tool for variable frequency drives and line operated motors*. [Online]. Available: https://es.megger.com/products/motor-and-generator-testing/dynamic-analyzers/baker-exp4000/technical/instantaneous-torque-as-a-predictive-maintenance-t

[50] S. Nandi, S. Ahmed, H. A. Toliyat, and R. M. Bharadwaj, "Selection criteria of induction machines for speed-sensorless drive applications," *IEEE Transactions on Industry Applications*, vol. 39, no. 3, pp. 704–712, 2003, doi: 10.1109/TIA.2003.810651

[51] M. Ishida and K. Iwata, "A new slip frequncy detector of an induction motor utilizing rotor slot harmonics," *IEEE Transactions on Industry Applications*, vol. IA-20, no. 3, pp. 575–582, 1984, doi: 10.1109/TIA.1984.4504454

[52] A. Bellini *et al.*, "On-field experience with online diagnosis of large induction motors cage failures using mcsa," *IEEE Transactions on Industry Applications*, vol. 38, no. 4, pp. 1045–1053, 2002, doi: 10.1109/TIA.2002.800591

[53] J. Jung, J. Lee, and B. Kwon, "Online diagnosis of induction motors using mcsa," *IEEE Transactions on Industrial Electronics*, vol. 53, no. 6, pp. 1842–1852, 2006, doi: 10.1109/TIE.2006.885131

[54] O. Keysan and H. B. Ertan, "Real-time speed and position estimation using rotor slot harmonics," *IEEE Transactions on Industrial Informatics*, vol. 9, no. 2, pp. 899–908, 2013, doi: 10.1109/TII.2012.2210231

[55] U. A. Orji and et al., "Non-intrusive induction motor speed detection," *IET Electric Power Applications*, vol. 9, no. 5, pp. 388–396, 2015, doi: 10.1049/iet-epa.2014.0274

[56] W. L. Silva, A. M. N. Lima, and A. Oliveira, "Speed estimation of an induction motor operating in the nonstationary mode by using rotor slot harmonics," *IEEE Transactions on Instrumentation and Measurement*, vol. 64, no. 4, pp. 984–994, 2015, doi: 10.1109/TIM.2014.2361554

[57] A. G. Yepes, J. Doval-Gandoy, F. Baneira, and H. A. Toliyat, "Speed estimation based on rotor slot harmonics in multiphase induction machines under open-phase fault," *IEEE Transactions on Power Electronics*, vol. 33, no. 9, pp. 7980–7993, 2018, doi: 10.1109/TPEL.2017.2773649

[58] A. Ferrah, K. Bradley, and G. Asher, "Sensorless speed detection of inverter fed induction motors using rotor slot harmonics and fast fourier transform," in *PESC '92 Record. 23rd Annual IEEE Power Electronics Specialists Conference*, 1992, pp. 279–286 vol.1, doi: 10.1109/PESC.1992.254661

[59] R. Blasco-Gimenez, G. M. Asher, M. Sumner, and K. J. Bradley, "Performance of fft-rotor slot harmonic speed detector for sensorless induction motor drives," *IEE Proceedings - Electric Power Applications*, vol. 143, no. 3, pp. 258–268, 1996, doi: 10.1049/ip-epa:19960241

[60] Z. Gao, L. Turner, R. S. Colby, and B. Leprettre, "A frequency demodulation approach to induction motor speed detection," *IEEE Transactions on Industry Applications*, vol. 47, no. 4, pp. 1632–1642, 2011, doi: 10.1109/TIA.2011.2153813

[61] S. Luecke, J. Koupeny, and A. Mertens, "Induction machine speed tracking based on rotor slot harmonics using a modified pll approach," in *2016 18th European Conf. on Power Electron. and Applicat. (EPE'16 ECCE Europe)*, 2016, pp. 1–10, doi: 10.1109/EPE.2016.7695518

[62] K. Hurst and T. Habetler, "Sensorless speed measurement using current harmonic spectral estimation in induction machine drives," *IEEE Transactions on Power Electronics*, vol. 11, no. 1, pp. 66–73, 1996, doi: 10.1109/63.484418

[63] O. Keysan and H. B. Ertan, "Determination of rotor slot number of an induction motor using an external search coil," *Facta universitatis-series: Electronics and Energetics*, vol. 22, pp. 227–234, 2009, doi: 10.2298/FUEE0902227K

[64] W. J. Bradley, B. Mason, A. Pezouvanis, and K. M. Ebrahimi, "A sensorless speed estimation algorithm for use in induction motor fault detection applications." *Journal of Systems and Control Engineering*, vol. 228, no. 4, pp. 257–264, 2013, doi: 10.1177/0959651813511613

[65] M. Chirindo, M. A. Khan, and P. Barendse, "Analysis of non-intrusive rotor speed estimation techniques for inverter-fed induction motors," *IEEE Transactions on Energy Conversion*, vol. 36, no. 1, pp. 338–347, 2021, doi: 10.1109/TEC.2020.3007409

Chapter 2

Sensorless speed estimation for the diagnosis of induction motors via MCSA. Review and commercial devices analysis

This paper was published on July 25, 2021 in Sensors journal, belonging to the MDPI publishing house, under the reference:

J. Bonet-Jara, A. Quijano-Lopez, D. Morinigo-Sotelo, and J. Pons-Llinares, "Sensorless speed estimation for the diagnosis of induction motors via mcsa. Review and commercial devices analysis," *Sensors*, vol. 21, no. 15, p. 5037, Jul. 2021, doi: 10.3390/s21155037.

In the next sections, the full author's version of the manuscript is reproduced, including abstract, appendixes and bibliography. Footnotes, which are not present in the original publication, are added in order to clarify some aspects within the general frame of this thesis.

Abstract

Sensorless speed estimation has been extensively studied for its use in control schemes. Nevertheless, it is also a key step when applying Motor Current Signature Analysis to induction motor diagnosis: accurate speed estimation is vital to locate fault harmonics, and prevent false positives and false negatives, as shown at the beginning of the paper through a real industrial case. Unfortunately, existing sensorless speed estimation techniques either do not provide enough precision for this purpose or have limited applicability. Currently, this is preventing Industry 4.0 from having a precise and automatic system to monitor the motor condition. Despite its importance, there is no research published reviewing this topic. To fill this gap, this paper investigates, from both theoretical background and an industrial application perspective, the reasons behind these problems. Therefore, the families of sensorless speed estimation techniques, mainly conceived for sensorless control, are here reviewed and thoroughly analyzed from the perspective of their use for diagnosis. Moreover, the algorithms implemented in the two leading commercial diagnostic devices are analyzed using real examples from a database of industrial measurements belonging to 79 induction motors. The analysis and discussion through the paper are synthesized to summarize the lacks and weaknesses of the industry application of these methods, which helps to highlight the open problems, challenges and research prospects, showing the direction in which research efforts have to be made to solve this important problem.

Key words: fault diagnosis; induction motors; MCSA; sensorless speed estimation; Industry 4.0.

2.1 Introduction

Over the last three decades, Sensorless Speed Estimation (SSE) for rotating machines has undergone a great advance. From the very first moment, SSE techniques were mainly applied in the field of electric motor control (e.g., Field Oriented Control) [1]. Therefore, their development has always been linked to the improvement of control methods and frequency converters. However, despite their natural link to sensorless control, SSE algorithms also play a key role in fault detection methods for Induction Machines (IMs), specifically in those that assess motor condition by localizing speed-dependent fault harmonics in the frequency spectrum of the stator current [2]–[6]. First, because in order to extract and quantify these harmonics, a good speed estimation is previously needed to accurately determine their position [7], [8]. Second, because most industrial motors are neither coupled to physical speed sensors nor do they have the shaft accessible to perform manual measurements. Yet, although the basis is the same, the requirements that SSE methods have to meet depend on the field of application.

On the one hand, in order to carry out a good control, it is imperative to obtain a real-time response of the estimated parameters, specifically, that of the speed. This necessary real-time response generally involves a trade-off with accuracy, as it requires the SSE algorithm to use short voltage and current records. Furthermore, speed estimation methods also have to meet the requirement of a stable performance over a wide range to provide more versatility (e.g., low-speed operation). Regarding these two needs, in the last decade, an effort has been made to increase accuracy and stability using modern techniques such as neural networks, genetic algorithms, etc. [9]–[17]. Nevertheless, since the possibility of working with large data records is restricted in the field of controlled AC drives, the maximum degree of accuracy is yet to be fully exploited.

On the other hand, there are procedures in the field of IM diagnosis in which SSE algorithms can be implemented, where time response and data record length are less critical. As a consequence, accuracy can be increased. One of these procedures is Motor Current Signature Analysis (MCSA). This method is mainly applied to detect speed-dependent fault harmonics in the frequency spectrum of stator current [18], although other magnitudes can also be used (e.g., instantaneous power, reactive power or apparent power [19]–[21]). Many research papers, whose main purpose is not localizing the fault harmonic, since they test lab motors with perfectly-known conditions, analyze the expected fault harmonic frequency band assuming that the highest peak of the band will be the fault harmonic [22]–[30]. Some other authors use filters as wavelet transform to extract sub-signals related to frequency bands where the harmonic is supposed to be [31]–[33]. Nevertheless, these are dangerous strategies in real non controlled industrial environments, since these harmonics can show frequencies very close to those of healthy state caused by multiple factors (winding harmonics[1], load oscillations, gear boxes, etc.), and be confused with them. To avoid these false positives and negatives, some authors directly measure the speed to localize the faulty harmonics perfectly [34], [35]. Nevertheless, speed sensors are rarely present in industrial environments. Therefore, a SSE algorithm with high accuracy is vital to precisely track fault harmonics and reduce both false positives and negatives. In this regard, SSE techniques based on extracting speed-dependent harmonics (fault or healthy) using the Fast Fourier Transform (FFT) can increase the degree of precision without using sophisticated signal processing methods. This might be done by recording long periods of stator current (50 s, 100 s, even 200 s) in applications with little load oscillations and connected to stable grids (as is the case for a large number of industrial applications), which in turn would not be a problem for the diagnostic method, since rotor bar and eccentricity faults, usually detected by MCSA evolve slowly. Moreover, as both the diagnostic method and the SSE method would use the FFT to extract respectively fault and healthy/fault harmonics of the same stator current, they could be put together in one single algorithm. Finally, other authors have proposed to measure additional quantities as the external flux [36] to estimate the speed; nevertheless, this leads to a less robust method, as the flux sensor must be placed near the motor housing, which in some applications is not possible (e.g., submersible motor-pumps).

SSE techniques, regardless of whether they are used for diagnostic or sensorless control, can be classified into two large groups of methods: Fundamental Model-Based (FMB) [1], [9]–[17], [37]–[58] and Magnetic Anisotropy-Based (MAB). The latter can be subdivided into two more groups of methods: Signal Injection-Based (SIB) [59]–[64] and Slotting and Eccentricity Harmonics Based (SaEHB)[2] [4], [65]–[79]:

- FMB methods require to estimate or to know in advance a wide range of parameters (stator resistance, inductance, rotor time constant, number of slots, etc.). As many of them are time-varying (e.g., stator resistance can have variations in a range of 1:2 [60]), there are two possible scenarios: if they are assumed to be constant, an error is added to the speed estimation; on the other hand, if they are estimated over time, the algorithm can get more complicated and unstable.

[1]The term "winding harmonics" is used in this thesis to refer to those harmonics that appear in the stator current at frequencies that are multiple of the fundamental frequency and that are caused by the discrete distribution of the stator winding, the non-linearity of the iron and/or the presence of time harmonics in the supply.

[2]Rotational Frequency Sideband Harmonics are also known in literature as Mixed Eccentricity Harmonics. The first nomenclature is used throughout the thesis except in this chapter, Chapter 4, and Chapter 5, where the second one is used instead. This is because a reviewer of the publication of Chapter 3 suggested this change of nomenclature, and as a result, the entire thesis was adapted to it, with the exception of these three chapters, since they must reflect their associated publications as they appear in the accepted version of the manuscripts. Therefore, in this thesis, RFSH is equivalent to MEH, LRFSH to LMEH, URFSH to UMEH, and SRFSHB to SaEHB.

- SIB methods do no depend on any time-varying parameter. However, they require a much more complicated implementation, and besides, not all drives are compatible with their requirements [61], [80]. All this makes them hardly applicable on an industrial scale.

- SaEHB techniques do not depend on any time-varying parameter either. Yet, when based on Rotor Slot Harmonics, they depend on a machine characteristic that is rarely known by the motor owner: the number of rotor slots. Conversely, if they are based on Mixed Eccentricity Harmonics, which only depend on an easy to know parameter (number of poles), precision and detectability problems may arise due to their narrow bandwidth [72].

The previous knowledge of specific parameters or the need to estimate them is a classic problem in SSE techniques no matter if they are used in diagnostic or control applications. This means a big drawback when it comes to obtaining a general method that can be applied to any motor in industry. That is because, in most cases, operators and technicians do not know data beyond those indicated on the nameplate.

Therefore, online condition assessment methods based on frequency spectrum information need a precise SSE algorithm that allows to automatically localize speed-dependent fault harmonics and reduce both false positives and negatives. Moreover, the set formed by the SSE algorithm and the diagnostic method should also be able to be easily integrated into Industry 4.0 systems in order to provide a complete monitoring of motor condition over time. Traditional SSE control-oriented methods are not a good option for these purposes as they provide a real-time response at the expense of a lower accuracy. Yet, if integrated into diagnostic procedures, and thus relieved of a need for real-time response, some of the traditional SSE techniques might be able to provide a much more precise fault harmonic positioning, which in turn would translate into a much more reliable diagnostic.

The paper analyses for the first time the SSE methods present in the technical literature from the perspective of its application to induction motors diagnosis via MCSA. This work aims to reveal which are the open problems, challenges and research prospects that the scientific community has yet to work on to finally bring a precise, general and automatic algorithm able to work in the context of a 4.0 industry. To that end, the limitations of each technique are analyzed, from both theoretical and industry applications perspective. First, taking as a starting point the work presented at [81], this paper shows, through an industrial case (Section 2.2), how important an accurate and automatic SSE is for fault diagnostic methods based on localizing, extracting and quantifying speed-dependent harmonics. Then, the paper thoroughly reviews and analyzes the two main groups of SSE techniques, pointing out their limitations when applied with diagnostic procedures (Sections 2.3 and 2.4). Moreover, using again industrial cases thanks to a database of industrial measurements belonging to 79 IM, it is shown how the two leading commercial devices for diagnosis work, which are the principles of the algorithms they implement and what are their weakness and sources of errors (Section 2.5). Concluding, SSE in diagnostic procedures is not a solved issue; thus, the analysis and discussion performed in this paper, related to the industry application of these techniques, enables to finally synthesize and highlight the lines of research in which academia should focus its efforts in order to provide a truly effective SSE industrial method that could help obtain automatic and reliable diagnostic results.

2.2 Importance of SSE in diagnosis

Speed estimation is a key factor in steady-state fault diagnosis via MCSA. Certain faults, such as rotor bars breakage and eccentricities, induce speed-dependent harmonics in the stator current. For example, the frequencies of the main harmonics related to rotor bars breakage in the spectrum of the stator current are given by:

$$f_{BBH} = (1 \pm 2ks) f_0 \tag{2.1}$$

When k is equal to one, those harmonics are commonly known as the Upper Sideband Harmonic (USH), positive sign, and the Lower Sideband Harmonic (LSH), negative sign. The fundamental frequency (f_0) can be easily identified as it is the highest peak in the spectrum. Then, if the speed is also known or estimated, the slip (s) can be determined and with it the position of these harmonics. Finally, they can be quantified in order to issue a diagnosis.

Regarding the diagnosis, from now on, the following criterion will be used to determine the condition of the rotor bars in an IM: if the amplitude is below -48 dB the IM is considered to be healthy, between -48 and -36 dB there might be one or several broken/cracked bars, and above -36, there are multiple broken bars. This criterion is well established in the field of diagnosis [7], proved valid for different sizes of motors [18], [82] and shared by commercial devices (with slight variations in the thresholds, as shown in Section 2.5). It is also worth mentioning that, as these are empirically obtained limits, two different motors with the same amplitude of broken bar harmonics may have different numbers of broken or cracked bars. Yet, it should not be forgotten that the aim of the examples that will be used in this paper is to show that: given a failure criterion, a small error in speed estimation can lead to a wrong diagnosis. Therefore, the important point here analyzed is if the speed estimation method allows to precisely determine the frequency of the fault harmonic, while the exact value of the fault thresholds is secondary.

Next, to illustrate how important it is to know the speed accurately, the current of a two-pole 90 kW IM driving a submerged pump has been analyzed by the FFT. Figure 2.1a shows the spectrum of the stator current (blue line) with the fault thresholds (red lines), in which a deviation of only 3 rpm means to identify two healthy state harmonics (marked with green diamonds) as two broken bar harmonics (marked with red circles). The harmonics marked with green diamonds belong to the healthy state since they do not satisfy any of the formulas related to rotor electrical asymmetries, rotor-stator misalignments and stator electrical asymmetries. They could be caused by the operating conditions of the load, since after zooming out the spectrum (Fig. 2.1b), it can be observed a smearing effect around the fundamental frequency, as well as several sets of sideband harmonics not predicted by (2.1), but separated from the fundamental a multiple of a certain bandwidth: as stated in [18], these effects are usually related to the operation with gear boxes and/or load oscillations. Therefore, the error leads to diagnose the motor as faulty (green diamonds within the red lines) when, actually, the broken bars harmonics are in the healthy zone (red circles below red lines).

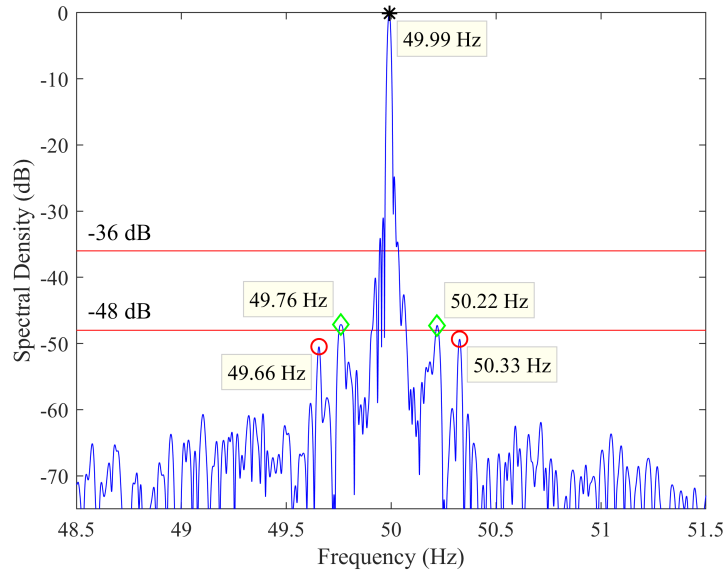

(a)

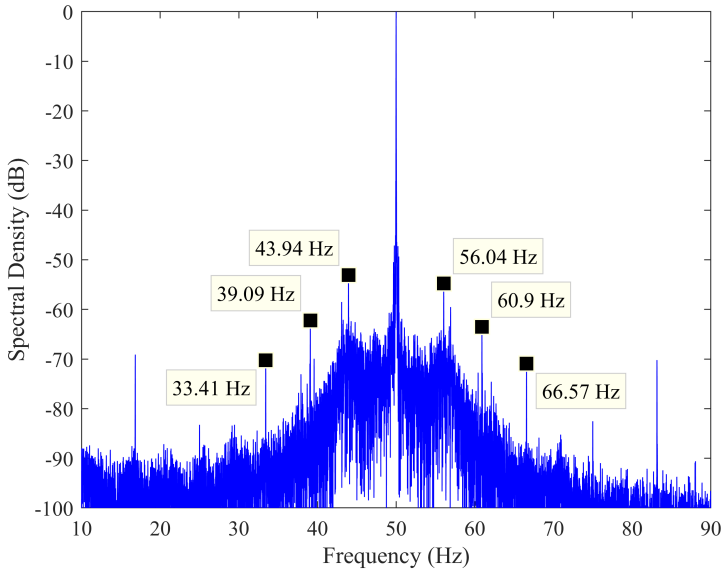

(b)

FIGURE 2.1: (a) Stator current spectrum of a two-pole 90 kW IM with healthy state harmonics (diamonds) close to the broken bar harmonics (circles) and (b) zoomed out spectrum showing the smearing effect around the fundamental and other harmonics caused by load oscillations.

From the above example, it is clear the need for accurate speed information in order to make a reliable diagnosis given a certain fault threshold. This information can come from a physical speed sensor or be estimated using an SSE technique. The cost of a physical sensor increases proportionally to the level of accuracy required, being sometimes a significant amount of the total price of the IM, especially when a custom design is required for its correct coupling. Moreover, they are very sensitive to the conditions of operation and location. Variations in temperature or large lengths of data transmission cable can lead to erroneous measurements.

In addition, a precise and careful assembly on the shaft is required. Conversely, sensorless techniques are able to overcome these drawbacks since they are: lower-cost options for the same accuracy (easy integration in existing control and measuring devices), more robust (measurements far from motor location implies better isolation; it also prevents motor disassembling in case of problems in measurement systems), and the only reliable option in certain industrial applications where physical sensors are very difficult to install (e.g., pumps submerged at great depths).

Alternatively, some authors propose to avoid the speed estimation problem by diagnosing the IM based on the following principle: since the fault-related harmonics have a certain operating bandwidth, determined for instance by (2.1) varying the slip from 0 to its rated value, it is possible to locate the fault harmonics in the spectrum by calculating the maximum in that bandwidth after a pre-treatment process [31], [83]. This diagnostic procedure relies on the fact that no other significant harmonic will be present in the search band. Nevertheless, as seen through the example presented in this section, that does not always hold true, and therefore, it can be a source of false positives. Thus, an algorithm that can accurately estimate speed, and consequently, the position of fault harmonics, is essential in the predictive maintenance of IM via MCSA.

Furthermore, in recent years, new requirements have started to emerge among those industries that are adopting an Industry 4.0 philosophy: collect considerable amounts of data related to different systems, process them with specific algorithms to obtain information and act through this set of interconnected systems to achieve optimal autonomous production. In terms of diagnosis, this means:

- Real-time condition monitoring: motors must be continuously diagnosed to achieve perfect operation.
- Noninvasive methods: production must not be altered (just when maintenance is needed).
- High reliability: avoid actions based on a false diagnosis.
- Automated process without human intervention: efficient and fast diagnosis of big amounts of motors.
- Intelligent operation of the facility: take the proper actions based on a correct diagnosis.
- Interoperability via the Internet of Things: information related to the state of the machines must be shared with the rest of the systems and take decisions collectively.

Then, there is not only the need for reliable and accurate diagnostic algorithms, but also for them to operate continuously, fully autonomously without requiring an expert intervention, and without altering the production process. Nevertheless, as it will be demonstrated later, current SSE algorithms implemented in commercial diagnostic devices do not meet these requirements, as they need human intervention to double-check the diagnostic due to the lack of reliability. The reliability is further reduced when the motor works in the presence of load oscillations and is fed by a frequency converter, the latter condition becoming more and more common in certain industries (e.g., water supply facilities). Moreover, it will also be shown that even those techniques that are able to provide a very accurate speed estimation and to be compatible with MCSA, also need the intervention of an expert to determine some of their initial parameters. Therefore, academia has yet to provide the modern industry with high-precision

and automatic SSE techniques that can serve as the cornerstone for the development of more reliable continuous condition monitoring systems based on MCSA.

2.3 Methods Based on the Fundamental Model

In this section, FMB methods are described, reviewing both the two most common techniques (Sections 2.3.1 and 2.3.2), and their respective improvements through the use of Artificial Intelligence (AI) (Section 2.3.3). Nevertheless, the key point, once the methods are reviewed, is to analyze their suitability for their use in IM diagnosis via MCSA (Section 2.3.4).

FMB methods describe the machine assuming a sinusoidal distribution of the air-gap flux (spatial harmonics of a higher order than the fundamental are neglected) and mainly using the d-q axes as the reference system. An open-loop scheme, depicted in Fig. 2.2a, is their simple way of implementation: the model outputs the speed (among other variables) using as inputs voltages and currents. However, this open loop model does not take into account the variations in parameters that occur during normal machine operation, such as the change in stator resistance with temperature [84]. Hence, as the model parameters remain constant but not the machine ones, there are deviations between the estimated speed and the actual one. This problem can be mitigated using closed-loop schemes (Fig. 2.2b) where error signals between measured and estimated magnitudes are used to adapt the response and/or the parameters of the model. Despite the variety of closed-loop schemes that exist, they can be subdivided into: Model Reference Adaptive Systems (MRASs), observer schemes and schemes that incorporate AI.

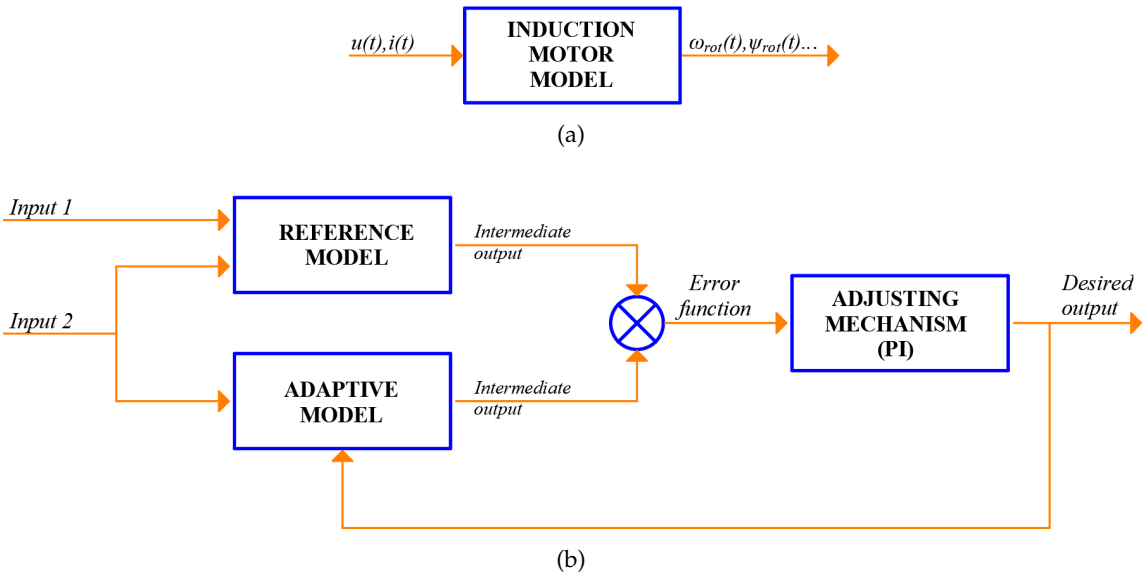

FIGURE 2.2: (a) Open-loop model and (b) a traditional scheme for a closed-loop MRAS.

Within the second group, there are different types of observers such as Sliding Mode Observer [48], Luenberger Observer [49], or observers based on the Extended Kalman Filter (EKF) [50]–[57]. Although with different characteristics from the control point of view (SMO and LO have better parameter robustness, dynamic performance and low-speed operation, while EKF has the best noise immunity [58]), their advantages and disadvantages regarding their

implementation in online diagnosis via MCSA are very similar (pros and cons later analyzed). Moreover, in high-speed steady-state operation, which is the range where MCSA is applied, the three observers exhibit very similar accuracy (relative error of 0.2% at 1500 rpm: perform similarly in the MCSA operation zone). Therefore, since the aim of this paper is not to review in detail each of the observer schemes, but to present their general characteristics and then analyze their compatibility with MCSA, only the EKF will be used as an example. The reasons behind this selection is that this type of scheme is one of the most used in the problem of speed estimation in the induction motor, thanks to its ability to deal with model uncertainties, measurement noise and its nonlinearity.

2.3.1 Model Reference Adaptive Systems

MRASs are schemes that consist of a reference model, an adaptive model and an adjustment mechanism (Fig. 2.2b). Reference and adaptive models estimate the same intermediate output but from different inputs. The desired magnitude to be estimated, in this case speed, is an input of the adaptive model, but not of the reference model. Finally, speed is estimated by minimizing the error between the intermediate outputs through a controller.

The first MRAS for SSE used the rotor flux as the error function and was presented by Tamai et al. [37] in 1985. However, it was complex, highly sensitive to machine parameter variations and unstable under certain conditions. On the one hand, complexity was mainly addressed in [38] (1992, Schauder) through a simplified and modified version of Tamai's work that rapidly became popular for its ease of implementation. On the other hand, sensitivity to parameter variations and instability were addressed through the use of other error functions such as back-EMF [39], reactive power [40], stator current [41] or fictional quantities [42]. Two excellent and wider reviews on these different MRAS schemes were conducted in [1], [43]. From these works, it can be concluded that classical reactive power-error-based MRAS schemes are the best to provide insensitivity to stator resistance variations, while classical fictional quantities-error-based MRAS schemes are a better option to provide stability in all zones of operation. In this regard, providing MRAS schemes that combine both qualities has been an aim of academia in recent years [44]–[46]. Finally, other authors have focused their research in reducing the computational time by replacing the PI controller with other structures [47].

2.3.2 Extended Kalman Filter Observer

An observer scheme is a dynamic structure that uses a model of the real system (e.g., IM) to estimate internal/no-measurable variables (e.g., flux, speed, position, etc.) from measurable inputs/outputs (e.g., stator currents and voltages). In the case of the EKF, the machine is modeled as a non-linear 5th-order system, where the mechanical speed is regarded as an additional state variable. Using this system, the EKF applies a two-stage recursive algorithm with a stochastic approach that accounts for the noise in the system, regarded as a Gaussian white noise environment. Then, in the first stage of the algorithm, the state variables are predicted, while in the second stage (filtering stage), the predicted variables are corrected.

One of the first successful applications of the EKF observer for SSE in IM was presented by Kim et al. in 1994 [50]. Since then, different approaches have been presented to increase speed accuracy. In [51], the problem was addressed from the perspective of improving the correct choice of noise covariance and weight matrices, while in [52] from the perspective of simultaneous estimation of speed and rotor resistance variations. Finally, in [53], the approach

was based on using an observer that does not use any linearization: the UKF. Using this observer, the authors stated that it was possible to obtain better results than using the EKF, especially in low-cost applications. However, this claim has been recently disputed in [54]. In this study, a comprehensive comparison of both methods is done under challenging conditions. It is shown that while equal in terms of performance, EKF is superior in terms of computational burdens and therefore a better choice for IM estimation problems. Yet, it is still debated which may be the best observer for the IM speed estimation problem. In this regard, works continue to be published where modified versions of the EKF are proposed to deal with the classical problems of choosing the noise covariance matrices and increasing the robustness against parameter variations [55]–[57].

2.3.3 Artificial Intelligence

In the early 2000s, AI techniques emerged as complementary tools for MRAS and EKF closed-loop schemes aimed to overcome three of their major problems: complexity of non-linear mathematical models, instability and parameter compensation [80]. Among them, the most used for these purposes are: Artificial Neural Networks [9]–[12] (ANNs), Fuzzy Logic [13]–[15] (FL) and Genetic Algorithms [16], [17] (GAs).

Having the role of complementary tools, these techniques are used to replace parts of closed loop schemes in order to obtain a better performance in the estimation process. For example, in [9], an ANN system replaced the adjustment mechanism of a classic MRAS scheme for a more robust behavior against machine parameter variations, while in [10], another ANN system replaced the adaptive mathematical model to improve stability in the four quadrants of operation. In [11], the approach was to use two kinds of ANN simultaneously: one for rotor speed estimation and the other for rotor resistance. In [12], different training algorithms for an ANN that replaces the flux estimator of a MRAS scheme were compared. In [13], a FL system replaced the adjustment mechanism of an MRAS scheme in order to obtain a synchronous speed estimator unaffected by variations in temperature. In [14], an adaptive supervisory sliding fuzzy cerebellar model is used as a speed controller in order to maintain the speed error within predefined boundaries. In [15], an FL control mechanism was used for stator resistance adaptation in order to improve speed estimation. In [16], [17], GAs were used to optimize the right choice of covariance filters matrices so as to enhance dynamic performance of EKF speed estimators. However, although these techniques have been proved to be a good tool to minimize the effects of parameter variations, their larger computational time and their need for training (ANN) can be a drawback in industrial applications.

2.3.4 Methods Based on the Fundamental Model in Online Diagnosis

Since the early nineties, all efforts have been put into developing FMB speed estimation techniques for sensorless control. No specific research has been done on developing these methods for diagnostic procedures. This may be due to the fact that the requirements of MCSA and FMB techniques do not fit together easily in an industrial environment, especially when implemented in portable devices, as explained below.

On the one hand, an MCSA-based commercial portable device needs to be as less invasive as possible: the diagnostic must be performed online and without interfering with the production process. MCSA only needs to sense stator currents (sometimes just one), whereas FMB methods need to sense both stator currents and voltages (inputs of the reference or adaptive

models). In this regard, although current sensing can be done in a non-invasive way using current clamps, voltage sensing requires the motor to be stopped in order to couple the probes without electrical hazard. Furthermore, another inconvenient from an industrial point of view is that in order to carry out the first stage of parameter identification that these methods require (parameters of the model), it is necessary to purposely stop the motor or wait for a scheduled stop.

On the other hand, a MCSA diagnostic procedure also needs to be as reliable as possible. Reliability is greatly improved if an accurate speed estimation algorithm is used. In FMB methods, the degree of accuracy depends on the degree of robustness against parameter variations. Over the last few years, there has been a considerably improvement in this regard. Current methods, such as [46], [57], can now obtain maximum errors of only a few rpm when there are changes in the parameters. However, while this degree of accuracy may be enough for sensorless control, this might not hold true for MCSA, especially at low slips and in an industrial environment. As shown in Section 2.2, only an error of 3 rpm is enough to issue a false positive. Moreover, if the motor is also working with load oscillations, the error needed to commit a mistake is even lower. Therefore, it is always preferable to use an SSE technique that does not depend on any changing parameter.

All the aforementioned drawbacks make FMB methods seemingly unsuitable for providing the speed information required by MCSA-based portable devices. However, MCSA-based continuous monitoring systems can open the door to use FMB techniques. If implemented in the driver, the set formed by the MCSA diagnostic procedure and the FMB method could use the same voltage and current measurements as the control system. Moreover, the system could also take advantage of the natural stops to perform the parameter identification. If designed as a separate device, it could be installed in the distribution board, and the same would apply. Yet, it is still necessary to study whether the accuracy provided by a method like this is enough for its use in high-reliability diagnostic procedures via MCSA in comparison with other SSE techniques. Furthermore, if complemented with AI, it would also be necessary to address in future comparative research, their feasibility in diagnostic devices, as these techniques require previous training and are computationally intensive.

2.4 Methods Based on Magnetic Anisotropy

These techniques exploit the effects of magnetic saturation and rotor slotting in IM. Their main advantage is their total independence to machine parameter variations (stator resistance, rotor time constant, etc.). This makes them really robust and often preferable to FMB methods. However, the existence or lack of certain anisotropies, as well as the intensity with which the effects due to slotting are manifested, depend on the machine design, which may reduce the applicability. Therefore, in many cases, a preliminary study of the motor (number of bars, rotor type, depth of slots, etc.) is required.

MAB methods can be classified into two groups: Signal Injection Based methods and Slotting and Eccentricity Harmonics Based methods. In Section 2.4.1, only a general description of SIB methods is given (without going into reviewing its evolution through time), since these techniques were developed to meet a specific need for control systems that is not found in diagnosis via MCSA. For this purpose, three excellent papers published by Holtz [59]–[61] are used. Conversely, in Section 2.4.2, the description and review of SaEHB methods are more in-depth and extensive, given that these techniques are more suitable to be used in diagnostic procedures in an Industry 4.0 environment, as analyzed in Section 2.4.3.

2.4.1 Methods Based on Signal Injection

SIB methods were born in the late 1990s as a response to the unstable performance of FMB at low or zero stator frequency. At these frequencies, the voltage induced in stator by rotor currents is practically zero, which makes the model unobservable: it is not possible to obtain information on rotor dynamics from stator terminals. However, it is possible to obtain accurate information about rotor position and rotor speed if the machine magnetic anisotropies are exploited [59].

Magnetic anisotropies can be caused in an IM mainly by: magnetic saturation of the fundamental field and the discrete structure of the squirrel cage. However, as Holtz states in [60], "a rotor may be custom designed so as to exhibit periodic variations within a fundamental pole pitch of local magnetic or electrical characteristics". An example of this could be the periodic variation of the widths of rotor slot openings, the resistance of the outer conductors or the depths of the rotors bars [60].

The technique consists of adding a high frequency and low amplitude voltage to the fundamental excitation in order to exploit these anisotropies. As explained by Holtz in [61]: "The resulting high-frequency currents generate flux linkages that close through the leakage paths in the stator and the rotor, leaving the mutual flux linkage with the fundamental wave almost unaffected". This signal, called carrier, is modulated periodically by the spatial orientation of the magnetic anisotropies present in the IM. Finally, by extracting and processing the modulated carrier it is possible to obtain information about the rotor angle and the rotor speed [61].

The injected signal can be of two types: a revolving signal [62] or an alternating signal [63]. On the one hand, revolving carriers provide a general view of all machine positions in order to locate the spatial orientation of a particular machine anisotropy. On the other hand, alternating carriers provide a high-sensitive view in a specific spatial direction, which is chosen based on previous knowledge [61]. As an alternative to revolving or alternating carriers, transient signals injected by PWM switches can be exploited. In words of Holtz in [61]: "the transient flux components, owing to their high-frequency content, do not penetrate sufficiently fast through rotor surface to establish mutual flux linkages. These fluxes, instead, create only separate linkages with the respective stator and rotor windings, thus contributing to the total leakage flux". Therefore, as the mutual flux also remains unaffected, the same principles apply as when external signals are used. Finally, it is also possible to use AI methods in order to improve some of the drawbacks of the technique, such as the need of having to determine with the help of an expert the magnetic fingerprint of each machine [64].

2.4.2 Methods Based on Slotting and Eccentricity Harmonics

Unlike SIB methods, SaEHB algorithms exploit magnetic anisotropies using the machine response to the fundamental excitation signal and its low-order harmonics (3rd, 5th, 7th ...). Particularly, these techniques track those anisotropies that are due to slotting and constructional/coupling imbalances such as static or dynamic eccentricity. In a simplified and brief way, the discrete nature of the squirrel cage bars causes the rotor system to generate MMF spatial harmonics as well as a periodic variation of the air-gap permeance. By interacting, they produce air-gap flux components that are responsible for inducing a set of harmonics in the stator windings called Rotor Slot Harmonics (RSH). When there are also misalignments between the rotor and the stator, the air-gap permeance is further modified, giving rise to additional air-gap flux components that can induce, depending on the characteristic of the misalignment, Static

Eccentricity Harmonics (SEH), Dynamic Eccentricity Harmonics (DEH) or Mixed Eccentricity Harmonics (MEH). The relationship between the frequencies of these harmonics in the current stator spectrum and the machine characteristics has been extensively studied in [85], [86] and can be given in a compact form by:

$$f_h = \left[\frac{(kR \pm n_d)}{p} (1 - s) \pm \nu \right] f_0 \tag{2.2}$$

$$f_{MEH} = \left[1 \pm k \frac{(1 - s)}{p} \right] f_0 \tag{2.3}$$

where k is a natural number $1, 2, 3 \ldots$, p the number of fundamental pole pairs, s the slip, ν the order of the time harmonic present in the stator current $1, 3, 5 \ldots$, f_0 the fundamental supply frequency, R the number of rotor bars, $n_d = 0$ for both SEH and RSH and $n_d = 1, 2, 3 \ldots$ for DEH. Finally, when k is equal to one in (2.3), those harmonics are known as the Upper Mixed Eccentricity Harmonic (UMEH), positive sign, and the Lower Mixed Eccentricity Harmonic (LMEH), negative sign.

As can be seen, both equations contain information on motor speed through the slip. Therefore, what these techniques do is to process the line current in order to determine the frequency of one or more of these harmonics and then, using (2.2) or (2.3), calculate the slip and with it, the mechanical speed. Finally, among the four sets of harmonics, RSH and MEH are usually the targets of these algorithms, since they are present in most IM.

The first works where RSH and MEH were used can be traced back to the middle of the 1980s and the beginning of the 1990s. In 1984, Ishida et al. [65] presented a work where, knowing the number of rotor bars and using analogue filters and zero cross detection, they were able to extract the RSH. This method achieved an accuracy of 0.1 Hz and a minimum operating frequency of 10 Hz. In a later work (Williams et al., 1990, [66]), MEH together with switched-capacitor filters and phase lock loops were used to estimate the rotor speed. In this case, no information about precision was provided. These methods laid down the foundations for the use of RSH and MEH in SSE.

During the 1990s, the accuracy and operating range of these SSE techniques was improved thanks to the use of digital methods such as FFT. Regarding this, RSH were first extracted using FFT in steady-state operation and over a wide range of load levels by A. Ferrah et al., in 1992 [67]. Results showed errors between -10 and 10 rpm when compared to an opto-electrical speed transducer. Furthermore, the speed detector performed satisfactorily down to 2 Hz and had a time response of 3 s. On the other hand, since the harmonics being tracked were RSH, the number of rotor slots needed to be known. Trying to address the problem, they presented a method to determine this parameter from a set of stator current records at rated frequency and under decreasing load levels. In 1996, a new improved method with a maximum error of 5 rpm, a time response of 1 s and an operating range down to 1 Hz was introduced by Hurst and Habetler [68]. In order to locate and extract the RSH, MEH and a recursive algorithm were used to ascertain the parameters R/p and ν.

In FFT techniques, the frequency resolution has a direct relation to signal capture time: the longer the capture time is, the better the resolution. Nevertheless, in the field of electric motor control, the length of data records is limited in order to obtain an appropriate time response. So, since the bases of SSE using FFT were set in [67], the effort was put in both reducing time response without losing accuracy and extending the method to transient conditions.

Considering this, in 1996, a study addressing these problems was presented by Blasco et

al [69]. It was stated that even with small data records, it is possible to achieve good accuracy through interpolation, windowing methods and choosing the appropriate RSH from the spectrum. The accuracy was less than 0.1 rpm, and the time response less than 1 s and in occasions much less than 1 s. A transient-state study was also presented. The results showed that the speed predictor followed the real speed after a delay which could be determined. Furthermore, two algorithms to detect RSH, where the number of rotor slots per pole and the parameter ν had to be known in advance, were described. In both methods, the problem about RSH crossing PWM harmonics was addressed. The first one, based on the detection of one RSH, showed reliability from 50 Hz to 5 Hz. The second one, based on the detection of two RSH, improved reliability until 2 Hz. Finally, a discussion about how to generalize the RSH detection for any squirrel cage IM was also presented. It was stated that the main problem was to know R and ν as they were parameters that were neither available in the nameplate nor in the motor datasheet. To work around this issue, they proposed that the motor/drive manufacturer, who can ascertain these parameters, sold each particular motor with its particular RSH detector embedded in the drive or, alternatively, that human operator derived their values through visual inspection of the frequency spectrum.

Since then, many studies have been published aimed at studying and improving different aspects of the technique such as: accuracy, real-time response, applicability, new signal processing methods, computational time and its use in unconventional machines. For example, in 1998 [70], a speed identifier was proposed with an error of less than 0.6 rpm and a real-time speed update of less than a sample period. This was achieved by extracting the RSH via adaptive digital filtering. Years later, in [71], [72], the relationship between the number of rotor slots, the number of pole pairs, the stator winding characteristics and the presence of RSH and other harmonics under healthy and eccentricity machine conditions was studied. This led the authors to establish a norm in selecting motors for SSE. In 2006 [4], an optimal slip estimation algorithm embedded in a diagnostic system using MCSA was proposed. This algorithm, assuming that the number of rotor slots was known, used broken bar harmonics, RSH and the Bayesian method of estimation to compute mechanical speed. The accuracy, in terms of slip frequency average error, was 2.97%. In 2013 [73], in order to reduce computation time, a novel approach that did not require spectral analysis was presented. It was based on extracting high order RSH (with previous knowledge of the number of rotor slots) through demodulating the information captured by an external search coil. By this method, a maximum speed error of 0.4% was achieved ($\approx$11 rpm). In 2015 [74], a new RSH-based method to estimate speed in non-stationary conditions was introduced. The proposed algorithm, assuming that the number of rotor slots was known, used short time Chirp-Z transform to search the supply frequency and the RSH. In this case, the maximum deviation found between the estimated and the measured speed using an optical tachometer was: 0.044% ($\approx$0.7 rpm) for the lab test and 0.163% ($\approx$2.4 rpm) for the industrial test. In 2016 [75], in order to improve the dynamics of speed estimation, a new algorithm that combines RSH detection, phase lock loop and AI was presented. In this work, the number of rotor slots was determined by comparing two current sequences at different load conditions with a fixed supply frequency. The maximum speed error in steady-state was found to be 0.083% ($\approx$0.7 rpm). In 2017 [76], MEH was used to estimate the slip in an online and real-time system for detecting partial broken rotor bars. The harmonics were found using a spectral estimator based on Rayleigh quotient theory, achieving a mean square error of 1.91×10^{-7} when compared to a physical sensor. Finally, in recent years, an effort has been made to extend SaEHB techniques to multi-phase IMs [77], [78].

2.4.3 Methods Based on Magnetic Anisotropy in Online Diagnosis

SIB methods were born to meet a very specific need for sensorless control: good performance at zero or very low speed. Nevertheless, the most common diagnostic procedures such as MCSA require the motor to be operating with relatively high speed and load. Therefore, these SSE techniques are not suitable to be integrated into this type of automatic fault diagnosis devices, since, outside the low-speed range, the robustness gained does not compensate for their excessive complexity of implementation.

Conversely, SaEHB methods are a great option for diagnostic algorithms via MCSA, since they are:

- Accurate: when based on RSH, errors can be less than 0.1 rpm.
- Robust: they do not depend on any time-varying parameter.
- Easy to implement: no need to subject the motor to a signal other than the one provided by its normal power supply.
- Compatible with MCSA: similar signal processing techniques and speed range.

Despite this, there are some drawbacks that have not been solved yet. On the one hand, in MEH-based methods, only the number of poles need to be known, which is a parameter available on the nameplate. This makes them the preferred methods for commercial diagnostic devices. However, they have a very narrow bandwidth. This means that they only vary a few fractions of hertz over its normal operating range. Therefore, a small error in the estimation of their frequencies implies a large error in the estimation of the speed (see Section 2.5). On the other hand, RSH-based methods can achieve very accurate estimates due to their wider operating bandwidth. That is the reason why they are so popular in academia, as shown in the literature review of previous subsection. However, these methods need to know the number of rotor slots to work, which is a problem for industry applications, as motor owners are rarely aware of this parameter. Therefore, the applicability of the method is dramatically reduced outside the laboratory.

The estimation of the $[R/p, \nu]$ is the main limitation to bring this type of algorithms to industrial scale. However, there is very little research addressing the problem. In fact, most of the papers about RSH-based algorithms either do not provide any information on how to obtain those parameters [4], [65], [66], [73], [74], [78], or propose non-automatic/invasive methods requiring human visual inspection, which limits their applicability in industrial environments [67], [69], [70], [75]. Only a few papers have proposed self-commission methods to ascertain this set [68], [79]. For example, in [68], the method relies on a preliminary speed estimation using the MEH, which, as already stated, is an unreliable source since small errors in frequency estimation mean big errors in speed. Moreover, there is also the disadvantage that MEH often do not manifest themselves with sufficient intensity to be distinguished from the noise level (see Section 2.5.1), being necessary in this case, as the authors comment, a no-load test to determine the number of rotor slots and the index ν associated with each RSH (increasing invasiveness). Something similar happens with the method proposed in [79], where in this case the unreliable source is the preliminary speed estimation based on nameplate data (see Section 2.5.2).

The unreliability of R/p and ν estimation can lead to misdiagnosing the IM due to the reasons exposed in Section 2.2. For example, Table 2.1 shows the speed and LSH frequency

errors caused by assigning $v = 1$ and $R/p = 26$ to the actual RSH (-1) for different motors with $R/p = 28$ working at two different slips. As can be seen, the speed error decreases as the number of pole pairs increases or the slip decreases. Yet, looking at the error committed in LSH frequency due to the wrong speed estimation, we find that it is independent of the number of pole pairs and that the error committed. Moreover, this error is of the same magnitude that the one necessary to issue a false positive in Fig. 2.1. Therefore, it is not only necessary for the method to be non-invasive, but also absolutely accurate to avoid false negatives and positives during diagnosis in any type of IM.

Finally, Table 2.2 summarizes the compatibility analysis between MCSA and the major families of SSE methods. From this analysis, it can be concluded that RSH-based methods are the best option for accurate diagnosis. Nevertheless, there is not yet a method to obtain R/p and v in a reliable, automatic and non-invasive way. That is precisely what makes RSH methods currently unsuitable for its use in high-reliability and high-applicability automatic diagnostic procedures via MCSA, and therefore, an aspect where academia should put its efforts.

TABLE 2.1: Speed and LSH frequency errors caused by assigning $\nu = 1$ and $R/p = 26$ to the actual RSH(-1) for different motors with $R/p = 28$ working at two different slips.

	p = 1, s = 0.01	**p = 1, s = 0.03**	**p = 2, s = 0.01**	**p = 2, s = 0.03**	**p = 3, s = 0.01**	**p = 3, s = 0.03**
Speed error (rpm)	2.31	6.92	1.15	3.46	0.76	2.30
LSH error (Hz)	0.08	0.23	0.08	0.23	0.08	0.23

TABLE 2.2: Compatibility analysis between MCSA and the major families of SSE methods.

Methods / **Characteristics**	**MRAS**	**EKF**	**AI**	**SIB**	**RSH-Based**	**MEH-Based**
Only one current sensing	x	x	x	x	✓	✓
No need for voltage sensing	x	x	x	x	✓	✓
No need for an additional power supply	✓	✓	✓	x	✓	✓
Highly accurate estimations (<1 rpm)	x	x	x	x	✓	x
High speed as one of the target zones of operation	✓	✓	✓	x	✓	✓
Insensitive to parameter variations	x	x	✓	✓	✓	✓
No need for previous training	✓	✓	x	✓	✓	✓
No need for parameter estimation	x	x	✓	x	x	✓
Simple implementation	✓	✓	✓	x	✓	✓
Compatibility with MCSA	Medium	Medium	Medium	Low	High	High

2.5 Commercial Devices

In this section, the two industry-leading commercial devices for IM diagnosis are analyzed. The analysis focuses on the speed-dependent online tests performed by these devices to detect motor faults. In this regard, Sections 2.5.1 and 2.5.2 first describe both the principles of the SSE algorithm and the diagnostic method (MCSA-based) of each device, and then analyze their weaknesses relying on the use of theoretical examples and real industrial cases from a database of measurements belonging to 79 different IM (Appendix A. Industrial motors data), which were taken using a high-resolution DAQ system (Appendix B. DAQ system) in order to reduce the measurement errors as much as possible, and thus to be able to focus only on the characteristics of each SSE algorithm. Finally, in Section 2.5.3 the results are discussed to highlight possible lines of improvement.

As explained in the following subsections, both commercial devices estimate the speed to approximately calculate the position in the spectrum of the faulty harmonic frequency, set a search frequency band around it, and finally calculate the maximum amplitude harmonic inside. Therefore, one of the key factors for a correct diagnosis is the search window. Window quality depends directly on the accuracy of the speed estimation. If the estimation is very accurate, the center of any search window will be very close to the fault harmonic frequency, which in turn will allow narrowing the band enough to prevent other significant healthy harmonics from entering it (reducing false positives), while still ensuring that it will contain the fault harmonic frequency (reducing false negatives). Therefore, as analyzed below, since both devices may suffer from wrong speed estimations, their capability to accurately assess the motor condition is affected.

2.5.1 EXPLORER 4000

EXP4000 from Megger is a device whose main purpose is to estimate power quality and efficiency in electrical machines. Yet, as it also allows to evaluate the rotor bars condition through MCSA, it has become a very popular tool when it comes to diagnosing this particular fault in induction motors.

The EXP4000 estimates the rotor speed using an algorithm based on detecting the LMEH in a series of instantaneous signals such as: phase current, current vector, sum of imaginary powers, angle of impedance, etc. [87], [88]. It should be noted that Equation (2.3) predicts the frequency of the LMEH ($k = 1$, $-$ sign) only for the spectrum of the stator current. According to [88], for the rest of the magnitudes analyzed by EXP4000, the frequency of the LMEH is given by $f^*_{LMEH} = f_0\,(1 - s)\,/\,p$. Taking this into account, the bases of the algorithm are:

In the stator current spectrum, the LMEH is located in a position slightly higher than $(1 - 1/p)\,f_0$ Hz, which is known if p is also known. Therefore, the algorithm sets a window whose lower limit is $(1 - 1/p)\,f_0$ Hz, which is the result of making $s = 0$ in (2.3), and whose upper limit is $(1 - (1 - s_{max})\,/\,p)\,f_0$ Hz, being s_{max} the slip correspondent to the maximum expected load (in [88] it is assumed to be $s_{max} = 180/n_{sync}$). Then, the maximum peak in the band is recorded assuming it is the LMEH. A similar process is repeated for each signal considered, but taking into account that, in their spectra, the formula that predicts the LMEH frequency is $f^*_{LMEH} = f_0\,(1 - s)\,/\,p$. Finally, the low amplitude peaks are discarded and the speed is estimated as the average of the largest group of estimations whose predictions coincide within a margin of 2 rpm.

As for the evaluation of rotor bars condition, the EXP4000 relies on localizing and quantifying the LSH. To do so, using the estimated speed and applying (2.1), the device calculates an estimated position for the LSH. Then, it sets a frequency window around this position and quantifies the maximum peak assuming it is the LSH. Finally, the EXP4000 applies the following default criterion to output a diagnosis: no damage to rotor bars if its amplitude is below -45 dB, possible damage to one or several bars if it is between -45 dB and -36 dB, and several broken bars if it is above -36 dB.

Mixed Eccentricity Harmonics: Detectability Problems in Two-Pole Machines

Mixed eccentricity is a problem inherent to any IM. It is caused by inaccuracies in the manufacturing process and misalignments during the motor-load coupling. Therefore, MEH are found in almost any IM, which does not mean that they always have a high amplitude. For example, in new and carefully coupled motors, they are normally only a few dB (if any) above the noise level. Moreover, the presence of nearby harmonics (not associated with motor faults) can complicate the detection process, especially, in two-pole motors (as analyzed below). This particular problem has been studied through the spectral analysis of 79 industrial motors (motor data can be found in Table 2.7 of Appendix A). The results of the analysis are summarized in Fig. 2.3 (UMEH) and Fig. 2.3b (LMEH), where blue bars represent their amplitudes, and red bars the amplitude of the highest harmonic found in the band determined by (2.3) when s is varied from zero to its rated value. A blue bar completely overlapping the red bar means that the highest harmonic corresponds to the MEH.

The analysis shows that in 48.10% of the cases, there is a higher harmonic than the UMEH in the search band, which for all these cases is the harmonic at $f_0 + f_0/p$ Hz (speed independent and placed at the upper limit of the search band). In two-pole machines, this frequency is $2f_0$ Hz (an even multiple of the fundamental), while in four and six-pole machines it coincides with a non-integer multiple of f_0. Theoretically, there should not be even multiples in the stator line current; however, as no real motor is perfectly symmetric, the existence of this harmonic is very common. Therefore, this explains why MEH detection can be especially difficult in two-pole machines. Figure 2.3c (right) shows one of these speed-independent harmonics (SIH) belonging to a two-pole 45 kW IM.

Regarding the LMEH, the same detectability problem has been observed with the same proportion of cases (48.10%) where the LMEH is not the highest harmonic in the search band. As with the UMEH, the majority of these motors corresponds to two-pole machines. In this case, the SIH harmonic that is causing problems is placed at 0 Hz (which is the lower limit of the search band), that is, the DC harmonic. Moreover, it has also been observed that, even when this component is filtered, for example, subtracting the mean value of the signal, it is still not possible to locate the LMEH in the line current spectrum, since it is submerged by the noise floor (see Fig. 2.3c (left)). Yet, if other electrical quantities are analyzed, as the EXP4000 does, the LMEH may become visible. For instance, Fig. 2.3d shows the spectrum of the instantaneous power signal of the same two-pole 45 kW IM. In this signal, the LMEH is expected to be at $f^*_{LMEH} = f_0\,(1-s)\,/\,p$ Hz. As can be seen, the LMEH is now visible. Nevertheless, the detectability problem does not disappear since there is still an SIH in the upper limit of the band.

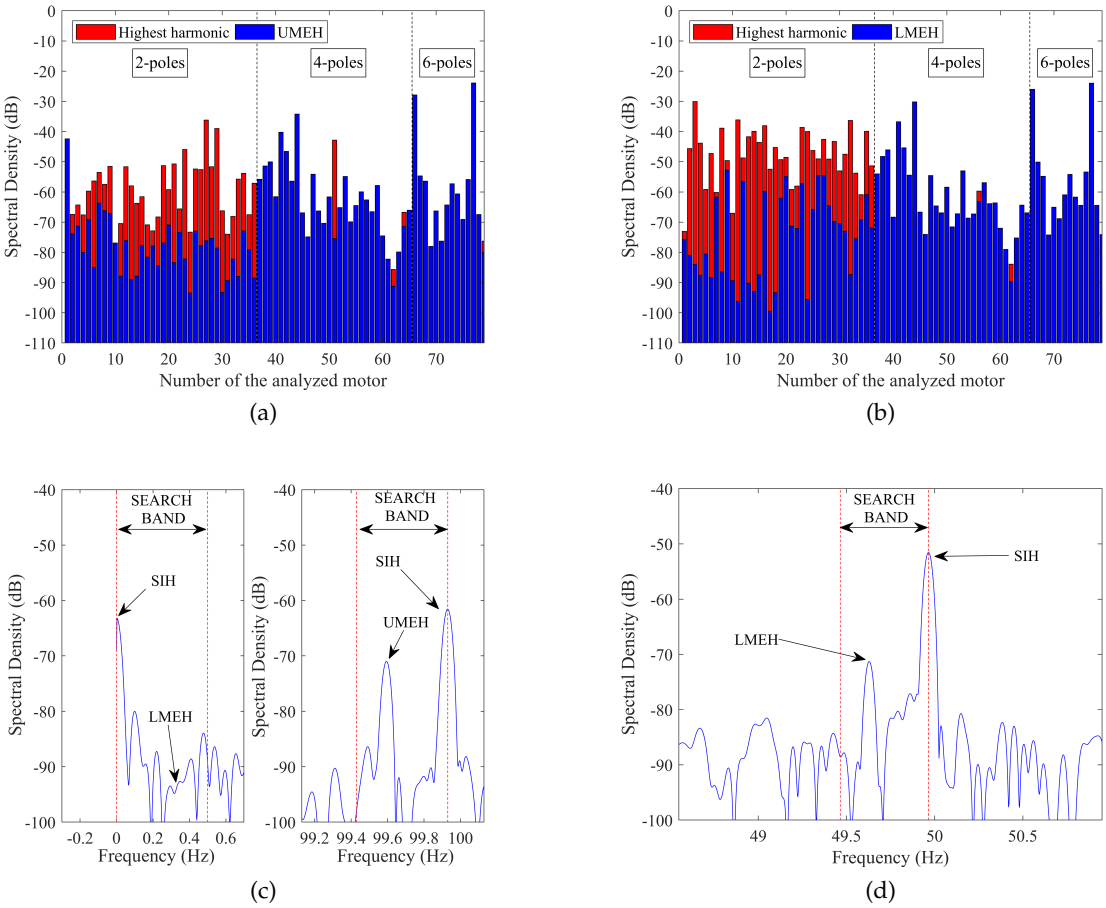

FIGURE 2.3: (a) UMEH and (b) LMEH detectability analysis for 79 IM covering a search band from zero to rated slip in the spectrum of the line current. Example of a two-pole 45 kW IM where: (c) the SIH is the highest harmonic in the search band defined for the UMEH and LMEH in the line current spectrum and (d) in the search band defined for the LMEH in the instantaneous power signal.

Mixed Eccentricity Harmonics: Narrow Bandwidth Implications in Rotor Diagnosis

As mentioned in Section 2.4.3, MEH cover a narrow frequency bandwidth (from no to full load), which means that small errors in estimating their frequencies (given by (2.3)), lead to significant errors in the estimated slip. Therefore, as this slip is used to set the search window where to find the fault harmonics, the diagnosis reliability is also affected by errors made in MEH frequency estimation. Next, in order to show more in depth the implications of harmonic bandwidth, we proceed to analyze the error committed in calculating the LSH frequency when slip is estimated from a narrow bandwidth harmonic (MEH) and a wide bandwidth harmonic (RSH).

Combining (2.1) and (2.3) with $k = 1$, LSH frequency can be expressed as a function of the MEH and fundamental harmonic frequencies:

$$f_{LSH} = -(1 \pm 2p) f_0 \pm 2p f_{MEH} \tag{2.4}$$

An error in the LSH frequency calculation can come either from a wrong frequency estimation

of the fundamental harmonic or the MEH. Therefore, if the previous equation is differentiated with respect to these two components and then discretized, we can express the error committed in the LSH frequency as a function of the errors committed in the MEH and fundamental harmonic frequencies:

$$\begin{cases} \frac{df_{LSH}}{df_0} = -(1 \pm 2p) \\ \frac{df_{LSH}}{df_{MEH}} = \pm 2p \end{cases} \rightarrow \Delta f_{LSH} = -\left[1 \pm 2p\right] \Delta f_0 \pm \left[2p\right] \Delta f_{MEH} \tag{2.5}$$

Finally, following the same reasoning, but in this case combining (2.1) and (2.2) with $k = 1$ and $n_d = 0$, we obtain the error committed in LSH frequency as a function of the RSH and fundamental harmonic frequency errors:

$$\begin{cases} \frac{df_{LSH}}{df_0} = -\left(1 \pm \frac{2\nu}{R/p}\right) \\ \frac{df_{LSH}}{df_{RSH}} = \frac{2}{R/p} \end{cases} \rightarrow \Delta f_{LSH} = -\left[1 \pm \frac{2\nu}{R/p}\right] \Delta f_0 + \left[\frac{2}{R/p}\right] \Delta f_{RSH} \tag{2.6}$$

As the number of rotor bars per poles pairs is normally higher than $R/p = 14$ for the majority of IM, the maximum coefficient multiplying Δf_{RSH} is $2/14 = 0.14$, while the coefficient multiplying Δf_{MEH} is much higher and increases with the pole pairs: $2p = 2, 4, 6 \ldots$ Assuming $\nu = +1$, which is the most common case, the maximum absolute value of the coefficient multiplying Δf_0 for the RSH is: $1 + 2/14 = 1.14$, while for the MEH increases as $1 + 2p = 3, 5, 7 \ldots$ or $1 - 2p = 1, 3, 5 \ldots$ Therefore, for the same frequency error Δf_0, and the same error estimating the RSH and MEH $\Delta f_{RSH} = \Delta f_{MEH}$, the RSH provides a much more accurate estimation of the LSH frequency. The errors Δf_0, Δf_{RSH} and Δf_{MEH} can mainly come from three sources:

1. Harmonic misidentification: the harmonic is confused with another close to it.
2. Harmonic in movement during capture time: the harmonic energy spreads over a range of frequencies instead of being concentrated in a single peak.
3. Frequency resolution error: the real harmonic frequency is between two FFT consecutive bins.

Sources 1 and 2 can be neglected for the fundamental harmonic, given that it is the highest harmonic in the spectrum and that its frequency is unlikely to significantly change in a short time capture (5 to 20 s). As for the MEH, source 1 has already been addressed in the previous subsection, while source 2 can be neglected if it is also assumed that speed will not change in a short time period. Therefore, if there is no harmonic misidentification and the regime is stable, the frequency resolution can be considered as the only source of error.

The FFT is a discrete transform calculated at a set of frequencies starting at 0 Hz, increasing by $1/T_{cap}$ Hz (being T_{cap} the capture time), and ending at half the sampling frequency. Each of these frequencies analyzed is called a bin. Thus, a harmonic whose real frequency is between two consecutive bins is assigned to the closest bin, while spreading part of its energy in the other. This generates the so-called frequency resolution error. In this regard, the maximum frequency resolution error occurs when the actual harmonic frequency is found just in the middle of two bins, which corresponds to $1/(2T_{cap})$ Hz. Figure 2.4 represents the deviation in LSH frequency (calculated using the absolute value of each term of (2.5) and (2.6), so that both errors add up) when the fundamental harmonic, the UMEH, the LMEH and the RSH(± 1) frequencies are estimated with an error equal to the maximum frequency resolution error: $\Delta f_0 = \Delta f_{RSH} = \Delta f_{MEH} = 1/(2T_{cap})$. This LSH error is quantified for $2p = 2$, $2p = 4$,

$2p = 6$ and $R/p = 28$ (typical number for IM). For instance, for an industry-standard capture time of 25 s, which corresponds to a maximum frequency resolution error of 0.02 Hz, the error committed in LSH frequency is, with respect to 0.02 Hz: of the same order for the RSH($\pm$1); 3, 7, or 11 times bigger for the LMEH and 5, 9 or 13 times bigger for the UMEH. It should be noted how inaccurate the estimation of the LSH frequency through MEH could be when compared to a RSH method.

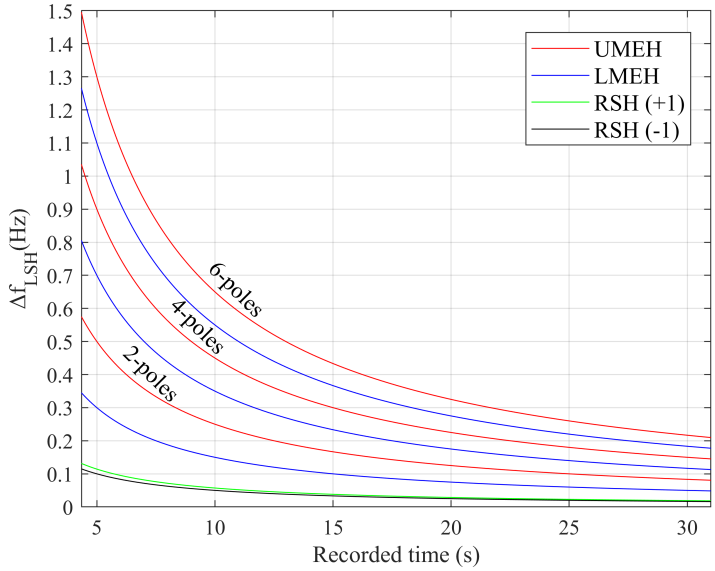

FIGURE 2.4: LSH absolute deviation due to the maximum frequency resolution error in RSH, MEH and f_0 .

To show how this error might lead to an erroneous diagnosis, two industrial motors were analyzed using the EXP4000 (based on the LMEH) and a RSH-based algorithm. The first is a four-pole 1500 kW IM, while the second a six-pole 800 kW IM. Table 2.3 summarizes the results for each machine, while Figs. 2.5 and 2.6 show the RSH-based algorithm result on the left (applied to the original current captured by the EXP4000) and the figure generated by the EXP4000 on the right (in both cases horizontal lines show the default limits for healthy and faulty state used by the EXP4000, while the vertical line shows the frequency at which each algorithm placed the LSH). The differences between the spectra were due to very small differences in signal processing: the way EXP4000 applied the FFT was not perfectly reproduced when analyzing the current extracted from the device, since this information ws not provided by the manufacturer. Nevertheless, since both were practically identical in frequency and amplitude (see the first two rows of Table 2.3), the differences in diagnosis could be considered to be caused exclusively by the differences between the SSE algorithms.

TABLE 2.3: Results of the rotor condition analysis for a four-pole 1500 kW IM and for a six-pole 800 kW IM. Frequencies are in Hz, speeds in rpm and amplitudes in dB.

	f_{res}	$f_{0,est}$	n_{est}	s_{est}	$f_{LSH,est}$	$f_{LSH,real}$	$f_{LSH,dev}$	$Amp.$	$Diag.$
EXP4000	0.039	59.98	1792.2	0.0040	59.501	59.462	0.039	−31.84	Damaged
RSH-based algorithm	0.039	59.98	1791.6	0.0042	59.467	59.462	0.005	−31.99	Damaged
EXP4000	0.036	60.01	1184.7	0.0129	58.463	59.029	0.566	−56.04	Healthy
RSH-based algorithm	0.036	60.01	1190.4	0.0081	59.032	59.029	0.003	−43.46	Damaged

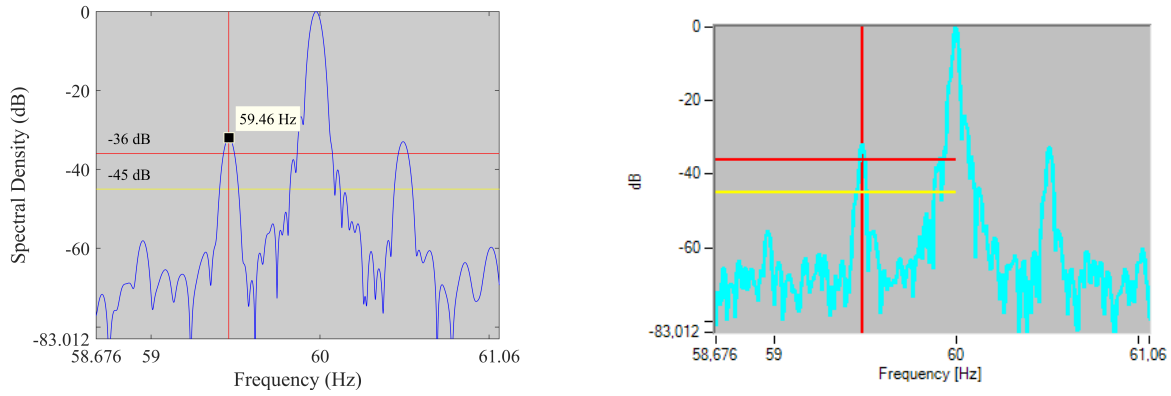

FIGURE 2.5: Rotor condition analysis of a four-pole 1500 kW IM using (a) a RSH-based algorithm and (b) the EXP4000.

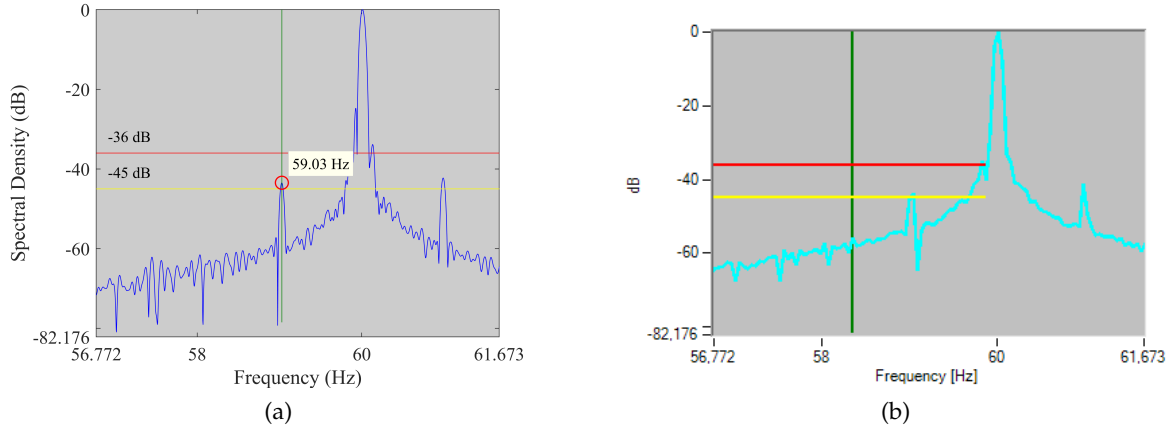

FIGURE 2.6: Rotor condition analysis of a six-pole 800 kW IM using (a) a RSH-based algorithm and (b) the EXP4000.

Regarding the difference in diagnosis, the RSH-based algorithm was able to estimate the LSH frequency very accurately in both motors (Figs. 2.5a and 2.6a), being the error committed ($f_{LSH,dev} = 0.005$ Hz and $f_{LSH,dev} = 0.003$ Hz), 7 and 11 times smaller than the frequency resolution ($f_{res} = 0.039$ Hz and $f_{res} = 0.036$ Hz), thereby issuing a correct diagnosis. Conversely, the EXP4000 was able to diagnose satisfactorily only the first motor (Fig. 2.5b): the error $f_{LSH,dev} = 0.039$ Hz was of the same magnitude as the frequency resolution $f_{res} = 0.039$ Hz. As for the second motor, it delivered a false negative (Fig. 2.6b): in this case, the deviation with respect to the LSH frequency was $f_{LSH,dev} = 0.566$ Hz (16 times bigger than the frequency resolution $f_{res} = 0.036$ Hz). This error was larger than the one predicted in (2.5), which meant that there might be an additional source of error. In this case, it could be a harmonic misidentification, given that the LMEH had an amplitude above the noise level of less than 6 dB in the line current spectrum. Moreover, it should be noted that the 0.566 Hz deviation only corresponded to an error of 0.09 Hz in the MEH frequency estimation, which showed how unreliable a MEH method could be.

Finally, in the signals where the LMEH had a frequency of $f^*_{LMEH} = f_0\,(1-s)\,/\,p$ (as the instantaneous power signal), the error in LSH frequency was expressed as:

$$\Delta f_{LSH} = -\,[1]\,\Delta f_0 + [2p]\,\Delta f^*_{LMEH} \tag{2.7}$$

As seen, when compared to (2.5) and for the same frequency resolution error, the deviation caused by the fundamental frequency was always equal or inferior, while the deviation caused by the LMEH frequency was the same. This improved LSH frequency estimation a bit, since, according to [88], EXP4000 uses several signals where LMEH has a frequency of $f_0\,(1-s)\,/\,p$ Hz. However, the coefficients of (2.7) were still further from those given by (2.6).

2.5.2 MCEMAX

MCEMAX is a device from PdMA that conducts three online speed-dependent tests to diagnose rotor asymmetries and eccentricities in an IM: Demodulation Test (DT), Rotor Evaluation Test (RET), and Eccentricity Test (ET). The first is used to estimate the speed, while the others are used to identify, respectively, rotor electrical asymmetries (such as bars breakage) and rotor-stator misalignments.

During the DT, the rotor speed information is extracted from two slip dependent harmonics related to bars breakage and mixed eccentricity [89]. In the spectrum of the demodulated current, they appear respectively, at $f^{Demod}_{BBH} = 2sf_0$ Hz and $f^{Demod}_{MEH} = f_0\,(1-s)\,/\,p$ Hz. In order to extract their frequencies, a track and find algorithm is performed. Finally, slips and speeds are calculated using the above formulas. The bases of the track and find algorithm are:

A preliminary speed estimation is carried out using nameplate data and current level. Then, with this estimation, f^{Demod}_{BBH} and f^{Demod}_{MEH} are calculated in order to set around each one a frequency band of ± 0.3 and ± 0.12 Hz, respectively (the rationale for using these fixed limits and not others is not disclosed by the company). Finally, the highest peak within each frequency band is identified. If one peak is below the noise level or speeds do not match, MCEMAX asks the user to estimate speed manually. If both peaks are above noise level and both speeds match, the MCEMAX considers this speed as valid.

Once the speed is estimated, either by the DT or the preliminary estimation, the MCEMAX can assess motor condition via MCSA. Using the RET, it tries to find the LSH in the line current spectrum to assess rotor health. Once this harmonic is identified, if its amplitude exceeds the limit bands set by the manufacturer (first alarm band from -48 dB to -42 dB, second from -42 dB to -36 dB), the device warns the user about a possible damage to rotor bars. Finally, through the ET, the MCEMAX tries to track and find the SEH. In particular, it focuses on the amplitude of those associated with $\nu = \pm 1$ and $\nu = \pm 3$ in (2.2). In this case, the criterion used is to consider that an eccentricity problem exists if their amplitudes are 20 dB above the noise level.

Implications of Nameplate-Based Approximations

In nameplate-based methods, speed is estimated through linearization of the current-speed curve using two sets of points: $[I_N, n_N] - [I_0, n_{sync}]$. As the no-load current cannot be neglected in IM ($0.9I_N > I_0 > 0.20I_N$), it has to be estimated, thus being the first source of error. Moreover, for motors with rated power >1 kW, a maximum tolerance of $\pm 20\%$ is allowed on the

nameplate rated slip [90], [91]. If this is added to the effects of degradation due to use, we have that the rated operation point can be quite far from the one stated on the nameplate. Therefore, making a speed estimation from nameplate values may lead to set frequency bands not containing the harmonics sought, which for the MCEMAX are: the Broken Bars Harmonic (BBH) and the MEH. To study this problem in the 79 industrial motors, the MCEMAX algorithm has been replicated.

Preliminary slip estimation is carried out using the following formula:

$$s_{pre} = \frac{I_L}{I_N} \cdot s_N \cdot k_{exp} \tag{2.8}$$

where I_L and I_N are, respectively, the operating and rated current, s_N the rated slip and k_{exp} an experimental factor that allows to obtain very similar results to those of the MCEMAX. Then, using this slip, f_{BBH}^{Demod} and f_{MEH}^{Demod} are calculated according to Section 2.5.2. Finally, a frequency band of ± 0.3 Hz for the BBH and ± 0.12 Hz for the MEH is set, just as MCEMAX does.

Using this algorithm, the actual frequency of the BBH remained outside the search window in 36.71 % of the cases, while the actual frequency of the MEH did so in 32.91% of the cases. Figure 2.7 shows one of the cases where the BBH remained outside the search band in a four-pole 37 kW IM, with 0.02 rated slip and operating at 87% of the rated current, while Fig. 2.7 shows one of the cases where the MEH is the one that remained outside the search band in a two-pole 45 kW IM, with 0.01 rated slip and operating at 75% of the rated current. Therefore, for the motors analyzed, the device would ask the user for a manual estimation in a considerable number of times, thereby losing its automatic characteristic and leaving the speed estimation quality up to the user's ability. Finally, if the user tries to visually identify the MEH and BBH, they might not appear as prominent peaks like the ones depicted in Fig. 2.7, and besides, a prominent peak in that area might be caused by another harmonic (as discussed below).

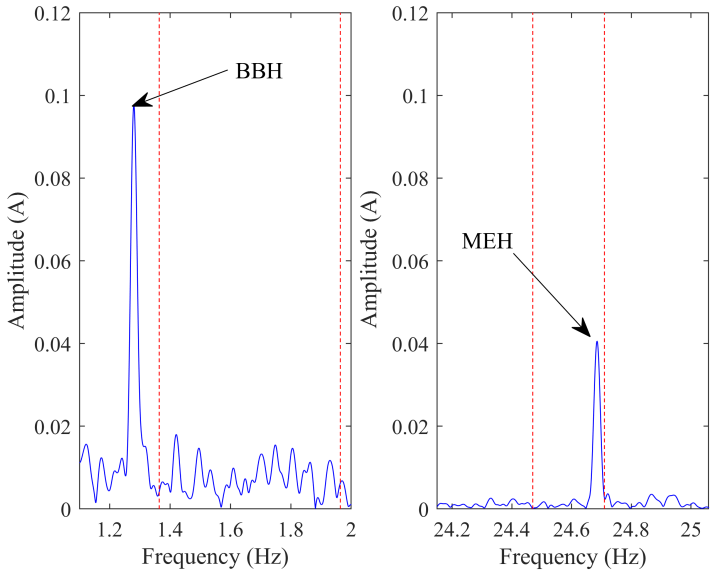

(a)

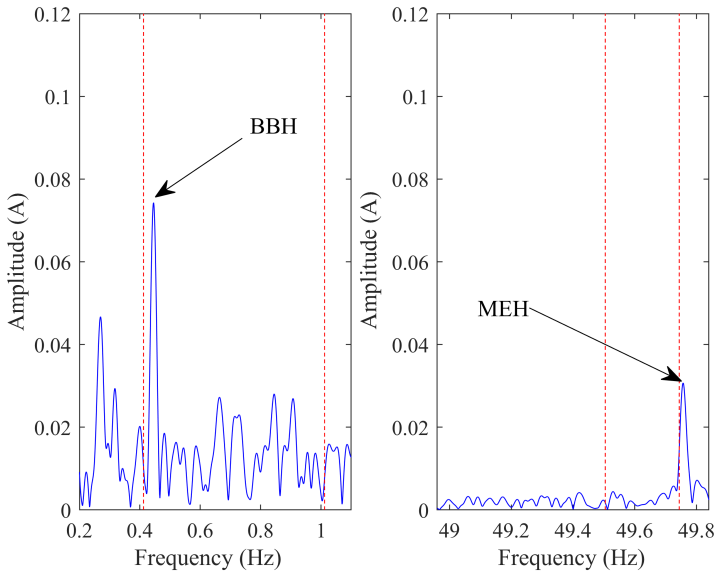

(b)

FIGURE 2.7: Spectrum of the demodulated current of: (a) a four-pole 37 kW IM and (b) a two-pole 45 kW IM, with the search windows established by the MCEMAX for the broken bars harmonic (left) and mixed-eccentricity harmonic (right).

Broken Bars Harmonic: Detectability Problems

The amplitude of the BBH that appears in the spectrum of the demodulated current (used by MCEMAX, together with MEH, to estimate the speed) is related to the amplitude of the harmonics predicted by Equation (2.1) (with $k = 1$) in the line current spectrum (sideband harmonics). However, this relationship is complex, as it depends on both the constructional parameters of the machine and the characteristics of the load [92].

In motors that operate with relative high slips, it should be possible to see (if exist) the sideband harmonics in the line current spectrum with a high enough capture time (10 to 40 s). Yet, in motors that operate with very low slip indexes, it may become impossible to detect these harmonics for the same capture time, since they can be masked by the spectral leakage of the fundamental component. Therefore, it is precisely in these cases where the spectrum of the demodulated current offers a great advantage in comparison to the line current spectrum thanks to the removal of this component [93]. In this regard, Fig. 2.8a shows the line current spectrum of a two-pole 90 kW IM operating at 34% of its rated slip, where the sideband harmonics are masked by the spectral leakage of the fundamental component, while Fig. 2.8b shows the spectrum of the demodulated current where the BBH is clearly visible.

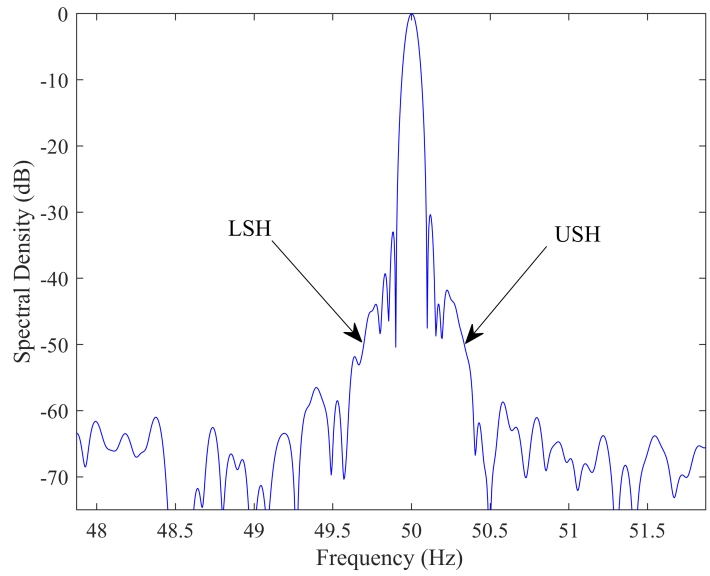

(a)

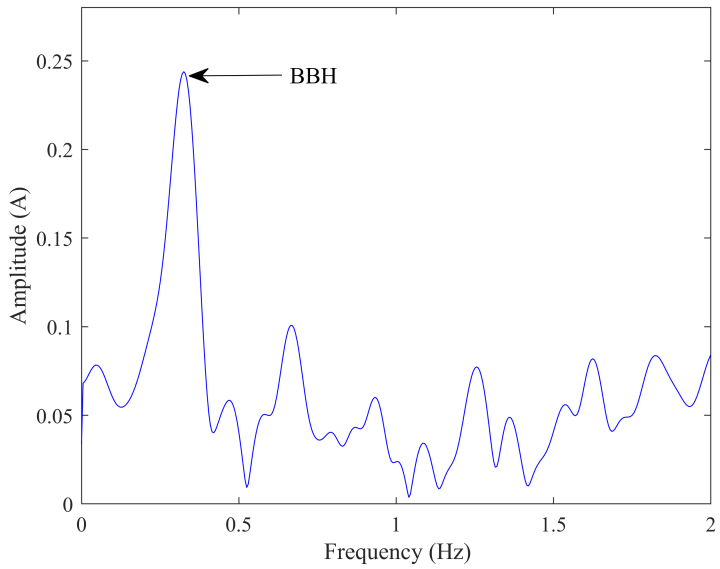

(b)

FIGURE 2.8: Broken bars harmonics in the spectrum of a two-pole 90 kW induction motor operating at 33.6% of its rated slip: (a) stator current and (b) demodulated stator current.

Despite the advantage of removing the fundamental component, the detectability of the BBH in the spectrum of the demodulated current can still be problematic, for instance, due to the presence of other nearby harmonics related to load variations or because its amplitude is below the noise floor. In this regard, the effectiveness of estimating speed through this harmonic was tested by analyzing the spectrum of the demodulated current of the 79 industrial motors using two methods. Both of them computed the FFT of the demodulated current, which was calculated as the absolute value of the analytic signal $\vec{i}_h(t) = i(t) + j \cdot H\left(i(t)\right)$, where $i(t)$ is the stator current and H the Hilbert transform. Method 1 employed a track and find algorithm consisting of detecting the maximum peak in a frequency band that was calculated as described in the previous subsection, while Method 2 used the same technique but establishing the frequency band around the exact frequency of the harmonic. The aim of Method 2 was to check if, under the most favorable conditions (perfect preliminary speed estimation), there were still problems in detecting the broken bars harmonic.

Table 2.4 shows the number of motors (as a percentage of the total analyzed) whose errors with respect to the actual speed were greater than 0.5, 1.5, 2.5, 3.5 and 4.5 rpm. As can be seen, Method 1 (the one similar to MCEMAX) presented more detectability problems than Method 2. These problems were mostly due to the nameplate-based approximations, as discussed previously. Yet, in the most favorable case (Method 2), where the frequency band covered the broken bars harmonic position, there was also a considerable amount of motors (18.99%) with a speed error greater than 0.5 rpm. In this regard, Fig. 2.9 shows examples of real industrial measures, along with the search bands and absolute speed error, where both Method 1 and 2 failed to provide a correct speed estimation, either for the presence of a higher harmonic in the search band (Figs. 2.9a and 2.9b) or an insufficient amplitude of the BBH (Figs. 2.9c and 2.9d).

TABLE 2.4: Number of motors, as a percentage of the total analyzed, whose errors with respect to the actual speed are greater than 0.5, 1.5, 2.5, 3.5 and 4.5 rpm, when BBH is used to estimate speed.

	>0.5 rpm	**>1.5 rpm**	**>2.5 rpm**	**>3.5 rpm**	**>4.5 rpm**
Method 1	45.57%	43.04%	37.97%	35.44%	27.85%
Method 2	18.99%	12.66%	7.59%	6.33%	2.53%

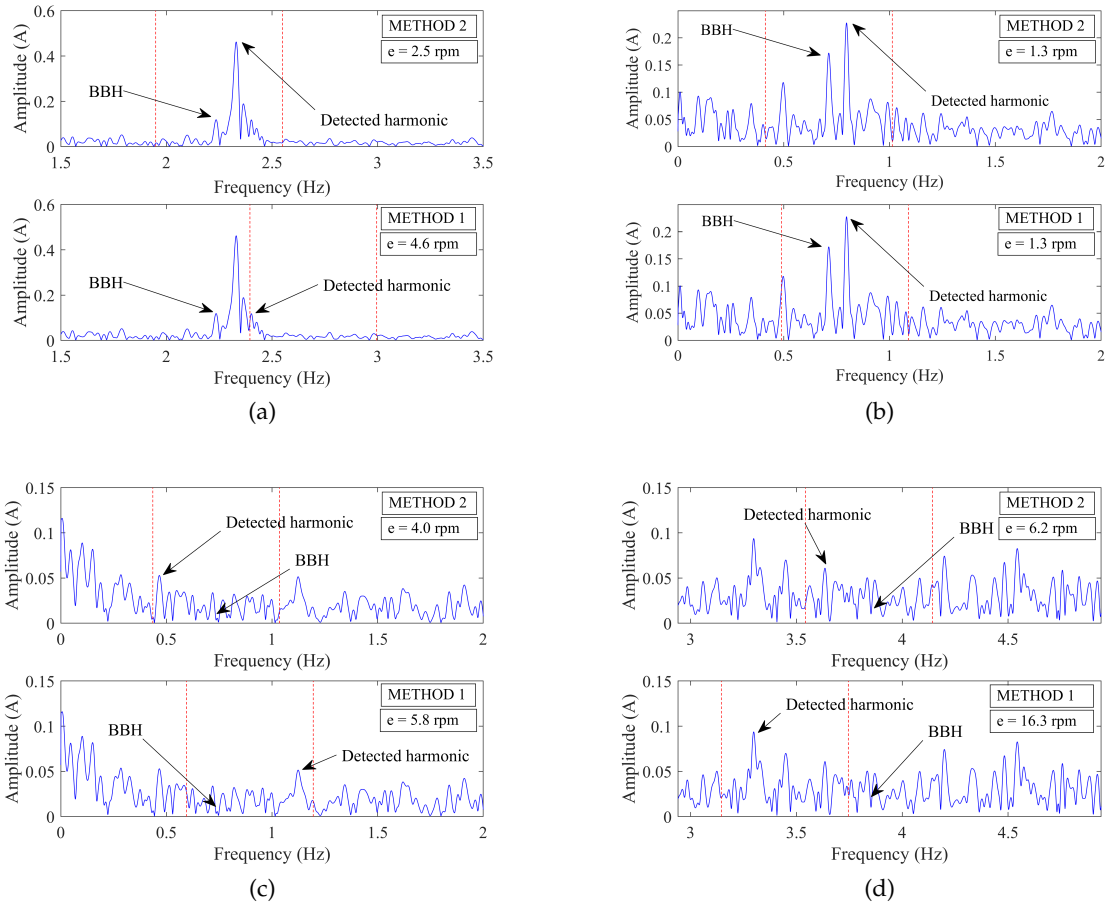

FIGURE 2.9: Examples where Method 1 and 2 failed to provide a correct speed estimation in the spectrum of the demodulated current of a: (a) two-pole 248 kW IM at 67.7% of its rated slip, (b) four-pole 90 kW IM at 60.5% of its rated slip, (c) four-pole 55 kW at 61.2% of its rated slip, and (d) a two-pole 139 kW IM at 96.1% of its rated slip.

Mixed Eccentricity Harmonic: Detectability and Accuracy Problems

MCEMAX uses both the BBH and the MEH in the demodulated current spectrum to estimate the speed (Section 2.5.2). As with the BBH, the MEH of the demodulated current spectrum is related to the analogous harmonics in the line current given by Equation (2.3) with $k = 1$. Unlike what happens with the BBH, the spectrum of the demodulated current does not provide such a relevant advantage at low slips. That is because, in the normal spectrum, the MEH is sufficiently separated from the fundamental component so as not to be masked by its spectral leakage. Thus, the removal of this component does not make a big difference in MEH detection. Yet, it seems logical that the MCEMAX algorithm uses the same spectrum for both MEH and BBH in order to save computational effort.

Since the fundamental component does not influence MEH detectability, the problems may be due to: a search window not covering the actual MEH frequency, the presence of other nearby harmonic with higher amplitude or an MEH amplitude below the noise level. The first problem has already been addressed in Section 2.5.2. As for the second, it was found in Section 2.5.1 that the most problematic harmonics that can cause a misidentification are the ones

placed at $f_0(1 \pm 1/p)$ Hz in the line current spectrum, particularly, in two-pole machines. In the spectrum of the demodulated current, these harmonics are shifted to f_0/p, thereby being also close to $f_{MEH}^{Demod} = f_0(1-s)/p$ Hz. However, unlike the EXP4000 algorithm, the MCEMAX uses a frequency band of ± 0.12 Hz centered in a preliminary frequency estimation, instead of a search band covering the range from zero to the expected full-load slip. Then, it is less likely that the band will cover the harmonic at f_0/p. In fact, using the replicated algorithm, it was found that the search band covered this SIH in only 8.86% of the cases and that all belonged to four- and six-pole machines, where the SIH has a very low amplitude. Therefore, detectability problems will be mostly related to an insufficient amplitude of MEH and/or the presence of load oscillations/imbalances harmonics.

Table 2.5 shows the number of motors (as a percentage of the total analyzed) whose errors with respect to the actual speed were greater than 0.5, 1.5, 2.5, 3.5 and 4.5 rpm. As can be seen, the number of wrong speed estimations increased when compared to BBH (Table 2.4).

TABLE 2.5: Number of motors, as a percentage of the total analyzed, whose errors with respect to the actual speed are greater than 0.5, 1.5, 2.5, 3.5 and 4.5 rpm, when MEH is used to estimate speed.

	>0.5 rpm	**>1.5 rpm**	**>2.5 rpm**	**>3.5 rpm**	**>4.5 rpm**
Method 1	50.63%	44.30%	41.77%	40.51%	39.24%
Method 2	29.11%	25.32%	24.05%	22.78%	17.72%

The increase was due to both a higher number of motors with an insufficient amplitude of MEH and the fact that this harmonic had a narrower bandwidth. Following a similar reasoning as in Section 2.5.1, the speed errors as a function of the errors committed in estimating MEH or BBH frequencies in the spectrum of the demodulated current were:

$$\begin{cases} \Delta n = \left[\frac{60}{p}\right] \Delta f_0 - \left[\frac{30}{p}\right] \Delta f_{BBH}^{Demod} \\ \Delta n = [0]\,\Delta f_0 - [60]\,\Delta f_{MEH}^{Demod} \end{cases} \tag{2.9}$$

Unlike what happens with MEH, the speed estimation through BBH was not independent of f_0 error. Yet, as the fundamental frequency tended to be very stable and it was easy to detect, the error committed in estimating it is normally very low when compared to the ones committed with the BBH and the MEH. Therefore, neglecting Δf_0, assuming the same frequency error and for a six-pole machine, the error committed in speed could be six times larger when using the MEH, thereby leading to a mismatch in speed estimations, and therefore, to user intervention, even when both peaks were detected.

Diagnosing with Static Eccentricity Harmonics

Regarding motor eccentricity, the problem relies on using SEH to diagnose (frequencies given by (2.2) making $n_d = 0$). These harmonics depend on the number of rotor bars (R). Therefore, three scenarios are possible. If R and speed are known, which is not usual, MCEMAX automatically locates the SEH and performs the diagnosis as explained in Section 2.5.2. If R is known but not speed, MCEMAX asks the user to manually choose the highest peak in the spectrum to the left of $(R/p - 1)\, f_0$ Hz as the SEH(-1). Then, MCEMAX automatically locates the rest of SEH and estimates the speed from this set. Finally, if R is not known, the MCEMAX has a feature to estimate this parameter as long as the speed has been previously estimated either by DT or other means. This feature consists of a manual assistant where the user has to choose

a candidate to be the SEH(-1). Next, alleged peaks SEH(+1) and SEH(± 3) are automatically detected. Then, the user has to check if the amplitudes and layout of the set is similar to the typical adopted by SEH to finally estimate the number of rotor bars.

This approach has several problems: it is not automatic, requires an advanced knowledge of SEH distribution, and it may easily lead to wrong estimations of R. To illustrate the latter, Fig. 2.10 shows the spectrum of a six-pole 132 kW IM. In it, instead of a set of ± 1 and ± 3 harmonics where the -1 is the one of highest amplitude (which is a common but not always true assumption when identifying RSH or SEH), what we have is a set of -1, +3 and +5 where +3 is the one of highest amplitude. Hence, the user could identify the +3 as the -1, and therefore, estimate the number of bars as 54 instead of the actual 42 bars. That is the reason why the manufacturer asks the owner to verify this number through the motor provider or motor workshop. Yet, as this is not always possible, the applicability of the test is reduced.

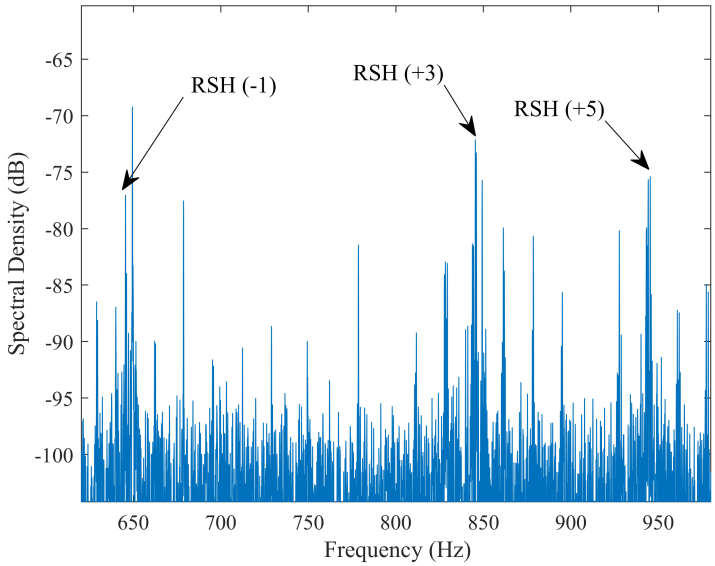

FIGURE 2.10: RSH layout in the stator current spectrum of a six-pole 132 kW IM.

2.5.3 Discussion and Lines of Improvement

Regarding MCEMAX, two main drawbacks has been identified in their SSE algorithm. The first, found in the initial stage of its SSE algorithm, is the error made in estimating the center of the band in which the MEH and BBH are sought. This error is mainly due to the no-load current and the fact of assuming as valid the nameplate rated speed (where the norm allows a tolerance in slip up to 20%). This, along with the bands used for each harmonic, causes that, for the 79 industrial motors analyzed, the BBH is outside the search window in 36.71% of the cases, while the MEH in 32.91%. The second drawback, related to detectability and accuracy, is found in the last stage of the algorithm. On the one hand, it has been proved that, even in the case of the band covering the BBH or MEH frequency, their detection can still be problematic, since they can be submerged by the noise floor or be confused with other healthy state harmonics caused, for example, by load oscillations. In particular, the speed error has been higher than 0.5 rpm in 18.99% of the cases for the BBH, and in 29.11% of the cases for the MEH. On the other hand, it has also been analyzed theoretically the disparity between the errors in speed estimation when using the BBH and the MEH of the demodulated current. The analysis has

shown that the MEH speed error can be from two times (two-pole machine) to eight times (eight-pole machine) larger than the BBH for the same resolution error, which means that, even if both peaks are detected, the MCEMAX could ask for user intervention.

The first problem can be mitigated without changing the basis of the algorithm by making the search bands of each harmonic proportional to their bandwidths. MEH and BBH bandwidth are, respectively, sf_0/p and $2sf_0$, that is, the BBH bandwidth is $2p$ times bigger than the MEH one. Then, if we assumed a fixed search band for the MEH of ± 0.12 Hz, the BBH window should have an amplitude of $\pm 0.12 \cdot p$ Hz. Applying this change to the replicated MCEMAX algorithm, the percentage of cases where the BBH remains outside the search window is reduced from 36.71% to 32.91%, therefore, being equal to that of the MEH.

As for the EXP4000, two main drawbacks has also been identified. The first is related to LMEH detectability in the search band covering from zero to the full-load expected slip. It has been shown in Section 2.5.1 that there is a high-amplitude SIH in two-pole machine placed at 0 Hz (line current) or f_0 Hz (current vector, instantaneous power...) that reduces LMEH detection. Two possible solutions can be applied to avoid this harmonic: to displace the band or to filter the SIH. The first solution requires a good enough frequency resolution so as not to lose too much detectability range. For example, a two-pole high-power IM, where rated slip can be as low as 0.5%, fed at 40 Hz gives us a MEH frequency bandwidth of 0.2 Hz. This means that a search band displacement of only 0.1 Hz (the frequency resolution of a 10 s record) would translate into losing 50% of the detectability range. The second solution, requires the filter to be as sharp as possible for the same reasons, thereby complicating the algorithm. Yet, even in the case of this SIH being filtered or not included in the search band, there might still be detection problems caused by an insufficient amplitude of the LMEH or the presence of nearby harmonics as in the case of MCEMAX. The second drawback is related to LMEH accuracy. As discussed in Section 2.5.1, small errors in estimating LMEH lead to large errors in LSH frequency, and therefore, to the possibility of issuing wrong diagnosis.

As discussed along the section, both devices suffer from detectability and accuracy issues due to the harmonics they use. This might be improved if RSH were used instead, since they appear at higher frequencies (far from other high-amplitude harmonics) and since they have a wider bandwidth (better accuracy). In this regard, three RSH-based algorithms has been tested with the data of the 79 industrial motors so as to compare their performance with the MCEMAX and EXP4000 alike algorithms. These algorithms are:

1- RSH-based algorithm using a search band covering from $s = 0$ to $s = s_N$.

2- RSH-based algorithm equal to 1 but displacing the band 0.5 Hz so as not to cover the harmonic at $(n \cdot f_0)$.

3- RSH-based algorithm using a search band centered in a preliminary frequency estimation using nameplate data. The band amplitude is proportional to that of the MCEMAX for the MEH (± 0.12 Hz).

4- The replicated MCEMAX algorithm. A speed match is considered if the difference between BBH and MEH speeds are less than 0.5 rpm.

5- LMEH-based algorithm using a search band covering from $s = 0$ to $s = s_N$. Speed is obtained as the weighted average of the ones extracted from the spectrum of the line current and the absolute value of the current vector (similar to EXP4000).

Table 2.6 summarizes the results of this analysis. As can be seen, the RSH-based algorithms (Alg. 1, Alg. 2 and Alg.3), where the number of rotor bars is already known, outperforms the MCEMAX-like (Alg. 4) and EXP4000-like (Alg. 5). Despite the clear advantage of using RSH algorithms for SSE, the current lack of a method to obtain the number of rotor bars in an automatic, online, and reliable way prevents its use in industrial devices such as MCEMAX or EXP4000.

TABLE 2.6: Number of motors, as a percentage of the total analyzed, whose errors with respect to the actual speed are greater than 0.5 rpm for 5 different algorithms.

	Alg. 1	**Alg. 2**	**Alg. 3**	**Alg. 4**	**Alg. 5**
Error > 0.5 rpm	21.52%	5.06%	36.71%	65.82%	51.90%

Finally, it is fair to mention that, despite the weaknesses highlighted in this section, MCEMAX and EXP4000 are still powerful and user-friendly tools that can be useful in certain conditions to assess rotor bars or eccentricity, as demonstrated by their wide use in industry.

2.6 Conclusions

In the field of induction motor diagnosis via MCSA, even if some papers have mentioned the necessity of accurate SSE, this is the first to highlight and analyze its importance, especially for the modern industry. The analysis presented in this paper is meant to achieve a large consensus on how important it is to have accurate speed information in order to reduce both false positives and negatives. Moreover, to date, there is no research that has gone into an in-depth assessment of the problems and challenges behind obtaining a method to achieve an accurate and automatic speed estimation that is valid for any motor. This is a key step towards Industry 4.0. In this regard, the paper fills this gap for the first time by investigating the major families of SSE techniques, which were mainly conceived for sensorless control, from the perspective of its application in the diagnosis of the induction motor, showing the lacks that yet remain unsolved. In addition, the investigation is enhanced with the analysis, supported by a database of measurements belonging to 79 different induction motors, of the SSE algorithms of the two leading commercial devices highlighting their weaknesses and lines of improvements. From those analyses, it is concluded that:

- FMB methods are apparently not the most suitable for portable devices, since they are invasive due to the need of voltage sensing and a first stage of parameter identification. However, they can be a good option for a continuous monitoring system, since, if implemented in the driver, the set formed by the MCSA diagnostic procedure and FMB method could use the same voltages and current measurements than the control system, as well as take advantage of the natural stops for the parameter identification. Nevertheless, further research is still necessary in order to study whether the accuracy provided by a method like this is enough for its use in high-reliability diagnostic procedures via MCSA.

- SIB methods introduce excessive complexity either for a portable device or for a continuous monitoring system. The complexity is only compensated by their performance at low or zero speed, which is not the range where MCSA is used. Thus, it can be discarded as a promising candidate for SSE in online diagnosis via MCSA.

- SaEHB are the best option for continuous or occasional monitoring due to its compatibility with MCSA in terms of accuracy, robustness, ease of implementation and independence to parameter variations. Among them, MEH-based methods are preferred in industry since they only depend on the number of pole pairs, which is a parameter available on the nameplate. As a counterpart, they provide low accuracy due to the narrow bandwidth of these harmonics. Conversely, RSH-based methods are preferred in academy since they provide higher accuracy, being the drawback in this case its reduced applicability due to the need of knowing the number of rotor slots, which is a parameter rarely known by motor owners.
- Current SaEHB techniques used in commercial devices do not provide reliability in a considerable amount of cases. On the one hand, EXP4000 has the main problem of using MEH, which do not provide enough accuracy due to its narrow bandwidth and the difficulty of being detected, particularly in two-pole machines. On the other hand, MCEMAX uses the BBH and MEH of the demodulated current. In this case, the major drawback is that to locate these harmonics, it uses an algorithm that depends on a preliminary speed estimation whose accuracy is subjected to the magnitude of the no-load current and the consistency between nameplate data and actual values. Nevertheless, detection difficulties also arise in these two harmonics, and besides, their different speed estimation errors may generate inconsistencies, leading the device to ask for a human check.

Thus, commercial diagnostic systems still need a reliable SSE algorithm. According to scientific literature, RSH-based methods are the ones that can provide the highest accuracy and reliability due to its wider bandwidth and ease of detection. Nevertheless, they lack of a general and non-invasive method to automatically determine the number of rotor slots (R) and the order of the time harmonic associated to each RSH (ν). This prevents them from being efficiently integrated into Industry 4.0 smart diagnostic systems. Therefore, the authors conclude that, despite SSE techniques have been investigated for a long time in the field of controlled AC drives, the scientific community has yet to provide a precise, automatic and general method that helps to achieve a highly reliable MCSA-based online condition monitoring system for the modern industry.

Appendix A. Industrial Motors Data

This database is the result of several years of consulting work with different types of industry. As a consequence, there are signals of motors driving vertical/horizontal pumps, conveyors, compressors, worm gears, shredders, etc. This fact, together with the wide range of powers and slips, makes the database a robust statistical sample to evaluate the bases of the algorithms described in this paper.

TABLE 2.7: Industrial motors data.

2-poles				4-poles				6-poles			
$P_N(kW)$	s_N	$s/s_N(\%)$	*Fig.*	$P_N(kW)$	s_N	$s/s_N(\%)$	*Fig.*	$P_N(kW)$	s_N	$s/s_N(\%)$	*Fig.*
1.50	0.047	32.27%		0.75	0.070	3.23%		132.00	0.011	52.45%	2.10
30.00	0.017	71.34%		0.75	0.070	9.39%		132.00	0.011	49.51%	
30.00	0.017	69.81%		0.80	0.040	74.05%		132.00	0.011	52.95%	
30.00	0.033	141.56%		0.80	0.040	96.82%		200.00	0.010	47.23%	
45.00	0.010	43.23%	2.3, 2.7b	1.10	0.057	100.44%		250.00	0.030	16.41%	
55.00	0.013	62.78%		1.10	0.057	10.21%		250.00	0.010	39.05%	
63.00	0.033	50.22%		2.20	0.053	79.05%		253.00	0.010	65.79%	
90.00	0.010	33.63%	2.1, 2.8	2.98	0.070	24.83%		253.00	0.010	93.75%	
90.00	0.033	66.56%		37.00	0.020	53.90%	2.7a	253.00	0.010	65.96%	
110.00	0.007	56.17%		37.00	0.020	44.62%		253.00	0.010	59.46%	
112.00	0.033	75.18%		45.00	0.014	36.01%		375.00	0.014	65.72%	
112.00	0.033	69.43%		55.00	0.012	61.22%	2.9c	375.00	0.014	37.98%	
112.00	0.033	88.00%		75.00	0.010	62.68%		375.00	0.014	33.60%	
112.00	0.033	98.72%		90.00	0.013	24.93%		800.00	0.017	48.82%	2.6
112.00	0.033	81.50%		90.00	0.015	60.51%	2.9b				
117.00	0.033	69.97%		110.00	0.013	30.25%					
132.00	0.007	76.98%		110.00	0.008	73.78%					
132.00	0.007	99.54%		110.00	0.008	83.85%					
134.00	0.033	62.57%		110.00	0.008	72.16%					
134.00	0.033	81.81%		110.00	0.008	100.47%					
139.00	0.040	96.08%	2.9d	160.00	0.013	36.90%					
150.00	0.033	79.94%		160.00	0.007	84.36%					
171.00	0.017	90.23%		160.00	0.007	91.88%					
223.00	0.033	74.69%		160.00	0.007	61.25%					
230.00	0.040	86.26%		160.00	0.007	68.10%					
231.00	0.033	68.59%		160.00	0.007	39.65%					
232.00	0.033	74.96%		300.00	0.010	58.53%					
234.00	0.033	88.36%		580.00	0.008	71.90%					
239.00	0.028	81.77%		1500.00	0.007	58.57%	2.5				
248.00	0.033	67.73%	2.9a								
248.00	0.033	61.55%									
248.00	0.033	65.63%									
270.00	0.033	96.27%									
270.00	0.033	61.85%									
372.00	0.033	44.23%									
2200.00	0.012	36.01%									

Appendix B. DAQ System

The measurements of the 79 industrial motors were performed with the following DAQ system:

- High-resolution oscilloscopes:
  - PicoScope 4262:
    - Channels: 2.
    - Vertical resolution: 16-bit.
    - Sampling frequency: 10 MS/s.
  - PicoScope 4824:
    - Channels: 8.
    - Vertical resolution: 12-bit.
    - Sampling frequency: 80 MS/s.
- High-precision current probes:
  - TA189:
    - Measuring range: 30 A.
    - Accuracy: 1% of reading $\pm$2 mA.
    - Frequency range: DC to 100 kHz.
  - TA167:
    - Measuring range: 200/2000 A.
    - Accuracy (0–200/1500 A): 1% of reading $\pm$100/$\pm$ 500 mA.
    - Accuracy (1500–2000 A): $\pm$5 % of reading.
    - Frequency range: DC to 20 kHz.

Regarding the characteristics of the signals, they were always recorded with a minimum capture time of 100 s, at 10 kHz and adjusted scale. Finally, for the analyses performed on the 79 induction motors in this paper, the signal duration was shorten to 81.9 s, as this is the maximum recording time allowed by MCEMAX.

Bibliography

[1] M. Korzonek, G. Tarchala, and T. Orlowska-Kowalska, "A review on mras-type speed estimators for reliable and efficient induction motor drives," *ISA Transactions*, vol. 93, pp. 1 – 13, 2019, doi: 10.1016/j.isatra.2019.03.022

[2] M. El Hachemi Benbouzid, "A review of induction motors signature analysis as a medium for faults detection," *IEEE Transactions on Industrial Electronics*, vol. 47, no. 5, pp. 984–993, 2000, doi: 10.1109/41.873206

[3] M. Benbouzid and G. Kliman, "What stator current processing-based technique to use for induction motor rotor faults diagnosis?" *IEEE Transactions on Energy Conversion*, vol. 18, no. 2, pp. 238–244, 2003, doi: 10.1109/TEC.2003.811741

[4] J. Jung, J. Lee, and B. Kwon, "Online diagnosis of induction motors using mcsa," *IEEE Transactions on Industrial Electronics*, vol. 53, no. 6, pp. 1842–1852, 2006, doi: 10.1109/TIE.2006.885131

[5] Y. Merizalde, L. Hernández-Callejo, and O. Duque-Perez, "State of the art and trends in the monitoring, detection and diagnosis of failures in electric induction motors," *Energies*, vol. 10, no. 7, 2017, doi: 10.3390/en10071056

[6] V. Fernandez-Cavero, J. Pons-Llinares, O. Duque-Perez, and D. Morinigo-Sotelo, "Detection and quantification of bar breakage harmonics evolutions in inverter-fed motors through the dragon transform," *ISA Transactions*, 2020, doi: 10.1016/j.isatra.2020.10.020

[7] S. B. Lee, D. Hyun, T. Kang, C. Yang, S. Shin, H. Kim, S. Park, T. Kong, and H. Kim, "Identification of false rotor fault indications produced by on-line mcsa for medium voltage induction machines," in *2015 61st IEEE Pulp and Paper Industry Conference (PPIC)*, 2015, pp. 1–9, doi: 10.1109/PPIC.2015.7165709

[8] P. Gangsar and R. Tiwari, "Signal based condition monitoring techniques for fault detection and diagnosis of induction motors: A state-of-the-art review," *Mechanical Systems and Signal Processing*, 2020, doi: 10.1016/j.ymssp.2020.106908

[9] Seong-Hwan Kim, Tae-Sik Park, Ji-Yoon Yoo, and Gwi-Tae Park, "Speed-sensorless vector control of an induction motor using neural network speed estimation," *IEEE Transactions on Industrial Electronics*, vol. 48, no. 3, pp. 609–614, 2001, doi: 10.1109/41.925588

[10] S. Maiti, V. Verma, C. Chakraborty, and Y. Hori, "An adaptive speed sensorless induction motor drive with artificial neural network for stability enhancement," *IEEE Transactions on Industrial Informatics*, vol. 8, no. 4, pp. 757–766, 2012, doi: 10.1109/TII.2012.2210229

[11] J. M. Gutierrez-Villalobos, J. Rodriguez-Resendiz, E. A. Rivas-Araiza, and M. A. Martínez-Hernández, "Sensorless foc performance improved with on-line speed and rotor resistance estimator based on an artificial neural network for an induction motor drive," *Sensors*, vol. 15, no. 7, pp. 15 311–15 325, 2015, doi: 10.3390/s150715311

[12] S. V. B. S. Reddy, B. Kumar, and D. Swaroop, "Investigations on training algorithms for neural networks based flux estimator used in speed estimation of induction motor," in *2019 6th International Conference on Signal Processing and Integrated Networks (SPIN)*, 2019, pp. 1090–1094, doi: 10.1109/SPIN.2019.8711623

[13] Y. Luo and C. Lin, "Fuzzy mras based speed estimation for sensorless stator field oriented controlled induction motor drive," in *2010 International Symposium on Computer, Communication, Control and Automation (3CA)*, vol. 2, 2010, pp. 152–155, doi: 10.1109/3CA.2010.5533625

[14] S.-Y. Wang, C.-L. Tseng, S.-C. Lin, C.-J. Chiu, and J.-H. Chou, "An adaptive supervisory sliding fuzzy cerebellar model articulation controller for sensorless vector-controlled induction motor drive systems," *Sensors*, vol. 15, no. 4, pp. 7323–7348, 2015, doi: 10.3390/s150407323

[15] S. Mohan Krishna and J. Febin Daya, "Mras speed estimator with fuzzy and pi stator resistance adaptation for sensorless induction motor drives using rt-lab," *Perspectives in Science*, vol. 8, pp. 121 – 126, 2016, doi: 10.1016/j.pisc.2016.04.013

[16] Li Cai, Yinhai Zhang, Zhongchao Zhang, Chenyang Liu, and Zhengyu Lu, "Application of genetic algorithms in ekf for speed estimation of an induction motor," in *IEEE 34th Annual*

Conference on Power Electronics Specialist, 2003. PESC '03., vol. 1, 2003, pp. 345–349 vol.1, doi: 10.1109/PESC.2003.1218317

[17] I. M. Alsofyani, N. R. N. Idris, M. Jannati, S. A. Anbaran, and Y. A. Alamri, "Using nsga ii multiobjective genetic algorithm for ekf-based estimation of speed and electrical torque in ac induction machines," in *2014 IEEE 8th International Power Engineering and Optimization Conference (PEOCO2014)*, 2014, pp. 396–401, doi: 10.1109/PEOCO.2014.6814461

[18] W. T. Thomson and M. Fenger, "Current signature analysis to detect induction motor faults," *IEEE Industry Applications Magazine*, vol. 7, no. 4, pp. 26–34, 2001, doi: 10.1109/2943.930988

[19] M. Drif and A. J. M. Cardoso, "The use of the instantaneous-reactive-power signature analysis for rotor-cage-fault diagnostics in three-phase induction motors," *IEEE Transactions on Industrial Electronics*, vol. 56, no. 11, pp. 4606–4614, 2009, doi: 10.1109/TIE.2009.2027922

[20] J. Kim, S. Shin, S. B. Lee, K. N. Gyftakis, M. Drif, and A. J. M. Cardoso, "Power spectrum-based detection of induction motor rotor faults for immunity to false alarms," *IEEE Transactions on Energy Conversion*, vol. 30, no. 3, pp. 1123–1132, 2015, doi: 10.1109/TEC.2015.2423315

[21] K. Yahia, M. Sahraoui, A. J. M. Cardoso, and A. Ghoggal, "The use of a modified prony's method to detect the airgap-eccentricity occurrence in induction motors," *IEEE Transactions on Industry Applications*, vol. 52, no. 5, pp. 3869–3877, 2016, doi: 10.1109/TIA.2016.2582146

[22] R. Schoen, B. Lin, T. Habetler, J. Schlag, and S. Farag, "An unsupervised, on-line system for induction motor fault detection using stator current monitoring," *IEEE Transactions on Industry Applications*, vol. 31, no. 6, pp. 1280–1286, 1995, doi: 10.1109/28.475698

[23] J. Cusidó, L. Romeral, J. A. Ortega, A. Garcia, and J. Riba, "Signal injection as a fault detection technique," *Sensors*, vol. 11, no. 3, pp. 3356–3380, 2011, doi: 10.3390/s110303356

[24] C.-C. Kuo, C.-H. Liu, H.-C. Chang, and K.-J. Lin, "Implementation of a motor diagnosis system for rotor failure using genetic algorithm and fuzzy classification," *Applied Sciences*, vol. 7, no. 1, 2017, doi: 10.3390/app7010031

[25] O. Duque-Perez, C. Del Pozo-Gallego, D. Morinigo-Sotelo, and W. Fontes Godoy, "Condition monitoring of bearing faults using the stator current and shrinkage methods," *Energies*, vol. 12, no. 17, 2019, doi: 10.3390/en12173392

[26] J. Tang, Y. Yang, J. Chen, R. Qiu, and Z. Liu, "Characteristics analysis and measurement of inverter-fed induction motors for stator and rotor fault detection," *Energies*, vol. 13, no. 1, 2020, doi: 10.3390/en13010101

[27] D. A. Elvira-Ortiz, D. Morinigo-Sotelo, A. L. Zorita-Lamadrid, R. A. Osornio-Rios, and R. d. J. Romero-Troncoso, "Fundamental frequency suppression for the detection of broken bar in induction motors at low slip and frequency," *Applied Sciences*, vol. 10, no. 12, 2020, doi: 10.3390/app10124160

[28] W. Fontes Godoy, D. Morinigo-Sotelo, O. Duque-Perez, I. Nunes da Silva, A. Goedtel, and R. H. C. Palácios, "Estimation of bearing fault severity in line-connected and inverter-fed three-phase induction motors," *Energies*, vol. 13, no. 13, 2020, doi: 10.3390/en13133481

[29] A. Duda and P. Drozdowski, "Induction motor fault diagnosis based on zero-sequence current analysis," *Energies*, vol. 13, no. 24, 2020, doi: 10.3390/en13246528

[30] J. Petryna, A. Duda, and M. Sułowicz, "Eccentricity in induction machines—a useful tool for assessing its level," *Energies*, vol. 14, no. 7, 2021, doi: 10.3390/en14071976

[31] S. H. Kia, H. Henao, and G. Capolino, "Diagnosis of broken-bar fault in induction machines using discrete wavelet transform without slip estimation," *IEEE Transactions on Industry Applications*, vol. 45, no. 4, pp. 1395–1404, 2009, doi: 10.1109/TIA.2009.2018975

[32] S. Zolfaghari, S. B. M. Noor, M. Rezazadeh Mehrjou, M. H. Marhaban, and N. Mariun, "Broken rotor bar fault detection and classification using wavelet packet signature analysis based on fourier transform and multi-layer perceptron neural network," *Applied Sciences*, vol. 8, no. 1, 2018, doi: 10.3390/app8010025

[33] R. Nishat Toma and J.-M. Kim, "Bearing fault classification of induction motors using discrete wavelet transform and ensemble machine learning algorithms," *Applied Sciences*, vol. 10, no. 15, 2020, doi: 10.3390/app10155251

[34] C. Qiu, X. Wu, C. Xu, X. Qiu, and Z. Xue, "An approximate estimation approach of fault size for spalled ball bearing in induction motor by tracking multiple vibration frequencies in current," *Sensors*, vol. 20, no. 6, 2020, doi: 10.3390/s20061631

[35] J. Chen, N. Hu, L. Zhang, L. Chen, B. Wang, and Y. Zhou, "A method for broken rotor bars diagnosis based on sum-of-squares of current signals," *Applied Sciences*, vol. 10, no. 17, 2020, doi: 10.3390/app10175980

[36] F. Zidat, J.-P. Lecointe, F. Morganti, J.-F. Brudny, T. Jacq, and F. Streiff, "Non invasive sensors for monitoring the efficiency of ac electrical rotating machines," *Sensors*, vol. 10, no. 8, pp. 7874–7895, 2010, doi: 10.3390/s100807874

[37] S. Tamai, H. Sugimoto, and P. Yano, "Speed sensorless vector control of induction motor applied model reference adaptive system," in *1985 Conference Record IEEE/MS Annual Meeting 6th*, 1985, pp. 613–620.

[38] C. Schauder, "Adaptive speed identification for vector control of induction motors without rotational transducers," *IEEE Transactions on Industry Applications*, vol. 28, no. 5, pp. 1054–1061, 1992, doi: 10.1109/28.158829

[39] Fang-Zheng Peng and T. Fukao, "Robust speed identification for speed-sensorless vector control of induction motors," *IEEE Transactions on Industry Applications*, vol. 30, no. 5, pp. 1234–1240, 1994, doi: 10.1109/28.315234

[40] S. Maiti, C. Chakraborty, and S. Sengupta, "Adaptive estimation of speed and rotor time constant for the vector controlled induction motor drive using reactive power," in *IECON 2007 - 33rd Annual Conference of the IEEE Industrial Electronics Society*, 2007, pp. 286–291, doi: 10.1109/IECON.2007.4460396

[41] M. Dybkowski and T. Orlowska-Kowalska, "Application of the stator current-based mras speed estimator in the sensorless induction motor drive," in *2008 13th International Power Electronics and Motion Control Conference*, 2008, pp. 2306–2311, doi: 10.1109/EPEPEMC.2008.4635607

[42] A. V. Ravi Teja, C. Chakraborty, S. Maiti, and Y. Hori, "A new model reference adaptive controller for four quadrant vector controlled induction motor drives," *IEEE Transactions on Industrial Electronics*, vol. 59, no. 10, pp. 3757–3767, 2012, doi: 10.1109/TIE.2011.2164769

[43] R. Kumar, S. Das, P. Syam, and A. K. Chattopadhyay, "Review on model reference adaptive system for sensorless vector control of induction motor drives," *IET Electric Power Applications*, vol. 9, no. 7, pp. 496–511, 2015, doi: 10.1049/iet-epa.2014.0220

[44] A. V. Ravi Teja, V. Verma, and C. Chakraborty, "A new formulation of reactive-power-based model reference adaptive system for sensorless induction motor drive," *IEEE Transactions on Industrial Electronics*, vol. 62, no. 11, pp. 6797–6808, 2015, doi: 10.1109/TIE.2015.2432105

[45] Y. B. Zbede, S. M. Gadoue, and D. J. Atkinson, "Model predictive mras estimator for sensorless induction motor drives," *IEEE Transactions on Industrial Electronics*, vol. 63, no. 6, pp. 3511–3521, 2016, doi: 10.1109/TIE.2016.2521721

[46] S. Das, R. Kumar, and A. Pal, "Mras-based speed estimation of induction motor drive utilizing machines' d- and q-circuit impedances," *IEEE Transactions on Industrial Electronics*, vol. 66, no. 6, pp. 4286–4295, 2019, doi: 10.1109/TIE.2018.2860530

[47] K. S. Gaeid, H. W. Ping, M. Khalid, and A. Masaoud, "Sensor and sensorless fault tolerant control for induction motors using a wavelet index," *Sensors*, vol. 12, no. 4, pp. 4031–4050, 2012, doi: 10.3390/s120404031

[48] M. S. Zaky, M. M. Khater, S. S. Shokralla, and H. A. Yasin, "Wide-speed-range estimation with online parameter identification schemes of sensorless induction motor drives," *IEEE Transactions on Industrial Electronics*, vol. 56, no. 5, pp. 1699–1707, 2009, doi: 10.1109/TIE.2008.2009519

[49] M. Jouili, Y. Agrebi, Y. Koubaa, and M. Boussak, "A luenberger state observer for simultaneous estimation of speed and stator resistance in sensorless irfoc induction motor drives," in *2015 16th International Conference on Sciences and Techniques of Automatic Control and Computer Engineering (STA)*, 2015, pp. 898–904, doi: 10.1109/STA.2015.7505225

[50] Young-Real Kim, Seung-Ki Sul, and Min-Ho Park, "Speed sensorless vector control of induction motor using extended kalman filter," *IEEE Transactions on Industry Applications*, vol. 30, no. 5, pp. 1225–1233, 1994, doi: 10.1109/28.315233

[51] K. L. Shi, T. F. Chan, Y. K. Wong, and S. L. Ho, "Speed estimation of an induction motor drive using an optimized extended kalman filter," *IEEE Transactions on Industrial Electronics*, vol. 49, no. 1, pp. 124–133, 2002, doi: 10.1109/41.982256

[52] M. Barut, S. Bogosyan, and M. Gokasan, "Speed sensorless direct torque control of ims with rotor resistance estimation," *Energy Conversion and Management*, vol. 46, no. 3, pp. 335 – 349, 2005, doi: 10.1016/j.enconman.2004.04.002

[53] B. Akin, U. Orguner, A. Ersak, and M. Ehsani, "Simple derivative-free nonlinear state observer for sensorless ac drives," *IEEE/ASME Transactions on Mechatronics*, vol. 11, no. 5, pp. 634–643, 2006, doi: 10.1109/TMECH.2006.882996

[54] R. Yildiz, M. Barut, and E. Zerdali, "A comprehensive comparison of extended and unscented kalman filters for speed-sensorless control applications of induction motors," *IEEE Transactions on Industrial Informatics*, vol. 16, no. 10, pp. 6423–6432, 2020, doi: 10.1109/TII.2020.2964876

[55] P. Rokhforoz and J. Poshtan, "Rotor speed and resistance estimation using robust extended kalman filter for sensorless vector control of induction motor drives," in *The 6th Power Electronics, Drive Systems Technologies Conference (PEDSTC2015)*, 2015, pp. 304–309, doi: 10.1109/PEDSTC.2015.7093292

[56] Z. Yin, G. Li, Y. Zhang, J. Liu, X. Sun, and Y. Zhong, "A speed and flux observer of induction motor based on extended kalman filter and markov chain," *IEEE Transactions on Power Electronics*, vol. 32, no. 9, pp. 7096–7117, 2017, doi: 10.1109/TPEL.2016.2623806

[57] E. Zerdali, "Adaptive extended kalman filter for speed-sensorless control of induction motors," *IEEE Transactions on Energy Conversion*, vol. 34, no. 2, pp. 789–800, 2019, doi: 10.1109/TEC.2018.2866383

[58] Y. Zhang, Z. Zhao, T. Lu, L. Yuan, W. Xu, and J. Zhu, "A comparative study of luenberger observer, sliding mode observer and extended kalman filter for sensorless vector control of induction motor drives," in *2009 IEEE Energy Conversion Congress and Exposition*, 2009, pp. 2466–2473, doi: 10.1109/ECCE.2009.5316508

[59] J. Holtz, "Sensorless position control of induction motors-an emerging technology," *IEEE Transactions on Industrial Electronics*, vol. 45, no. 6, pp. 840–851, 1998, doi: 10.1109/41.735327

[60] J. Holtz, "Sensorless control of induction motor drives," *Proceedings of the IEEE*, vol. 90, no. 8, pp. 1359–1394, 2002, doi: 10.1109/JPROC.2002.800726

[61] J. Holtz, "Sensorless control of induction machines—with or without signal injection?" *IEEE Transactions on Industrial Electronics*, vol. 53, no. 1, pp. 7–30, 2006, doi: 10.1109/TIE.2005.862324

[62] M. W. Degner and R. D. Lorenz, "Using multiple saliencies for the estimation of flux, position, and velocity in ac machines," *IEEE Transactions on Industry Applications*, vol. 34, no. 5, pp. 1097–1104, 1998, doi: 10.1109/28.720450

[63] Jung-Ik Ha and Seung-Ki Sul, "Sensorless field-orientation control of an induction machine by high-frequency signal injection," *IEEE Transactions on Industry Applications*, vol. 35, no. 1, pp. 45–51, 1999, doi: 10.1109/28.740844

[64] T. M. Wolbank, M. A. Vogelsberger, R. Stumberger, S. Mohagheghi, T. G. Habetler, and R. G. Harley, "Autonomous self-commissioning method for speed-sensorless-controlled induction machines," *IEEE Transactions on Industry Applications*, vol. 46, no. 3, pp. 946–954, 2010, doi: 10.1109/TIA.2010.2046288

[65] M. Ishida and K. Iwata, "A new slip frequncy detector of an induction motor utilizing rotor slot harmonics," *IEEE Transactions on Industry Applications*, vol. IA-20, no. 3, pp. 575–582, 1984, doi: 10.1109/TIA.1984.4504454

[66] B. W. Williams, J. K. Goodfellow, and T. C. Green, "'sensorless' speed measurement of inverter driven squirrel cage induction motors," in *1990 Fourth International Conference on Power Electronics and Variable-Speed Drives (Conf. Publ. No. 324)*, 1990, pp. 297–300. [Online]. Available: https://ieeexplore.ieee.org/document/114657

[67] A. Ferrah, K. G. Bradley, and G. M. Asher, "Sensorless speed detection of inverter fed induction motors using rotor slot harmonics and fast fourier transform," in *PESC '92 Record. 23rd Annual IEEE Power Electronics Specialists Conference*, 1992, pp. 279–286 vol.1, doi: 10.1109/PESC.1992.254661

[68] K. D. Hurst and T. G. Habetler, "Sensorless speed measurement using current harmonic spectral estimation in induction machine drives," *IEEE Transactions on Power Electronics*, vol. 11, no. 1, pp. 66–73, 1996, doi: 10.1109/63.484418

[69] R. Blasco-Gimenez, G. M. Asher, M. Sumner, and K. J. Bradley, "Performance of fft-rotor slot harmonic speed detector for sensorless induction motor drives," *IEE Proceedings - Electric Power Applications*, vol. 143, no. 3, pp. 258–268, 1996, doi: 10.1049/ip-epa:19960241

[70] A. Ferrah, K. J. Bradley, P. J. Hogben-Laing, M. S. Woolfson, G. M. Asher, M. Sumner, J. Cilia, and J. Shuli, "A speed identifier for induction motor drives using real-time adaptive digital filtering," *IEEE Transactions on Industry Applications*, vol. 34, no. 1, pp. 156–162, 1998, doi: 10.1109/28.658741

[71] S. Nandi, S. Ahmed, and H. A. Toliyat, "Detection of rotor slot and other eccentricity related harmonics in a three phase induction motor with different rotor cages," *IEEE Transactions on Energy Conversion*, vol. 16, no. 3, pp. 253–260, 2001, doi: 10.1109/60.937205

[72] S. Nandi, S. Ahmed, H. A. Toliyat, and R. M. Bharadwaj, "Selection criteria of induction machines for speed-sensorless drive applications," *IEEE Transactions on Industry Applications*, vol. 39, no. 3, pp. 704–712, 2003, doi: 10.1109/TIA.2003.810651

[73] O. Keysan and H. B. Ertan, "Real-time speed and position estimation using rotor slot harmonics," *IEEE Transactions on Industrial Informatics*, vol. 9, no. 2, pp. 899–908, 2013, doi: 10.1109/TII.2012.2210231

[74] W. L. Silva, A. M. N. Lima, and A. Oliveira, "Speed estimation of an induction motor operating in the nonstationary mode by using rotor slot harmonics," *IEEE Transactions on Instrumentation and Measurement*, vol. 64, no. 4, pp. 984–994, 2015, doi: 10.1109/TIM.2014.2361554

[75] S. Luecke, J. Koupeny, and A. Mertens, "Induction machine speed tracking based on rotor slot harmonics using a modified pll approach," in *2016 18th European Conference on Power Electronics and Applications (EPE'16 ECCE Europe)*, 2016, pp. 1–10, doi: 10.1109/EPE.2016.7695518

[76] A. K. Samanta, A. Naha, A. Routray, and A. K. Deb, "Fast and accurate spectral estimation for online detection of partial broken bar in induction motors," *Mechanical Systems and Signal Processing*, vol. 98, pp. 63–77, 2018, doi: 10.1016/j.ymssp.2017.04.035

[77] A. G. Yepes, F. Baneira, J. Malvar, A. Vidal, D. Pérez-Estévez, O. López, and J. Doval-Gandoy, "Selection criteria of multiphase induction machines for speed-sensorless drives based on rotor slot harmonics," *IEEE Transactions on Industrial Electronics*, vol. 63, no. 8, pp. 4663–4673, 2016, doi: 10.1109/TIE.2016.2548979

[78] A. G. Yepes, J. Doval-Gandoy, F. Baneira, and H. A. Toliyat, "Speed estimation based on rotor slot harmonics in multiphase induction machines under open-phase fault," *IEEE Transactions on Power Electronics*, vol. 33, no. 9, pp. 7980–7993, 2018, doi: 10.1109/TPEL.2017.2773649

[79] W. J. Bradley, B. Mason, A. Pezouvanis, and K. M. Ebrahimi, "A sensorless speed estimation algorithm for use in induction motor fault detection applications," *Proceedings of the Institution of Mechanical Engineers, Part I: Journal of Systems and Control Engineering*, vol. 228, no. 4, pp. 257–264, 2014, doi: 10.1177/0959651813511613

[80] S. Rind, Y. Ren, and L. Jiang, "Traction motors and speed estimation techniques for sensorless control of electric vehicles: A review," in *2014 49th International Universities Power Engineering Conference (UPEC)*, 2014, pp. 1–6, doi: 10.1109/UPEC.2014.6934646

[81] J. Bonet-Jara and J. Pons-Llinares, "Sensorlees speed estimation. a review," in *2019 IEEE 12th International Symposium on Diagnostics for Electrical Machines, Power Electronics and Drives (SDEMPED)*, 2019, pp. 283–289, doi: 10.1109/DEMPED.2019.8864878

[82] S. Chetwani, M. Shah, and M. Ramamoorty, "Online condition monitoring of induction motors through signal processing," in *2005 International Conference on Electrical Machines and Systems*, vol. 3, 2005, pp. 2175–2179 Vol. 3, doi: 10.1109/ICEMS.2005.202952

[83] H. Guesmi, S. Ben Salem, and K. Bacha, "Smart wireless sensor networks for online faults diagnosis in induction machine," *Computers and Electrical Engineering*, vol. 41, no. 1, pp. 226–239, 2015, doi: 10.1016/j.compeleceng.2014.10.015

[84] J. W. Finch and D. Giaouris, "Controlled ac electrical drives," *IEEE Transactions on Industrial Electronics*, vol. 55, no. 2, pp. 481–491, 2008, doi: 10.1109/TIE.2007.911209

[85] P. Vas, *Parameter Estimation, Condition Monitoring, and Diagnosis of Electrical Machines*. Oxford Science Publications, 1993, [Online]. Available: https://global.oup.com.

[86] D. G. Dorrell, W. T. Thomson, and S. Roach, "Analysis of airgap flux, current, and vibration signals as a function of the combination of static and dynamic airgap eccentricity in 3-phase induction motors," *IEEE Transactions on Industry Applications*, vol. 33, no. 1, pp. 24–34, 1997, doi: 10.1109/28.567073

[87] Megger, *Instantaneous torque as a predictive maintenance tool for variable frequency drives and line operated motors*. [Online]. Available: https://es.megger.com/products/motor-and-generator-testing/dynamic-analyzers/baker-exp4000/technical/instantaneous-torque-as-a-predictive-maintenance-t

[88] E. Wiendenbrüg, "Measurement analysis and efficiency estimation of three phase induction machines using instantaneous electrical quantities," Ph.D. dissertation, Oregon State University, 1998. [Online]. Available: https://ir.library.oregonstate.edu/concern/graduate_thesis_or_dissertations/3f4628121?locale=en

[89] PDMA, *Introduction to MCEMAX*. [Online]. Available: https://www.pdma.com/PdMA-intro-mcemax.php

[90] *UNE-EN Maquinas electricas rotativas 60034-1*, 2011. [Online]. Available: https://www.une.org/encuentra-tu-norma/busca-tu-norma/norma/?c=N0047178

[91] *NEMA Motors and Generators, MG-1-2016*, 2016. [Online]. Available: https://www.nema.org/standards/view/motors-and-generators

[92] A. Bellini, F. Filippetti, G. Franceschini, C. Tassoni, and G. B. Kliman, "Quantitative evaluation of induction motor broken bars by means of electrical signature analysis," *IEEE Transactions on Industry Applications*, vol. 37, no. 5, pp. 1248–1255, 2001, doi: 10.1109/28.952499

[93] Zhenxing Liu, Xiaolong Zhang, Xianggen Yin, and Zhe Zhang, "Rotor cage fault diagnosis in induction motors based on spectral analysis of current hilbert modulus," in *IEEE Power Engineering Society General Meeting, 2004.*, 2004, pp. 1500–1503 Vol.2, doi: 10.1109/PES.2004.1373123

Chapter 3

A precise, general, non-invasive and automatic speed estimation method for MCSA diagnosis and efficiency estimation of induction motors

This paper was published on November 12, 2022 in IEEE Transactions on Energy Conversion journal, belonging to the IEEE publishing house, under the reference:

In the next sections, the full accepted author's version of the manuscript is reproduced, including abstract, appendixes and bibliography. Footnotes, which are not present in the original publication, are added in order to clarify some aspects within the general frame of this thesis.

Abstract

Efficiency estimation and diagnosis via MCSA require precise knowledge of speed. In an industrial environment, speed must be obtained with a non-invasive, automatic and general method. Recent studies have shown that Sensorless Speed Estimation techniques based on detecting Rotational Frequency Sideband Harmonics (RFSHs) or Rotor Slot Harmonics (RSHs) are best suited to these purposes. RFSHs-based methods are easier to apply as they only depend on the number of poles. RSHs-based are much more accurate due to their wider bandwidth. Yet, their use is not trivial as they require to identify the RSHs family, assign to each RSH its order of the current harmonic (ν) and determine the number of rotor slots (R), a rarely known parameter. This paper ends with this trade-off between accuracy and applicability by proposing a novel RSHs-based technique that, for the first time in technical literature, eliminates the need to estimate the number of rotor slots and provides a reliable and automatic procedure to locate the RSHs family and determine their ν indices. Finally, the method is validated under all types of conditions and motor designs, by simulations, lab tests and with 105 industrial motors, highlighting its high accuracy (errors below 0.05 rpm), and applicability.

Keywords: diagnosis; induction motors; MCSA; sensorless speed estimation; efficiency estimation.

3.1 Introduction

There are two key points when operating induction motors (IM) in industry: maintenance (to avoid untimely outages) and efficiency estimation (to minimize energy consumption). In order to estimate the efficiency it is necessary to measure voltages and currents [1]. Thus, a natural step is to use the same current sensor to diagnose the motor via MCSA (Motor Current Signature Analysis); compared with others, this technique is best suited to this industry context due to its non-invasiveness and remote measurement capability [2]. Moreover, both processes need very accurate speed information [3], [4]. To facilitate the industrial use, the speed must be obtained with a non-invasive and automatic (no-human intervention) method, valid for any IM.

Determining efficiency with good accuracy requires precise operating speed information (e.g., AGT or ORMEL96 [5]). In turn, speed is also vital to localize fault harmonics in the current spectrum, since they are speed-dependent [6]. In fact, speed estimation is the bottleneck of the diagnostic process: a reliable diagnosis requires a previous correct fault harmonic positioning. Some authors propose locating the fault harmonics without knowing the operating speed by calculating the maximum of the spectrum in the harmonic operating bandwidth (determined by the slip varying from 0 to its rated value) [7], [8] . Nevertheless, constructional characteristics, supply, load-oscillations, etc. might generate significant harmonics in these search bands, and produce false positives [9]. Moreover, the fault harmonic might be outside the search band due to an error in the name-plate rated slip, generating a false negative. Concluding, accurate speed knowledge is essential to avoid both false positives and negatives, and therefore, to conduct a reliable diagnosis via MCSA [6], [9].

A physical speed sensor (e.g., encoder) requires a precise and careful assembly and has a cost proportional to its accuracy. In addition, it is sensitive to the operation and location conditions (temperature, cable length, etc.). Finally, manual measurements with hand-held sensors (e.g. tachometers), apart from not being sufficiently accurate, require the shaft to be accessible,

which is not always the case. Therefore, giving these limitations, a Sensorless Speed Estimation (SSE) becomes a better option. These techniques (traditionally developed for electric motor control [10]), can be classified into two major families: Fundamental Model Based [11]–[13] and Magnetic Anisotropy Based. The latter can be subdivided into: Signal Injection Based [14]–[16] and Slotting and Rotational Frequency Sideband Harmonics Based (SRFSHB) [17]–[36].

SRFSHB methods are the most suitable for in-service IM efficiency estimation [3] and IM diagnosis via MCSA [4], as they only need to measure one current, do not depend on time-varying parameters (as fundamental model methods do) and do not need the machine to be excited with a source other than its normal power supply (as signal injection methods do). These methods consist of processing the line current in order to determine the frequency of one or more speed-dependent harmonics, and then, using the formulas that predict their frequencies, calculate slip [37]. Rotational Frequency Sideband Harmonics (RFSHs) and Rotor Slot Harmonics (RSHs) are commonly used in these techniques, although sometimes Broken Bar Harmonics (BBHs) may be a complement.

Since they only require the number of pole pairs (available on the nameplate), RFSHs-based methods are preferred by industry, being frequently used in online condition monitoring [20], in-situ efficiency estimation [17]–[19], and commercial diagnostic devices (MCEMAX [21], EXP4000 [22]). However, their frequencies only vary a few fractions of hertz from no to full load [38]. Therefore, a small error in their frequencies estimation implies a large error in the speed estimation. Moreover, they usually encounter detectability problems, especially in 2-pole machines [4].

RSHs-based methods are much more accurate due to their wider operating bandwidth [3], [4]. Yet, using these harmonics is not trivial. The first problem is to identify which harmonics in the spectrum constitute a RSHs family. Then, even assuming that they have been correctly identified, they must be assigned a ν index; there is an erroneous trend to assign $+1$ or -1 to the RSH with the highest amplitude. Finally, to estimate speed, the number of rotor bars (R) must be known. This is a problem, as motor owners are rarely aware of this parameter. Therefore, the applicability of this technique as a non-invasive method is dramatically reduced outside laboratory.

No method has yet solved the problems of this technique in a robust and reliable way. Most of the papers assume R, the position of the RSH in the spectrum and their ν values as known information [23]–[29]. To solve this lack of data, others propose non-automatic/invasive methods that require visual inspection and/or subject the motor to different operating conditions [30]–[33]. Finally, only three papers propose self-commission methods to ascertain this set [34]–[36]:

The method presented in [34], which relies on a preliminary slip estimation from RFSHs, has three disadvantages. First, R is constrained from 30 to 54, which leaves quite a few machines out below 30 (2-pole and small-medium 4-pole machines) and above 54 (medium-large 4-pole and 6-pole machines). Second, RFSHs are an unreliable source of information since small errors in frequency estimation mean big errors in speed. Finally, RFSHs do not often manifest themselves with sufficient intensity to be distinguished from the noise level (especially in 2-pole machines). When this happens, the paper proposes to perform a no-load test to determine the main RSH and asks the user to introduce R (increasing invasiveness and decreasing automaticity).

In [35], the method searches a RFSH and the RSH with $\nu = 1$ (not specifying how the bands are defined). Then, using these two harmonics and the value of the fundamental frequency, R

is calculated. If the decimal of R is lower than 0.1 or higher than 0.9, the number is rounded and the process ends; otherwise, the process is repeated (it is not specified how the band for the RSH is re-defined). The drawbacks of this method are the same as in [34] with respect to RFSHs, with the added disadvantage of assuming that RSH ($\nu = 1$) may always be identified automatically .

In [36], the method, which relies on a preliminary speed estimation based on nameplate data, has three disadvantages. First, as stated before, constraining the number of R to test may leave some motors out of the algorithm's scope. Although in this case the range is wider than in [34], large motors could still be left out. Another problem with this methodology, is that it uses a fixed band to localize RSHs (8.609 Hz), which could left some of them out of the window. Finally, the main problem is that the convergence criteria is based on a preliminary speed estimation from nameplate. This estimation can be quite unreliable because nameplate data, apart from being subjected to wide tolerances (especially rated slip), can change through time due to degradation.

Summarizing, RSHs-based methods are preferable due to their high accuracy. Nevertheless, no existing method has solved their low applicability: number of rotor slots needed is unknown, as well as the RSHs position in the spectrum, together with their ν indices. Trying to solve this lack of information, previous methods have proposed problematic solutions. Moreover, reliability is low for existing methods, since among all the RSHs, they only use the so called Principal Slot Harmonics (PSHs), which have low amplitudes for certain motor designs [38]. Finally, SSE methods presented have a poor validation: few laboratory motors (one to four with similar characteristics), and none industrial cases, not ensuring a high reliability.

Concluding, a new SSE method is needed, solving the RSHs-based methods drawbacks, to profit their accuracy necessary in diagnosis and efficiency estimation applications. This is the first SSE method which achieves to automatically localize the family of RSHs, properly assigning their ν indices, without knowing the number of rotor slots, without introducing errors as a preliminary estimate based on rated slip or use of RFSHs, without using invasive tests (e.g., no-load test), not restricting to PSHs, and not wrongly assuming that the highest amplitude corresponds to $\nu = 1$. To this end, a new formula for the RSHs frequencies is deducted, and a smart RSH search method is presented, to localize and characterize the RSHs family (Sections 3.2, 3.3 and 3.4). The algorithm has been extensively tested, not only through simulations (Section 3.5), lab tests under different load conditions and power supply (Section 3.6), but also through 105 field cases (covering all ranges of rated magnitudes), highlighting the high applicability of the proposed methodology (Section 3.7). The algorithm provides a SSE easy to be implemented in an industrial environment for IM steady state diagnosis via MCSA and in-situ efficiency estimation, which ends with the trade-off between accuracy, applicability and reliability of previous techniques.

3.2 Determining RSHs parameters

The discrete nature of the squirrel cage bars causes the rotor to generate magnetomotive force spatial harmonics as well as a periodic variation of the air-gap permeance. By interacting, they produce air-gap flux components which induce in the stator currents a set of speed-dependent harmonics called Rotor Slot Harmonics (RSHs). The relationship between the frequencies of these harmonics and the machine characteristics has been extensively studied [37], [38] and

can be given by:

$$f_{RSH} = \left[k\frac{R}{p}(1-s) \pm \nu \right] f_0 \tag{3.1}$$

where k is a natural number $1, 2, 3 \ldots$, p the number of pole pairs, s the slip, ν the order of the time harmonic present in the stator current $1, 3, 5 \ldots$, f_0 the fundamental supply frequency and R the number of rotor bars.

Formula (3.1) depends on the slip, which is directly related with rotor speed. Therefore, once a RSH is localized, if the other parameters in (3.1) are known, speed can be calculated. The number of pole pairs p and the fundamental frequency f_0 are obtained respectively from the nameplate and a FFT analysis (as f_0 is the highest peak in the spectrum). On the contrary, the number of rotor bars is an a priori unknown parameter: it is not listed on the nameplate or in the data sheet, nor can it be easily obtained from the manufacturer. Thus, to obtain an automatic, non-invasive, general and precise speed estimation algorithm, it is necessary to eliminate this parameter from the equation. To this end, let us first eliminate $\pm$ sign in (3.1), so now $\nu = \ldots, -3, -1, 1, 3, \ldots$, and rewrite it as follows:

$$f_{RSH} = \left[k\frac{R}{p} + \nu \right] f_0 - k\frac{R}{p} s f_0 \tag{3.2}$$

Next, consider the case of ideal no-load ($s = 0$):

$$f_{RSH}|_{s=0} = \left[k\frac{R}{p} + \nu \right] f_0 \tag{3.3}$$

Then, let us define O_ν, (where the subscript refers to the value of ν taken), as the quotient between the frequency of the RSH at zero slip and the frequency of the fundamental component:

$$O_\nu = \frac{f_{RSH}|_{s=0}}{f_0} = \left[k\frac{R}{p} + \nu \right] \tag{3.4}$$

Combining (3.2) and (3.4) we obtain:

$$f_{RSH} = O_\nu f_0 - [O_\nu - \nu]\, s f_0 \tag{3.5}$$

Therefore, we can finally calculate the slip as:

$$s = \frac{O_\nu f_0 - f_{RSH}}{[O_\nu - \nu]\, f_0} \tag{3.6}$$

RSHs only exhibit high amplitude in the stator current spectrum when the product kR/p is even [38]. If an odd number (ν) is added to or subtracted from this product, the result ($O_\nu = kR/p + \nu$) is always an odd number. Therefore, according to (3.5), the following rule can be established: in ideal no-load ($s = 0$) the most detectable RSHs are placed over an odd multiple of the fundamental frequency ($O_\nu f_0$), while in load, to its left (motor mode, $s > 0$), or to its right (generator mode, $s < 0$).

Taking into account the above rule, once a RSH has been localized in the spectrum, the odd multiple of the fundamental frequency closest to its right (motor mode) is $O_\nu f_0$: knowing f_0, O_ν can be calculated. Therefore, as the number of rotor bars has been eliminated in (3.6), it only remains to obtain ν for each RSH localized. Next, a novel method based on the steady-state

current is proposed to localize the RSHs and determine their related v.

3.2.1 Localizing the RSHs

According to (3.2) and (3.5), the distance of a RSH with respect to $O_v f_0$ is ksf_0R/p. R/p is constant and sf_0 (slip frequency) is the same for all RSHs. Therefore, if a set of RSHs are linked to the same k, all remain at the same distance (in Hz) from their respective $O_v f_0$. Let us define such set as a family of RSHs. Figure 3.1 shows three fragments of the stator current spectrum from a 248 kW IM where three RSHs are shown at the same distance (31.10 Hz) from the first odd multiple of f_0 at their right, thereby belonging to the same RSHs family. Considering this rule, the following Track & Find algorithm has been developed to localize a RSHs family (small clarifications in the next paragraph):

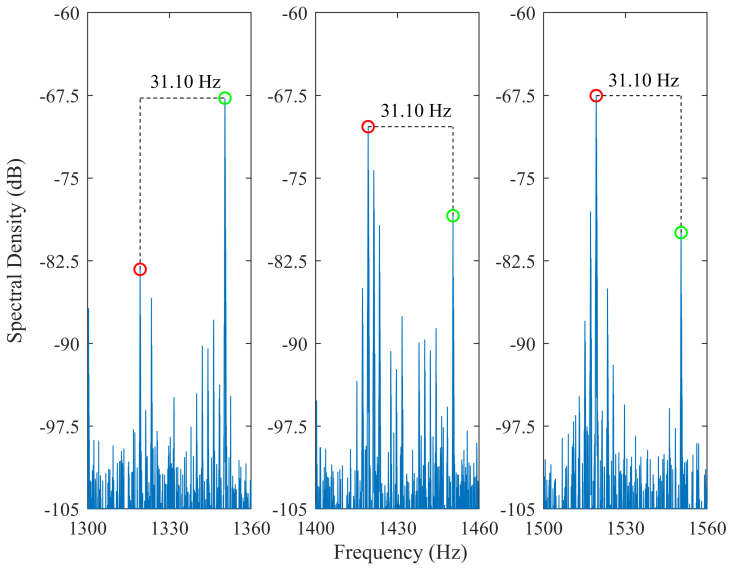

FIGURE 3.1: Distance between the RSHs of a same family (red circles) and their nearest odd multiple of f_0 (green circles) in the steady-state current of a 248 kW IM. From left to right: RSH(-3), RSH(-1) and RSH(+1).

- *Step 1:* The FFT spectrum of the line current is subdivided in windows of width $[f_0 \cdot (2n-1), f_0 \cdot (2n+1)]$ Hz (starting at $n = 4$, until it is entirely covered).
- *Step 2:* The widths of the windows are slightly reduced by subtracting 1.3 Hz to the upper limit and by adding $0.26 \cdot f_0$ to the lower.
- *Step 3:* The frequency of the highest peak within each window is recorded as a RSH candidate.
- *Step 4:* The RSH candidates are classified by families. Two candidates belong to the same family if they are at the same distance (with a tolerance of 0.5 Hz) from the upper limit (lower if generator mode) of their search window (the correspondent $O_v f_0$).
- *Step 5:* The family with the highest number of candidates is selected as a possible RSHs family. In case of a tie, all the tied families are selected.

In *Step 1*, n starts at 4 since RSHs are not expected to be found in windows with $n < 4$, given that a motor is normally made with $R/p > 10$. In *Step 2*, windows are reduced in order to avoid capturing odd multiples of f_0, as well as other harmonics that appear near them (e.g, Dynamic Eccentricity Harmonics (DEH)). The reduction parameters are determined experimentally and verified through a motor database of 105 IMs of different rated powers (see Section 3.7). Finally, in *Step 4*, the tolerance is also established empirically and accounts for slight speed variations during the signal capture.

3.2.2 Determining the parameter ν

Once the candidates RSHs families have been detected, it is necessary to determine the parameter ν of each RSH candidate. Here, an iterative method is proposed, whose convergence criteria is based on the information provided by 16 different speed-dependent harmonics (frequency formulas in Appendix A): BBHs first ($k = 1$ and $k = 2$) and second family ($k/p = 5$ and $k/p = 7$), RFSHs ($k = 1$ and $k = 2$) and DEHs ($n_D = 1$). To improve the effectiveness in low-slip motors, the BBHs ($k = 1$ and $k = 2$) present in the spectrum of the current Hilbert modulus are also included [39].

Next, the method for determining ν is described. This process is repeated for each RSH candidate of each family:

- *Step 1:* O_ν is calculated as explained in Section 3.2.
- *Step 2:* A value for ν is selected, beginning in -27 and ending in $O_\nu - 10$, and the following process is applied for each of these values:
  - *Step 2.1:* s is obtained from (3.6), using the calculated O_ν, the selected ν and the RSH candidate frequency.
  - *Step 2.2:* A frequency window is calculated for each harmonic considered in Appendix A using $[0.75s, 1.25s]$.
  - *Step 2.3:* The frequency of the highest peak within each window is recorded.
  - *Step 2.4:* If the distance between the highest peak and the centre of the window is less than 7% of the window amplitude, the tested value for ν is considered to correctly locate the correspondent fault harmonic.
- *Step 3:* The ν finally assigned to a given RSH candidate is the one that has correctly located (according to *Step 2.4* criteria) the largest number of fault harmonics (in case of a tie, the lowest ν is chosen).

Up to this point, each RSH candidate of each family has been assigned a pair $[O_\nu, \nu]$. Two RSH candidates are consistent if when applying $kR/p = O_\nu - \nu$ they give the same result. The most repeated kR/p in a candidate RSHs family is obtained, and the percentage of RSH leading to that value is called the consistency ratio of that family. This concept is used in the following validation process to discard the candidate families that are unlikely to be the RSHs family:

- *Step 4:* If one of the RSHs in a family fails to predict the position of all the fault harmonics for all ν, the whole family is discarded.
- *Step 5:* Consistency ratio is calculated as previously defined: if it is less than 50%, the whole family is discarded.

- *Step 6:* Finally, the family with the highest consistency ratio is selected as the definitive RSHs family; its inconsistent RSHs are discarded and the consistent stored.

In *Step 2*, the set of values for ν is empirically determined using the 105 IM database (see Section 3.7): it has never been found a ν index lower than -27 or greater than $O_\nu - 10$ (this would mean a motor with less than 10 R/p). In *Step 2.4*, the 7% margin accounts for speed variations during recording as well as for the frequency resolution error. In Hz, this margin is very small: e.g., between 0.01 and 0.05 Hz for the LSH of a motor with $R/p = 28$).

Among other important advantages, summarized in the conclusions section, at this point it can already be seen how the algorithm manages to perform a SSE without knowing the rotor slots, automatically localizing the RSHs family in the spectrum, and assigning their related O_ν and ν indices. It works without any restriction (general solution), even for motors not Principal Slot Harmonics (PSH) producers (RSHs with $k = 1$, [38]), since it also accounts for $k > 1$ in (3.1), and without using invasive procedures (just a steady state current). The algorithm result assures a perfect match between the slip information of the speed-dependent harmonics present in the current spectrum (RSHs and fault harmonics, which also appear in healthy conditions, as all motors have a certain level of electrical and constructive asymmetry). In other words, thanks to the novel criterion introduced, it is verified that the slip predicted by the RSHs agrees with the position of the remaining speed-dependent harmonics.

3.3 On the order k of the RSHs

The order k of the RSHs present in the spectrum depends on the number of rotor slots R and pole pairs p: kR/p must be even for a RSH of order k to appear. This condition leads to Table 3.1, which shows the orders k that appear for each combination of R and p (where $R/a \in \mathbb{N}$ means R can be divided by a, giving as a result an integer).

TABLE 3.1: Orders k of RSHs for each combination of R and p

	$p = 1$	$p = 2$	$p = 3$
R even	$\forall k \in \mathbb{N}$	$\forall k \in \mathbb{N}$ if $R/4 \in \mathbb{N}$ k even if $R/4 \notin \mathbb{N}$	$\forall k \in \mathbb{N}$ if $R/6 \in \mathbb{N}$ $k/3 \in \mathbb{N}$ if $R/6 \notin \mathbb{N}$
R odd	k even	$k/4 \in \mathbb{N}$	k even if $R/3 \in \mathbb{N}$ $k/6 \in \mathbb{N}$ if $R/3 \notin \mathbb{N}$

The most critical cases for the algorithm are those combinations which produce RSHs families whose minimum order k is a high number, since these harmonics tend to have a lower amplitude. Looking at the table, those cases are motors with $p = 2$ and R odd ($k_{min} = 4$) and motors with $p = 3$ and R odd number non-multiple of 3 ($k_{min} = 6$). Yet, manufacturers usually avoid odd numbers for R (especially if $kR/p \notin \mathbb{N}$ as in these cases), due to the appearance of unbalanced magnetic pull [40]. In fact, when analyzing the database contained in [41] with data about R and p of 3474 motors with $p = 1$, 2 and 3, these two cases account only for the 5.33% and 3.2% respectively.

Nevertheless, even if analyzing a motor without RSHs of orders $k = 1, 2$, and 3 is an uncommon case, in Section 3.5 it can be seen how the algorithm successfully detects the RSHs in a motor whose first appearing order is $k = 4$. As previously stated, every RSH operates at the left of some odd multiple of the fundamental component. According to (3.3), the frequency of this

multiple increases with the order k of the RSH. However, this makes no difference for the algorithm, since it searches in a bandwidth to the left of every odd multiple of f_0, no matter if they are at low or high frequencies. Therefore, if the minimum RSH order k present in the motor is for instance 4, it means that the first RSHs will be found at higher frequencies than those of $k = 1$ if they were also present, but the behavior of the algorithm is exactly the same. Although for higher k the amplitudes are lower, it is also true that they appear at higher frequencies, where there are less components with which they can be confused. Hence, the algorithm can also work well in these conditions.

Finally, it is also interesting to analyze what would happen if the frequency operation bandwidth of two RSHs of different order k overlap. To this end, let us consider two RSHs defined by $[k_1, \nu_1]$ and $[k_2, \nu_2]$, both operating at the left of: $[kR/p + \nu]f_0$. Therefore, the overlapping condition is $k_1 R/p + \nu_1 = k_2 R/p + \nu_2$. If $k_1 = 1$ and $k_2 = 2$, then $\nu_1 - \nu_2 = R/p$. In the database of [41], it is found that the minimum R/p is 9, that only 3.2% of the motors have $R/p < 14$, and that 68% of them have $R/p > 20$ (for powers greater than 100 HP, all $R/p > 15$). Therefore, the absolute value of ν_1 and ν_2 will unlikely be simultaneously small, since their difference (R/p) is usually high (most of the cases higher than 14). Since high RSHs amplitudes are usually related to low absolute values of ν, it is unlikely that two RSHs whose bandwidths overlap have simultaneously high amplitudes (one of them will probably be negligible).

Nevertheless, if both RSHs are not negligible, the algorithm will choose the one with the highest amplitude, determine its distance to the nearest odd multiple of f_0 and put it into the family associated to that distance. The second RSH will be discarded, and its family will lose a member, decreasing its chances to be chosen to determine the speed. Concluding, if two valid families of RSHs coexist in the spectrum, both can be used to determine the speed (algorithm picks the one with the highest number of RSHs), and makes no difference if the algorithm discards one RSH in a bandwidth in which two RSHs of different families can be found.

3.4 Algorithm

Figure 3.2 depicts the flux diagram of the proposed technique. As can be seen, the methodology is characterized by three different blocks: Filtering and pre-treatment (Block A), Determination of RSHs parameters (Block B) and Slip/Speed Estimation (Block C). For the sake of simplicity, Block B has been represented for the case in which only one RSHs family is proposed as a candidate at the end of Section 3.2.1. The SSE algorithm has been implemented using MATLAB in a PC with an Intel Core i7-8700 processor. The processing time is 2 s (A+B+C, new motor) or 1.8 s (A+C, already analyzed motor) for a 200 s signal at 10 kHz. Next, the three blocks are described.

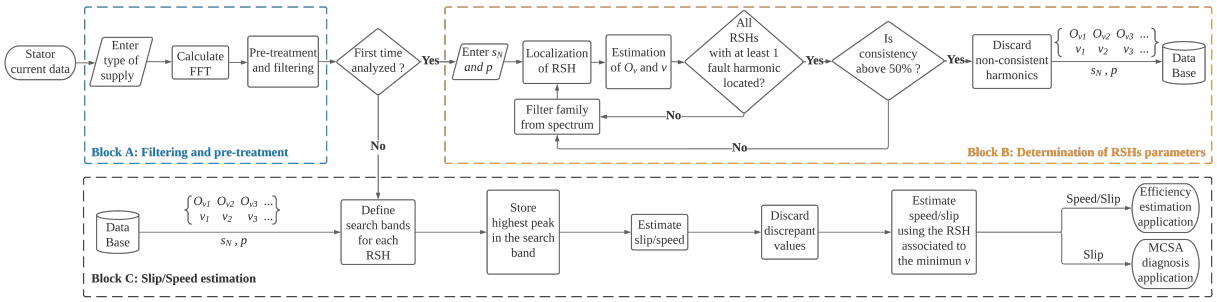

FIGURE 3.2: Flux diagram of the proposed algorithm.

3.4.1 Block A: Filtering and pre-treatment process

First, the algorithm requires the user to enter whether the motor is powered with a frequency converter or not. Then, the FFT is applied to the current, and to its Hilbert modulus, previously applying Hann window and zero-padding (x10). Next, a pre-treatment and filtering process is applied to the resultant current spectrum (later used to localize the RSHs):

- Estimate the noise level: mean value of the current spectral density multiplied by an experimental factor.
- Suppress harmonics below the estimated noise level.
- Suppress even harmonics of the fundamental frequency.
- If the motor is fed with a frequency converter, suppress the PWM harmonics.

3.4.2 Block B: Determination of RSHs parameters

If it is the first time that the motor is analyzed, family of RSHs must be localized, and its pairs $[O_\nu, \nu]$ must be ascertained. For this purpose, it is required to capture a signal of 50 to 200 s (frequency resolution between 0.02 Hz and 0.005 Hz to increase precision) at $200 f_0$ Hz (maximum frequency $100 f_0$ Hz to ensure RSHs detection). The number of pole pairs and the rated slip must be entered as input data. Then, the pairs $[O_\nu, \nu]$ are determined as described in Section 3.2, and finally stored in a database, together with the rated slip and number of pole pairs of the motor.

3.4.3 Block C: Slip/Speed estimation

If the motor has already been analyzed (minutes, days or months before), Block B has already been applied with a different current, determining the RSHs family, and their pairs $[O_\nu, \nu]$. In a new measurement, exact position of the RSHs might have changed, since the operating conditions might be different, but their pairs $[O_\nu, \nu]$ are the same. Therefore, using the Block B output contained in the database, a search window is defined for each RSH (see (3.5)):

$$\begin{aligned} f_{RSH,min} &= O_\nu f_0 - (O_\nu - \nu)\, k_1 s_N f_0 \\ f_{RSH,max} &= O_\nu f_0 - k_2 \end{aligned} \tag{3.7}$$

where k_1 and k_2 are experimental factors to compensate the tolerance in the rated slip (min) and to avoid detecting an odd multiple of the fundamental (max).

Then, using the frequency of the highest peak in each of these windows and applying (3.6), slip and speed are estimated. Some of these peaks might not be RSHs, as the feeding and loading conditions might be different from the time when the pairs $[O_\nu, \nu]$ were determined, and therefore, it might happen that some of the RSHs are no longer the highest peak in its search band. Peaks not being RSHs must be detected and discarded. To this end, the algorithm uses a classic criterion for outlier detection: peaks whose slip/speed estimation are more than three scaled median absolute deviations away from the median of all the slip/speed estimated. Once the outliers are discarded, the slip/speed output is computed using the RSH of the lowest ν, as it provides the lowest error. Furthermore, this Block only requires a current captured at $200 f_0$

(to ensure RSHs detection), while duration depends on the precision needed. Finally, it must be remarked that, up to date, the algorithm has been tested for steady state applications; further research will be conducted to prove its use under load oscillations, where a high frequency speed estimation is needed.

3.5 Simulation

This section proves through simulations the capability of the algorithm to precisely estimate the speed for an arbitrary number of R/p, load level or skewing angle. As stated in Section 3.2, the algorithm is designed to track any RSH predicted by (3.1). Therefore, even in an IM with an odd or non-integer number of R/p, where RSHs associated to $k = 1$ in (3.1) are not expected to appear, the algorithm could track those of higher order ($k = 2, 3, 4 \dots$). Nevertheless, the amplitude of these harmonics, and therefore their detectability, decreases with k, apart from being also affected by the load level and the skewing angle of the rotor bars. Therefore, it is important to test the ability of the algorithm to correctly determine the parameters associated with each RSH taking into account all these factors. To do so, the algorithm is input with simulated signals (100 s, 10 kHz) from a model of a 4-pole 4 kW IM (model information can be found in [42]). The rotor of the simulated motor is configured under three different number of bars: 26 (odd R/p), 27 (non-integer R/p) and 28 (even R/p). Then, each configuration is tested under 85% and 55% of the rated load (industrial motors are usually oversized, working usually around 85%, and rarely under 55%). Four typical skewing angles are used: 0° (straight bars), $180^\circ/R$ (half rotor slot pitch), $360^\circ/N_{est}$ (one stator slot pitch; N_{est}: stator slots) and $360^\circ/R$ (one rotor slot pitch).

In order to get the simulations as realistic as possible, the model is fed with a real three-phase voltage system measured in an industry. In addition, a white Gaussian noise is added to the resulting simulated currents to have a noise floor similar to reality. Finally, a slight electrical asymmetry is introduced in the rotor (common in industry, as seen in the results of the 105 IM analyzed in Section 3.7), through increasing the impedance of one of the bars by 10% (this motor needs a 900% increment to obtain a Lower Sideband Harmonic (LSH) with a -37 dB amplitude, which is considered as a broken bar).

The algorithm results are shown in Fig. 3.3, plotting the number of RSHs detected, for 85% (Fig. 3.3a) and 55% (Fig. 3.3a) of the rated load, for different number of bars (26, 27 and 28) and different skewing angles. The algorithm succeeds in 23 out of 24 cases. As explained further below, it fails (no RSH detected) in the case with low load, 26 bars and one rotor slot pitch skewed. In the successful cases (all the rest), the algorithm detects from 2 to 9 RSHs, even under nearly no load situation. The number of RSHs detected decreases when the bars are skewed, being the most severe cases when the bars are skewed one rotor slot pitch.

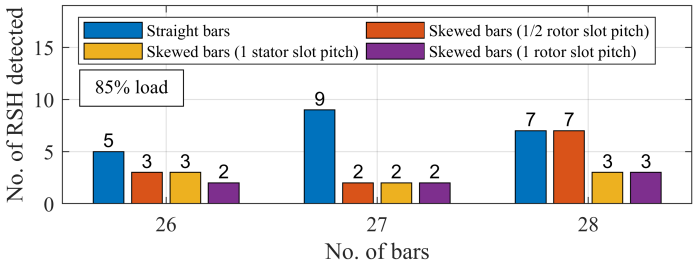

(a)

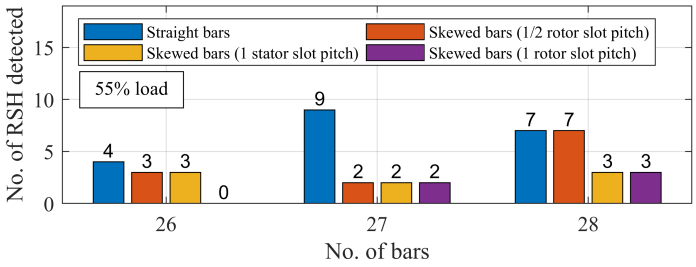

(b)

FIGURE 3.3: Number of RSHs detected by the algorithm for different number of rotor bars and skewing angles at two loads: 85% (a) and 55% (b).

With 27 and 28 bars, the algorithm detects the RSHs associated with $k = 4$ and $k = 1$ respectively. This is in accordance with theory as $k = 4$ and $k = 1$ are the lowest k for which kR/p is even, for 27 and 28 bars respectively (see Section 3.2).

Similar results are obtained for 26 bars (where the RSHs detected are the ones for $k = 2$), except under 55% of the load, with the bars skewed one rotor slot pitch. This is the only case in which the algorithm fails to detect the RSHs family. Error appears since only one RSH is the highest in its search window, and there are two speed-independent grid harmonics in the spectrum that also satisfy the rule set in Section 3.2.1 to be considered a RSHs family. This is caused by the skewing of the bars, which significantly reduces the RSHs amplitude: Fig. 3.4a (unskewed bars, 4 RSHs detected), Fig. 3.4b (one rotor slot pitch skewed bars, only 1 RSH detectable). Nevertheless, although skewing of the bars is a common practice in small motors, it is not in large ones, due to the difficulty in the manufacturing process and the increase in the iron losses, which are the most significant in this type of motors [43]. Moreover, in the only case in which the algorithm has failed, the motor works at an extremely low load level, nearly never found in an industrial environment.

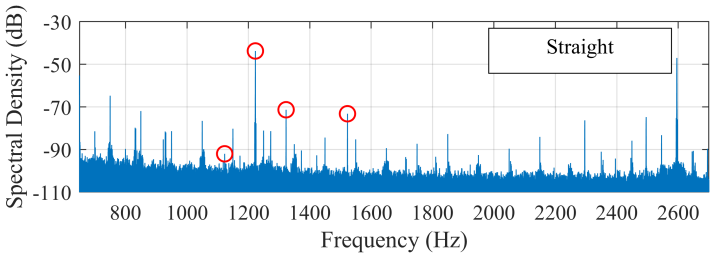

(a)

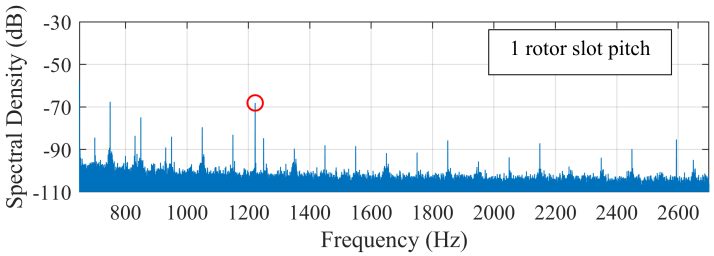

(b)

FIGURE 3.4: Number of RSHs detected by the algorithm for different number of rotor bars and skewing angles at two loads: 85% (a) and 55% (b).

Finally, it should be noted that, due to the ideal characteristic of the model, the number of detectable RSHs is inferior to real motors: the inherent asymmetries, as well as the non-linearity of the iron core, intensify some of the RSHs that are below noise level in the spectrum obtained through the model. In Section 3.7, it will be shown how the number of detectable RSHs in a database of 105 industrial IM is even superior to the results shown here.

3.6 Lab Test

In this section, the algorithm performance is evaluated, using signals from a 2.2 kW IM (28 bars skewed 1/2 rotor slot pitch, 1420 rpm, 230V Δ), which can be supplied from the grid or from a frequency converter. An identical IM is coupled to its shaft and fed with a second frequency converter, to act as a load. Speed is measured using a 1000-line incremental encoder installed on the shaft end, while current is measured using a current probe (PicoTech TA189). Both signals are simultaneously recorded using an oscilloscope (PicoTech 4262). In order to assess the capabilities of the algorithm in localizing the RSHs, determining their pairs $[O_\nu, \nu]$ (Block B) and obtaining the speed/slip (Block C), three different supply frequencies are used (20 Hz, 35 Hz and 50 Hz-line-fed), with three different slips at each of these frequencies (0.046, 0.02 and 0.0067). For testing Block B, signals of 200 s are used, while for testing Block C, 50 signals of 50 s per case are taken to obtain the average errors in speed and slip. A duration of 50 s is used because it provides the sufficient frequency resolution for a MCSA diagnostic application.

Figure 3.5a shows, for each of the cases analyzed (20, 35 and 50 Hz-Line-Fed, and three slips at each frequency), the number of RSHs detected: it varies from 5 to 6, which is in accordance with the results shown in the previous section for a motor with bars skewed 1/2 rotor slot pitch. In this IM, $R/p = 14$ and the pairs $[O_\nu, \nu]$ assigned by the algorithm to the RSHs detected give

$kR/p = O_\nu - \nu = 14$. Therefore, the algorithm perfectly detects the RSHs (using those associated to $k = 1$), and their related parameters $[O_\nu, \nu]$. Moreover, the RSHs help to detect from 5 up to 8 fault harmonics (Fig. 3.5b: number of fault harmonics localized). It is logic to expect a variation in this value depending on the supply frequency and the slip, as fault harmonics can be affected by them. Nevertheless, the value is still high in all cases, showing a good consistency between the slip estimation through RSHs, and the slip-dependent information contained in the spectrum through fault harmonics.

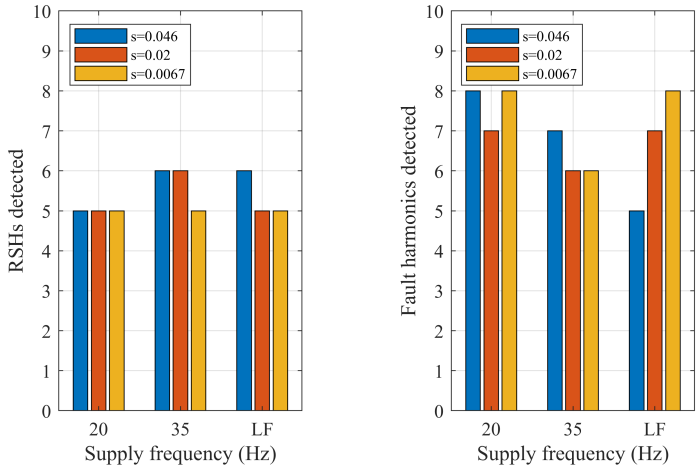

FIGURE 3.5: Number of RSHs (a) and fault harmonics detected (b) for three different supply frequencies (20 Hz, 35 Hz and 50 Hz-Line-Fed) and slips (0.046, 0.02 and 0.0067).

Concluding, the algorithm precisely identifies the RSHs family, and determines its parameters $[O_\nu, \nu]$, even under the most unfavorable conditions, which are a low supply frequency and a low slip. In this situation, some of the harmonics used in the algorithm can appear very near to other relevant harmonics and be masked by them (e.g., BBH near the fundamental frequency or RSHs near winding harmonics). Nevertheless, the fact of using an analysis based on the consistency of the speed information between the RSHs detected and up to 16 different fault harmonics makes it possible for the algorithm to identify the RSHs and resolve the correct values for the pairs $[O_\nu, \nu]$, which perfectly match with the exact number of $kR/p = O_\nu - \nu = 14$ present in the IM.

Figure 3.6 shows the absolute speed error (Fig. 3.6a and the relative slip error (Fig. 3.6b) between the 1000-line encoder and the algorithm. Errors are obtained for the three supply frequencies, and for the three slips at each supply frequency. Errors are extremely low in all cases: below 0.05 rpm and 0.5% (if the slip is 1% and the slip relative error is 0.5%, the measured slip is either 1.005% or 0.995%). It should be noted that, as the frequency converter is able to maintain a more stable supply frequency than the grid, the errors are much smaller ($e_{speed} <$ 0.01 rpm and $e_{slip} < 0.2\%$) . Finally, errors are especially low under high load, since the load level is influencing the speed stability in this motor, causing the error to increase as the load decreases. The error shown in each case is the average error of 50 signals captured under the same operating conditions. Therefore, the algorithm is highly reliable.

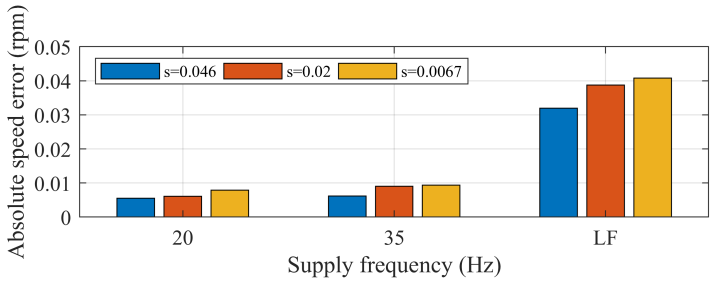

(a)

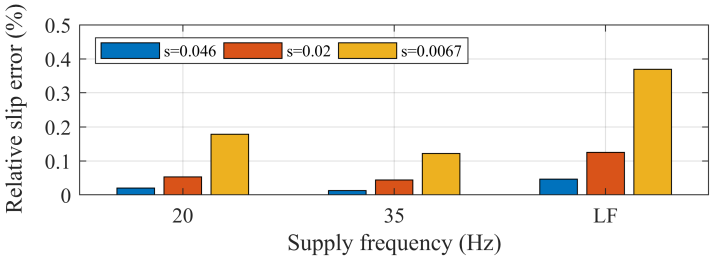

(b)

FIGURE 3.6: Absolute speed error (a) and relative slip error (b) for three different supply frequencies (20 Hz, 35Hz and 50 Hz-Line-Fed) and slips (0.046, 0.02 and 0.0067).

3.7 Field Test

In this section, the algorithm is validated using real measurements of 105 industrial IM. All signals have been obtained using an oscilloscope (PicoTech 4824) and a current probe (PicoTech TA167), except for ten motors that were measured using a device with a limited sampling frequency of 2.6 kHz. Most of the 105 motors have been monitored two or three times, while some of them have been diagnosed every six hours during nearly a year, using this algorithm in the process (results of failure cases presented in [42]).

Figure 3.7 shows the number of motors in the database for each of the ranges of rated power, slip, voltage and number of pole pairs. As can be seen, the database covers a wide range of different types of motors: from a few kW to 2 MW, 0.67% to 8% slip, 400 V to 6.6 kV and from 1 to 5 pole pairs. Figure 3.8 shows the rated slip (y-axis) and the supply frequency (x-axis) for all the motors supplied by the grid (blue circles) and by frequency converters (red circles). In this regard, it should be noted that the algorithm has been tested with a considerable amount of motors with low rated-slips (21 motors with slip lower than 1%), and converter-fed at low frequencies, which are the most challenging conditions for algorithms based on harmonic detection. Therefore, this database is a great tool to validate and demonstrate the high applicability of the proposed method.

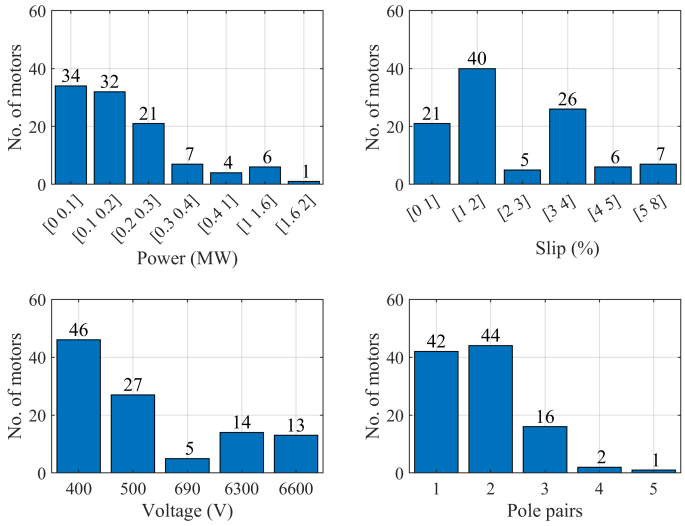

FIGURE 3.7: Summary of the rated characteristics of the motor database.

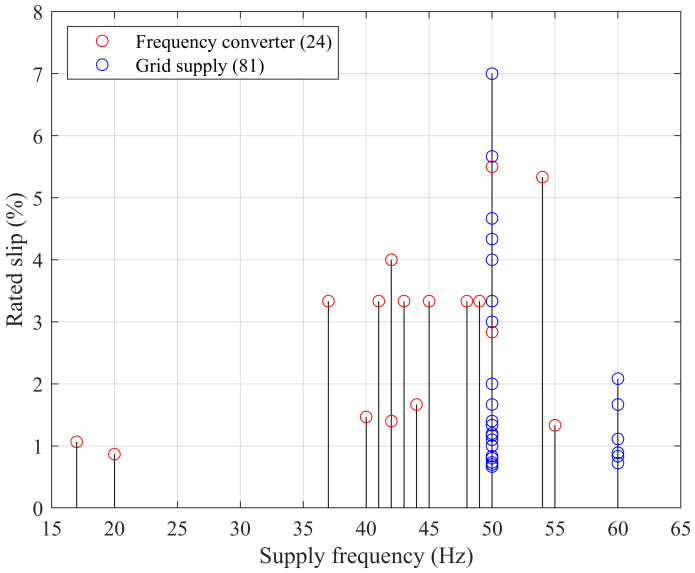

FIGURE 3.8: Rated slip and supply frequency of each motor of the database.

As for the validation methodology, whenever possible, the speed has been measured and a direct comparison with the speed estimated by the algorithm has been made. Otherwise (e.g, shaft not accessible), a visual inspection of the spectrum has been performed through three steps. First, the RSHs family localized by the algorithm has been identified in the spectrum. Second, it has been checked if there is another significant harmonic family, not detected by the algorithm, that satisfies the rules of Section 3.2 for being a RSHs family: harmonics at the same distance of their respective multiple of f_0. Third, a manual determination of parameters O_ν and ν has been conducted for all families accomplishing that rule, verifying that the family and its respective indices O_ν and ν selected by the algorithm are the ones that perfectly match with the rest of speed-dependent harmonics present in the spectrum.

In this regard, after applying the algorithm to the 105 IMs, there are only five of them where it has not been possible to assess whether the results are correct or not. This has been due to the fact that these measures were taken in conditions for which the algorithm is not designed for: high noise-floor (two IMs with -67 dB, while in the rest of motors the value is around -90 to -100 dB), very low load (one IM running at 37% of the rated current) and transient operation (two IMs with significant load variations).

3.7.1 Results: three critical examples

The three figures depicted in this subsection show the RSHs and fault harmonics localized by the algorithm for three different IMs. Subfigures (a) represent the spectrum with the number of RSHs detected (red circles) and the RSH used to estimate speed (black circle), while the rest of subfigures show the estimated position of the most relevant speed-dependent harmonics: the LRFSH (b), the URFSH (c), the first family of BBHs (d) and the second family of BBHs (e), (f).

Figure 3.9 shows the results for a four-pole, 90 kW IM running with a slip of 0.3% and a supply frequency of 20 Hz. This is one of the most challenging conditions for the algorithm since the spectrum is highly polluted (affecting the RSHs localization) and the speed-dependent harmonics appear very close to multiples of the fundamental frequency (affecting the estimation of ν). However, the algorithm precisely detects 6 RSHs and 5 fault harmonics localized through them (2 of them shown in Figs. 3.9b and 3.9c, 2 in 3.9d and 1 in 3.9e).

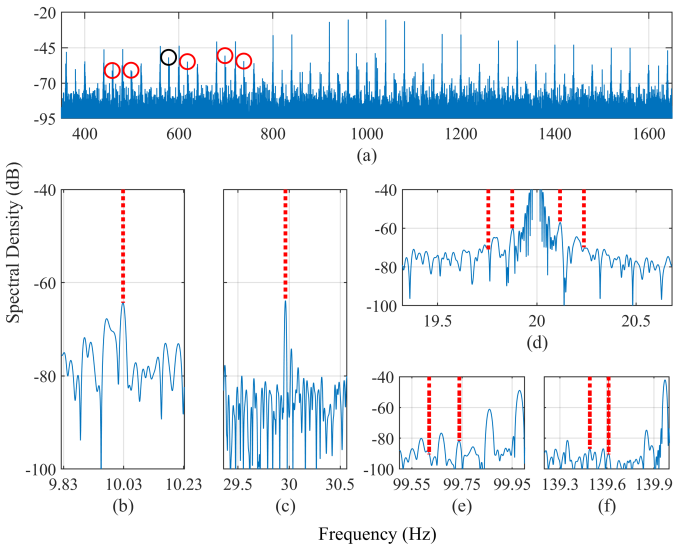

FIGURE 3.9: Algorithm performance in a four-pole 90 kW IM fed at 20 Hz: detected RSHs (a) and location of LRFSH (b), URFSH (c), first family of BBHs (D) and second family of BBHs (e) and (f).

Figure 3.10 shows the results for a two-pole, 112 kW, line-fed IM running with a slip of 2.9%. In this case, the algorithm has detected 17 RSHs, which enable to localize 11 fault harmonics (9 of them shown in Figs. 3.10c, 3.10d, 3.10e and 3.10f). It is worth to remark that, an algorithm based on detecting RFSHs would have failed, since there are two harmonics with a higher amplitude next to them, as shown in Figs. 3.10b and 3.10c.

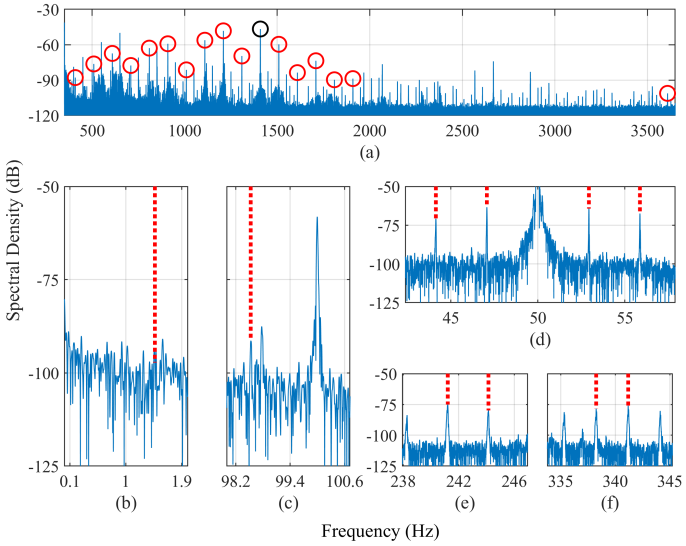

FIGURE 3.10: Algorithm performance in a two-pole 112 kW IM line-fed: detected RSHs (a) and location of LRFSH (b), URFSH (c), first family of BBHs (D) and second family of BBHs (e) and (f).

Figure 3.11 shows the results for a two-pole, 172 kW IM running with a slip of 1.5% and a supply frequency of 43.97 Hz. In this case, the spectrum is less polluted than in Fig. 3.9, so the number of detected RSHs increases to 10, and the number of fault harmonics localized is 8 (all of them shown in Figs. 3.11d, 3.11e and 3.11f). As before, an algorithm based on detecting RFSHs would have failed[1], since they are below noise level, as shown in Figs. 3.11b and 3.11c.

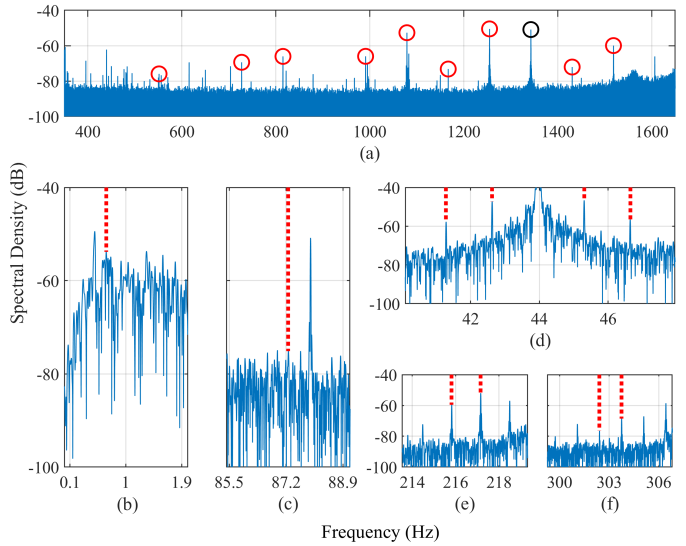

FIGURE 3.11: Algorithm performance in a two-pole 172 kW IM fed at 43.97 Hz: detected RSHs (a) and location of LRFSH (b), URFSH (c), first family of BBHs (D) and second family of BBHs (e) and (f).

[1]As shown in this field case and in the previous one, RFSHS are not very reliable for speed estimation, not only because of their greater margin of error, but also because of their low detectability, especially, in two-pole machines.

3.7.2 Statistical analysis

Figure 3.12a represents the number of RSHs detected by the algorithm in each of the motors analyzed along with the final mean and boxplot. According to it, the mean value of detections is 7.3, while the median is 6. It is also worth to remark that in 75% of the cases the number of RSHs detected is more than 4, and that in some cases it can reach values up to 24. Finally, there are 14 cases where the number of detected RSHs is equal to 2. However, 10 of them were measured with a 2.6 kHz sampling frequency. Therefore, it is highly likely that more harmonics would have been detected if the sampling frequency had been $200 f_0$, as in the rest of signals.

Figure 3.12b represents, for each of the motors analyzed, the number of fault harmonics properly localized through the detected RSHs family. According to it, the mean value for the database is 7.6, the median 8 and the first quartile 6. This gives us a measure on how robust the determination of O_ν and ν has been for all RSHs of the family, since it depicts the degree of coherency between the slip estimated through each RSH using the pair O_ν and ν obtained, and the rest of speed-dependent harmonics considered (fault harmonics).

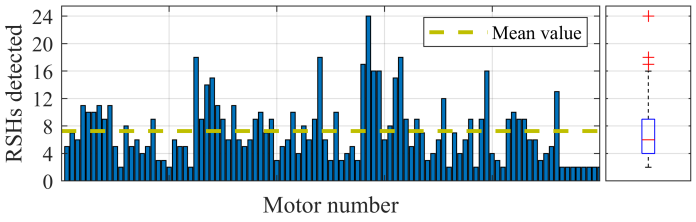

(a)

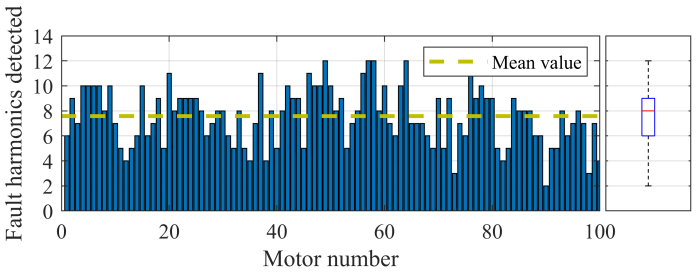

(b)

FIGURE 3.12: For each motor of the database: number of RSHs detected (a) and number of fault harmonics properly localized through the RSHs (b).

Concluding, the algorithm has been tested with an extensive and varied database giving a mean value of: 7.3 RSHs detected per motor, and 7.6 average number of fault harmonics localized. These results demonstrate the robustness of the method, since the slips estimated through the RSHs localized and their assigned pairs $[O_\nu, \nu]$ allow locating a high number of speed-dependent fault harmonics, thus verifying the coherence between the estimated O_ν and ν and the information available in the spectrum. Finally, it is also shown that the method is more robust in two-pole machines than those based on detecting RFSHs, as it was confirmed in more detail in [4].

3.8 Conclusions

A new SSE algorithm based on RSHs detection has been proposed, overcoming the main drawback of these techniques, i.e., need of knowing: the number of rotor slots R, the position of the RSHs in the spectrum, and their assigned ν index. The algorithm does not use as starting point the RFSHs (avoiding their low accuracy and low detectability for $p = 1$), neither assumes a certain interval for R or erroneously assigns $\nu = 1$ to the highest amplitude RSH, nor uses invasive solutions as no-load test, or inaccurate information, as the rated slip in the nameplate (as previous methods do).

This is the first SSE algorithm that automatically localizes the RSHs family, tracking several RSHs at the same time with one steady state current. It is completely general: works with different skewing angles, and with odd, even or not integer R/p (since it also detects RSHs with $k > 1$, even if for higher k, the RSHs amplitudes are lower). It precisely estimates the speed with high or low load, grid or frequency converter-fed (high or low fundamental frequency), and high or low slip (specifically tested under the most challenging conditions: low fundamental frequency and low slip).

This is achieved through a new RSHs frequency formula, used by a novel smart search method, which enables to automatically localize and characterize the RSHs (fixing its parameters O_ν and ν), converging when the slip information of the speed-dependent harmonics present in the spectrum (RSHs and up to 16 fault harmonics) matches, thus assuring the accuracy and reliability of the SSE.

The extensive experimental test demonstrates that the SSE algorithm can replace a 1000-line encoder, thanks to its high accuracy: absolute speed error is always below 0.05 rpm and the relative slip error is below 0.5% (0.01 rpm and 0.2% with a frequency converter; error obtained as the average error of 50 tests for each case analyzed). Finally, the field tests show the robustness of the method, since it is proved to work in 100 industrial motors covering all types of rated powers, voltages, speeds, poles pairs, and different operating conditions (21 motors with slips lower than 1%).

Concluding, it is an automatic, non-invasive, accurate, generally applicable and robust speed estimation method for induction motors, which, in addition, can be easily implemented in field monitoring systems due to its low computational burden and simple signal processing. This makes the algorithm a great candidate for use in continuous monitoring systems of motor health and efficiency in industrial environments.

Appendix A

Harmonics considered in Section 3.2.2:

$$f_{BBH_1} = (1 \pm k2s)\, f_0 \qquad f_{BBH_2} = \left[\tfrac{k}{p}(1-s) \pm s\right] f_0$$

$$f_{BBH_{Hilb}} = k2sf_0 \qquad f_{RFSH} = \left[1 \pm k\tfrac{(1-s)}{p}\right] f_0$$

$$f_{DEH} = \left[\tfrac{p(O_\nu - \nu) \pm n_D}{p}\,(1-s) + \nu\right] f_0$$

Bibliography

[1] J. Hsu, J. Kueck, M. Olszewski, D. Casada, P. Otaduy, and L. Tolbert, "Comparison of induction motor field efficiency evaluation methods," *IEEE Transactions on Industry Applications*, vol. 34, no. 1, pp. 117–125, 1998, doi: 10.1109/28.658732

[2] W. T. Thomson and M. Fenger, "Current signature analysis to detect induction motor faults," *IEEE Transactions on Industry Applications*, vol. 7, no. 4, pp. 26–34, 2001, doi: 10.1109/2943.930988

[3] M. Chirindo, M. A. Khan, and P. Barendse, "Analysis of non-intrusive rotor speed estimation techniques for inverter-fed induction motors," *IEEE Transactions on Energy Conversion*, vol. 36, no. 1, pp. 338–347, 2021, doi: 10.1109/TEC.2020.3007409

[4] J. Bonet-Jara, A. Quijano-Lopez, D. Morinigo-Sotelo, and J. Pons-Llinares, "Sensorless speed estimation for the diagnosis of induction motors via mcsa. Review and commercial devices analysis," *Sensors*, vol. 21, no. 15, 2021, doi: 10.3390/s21155037

[5] B. Lu, T. Habetler, and R. Harley, "A survey of efficiency-estimation methods for in-service induction motors," *IEEE Transactions on Industry Applications*, vol. 42, no. 4, pp. 924–933, 2006, doi: 10.1109/TIA.2006.876065

[6] P. Gangsar and R. Tiwari, "Signal based condition monitoring techniques for fault detection and diagnosis of induction motors: A state-of-the-art review," *Mechanical Systems and Signal Processing*, 2020, doi: 10.1016/j.ymssp.2020.106908

[7] S. H. Kia, H. Henao, and G. Capolino, "Diagnosis of broken-bar fault in induction machines using discrete wavelet transform without slip estimation," *IEEE Transactions on Industry Applications*, vol. 45, no. 4, pp. 1395–1404, 2009, doi: 10.1109/TIA.2009.2018975

[8] H. Guesmi, S. Ben Salem, and K. Bacha, "Smart wireless sensor networks for online faults diagnosis in induction machine," *Computers and Electrical Engineering*, vol. 41, no. 1, pp. 226–239, 2015, doi: 10.1016/j.compeleceng.2014.10.015

[9] S. B. Lee, D. Hyun, T.-j. Kang, C. Yang, S. Shin, H. Kim, S. Park, T.-S. Kong, and H.-D. Kim, "Identification of false rotor fault indications produced by online mcsa for medium-voltage induction machines," *IEEE Transactions on Industry Applications*, vol. 52, no. 1, pp. 729–739, 2016, doi: 10.1109/TIA.2015.2464301

[10] M. Korzonek, G. Tarchala, and T. Orlowska-Kowalska, "A review on mras-type speed estimators for reliable and efficient induction motor drives," *ISA Transactions*, vol. 93, pp. 1 – 13, 2019, doi: 10.1016/j.isatra.2019.03.022

[11] S. Maiti, V. Verma, C. Chakraborty, and Y. Hori, "An adaptive speed sensorless induction motor drive with artificial neural network for stability enhancement," *IEEE Transactions on Industrial Informatics*, vol. 8, no. 4, pp. 757–766, 2012, doi: 10.1109/TII.2012.2210229

[12] S. Das, R. Kumar, and A. Pal, "Mras-based speed estimation of induction motor drive utilizing machines' d- and q-circuit impedances," *IEEE Transactions on Industrial Electronics*, vol. 66, no. 6, pp. 4286–4295, 2019, doi: 10.1109/TIE.2018.2860530

[13] E. Zerdali, "Adaptive extended kalman filter for speed-sensorless control of induction motors," *IEEE Transactions on Energy Conversion*, vol. 34, no. 2, pp. 789–800, 2019, doi: 10.1109/TEC.2018.2866383

[14] Jung-Ik Ha and Seung-Ki Sul, "Sensorless field-orientation control of an induction machine by high-frequency signal injection," *IEEE Transactions on Industry Applications*, vol. 35, no. 1, pp. 45–51, 1999, doi: 10.1109/28.740844

[15] J. Holtz, "Sensorless control of induction machines—with or without signal injection?" *IEEE Transactions on Industrial Electronics*, vol. 53, no. 1, pp. 7–30, 2006, doi: 10.1109/TIE.2005.862324

[16] T. M. Wolbank, M. A. Vogelsberger, R. Stumberger, S. Mohagheghi, T. G. Habetler, and R. G. Harley, "Autonomous self-commissioning method for speed-sensorless-controlled induction machines," *IEEE Transactions on Industry Applications*, vol. 46, no. 3, pp. 946–954, 2010, doi: 10.1109/TIA.2010.2046288

[17] P. Phumiphak and C. Chat-uthai, "Non-intrusive method for induction motor field efficiency estimation using on-site measurement and modified equivalent circuit," in *2012 15th International Conference on Electrical Machines and Systems (ICEMS)*, 2012, pp. 1–5. [Online]. Available: https://ieeexplore.ieee.org/document/6401991

[18] A. G. Siraki and P. Pillay, "An in situ efficiency estimation technique for induction machines working with unbalanced supplies," *IEEE Transactions on Energy Conversion*, vol. 27, no. 1, pp. 85–95, 2012, doi: 10.1109/TEC.2011.2168563

[19] M. Al-Badri, P. Pillay, and P. Angers, "A novel in situ efficiency estimation algorithm for three-phase induction motors operating with distorted unbalanced voltages," *IEEE Transactions on Industry Applications*, vol. 53, no. 6, pp. 5338–5347, 2017, doi: 10.1109/TIA.2017.2728786

[20] A. K. Samanta, A. Naha, A. Routray, and A. K. Deb, "Fast and accurate spectral estimation for online detection of partial broken bar in induction motors," *Mechanical Systems and Signal Processing*, vol. 98, pp. 63–77, 2018, doi: 10.1016/j.ymssp.2017.04.035

[21] PDMA, *Introduction to MCEMAX*. [Online]. Available: https://www.pdma.com/PdMA-intro-mcemax.php

[22] Megger, *Instantaneous torque as a predictive maintenance tool for variable frequency drives and line operated motors*. [Online]. Available: https://es.megger.com/products/motor-and-generator-testing/dynamic-analyzers/baker-exp4000/technical/instantaneous-torque-as-a-predictive-maintenance-t

[23] M. Ishida and K. Iwata, "A new slip frequncy detector of an induction motor utilizing rotor slot harmonics," *IEEE Transactions on Industry Applications*, vol. IA-20, no. 3, pp. 575–582, 1984, doi: 10.1109/TIA.1984.4504454

[24] A. Bellini *et al.*, "On-field experience with online diagnosis of large induction motors cage failures using mcsa," *IEEE Transactions on Industry Applications*, vol. 38, no. 4, pp. 1045–1053, 2002, doi: 10.1109/TIA.2002.800591

[25] J. Jung, J. Lee, and B. Kwon, "Online diagnosis of induction motors using mcsa," *IEEE Transactions on Industrial Electronics*, vol. 53, no. 6, pp. 1842–1852, 2006, doi: 10.1109/TIE.2006.885131

[26] O. Keysan and H. B. Ertan, "Real-time speed and position estimation using rotor slot harmonics," *IEEE Transactions on Industrial Informatics*, vol. 9, no. 2, pp. 899–908, 2013, doi: 10.1109/TII.2012.2210231

[27] U. A. Orji and et al., "Non-intrusive induction motor speed detection," *IET Electric Power Applications*, vol. 9, no. 5, pp. 388–396, 2015, doi: 10.1049/iet-epa.2014.0274

[28] W. L. Silva, A. M. N. Lima, and A. Oliveira, "Speed estimation of an induction motor operating in the nonstationary mode by using rotor slot harmonics," *IEEE Transactions on Instrumentation and Measurement*, vol. 64, no. 4, pp. 984–994, 2015, doi: 10.1109/TIM.2014.2361554

[29] A. G. Yepes, J. Doval-Gandoy, F. Baneira, and H. A. Toliyat, "Speed estimation based on rotor slot harmonics in multiphase induction machines under open-phase fault," *IEEE Transactions on Power Electronics*, vol. 33, no. 9, pp. 7980–7993, 2018, doi: 10.1109/TPEL.2017.2773649

[30] A. Ferrah, K. G. Bradley, and G. M. Asher, "Sensorless speed detection of inverter fed induction motors using rotor slot harmonics and fast fourier transform," in *PESC '92 Record. 23rd Annual IEEE Power Electron. Spec. Conf.*, 1992, pp. 279–286 vol.1, doi: 10.1109/PESC.1992.254661

[31] R. Blasco-Gimenez, G. M. Asher, M. Sumner, and K. J. Bradley, "Performance of fft-rotor slot harmonic speed detector for sensorless induction motor drives," *IEE Proceedings - Electric Power Applications*, vol. 143, no. 3, pp. 258–268, 1996, doi: 10.1049/ip-epa:19960241

[32] Z. Gao, L. Turner, R. S. Colby, and B. Leprettre, "A frequency demodulation approach to induction motor speed detection," *IEEE Transactions on Industry Applications*, vol. 47, no. 4, pp. 1632–1642, 2011, doi: 10.1109/TIA.2011.2153813

[33] S. Luecke, J. Koupeny, and A. Mertens, "Induction machine speed tracking based on rotor slot harmonics using a modified pll approach," in *2016 18th European Conf. on Power Electron. and Applicat. (EPE'16 ECCE Europe)*, 2016, pp. 1–10, doi: 10.1109/EPE.2016.7695518

[34] K. D. Hurst and T. G. Habetler, "Sensorless speed measurement using current harmonic spectral estimation in induction machine drives," *IEEE Transactions on Power Electronics*, vol. 11, no. 1, pp. 66–73, 1996, doi: 10.1109/63.484418

[35] O. Keysan and H. B. Ertan, "Determination of rotor slot number of an induction motor using an external search coil," *Facta universitatis-series: Electronics and Energetics*, vol. 22, pp. 227–234, 2009, doi: 10.2298/FUEE0902227K

[36] W. J. Bradley, B. Mason, A. Pezouvanis, and K. M. Ebrahimi, "A sensorless speed estimation algorithm for use in induction motor fault detection applications." *Journal of Systems and Control Engineering*, vol. 228, no. 4, pp. 257–264, 2013, doi: 10.1177/0959651813511613

[37] S. Nandi, S. Ahmed, and H. A. Toliyat, "Detection of rotor slot and other eccentricity related harmonics in a three phase induction motor with different rotor cages," *IEEE Transactions on Energy Conversion*, vol. 16, no. 3, pp. 253–260, 2001, doi: 10.1109/60.937205

[38] S. Nandi, S. Ahmed, H. A. Toliyat, and R. M. Bharadwaj, "Selection criteria of induction machines for speed-sensorless drive applications," *IEEE Transactions on Industry Applications*, vol. 39, no. 3, pp. 704–712, 2003, doi: 10.1109/TIA.2003.810651

[39] Z. Liu, X. Zhang, X. Yin, and Z. Zhang, "Rotor cage fault diagnosis in induction motors based on spectral analysis of current hilbert modulus," in *IEEE Power Eng. Soc. Gen. Meet, 2004.*, 2004, pp. 1500–1503 Vol.2, doi: 10.1109/PES.2004.1373123

[40] G. Joksimović, E. Levi, A. Kajević, M. Mezzarobba, and A. Tessarolo, "Optimal selection of rotor bar number for minimizing torque and current pulsations due to rotor slot harmonics in three-phase cage induction motors," *IEEE Access*, vol. 8, pp. 228 572–228 585, 2020, doi: 10.1109/ACCESS.2020.3045766

[41] H. W. Penrose, "Appendix5: Stator slot and rotor bar tables," in *Electrical Motor Diagnostics 2nd Edition*. Sucess by Design, 2014. [Online]. Available: http://shop.btpubservices.com/Title/9780971245075

[42] J. Bonet-Jara, D. Morinigo-SOTELO, O. Duque-Perez, L. Serrano-Iribarnegaray, and J. Pons-Llinares, "End-ring wear in deep well submersible motor pumps," *IEEE Transactions on Industry Applications*, pp. 1–1, 2022, doi: 10.1109/TIA.2022.3166876

[43] C. McClay and S. Williamson, "The variation of cage motor losses with skew," *IEEE Transactions on Industry Applications*, vol. 36, no. 6, pp. 1563–1570, 2000, doi: 10.1109/28.887207

Chapter 4

End-ring wear in deep-well submersible motor pumps

This paper was published on April 12, 2022 in IEEE Transactions on Industry Applications journal belonging to IEEE publishing house with reference:

In the next sections, the full accepted author's version of the manuscript is reproduced, including abstract, appendixes and bibliography. Footnotes, which are not present in the original publication, are added in order to clarify some aspects within the general frame of this thesis.

Abstract

Wear of end-ring is to date an unreported and uninvestigated failure that very frequently takes place in deep well submersible motor pumps. The present paper first analyzes the particularities of these induction motors, especially their unusual rotor manufacturing process. Failure mechanism related to the end-ring wear is described, showing several examples of damaged rotors in a motor repair shop. Then, the difficulties of its diagnosis through conventional rotor asymmetry indicators are described, caused by the subtlety of this fault and the very easy appearance of false negatives. The end-ring wear detection through a multicomponent approach is researched through simulation, laboratory results and the diagnosis of two field motors showing that new fault alarm levels need to be defined. To perform this last step and for the first time in the technical literature, two induction motors working in a deep borehole have been continuously monitored (one measure every six operating hours) for almost one year.

Keywords: diagnosis; induction motor; pump; false negative; end-ring.

4.1 Introduction

The type of rotor faults in induction motors highly depends on the rotor manufacturing process [1]. In the case of copper or aluminium fabricated rotors, the failure mainly consists in the breakage of the bar (typically at the joint with the end-ring), and its detachment from it [2]. Once the rotor core is assembled in these motors, putting together a set of thin ferromagnetic laminations, previously copper or aluminium fabricated bars are inserted in the lamination holes and swaged. The bars slightly exceed the rotor core and are shortcircuited by brazing or welding them to an end-ring (a previously fabricated solid circumferential piece of copper or aluminium). A certain space is left between the end-ring and the rotor core, where the bars can be clearly seen. In that space is where the bar breaks and detaches from the end-ring [3]. In the case of die-cast aluminium, bars and end-ring are moulded altogether with the rotor core, being its main failure porosity or melting [4], since when end-rings and bars form a unique piece, crack and detachment problems disappear.

Rotor cage failure accounts for 5-15 % of induction motor failures [5]. Nevertheless, none or very few are related to the breakage of the end-ring itself. As analyzed in the present paper, the type of failure in deep well submersible motor pumps is very different. These motors use previously fabricated copper bars, but instead of being a solid piece, the end-ring is made of several copper sheets with the same shape as the ferromagnetic laminations. These sheets are stacked until they cover the bar endings that remain out of the rotor core. Then, the gaps between the end-ring sheets and the bars are filled with liquid copper soldering, and a coat of paint is applied to the rotor. This assembly process is shown in Fig. 4.1.

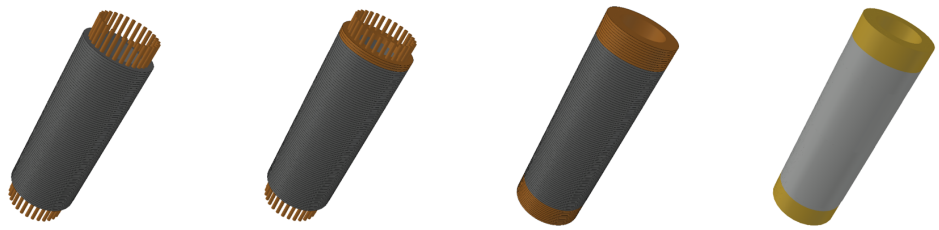

(a) (b) (c) (d)

FIGURE 4.1: Rotor assembly of a deep well submersible motor: copper bars with ferromagnetic laminations (a); some (b) and all (c) of the copper sheets of the end-ring and its final copper liquid soldering plus the paint coating (d).

As will be demonstrated with several real field cases throughout the article, the end ring wears very often due to internal cooling water and high-speed rotation. The liquid copper solder, which unites the bars and end-ring sheets, gradually losses material until the copper sheets appear. Then, pieces of the copper sheets themselves might detach, exposing the bars which are initially covered. At the beginning of the failure mechanism, wear appears on some end-ring segments, being too subtle to be detected. Then, the unequal wear uniformly extends to the whole end-ring, cancelling the initial asymmetry, which might cause the appearance of a false negative. Concluding, the detection of this type of failure is a challenging problem.

No papers have investigated end-ring wear and very few address end-ring breakage. It has been stated that broken end-ring segments cause a periodic fluctuation in the line current and rotor speed [6] (basis of rotor asymmetries detection via current spectrum). More precisely, end-ring faults produce the same harmonic components in the stator line current as rotor bar faults [7]. This has been confirmed by simulation using models of induction motors based on inductances calculation [8] and Finite Element Methods [9]; it has also been proven through simulation the appearance of harmonics in torque and speed [10].

Since in conventional motors, end-ring breakage is much less frequent than bar breakage, most studies focus on the latter failure. On the other hand, as stated through the paper, end-ring wear (typical of deep well motors) always causes false negatives. Therefore, to find similarities, it is important to survey the false negative caused by non-adjacent broken bars (which might also cancel rotor asymmetry) when only the Lower Sideband Harmonic (LSH) is monitored [11]–[13]. To solve the problem of false negatives, some authors propose to monitor fault harmonics different than LSH [14], [15]. Instead of using a single current, other authors have proposed to obtain the phase currents to calculate the zero-sequence current [16] and Park's vector [17], or analyze the spectrum of other magnitudes as the flux [18]–[21]. Nevertheless, phase currents are not always available for motors submerged at least 50 m, while it is impossible to measure the flux. Finally, only one paper shows the possible appearance of false negatives under several broken end-rings [22].

This paper, which is an extended version of the contribution presented at the IEEE 13th international SDEMPED conference [23], is the first in which end-ring wear in deep well submersible pump motors is investigated, which is a challenging problem due to the subtle appearance of the failure at its beginning, and the possible occurrence of false negatives when severity increases. Its detection is crucial in deep well motors predictive maintenance since

end-ring wear highly contaminates the water that internally cools the motor, increasing the chances to cause secondary damage in bearings and stator insulation.

4.2 Deep well submersible motor pumps: special features and failure mechanism.

The rotor manufacturing process for this type of motor, and particularly its end-ring, has been explained in the introduction. The widespread end-ring wear problem has also been presented. In this section, the end-ring wear failure mechanism is described using real field cases of damaged rotors (pictures from the motor repair shop are presented). Previously, the unique features of this type of motor are synthesized:

4.2.1 Special features of induction motors in deep well submersible pumps.

Submersible pumps are mainly used for water supply extracted from aquifers at depths from 50 to 500 m (Fig. 4.2) where the motor-pump set elevates the water to a tank through a pipeline. The motor-pump set works submerged in the aquifer, with the motor-pump shafts directly coupled and in vertical position (the motor underneath the pump and the water inlet between them). Sometimes, to externally cool the motor, a metal cover is placed embracing the motor to force water to flow between the cover and the motor surface before entering the inlet (Fig. 4.3). The motor frame, which is smooth and without heat sinks, is internally cooled by prefilling with a mixture of water and glycol[1]. Carbon or stainless steel thrust bearings are used to support the weight of the entire assembly.

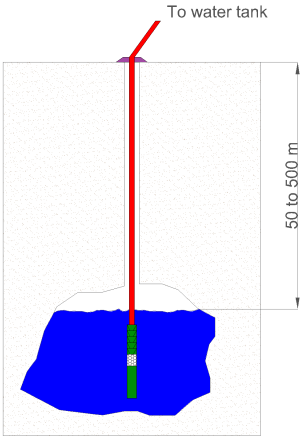

FIGURE 4.2: Motor-pump set submerged in an aquifer with a 50 to 500 m piping elevating the water to a tank.

[1]This cooling mechanism, followed by several big manufacturers as Pleuger, Aturia or Caprari, consists of prefilling the motor (before entering operation) with a fluid (normally a mixture of water and glycol), through a valve place on the casing of the motor. The fluid then acts as an internal cooler as it flows between the rotor outer surface and the stator inner surface, being moved by the rotational force generated by the rotor. In order to balance the pressure between the outside and the inside when the cooling fluid heats up due to operation, compensation valves are installed in the motor casing.

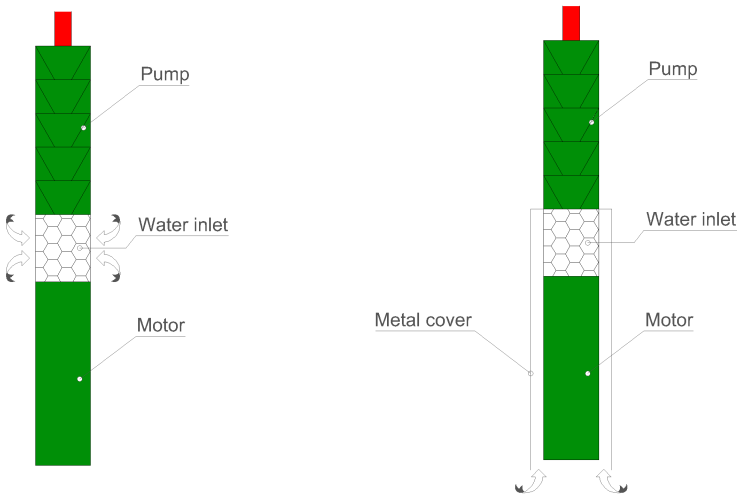

FIGURE 4.3: Motor-pump set without (a) and with (b) metal cover to force water flowing through the motor surface before entering the water inlet.

The borehole drilled to reach the aquifer has a small diameter to reduce excavation costs. This determines the motor design with a small diameter, together with the insulation needed for underwater operation. Rotor cage with skewed bars induction motors are used, with a length proportionally high compared with its small diameter. One-pole pairs design is used to achieve high power with a reduced motor size, as its high rotating speed increases output hydraulic power, but also components wear. Motors are fed at least with a soft-starter to prevent startup peak currents and preferably with a frequency converter, which also permits to adjust the pump speed. Nowadays, all new motors are converter-fed. Motors are operated at a fixed speed, without significant load or grid oscillations; therefore, FFT signal analysis can be applied for monitoring purposes.

4.2.2 Failure mechanism of deep well submersible motor rotor.

As stated in the introduction, once manufactured, the copper rotor structure is very similar to an Al die cast rotor (without porosity problems). Therefore, rotor bars cannot break as they do in standard copper rotors. The only rotor asymmetry that might take place is caused by the degradation of the end-ring liquid soldering, which glues the copper laminations and the bars together, constituting the end-ring. The internally cooling water flows in contact with the rotor and stator windings. The copper liquid soldering is especially delicate and very often starts to lose material. Water is propelled by the rotor, which rotates at a high-speed (due to the use of one-pole pairs), boosting the liquid soldering erosion: its degradation causes wear in the end-ring segments between the bars, together with loss of contact between the bars inserted in the lamination end-rings. Figure 4.4 shows photos of several rotor end-rings in a motor repair shop: new (a) and with different degrees of wear in (b), (c) and (d). Water suspended particles, detached from the rotor, are shoot to the inner part of the stator by the centrifuge force. Some

of these particles might impact the winding, breaking the insulation, which is what usually happens when parts of a rotor bar are detached in standard copper rotor induction motors.

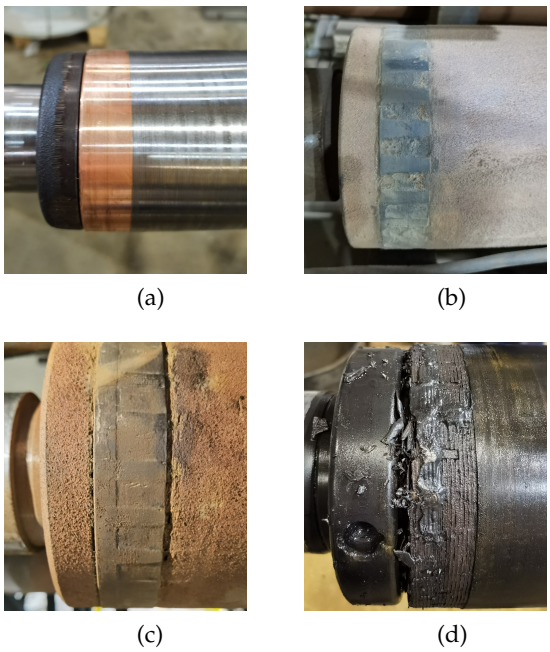

(a) (b)

(c) (d)

FIGURE 4.4: Rotor end-rings of deep well submersible motor pumps, in a motor repair shop: new (a) and different wear conditions (b), (c) and (d).

End-ring wear is not easy to be detected. Even if wear starts on some point of the end-ring (for instance, in a segment between two bars), it will spread over the whole end-ring; then, the process starts again, increasing the wear in another segment gradually spreading to the rest of the end-ring. Initially, the wear may be too subtle to cause fault harmonics to appear in the line current, making detection impossible. Once the failure has expanded to other segments, the effects may be cancelled out, leading to the appearance of false negatives.

Concluding, end-ring wear is a widespread failure in induction motors of submersible pumps (unlike end-ring breakage in standard induction motors), which might cause severe secondary damage in other components. It is difficult to detect since it might be too subtle at the beginning, and once it becomes widespread, it can lead to false negatives.

4.3 Rotor end-ring wear: false negatives.

In this section, the problem of issuing false negatives when diagnosing the wear of end-ring segments in deep well motors through the LSH monitoring is addressed for the first time (LSH is the main rotor asymmetry harmonic, with frequency at $(1-2s)f$ Hz, being f the fundamental supply frequency). To serve this purpose, a model of an induction motor (whose parameters are in Appendix A), has been used to study the harmonics present in the current under end-ring wear.

4.3.1 Squirrel cage induction model

The dynamic model used in this paper has been implemented in MATLAB and solved using a 4th order Runge-Kutta method with a simulation step size of 10^{-4} s and the following general characteristics: constant air-gap, infinite iron permeability, no saturation and arbitrary number of spatial harmonics considered in inductance and torque calculations.

As for the particular characteristic of the rotor, the electrical equation for the Nth rotor loop can be described as:

$$\begin{aligned} 0 = i_{l(n)} \left(R_{b(n)} + R_{b(n+1)} + R_{uers(n)} + R_{lers(n)} \right) - i_{l(n-1)} R_{b(n)} - \\ - i_{l(n+1)} R_{b(n+1)} - i_{er} R_{lers(n)} + \frac{d\Psi_{l(n)}}{dt} \end{aligned} \tag{4.1}$$

And for the lower end-ring:

$$0 = \sum_{n=1}^{Nr} \left(\left(i_{l(n)} - i_{er} \right) R_{lers(n)} + \frac{d\left(i_{l(n)} - i_{er} \right)}{dt} L_{\sigma lers(n)} \right) \tag{4.2}$$

Where $i_{l(n)}$ is the current of the Nth rotor loop, i_{er} the end-ring current, $\Psi_{l(n)}$ the total flux linkages of the Nth rotor loop, $R_{b(n)}$ the resistance of bar Nth, $R_{uers(n)}$ and $R_{lers(n)}$ the resistances of the Nth upper end-ring segment and the lower end-ring segment, and $L_{\sigma lers}$ the leakage inductance of the Nth lower end-ring segment.

The wear of an end-ring is modelled as an increase in the impedance of any of its segments. The model input is a three-phase, 400 V, 50 Hz, perfect sinusoidal voltage, sampled at 20 kHz. Finally, one of the resultant currents is processed to analyze the rotor asymmetry harmonics amplitude.

4.3.2 False negatives due to low severity of end-ring wear.

As stated in the introduction, end-ring faults cause the appearance of the same fault-related harmonics as bar breakages. To simulate the wear of an end-ring segment, the resistance of one of them has been multiplied by 1.25; Fig. 4.5 shows the spectral density of the simulated line current (in dB with respect to the fundamental component). End-ring wear affects both the resistance and the inductance of the end-ring. In this paper only the resistance is increased to simulate the rotor asymmetry. Nevertheless, the amplitude of the current in the bar progressively decreases, similarly as if the inductance is also increased. Therefore, there is no difference in the rotor asymmetry created in terms of amplitude of the LSH generated, which is the final objective of the analysis.

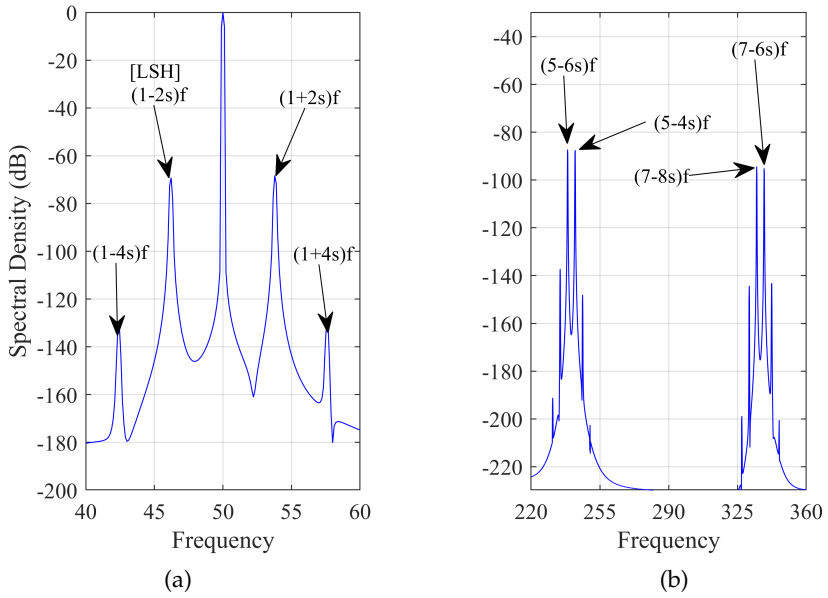

FIGURE 4.5: First (a) and second (b) family of the main harmonics produced by end-ring segment fault (resistance increased by 25%) in the spectrum of the simulated line current of a 4 kW IM operating at 0.038 slip (amplitude in dB with respect to the fundamental component).

As can be seen, the main rotor fault harmonics are present (first family Fig. 4.5a, second family Fig. 4.5b), but with low amplitudes. Classic rotor fault alarm thresholds use the LSH amplitude: between -45 and -36 dB, incipient failure with even one or two broken bars; above -36 dB, multiple broken bars. As stated through several simulations with this motor, segment resistance must be multiplied by 6.5 and 80 to achieve LSH amplitudes of -45 and -36 dB respectively. On the other hand, a complete segment breakage is more severe than a complete bar breakage: -34 and -38 dB respectively. Concluding, classic LSH thresholds cannot be used if end-ring wear is to be detected before it may be too late to avoid water contamination, as the failure might be too subtle for these limits, thus issuing a false negative.

4.3.3 False negatives in double segments wear.

The motor has been simulated for all possible combinations of double end-ring segment faults (segments: 1-2, 1-3,...,1-28) in one of the end-rings. The fault is modelled as an increase of 25% in the segment resistance. Since the pattern is repetitive, results are only depicted for one pole pitch (90 mechanical degrees, 7 combinations). Figures 4.6a and 4.6b show the amplitude of the LSH and the second family of fault harmonics under double fault, normalized with respect to the amplitude under single fault ($A_{1-2}/A_1, A_{1-3}/A_1, \ldots, A_{1-7}/A_1$) and as a function of the second fault position ($360/28, 2 \cdot 360/28, \ldots, 7 \cdot 360/28$), as well as the theoretical pattern for double bar faults (solid lines) [14]. As can be seen, under double end-ring segments faults, the normalized amplitude of the fault harmonics describes the same pattern as in the case of broken bars. Therefore, both cases, end-ring and bar faults, face the same diagnostic problem.

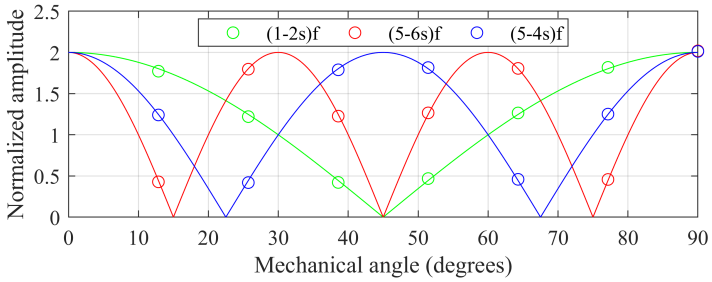

(a)

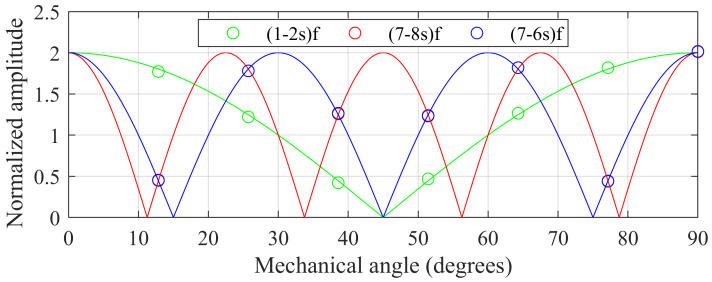

(b)

FIGURE 4.6: Theoretical (line) and simulated (circles) amplitude of the main fault harmonics under double faults, normalized with respect to the amplitude under single fault, for each combination of double end-ring segment faults (resistance increased by 25) in one pole pitch; (a): (1-2s)f, (5-6s)f, (5-4s)f ; (b): (1-2s)f, (7-8s)f, (7-6s)f.

It should be noticed that this problem is of significant importance in the rotor of the submersible motor pumps described in Subsection 4.2, since the degradation of the end-ring weld takes place in different segments, thereby leading to the false negative issues just discussed.

4.3.4 False negatives in multiple segments wear.

Amplitude patterns for double worn end-ring segments of the previous subsection give an excellent insight into dealing with non-adjacent faults. Nevertheless, as confirmed by visual inspection at the motor repair shop, the friction between the end-rings and the inner cooling-water and the particles that there might be in it wears the weld in almost every segment but with different severity. Therefore, at least in a first approximation, the wear process can be regarded as a randomly increasing wear of the end-ring segments.

To get an insight on harmonic amplitude patterns in this situation, four fault severity conditions have been defined for each segment of the rotor upper end-ring: resistance increased by 5, 10, 17 and 25%. Then, each segment has randomly gone through the different increasing fault states (e.g., Sim(#1): seg(#17) at fault state 1; Sim.(#2): seg(#17) at fault state 1 and seg(#10) at fault state 1; etc.). Moreover, the process has been designed so that between some consecutive simulations, the rotor fault condition may remain the same (e.g., Sim(#32) and Sim(#33) with the same segments worn and the same severity), as it could happen between consecutive measures in a real case.

Figure 4.7a shows the amplitude evolution (in dB with respect to the fundamental component) of the main fault harmonics from the first simulation to the simulation #200, in which 75% of the segments have reached their final fault state; Fig. 4.7b shows the fault evolution of each

segment of the upper end-ring for the same range of simulations. As can be seen, the $(5-6s)f$ component has the same pattern as the component at $(7-6s)f$, while both are different from the $(5-4s)f$ pattern. It should be noticed as well that, for this particular number of rotor bars, the harmonic at $(7-8s)f$ describes the same evolution as the ones at $(5-6s)f$ and $(7-6s)f$. These results are in agreement with those shown in Fig. 4.6 for double faults.

It can be concluded from Fig. 4.7a, that a long period condition monitoring (e.g., biannual measurements) based exclusively on the LSH followup can be especially unreliable for this wear process since its amplitude is always under classic rotor damage thresholds, being even nearly as low as in a healthy state when 75 % of the segments are damaged. Although the same problem might also be encountered with multiple non-adjacent broken bars (principally in HV machines with frequent transient stresses [13], [21]), the number of broken elements is small when compared to the number of segments that deteriorate in the rotors described in this paper. Therefore, given the extra difficulties with respect to non-adjacent broken bars, it is of particular interest for these machines to develop a reliable indicator to monitor the end-ring condition.

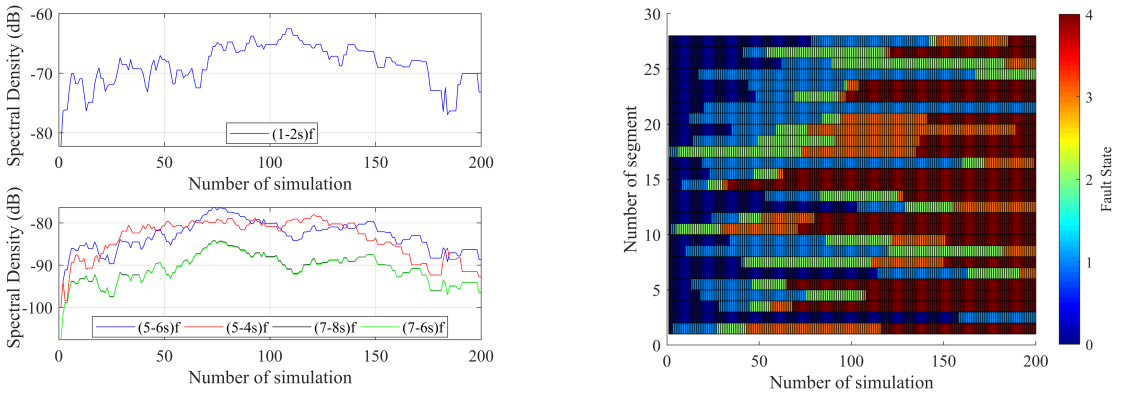

FIGURE 4.7: Amplitude evolution (in dB with respect to the fundamental component) of the main fault harmonics (A) and fault state evolution of each segment of the upper end-ring (B) from the first simulation to simulation #200, in which 75% of the segments have reached their final fault state.

4.4 Experimental results

The purpose of this section, which can be achieved by performing the test with a standard induction motors, is: first, an understanding of the behaviour of the rotor asymmetry harmonics under multiple and progressive segment degradation, and second, a procedure to identify that a fault is in progress in a real motor. Testing a submersible motor would require a well, a pump coupled to the motor, a crane to put the motor inside the well and a system of pipelines and valves to regulate the load. The critical aspect that prevents to test this type of motor outside a well is the surrounding water going inside the pump inlet to create convection heat transfer which cools the motor and avoids over-heating. Since these means cannot be found in an academic lab, a standard squirrel cage induction motor (2.2 kW, 2-p, 28-bars, 230 V, 8.5 A, 1420 rpm, Δ connection, line-fed) is tested instead, under several fault states. More precisely, two identical induction motors are coupled by their shafts, one fed by the grid, and the other by a frequency converter. By decreasing the feeding frequency of the second machine, the tested

motor is driven to its rated load. Then, the line current is measured to perform MCSA. Finally, the conclusions about motors behaviour under the end-ring degradation acquired with standard motors are verified with submersible pump motors in the real field cases shown in the next section.

Why not using vibrational analysis? It is hard to be performed in deep-well submersible motors, as it requires to place the sensors in the body of the machine, which in this case is located inside an aquifer up to 500 m depth. The long data transmission cable hinders the measurements, since it introduces capacitances into the sensor circuit distorting the vibration signal. Moreover, it is difficult to find a sensor robust enough to deal with such a harsh environment: underwater operation with dirt, mud, etc. Therefore, only Pt-100 temperature sensors, with motors especially designed to place the sensor inside the sealed motor, are used at these depths by water distribution system operators.

After testing the motor in a healthy state, holes have been drilled in different end-ring segments between the bars (as seen in Fig. 4.8). Segment 1 has been drilled to 11 mm depth out of 18.5 mm. Then, to compensate for the rotor asymmetry, segments 4 and 5 have been worn (exact compensation would be between these two segments) by producing holes of smaller amplitudes but similar depths (11 mm). Finally, segments 2 and 3 have also been worn with 14 mm deep holes. Figure 4.9 shows the final rotor state.

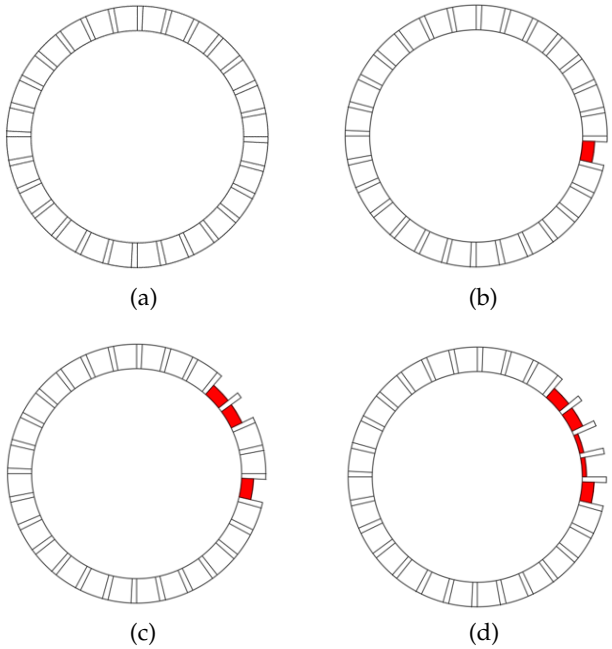

FIGURE 4.8: Transversal section of the end-ring, showing the segments between the bars, and the progressive fault tested: healthy (a), segment 1 drilled 11 mm (b), segments 1, 4 and 5 drilled 11 mm (c) and finally drilling 14 mm in segments 2 and 3 (d).

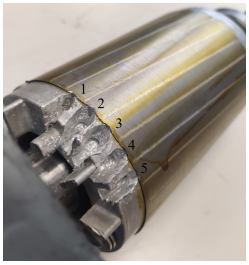

FIGURE 4.9: Rotor after wearing end-ring segments 1, 4 and 5 (11 mm deep hole), and segments 2 and 3 (14 mm deep hole).

Figure 4.10 shows the LSH amplitude(in dB with respect to the fundamental component) in the line current spectrum for these four states with the motor operating at 100 % of rated load. It can be seen how after the wear of segments 1, 4 and 5, the LSH amplitude is even smaller than when the motor was healthy. Moreover, when comparing fault state 1 (only segment 1 worn) with fault state 3 (segments 1, 2, 3, 4 and 5 worn), it is observed that the amplitude of the LSH is approximately the same. In none of the faulty states, the LSH reaches an amplitude usually considered as the starting of a rotor fault (-45 dB), even if the rotor has been seriously damaged, as seen in Fig. 4.9. Therefore, a single measurement of the LSH amplitude would not raise the alarm on the rotor condition in any of these four states. Moreover, even for severe faulty conditions, the indicator might be the same as in the healthy state due to asymmetry cancellation. Concluding, a single measurement of the LSH in a faulty rotor will cause a false negative.

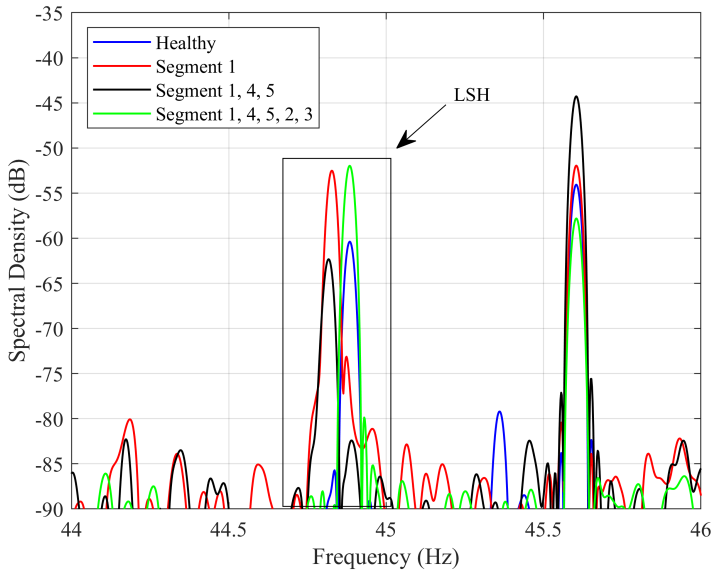

FIGURE 4.10: LSH amplitude in the line current spectrum for the four fault states tested (in dB with respect to the fundamental component).

Figure 4.11a shows the evolution of the LSH amplitude, from the healthy state to the wearing of the segments 1 to 5, passing through the two intermediate faulty states (only segment 1 worn and segments 1, 4, 5 worn). For each state, five measurements at full load are shown. Fig. 4.11b shows that same result related to four other rotor fault harmonics, selected, as explained in Section 4.3, for having significantly different amplitude patterns against double faults. These laboratory results emulate the periodic monitoring of a field motor.

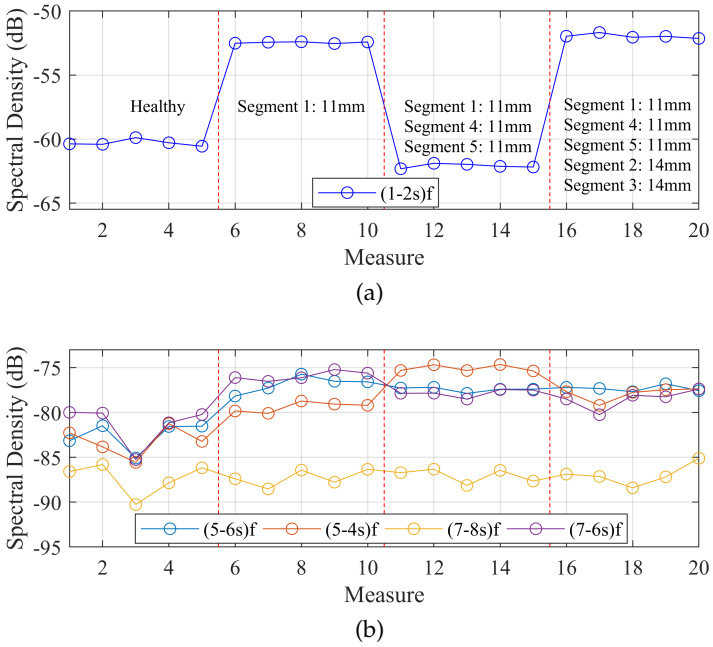

FIGURE 4.11: Lab emulation of a field periodic monitoring of the LSH amplitude (a) and four significant rotor fault harmonics (b): five measurements per fault state, separated with vertical dotted lines.

The analysis of the LSH amplitude from time to time measurements would not provide enough valuable information. The rotor would be categorized healthy, considering that, for every case analyzed, the LSH amplitude is significantly lower than the early stage alarm threshold (-45 dB) commonly used in industry. Nevertheless, the time evolution of the LSH amplitude clearly shows that a rotor failure is developing: changes of 7 to 10 dB are observed, while, as analyzed in the lab, load oscillations generate changes of only 0.5 dB approximately. If the measurements are from a deep-well motor, where end-ring wear is likely to occur, these changes are sufficient to alert maintenance personnel that a failure is occurring. Therefore, it is not important in these motors how large the LSH is, especially knowing that a severe fault might not show up as a large LSH since the rotor asymmetry might cancel out. Concluding, new alarm thresholds should be defined related to the rate of change in the LSH amplitude for this type of motors.

Concerning the evolution of the harmonics shown in Fig. 4.11b, the $(5-4s)f$ (red) is especially important: at the healthy state, the amplitude oscillates between -85 to -81 dB, increasing to -79 dB in the first faulty state, increasing again to -75 dB in the second faulty state (when LSH decreases to healthy state values) and finally decreasing to -78 dB in the last state (when LSH increases back to -52.5 dB). Therefore, it is a good complement for the LSH monitoring to detect the end-ring wear. On the other hand, the evolutions of the harmonics depicted in blue and black also show different complementary patterns, not decreasing that much as the LSH in the third state but also maintaining their amplitudes at the final state. Finally, the pattern of the harmonic plotted in green does not seem to give significant information.

Finally, it is worth noting that the operation of the motor in the harsh environment of a deep well does not affect the proposed indicator. The motor is sealed to prevent from contamination, and it is designed with pressure stabilizer; therefore, only changing temperature might affect the inside. The aquifer in which the motor is submerged at a high depth tends to stabilize

the temperature. Changes might appear as the year seasons take place, load increases, or malfunctioning appears (that is why Pt-100 temperature sensors are installed inside high power motors). Nevertheless, a temperature change would affect the whole rotor, without increasing its asymmetry. Therefore, changes in the LSH amplitude will only be related to an increase in end-ring wear.

4.5 Field cases

Two deep well motors from two different pumping stations are continuously monitored, measuring all their startups and a steady-state every six operating hours (500 s each). FFT is used to calculate the current spectrum, and faulty harmonics are localized and their amplitudes quantified.

4.5.1 Field case 1

The first motor is a Caprari M12230 (230 HP, 1-p, 30 bars, 380 V, 335 A, 2950 rpm), fed with a frequency converter (model SD7058055 from Power Electronics), installed in a deep well at 118.87 m from the ground. Figure 4.12 shows the time evolution (a measure every six operating hours) of the LSH amplitude (in dB with respect to the fundamental component) during nearly a year (2020). Horizontal dotted red lines represent the thresholds used in the industry to consider the appearance of bar breakages: between -45 and -36 dB, incipient failure with even one or two broken bars; above -36 dB, multiple broken bars. The data gaps in the middle of March, end of June, and end of August are periods in which problems with the remote control of the measurement equipment could not be rapidly solved due to the Covid situation.

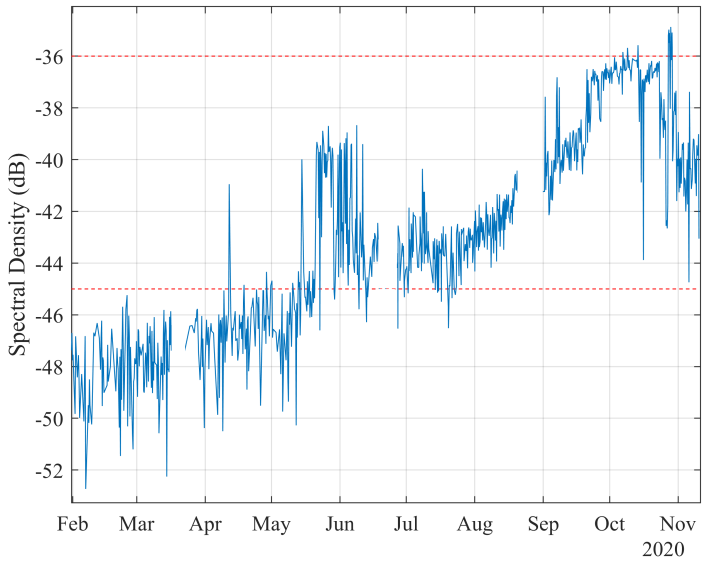

FIGURE 4.12: Time evolution (a measure every 6 operating hours) of the LSH amplitude (in dB with respect to the fundamental component) of the first pumping station motor continuously monitored.

As can be seen, the LSH amplitude starts to increase slowly very soon from the first measurement and, in approximately two and a half months, surpasses the -45 dB threshold. Then, in the middle of May (one month later), it increases very quickly to -40 dB, to suddenly drop to -44 dB after a month. Then, the tendency is to slowly but continuously increase until reaching -36 dB in October and approximately keep this level until descending again in November to -40 dB. This ratio of change in the LSH amplitude indicates the presence of severe end-ring wear. In addition, during the last month, stator winding fault harmonics $(n(1-s)/p \pm k)f$ increased dramatically as shown in Fig. 4.13. The pump replacement can be finally planned; the motor is drawn from the well at 118.87 m and send to the motor repair shop.

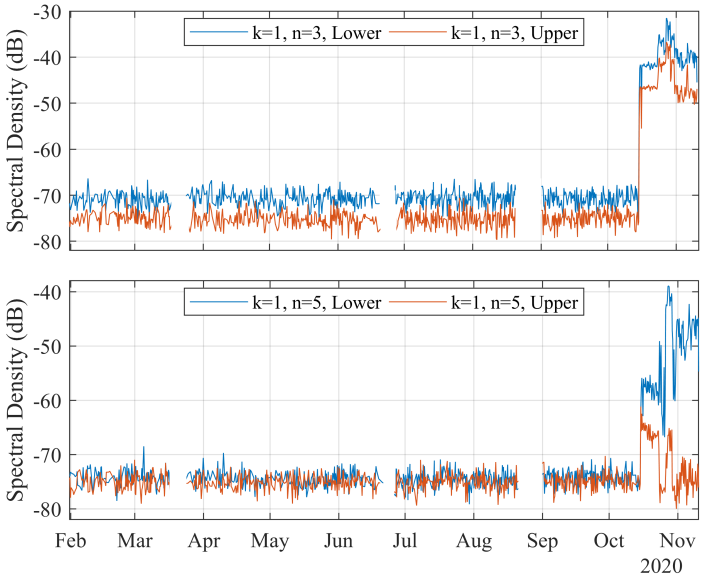

FIGURE 4.13: Time evolution (a measure every 6 operating hours) of the stator winding fault harmonics amplitude (in dB with respect to the fundamental component) of the first pumping station motor continuously monitored.

Figures 4.14a and 4.14c show two different perspectives of the rotor upper end-ring (near the coupling with the pump), while Figs. 4.14b and 4.14d show two different perspectives of the lower end-ring (at the bottom part of the motor-pump set). It can be observed how both end-rings have lost most of the copper liquid soldering: the copper sheets can be observed, even distinguishing the position of the copper bars (opposite to the healthy rotor shown in Fig. 4.4a). The upper end-ring is particularly damaged, with parts of the copper sheets detached, exposing some copper bars. In the lower end-ring, some material has been settled in the lower part of the side shown in Fig. 4.14d (probably due to gravitation).

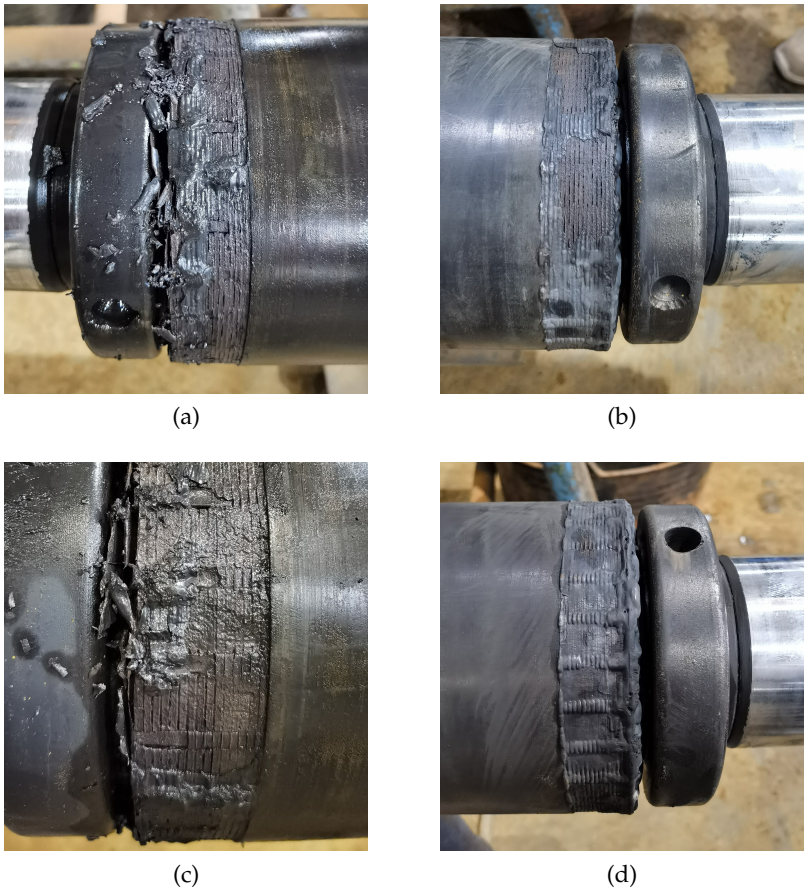

(a) (b)

(c) (d)

FIGURE 4.14: Worn rotor end-rings (upper in (a) and (c) and lower in (b) and (d)), of the first motor being monitored and repaired in the motor repair shop.

The unequal end-rings wear in their different perspectives explains the changes in the LSH amplitude: when some material is detached from some part of the end-ring, its asymmetry increases, while it balances when the rest is worn too. Not only the end-ring is worn, but also its contact with the bars through the loss of the copper liquid soldering that glues end-ring sheets and bars together, and the degradation of the end-ring sheets itself, particularly at the contact position with the bars, even exposing the bars which are covered initially. The ratio of change in the LSH enabled the fault detection and the motor replacement.

Unfortunately, the material detached from the end-ring polluted the water that internally cools the motor. Since the water, propelled by the rotor, rotates at high speed, suspended particles are naturally shoot to the inner part of the stator. Some of these particles might impact the winding, breaking the insulation, which is what usually happens when parts of a rotor bar are detached in standard copper rotor induction motors. Therefore, this is probably the cause of the stator winding insulation degradation, also detected in Fig. 4.13: the stator insulation resistance (measured in the motor repair shop) was below the company quality standards, prompting the stator rewinding.

It is worth to conclude that, continuously monitoring changes in the LSH amplitude can reveal early stage degradation of the rotor. Nevertheless, since the liquid soldering can be easily replaced in the motor repair shop, the true objective is to prevent the appearance of winding damages, caused by the detached rotor particles suspended in the internally cooling water, which propelled by the rotor might impact the stator, causing damage expensive to be

repaired.

4.5.2 Field case 2

The second motor is an Aturia N12-340 (340 HP, 1-p, 28 bars, 380 V, 475 A, 2900 rpm), fed with a soft-starter (model V50900 from Power Electronics) and installed in a deep well at 170.3 m from the ground. Figure 4.15 shows, from top to bottom, the time evolution of the LSH, the $(5-6s)f$ and the $(7-6s)f$ amplitudes (in dB with respect to the fundamental component) during nearly a year (2020). In this case, the LSH remains below the lower band of the classic LSH thresholds (-45 dB) during the whole period. However, as can be seen, from June onwards, the typical pattern of ups and downs begins to be observed. The LSH amplitude slowly decreases from -58 to -63.5 dB in August. Then, it goes up to -61.5 dB, where it remains stable until the end of September, when it reaches -59.7 dB. Finally, in the last month, several sharp changes are reported with variations between -2 and -4 dB. This could mean that the end-ring wear is developing. The pattern is even more evident with the $(5-6s)f$ and the $(7-6s)f$ harmonics, particularly in the latter, as the change ratio goes from 5 to 20 dB. Finally, it should be noted that the $(5-6s)f$ and $(7-6s)f$ patterns are very similar, which is in line with what has been shown in the previous sections.

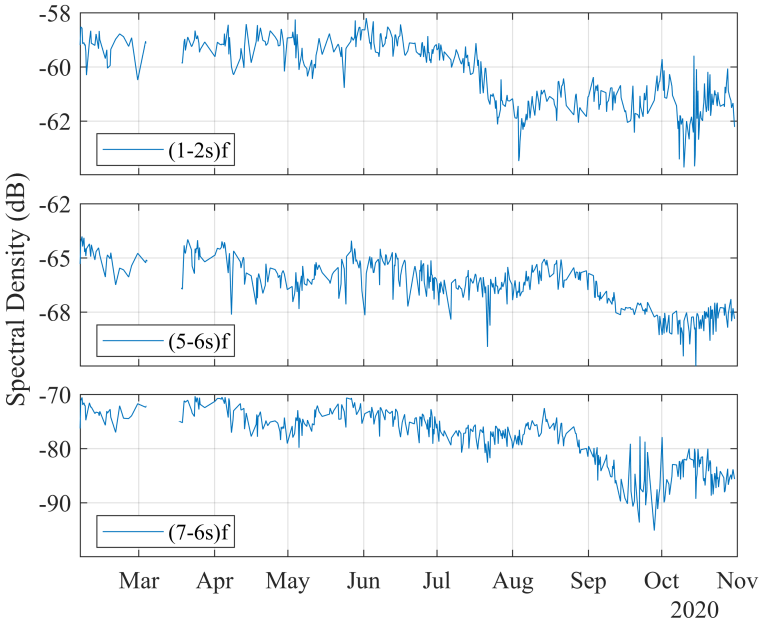

FIGURE 4.15: Time evolution (a measure every 6 operating hours) of the rotor asymmetry harmonic amplitudes (in dB with respect to the fundamental component) of the second pumping station motor continuously monitored.

The first intention was to continue monitoring this motor until the failure was more advanced. Unfortunately, the coupling between the motor and the pump broke down at the end of October, and as a result, the motor had to be drawn. Nevertheless, thanks to the continuous monitoring, it was possible to warn the company that an eccentricity problem was taking place, so they could make arrangements to avoid an unscheduled outage. The increase

in eccentricity was detected by measuring the Upper Mixed Eccentricity Harmonic (UMEH)[2]: $(1 + (1 - s)/p)f$; lower harmonic is not usually detected in this type of motor (it might also be removed when filtrating the DC component, due to its proximity). Figure 4.16a shows the UMEH time evolution and how, in the middle of September, the amplitude began to increase. Contrary to the LSH, eccentricity harmonics do not have a universally accepted threshold to correlate the UMEH amplitude with a certain degree of eccentricity. Nevertheless, the sudden change in its amplitude explains well what was finally analyzed in the motor repair shop. Figures 4.16b, 4.16c and 4.16d show the eventually broken down coupling between the motor and the pump. When the coupling breaks down, the forces that create the eccentricity highly decrease, and the rotor goes back to its natural position: that is why the UMEH amplitude decreases at the end of Fig. 4.16a. Since the motor is in the lower part of the system (Fig. 4.3), it receives the weight of all the water and the pump. Therefore, friction between the two broken shafts is high, and the pump stills rotating.

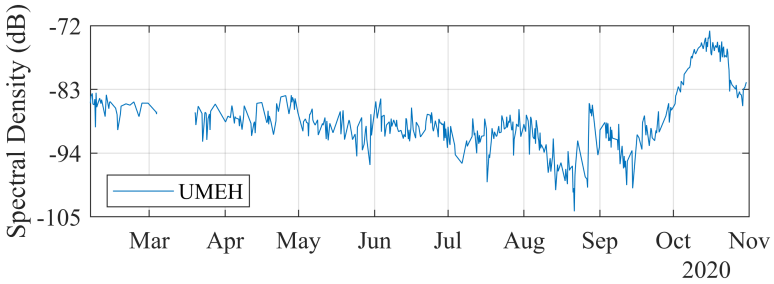

(a)

(b)

(c)

(d)

FIGURE 4.16: Time evolution (a measure every 6 operating hours) of the UMEH (in dB with respect to the fundamental component) of the second pumping station motor continuously monitored (a); photos of the broken coupling between the motor and the pump: part attached to the motor from two different perspectives (b) and (c) and part to be connected to the pump (d).

[2]Rotational Frequency Sideband Harmonics are also known in literature as Mixed Eccentricity Harmonics. The first nomenclature is used throughout the thesis except in this chapter, Chapter 2, and Chapter 5 where the second one is used instead. This is because a reviewer of the publication of Chapter 3 suggested this change of nomenclature, and as a result, the entire thesis was adapted to it, with the exception of these three chapters, since they must reflect their associated publications as they appear in the accepted version of the manuscripts. Therefore, in this thesis, RFSH is equivalent to MEH, LRFSH to LMEH, URFSH to UMEH, and SRFSHB to SaEHB.

4.6 Conclusions

Deep well submersible pump motors have a specific rotor end-ring manufacturing process: copper laminations with punching holes to place the bars, are glued to the end of these rotor bars with copper liquid soldering. Internally cooling water, which propelled by the rotor moves at a high speed, erodes the liquid soldering. Therefore, a particular type of fault appears, widespread in these motors: the end-ring wear, documented in this paper through several motor repair shop cases. The water suspended particles that end-ring wear generates, are impelled by the centrifugal force, and might impact the stator winding, causing serious damage.

As has been shown through simulation, lab tests, and field cases, a LSH monitoring with long periods between measurements (e.g., biannual) is insufficient for end-ring wear detection. First, in a single amplitude measurement, the wear might not be enough to raise the LSH amplitude to a level considered as faulty according to traditional rotor fault indicators. Second, once the wear spreads, rotor asymmetry might even be cancelled by multiple segments wear, lowering the LSH amplitude.

Continuous monitoring is needed to solve the problem: two field motors have been daily measured during nearly a year. Moreover, a new paradigm must be considered when monitoring deep well induction motors: the ratio of change in the LSH amplitude must be used as an indicator of end-ring wear, even if classic LSH thresholds are not reached (-45 dB). As shown through the field cases results, a changing LSH amplitude in time reveals the degradation of an end-ring. More precisely, ups and downs in the LSH amplitude reveal that the rotor asymmetry first increases and then is compensated as all the segments in the end-ring are equally worn. Therefore, instead of comparing the LSH amplitude with classic thresholds, changes in its amplitude must be monitored.

Changes in the secondary fault harmonics properly chosen are very useful to complement the LSH monitoring. Finally, stopping the motor at an early stage of end-ring wear might prevent this fault from contaminating the water that internally cools this type of motor and creates important secondary damage, as the winding failure that might appear if contaminating particles impact its coils at a high speed.

Appendix A. Simulated motor data

General	U = 400 V, Connection = Y, N_{bars} = 28 p = 2, h_{max} = 27, T = 26.6 N·m, J = 0.030 kg·m^2
Stator	R_{est} = 1.25 Ω, $L_{\sigma,est}$ = $3.57 \cdot 10^{-3}$ H, $L_{\mu,est}$ = 0.19 H
Rotor	R_b = $7.0 \cdot 10^{-5}$ Ω, $L_{\sigma,b}$ = $2.8 \cdot 10^{-7}$ H, $L_{\mu,rot}$ = $5.6 \cdot 10^{-6}$ H R_{ring} = $5.0 \cdot 10^{-5}$ Ω, $L_{\sigma,ring}$ = $5.0 \cdot 10^{-8}$ H

Bibliography

[1] W. R. Finley and M. M. Hodowanec, "Selection of copper versus aluminum rotors for induction motors," *IEEE Transactions on Industry Applications*, vol. 37, no. 6, pp. 1563–1573, 2001, doi: 10.1109/28.968162

[2] J. Pons-Llinares, D. Morinigo-Sotelo, O. Duque-Perez, J. Antonino-Daviu, and M. Perez-Alonso, "Transient detection of close components through the chirplet transform: Rotor faults in inverter-fed induction motors," in *IECON 2014 - 40th Annual Conference of the IEEE Industrial Electronics Society*, 2014, pp. 3386–3392, doi: 10.1109/IECON.2014.7048999

[3] L. Beneduce, G. Caruso, D. Lannuzzi, E. Pagano, and L. Piegari, "Analysis of a structural faiulure mode arising in cage rotors of induction machines," *Electrical Engineering*, vol. 93, pp. 179–191, 2011, doi: 10.1007/s00202-011-0204-8

[4] M. Jeong, J. Yun, Y. Park, S. B. Lee, and K. N. Gyftakis, "Quality assurance testing for screening defective aluminum die-cast rotors of squirrel cage induction machines," *IEEE Transactions on Industry Applications*, vol. 54, no. 3, pp. 2246–2254, 2018, doi: 10.1109/TIA.2018.2805828

[5] S. Nandi, H. A. Toliyat, and X. Li, "Condition monitoring and fault diagnosis of electrical motors—a review," *IEEE Transactions on Energy Conversion*, vol. 20, no. 4, pp. 719–729, 2005, doi: 10.1109/TEC.2005.847955

[6] H. Weichsel, "Squirrel-cage rotors with split resistance rings," *Transactions of the American Institute of Electrical Engineers*, vol. 47, no. 3, pp. 929–936, 1928, doi: 10.1109/T-AIEE.1928.5055080

[7] S. Williamson and A. C. Smith, "Steady-state analysis of 3-phase cage motors with rotor-bar and end-ring faults," *IEE Procedings B (Electric Power Applications)*, vol. 129, no. 3, pp. 93–100, 1982, doi: 10.1049/ip-b.1982.0014

[8] H. A. Toliyat and T. A. Lipo, "Transient analysis of cage induction machines under stator, rotor bar and end ring faults," *IEEE Transactions on Energy Conversion*, vol. 10, no. 2, pp. 241–247, 1995, doi: 10.1109/60.391888

[9] J. F. Bangura and N. A. Demerdash, "Diagnosis and characterization of effects of broken bars and connectors in squirrel-cage induction motors by a time-stepping coupled finite element-state space modeling approach," *IEEE Transactions on Energy Conversion*, vol. 14, no. 4, pp. 1167–1176, 1999, doi: 10.1109/60.815043

[10] S. J. Manolas and J. A. Tegopoulos, "Analysis of squirrel cage induction motors with broken bars and rings," *IEEE Transactions on Energy Conversion*, vol. 14, no. 4, pp. 1300–1305, 1999, doi: 10.1109/60.815063

[11] T. J. Sobczyk and W. Maciolek, "Does the component (1-2s)f0 in stator currents is sufficient for detection of rotor cage faults?" in *2005 5th IEEE International Symposium on Diagnostics for Electric Machines, Power Electronics and Drives*, 2005, pp. 1–5, doi: 10.1109/DEMPED.2005.4662509

[12] C. Kral, H. Kapeller, J. V. Gragger, A. Haumer, and B. Kubicek, "Phenomenon rotor fault — multiple electrical rotor asymmetries in induction machines," in *2009 IEEE International Symposium on Diagnostics for Electric Machines, Power Electronics and Drives*, 2009, pp. 1–9, doi: 10.1109/DEMPED.2009.5292769

[13] M. Riera-Guasp, M. F. Cabanas, J. A. Antonino-Daviu, M. Pineda-Sánchez, and C. H. R. García, "Influence of nonconsecutive bar breakages in motor current signature analysis for the diagnosis of rotor faults in induction motors," *IEEE Transactions on Energy Conversion*, vol. 25, no. 1, pp. 80–89, 2010, doi: 10.1109/TEC.2009.2032622

[14] M. Riera-Guasp, J. Pons-Llinares, F. Vedreño-Santos, J. A. Antonino-Daviu, and M. Fernández Cabanas, "Evaluation of the amplitudes of high-order fault related components in double bar faults," in *8th IEEE Symposium on Diagnostics for Electrical Machines, Power Electronics Drives*, 2011, pp. 307–315, doi: 10.1109/DEMPED.2011.6063641

[15] V. Climente-Alarcon, J. A. Antonino-Daviu, A. Haavisto, and A. Arkkio, "Evolution of high order fault harmonics during a bar breakage with compensation," in *2014 International Conference on Electrical Machines (ICEM)*, 2014, pp. 1888–1893, doi: 10.1109/ICELMACH.2014.6960441

[16] J. A. Antonino-Daviu, K. N. Gyftakis, R. Garcia-Hernandez, H. Razik, and A. J. Marques Cardoso, "Comparative influence of adjacent and non-adjacent broken rotor bars on the induction motor diagnosis through mcsa and zsc methods," in *IECON 2015 - 41st Annual Conference of the IEEE Industrial Electronics Society*, 2015, pp. 001 680–001 685, doi: 10.1109/IECON.2015.7392343

[17] K. N. Gyftakis, J. A. Antonino-Daviu, and A. J. Marques Cardoso, "A reliable indicator to detect non-adjacent broken rotor bars severity in induction motors," in *2016 XXII International Conference on Electrical Machines (ICEM)*, 2016, pp. 2910–2916, doi: 10.1109/ICELMACH.2016.7732937

[18] J. Antonino-Daviu, H. Razik, A. Quijano-Lopez, and V. Climente-Alarcon, "Detection of rotor faults via transient analysis of the external magnetic field," in *IECON 2017 - 43rd Annual Conference of the IEEE Industrial Electronics Society*, 2017, pp. 3815–3821, doi: 10.1109/IECON.2017.8216651

[19] P. A. Panagiotou, I. Arvanitakis, N. Lophitis, J. A. Antonino-Daviu, and K. N. Gyftakis, "A new approach for broken rotor bar detection in induction motors using frequency extraction in stray flux signals," *IEEE Transactions on Industry Applications*, vol. 55, no. 4, pp. 3501–3511, 2019, doi: 10.1109/TIA.2019.2905803

[20] M. E. Iglesias-Martínez, P. Fernández de Córdoba, J. A. Antonino-Daviu, and J. A. Conejero, "Detection of nonadjacent rotor faults in induction motors via spectral subtraction and autocorrelation of stray flux signals," *IEEE Transactions on Industry Applications*, vol. 55, no. 5, pp. 4585–4594, 2019, doi: 10.1109/TIA.2019.2917861

[21] Y. Park, H. Choi, S. B. Lee, and K. N. Gyftakis, "Search coil-based detection of nonadjacent rotor bar damage in squirrel cage induction motors," *IEEE Transactions on Industry Applications*, vol. 56, no. 5, pp. 4748–4757, 2020, doi: 10.1109/TIA.2020.3000461

[22] T. Ishikawa, S. Shinagawa, and N. Kurita, "Analysis and failure diagnosis of squirrel-cage induction motor with broken rotor bars and end rings," *IEEJ Journal of Industry Applications*, vol. 2, no. 6, pp. 292–297, 2013, doi: 10.1541/ieejjia.2.292

[23] J. Bonet-Jara, D. Morinigo-Sotelo, O. Duque-Perez, L. Serrano-Iribarnegaray, J. M. Llopis-Gomez, M. Ortiz-Gomez, and J. Pons-Llinares, "End-ring wear in deep well submersible motor pumps," in *2021 IEEE 13th International Symposium on Diagnostics for Electrical Machines, Power Electronics and Drives (SDEMPED)*, vol. 1, 2021, pp. 79–85, doi: 10.1109/SDEMPED51010.2021.9605520

Chapter 5

Comprehensive Analysis of Principal Slot Harmonics as Reliable Indicators for Early Detection of Inter-turn Faults in Induction Motors of Deep-Well Submersible Pumps

This paper was published on December 28, 2022 in IEEE Transactions on Industrial Electronics journal, belonging to the IEEE publishing house, under the reference:

In the next sections, the full accepted author's version of the manuscript is reproduced, including abstract, appendixes and bibliography. Footnotes, which are not present in the original publication, are added in order to clarify some aspects within the general frame of this thesis.

Abstract

Early detection of inter-turn faults is one of the most important issues in electrical machines, as the fault severity evolves very fast to a catastrophic failure due to the high thermal stress. However, as this paper shows, in submersible induction motors for deep-well pumps, it evolves slower. These motors are highly water-cooled, which significantly reduces the thermal stress caused by the fault, increasing the possibility of an early detection. Among fault detection methods, only those based on line current/voltage measurements can be used, as motors are at great depths. This article investigates the Principal Slot Harmonics as reliable indicators for early detection of inter-turn faults in this application. To this end, a comprehensive analysis is conducted using finite element analysis where the behavior of these harmonics is studied under different fault severities, both alone and coexisting with other asymmetries such as unbalanced voltages, eccentricity or rotor faults. The findings are used to develop a reliable diagnostic scheme based on the monitoring of the most fault-sensitive harmonics along with the voltage and current unbalance indexes. Finally, the scheme is applied, for the first time, in the context of a continuous monitoring of a 230 HP induction motor showing its efficacy.

Keywords: Condition monitoring; inter-turn faults; induction motors; fault diagnosis; MCSA; finite-element analysis; pumps;

5.1 Introduction

Deep well water pumps are starting to play an essential role in human's water supply, since superficial aquifers are drying due to climate change [1]. These pumps are normally driven by water-cooled squirrel cage submersible induction motors [2]. Therefore, monitoring the condition of this element is a key aspect to avoid catastrophic failures and unexpected shutdowns, which is quite a sensitive issue in this industry, due to the cost of replacement (motors are in wells of up to 500 m in depth) and the fact of leaving a part of the population without water supply.

Data provided by a Spanish water company on 20 water pumping facilities over the last three decades show that the main reason for pump replacement is found in stator faults (Fig. 5.1). A recent study has shown that end-rings of deep-well motors wear quite often [3]. This is due to the particular characteristics of their rotor cage (copper liquid soldering glues together bars and a set of die-cut thin end-ring sheets), the internal water cooling system and the high rotational speed (due to one pole pairs design). The particles detached from the end-ring wear is a possible trigger mechanism for the degradation of insulation in the stator coils.

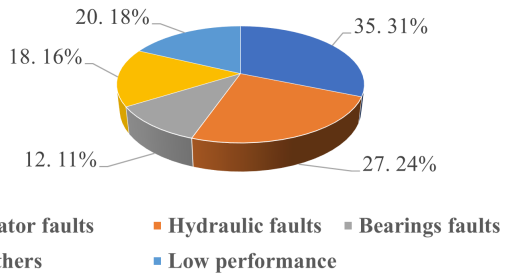

FIGURE 5.1: Distribution of reasons for pump replacement in a Spanish water company.

Another particular characteristic of these machines is their cooling system which is done both externally (by forcing the water to flow through the motor surface) and internally (by pre-filling the motor with a mixture of water and glycol). Thus, stator windings are subjected to a less thermal stress than in conventional surface motors, which delays the propagation of an inter-turn fault to a phase-to-phase or phase-to-ground short-circuit. Therefore, there is a higher probability of detecting the failure at an early stage.

In the field of online diagnostics, several methods have been proposed to detect inter-turn faults. However, some of them are unfeasible in their application to deep-well pumps. Flux [4]–[8] and vibration [9]–[11] methods require installing a sensor at or near the surface of the motor. This is a big challenge in deep-well motors, since the sensor must be able to withstand the impedance of an up to 500 m cable, be waterproof, be fixed in the smooth outer surface of the motor and survive the descent to the aquifer through a narrow borehole. In turn, methods that use the zero-sequence current or require access to the neutral point [12]–[14], cannot be applied, as coil end-connections are done internally in these motors, and therefore, phase magnitudes are not accessible. Thus, the only feasible solution in this application is to use methods based on line current/voltage measurements, as they are available at the motor control cabinet. In this regard, different approaches have been followed over the last two decades. Motor Current Signature Analysis (MCSA) has been proposed to monitor the amplitude of the third harmonic or the Principal Slot Harmonics (PSHs) [15]–[19], as well as instantaneous active/reactive power signature analysis to monitor the second harmonic [20]. The theory of symmetrical components has also been used based on the relationship between the asymmetry created by the stator fault and the negative sequence component [21], [22]. In recent years, advances have been made regarding model-based and artificial intelligence techniques [23]–[26].

Concluding, existing methods for inter-turn fault detection based on flux and vibration [4]–[11] are difficult to be applied in deep-well motors, since these motors are submerged at great depths (up to 500 m), while methods that use the zero-sequence current or neutral point cannot be applied, as phase magnitudes are not accessible [12]–[14]. Previous conclusions of line magnitude methods [15]–[26] have been deduced for conventional induction motors, and they are not necessarily valid in this specific context. Moreover, most of these line magnitude based works do not analyze in great detail the sensitivity and reliability of the proposed indicators in the presence of other asymmetries (in the most complete works the robustness of the method is studied only under eccentricity and voltage unbalance [20] and under broken bars and voltage unbalance [24]). In addition, these diagnostic schemes have not gone beyond laboratory tests where low power motors are used (with the exception of [16], [17] and [20]). All this calls into question the applicability of these methods to real and large industrial motors.

This is the first paper to investigate how the special characteristics of deep well induction motors (e.g., double water cooling, low number of turns per slot, two poles and even number of rotor bars) together with their operating conditions (long steady state under constant load) act as game changers in terms of inter-turn fault detection through PSHs, making them much more reliable indicators than what is shown in other papers of conventional motors. The paper proves that in deep-well motors there is always a set of PSHs that are nearly absent in the healthy machine, and highly increase when the inter-turn short-circuit takes place, deducing a formula to determine them (highly improved reliability with respect to using PSHs present in healthy state, as previous methods). Moreover, it is proven that an incipient stator fault in deep-well motors does not cause a destructive current (it can be even lower than rated current) and that the double water cooling system of these motors prevents from a fast insulation degradation (fault detected at an early stage before becomes catastrophic). These characteristics, together with a very sensitive indicator, enables an early short-circuit detection.

Apart from these very sensitive PSHs, two more indexes are proposed in order to discriminate inter-turn short-circuits from other asymmetries: Voltage Unbalance Index (VUI) and Current Unbalance Index (CUI). Theoretical findings are validated using up to 65 different simulations obtained through Finite Elements Analysis (FEA) on a 22 kW deep-well induction motor (high precision thanks to complete manufacturer data), and a detailed analysis is presented on the sensitivity and reliability of these harmonics under inter-turn faults, both alone and coexisting with different levels of voltage unbalance, rotor asymmetry and eccentricity. Finally, an original diagnostic scheme is presented to detect inter-turn faults through the use of PSHs, VUI and CUI, obtained only with line magnitudes, generating extremely sensitive indicators, even for early stages where other PSHs fail. Its efficacy is proven for the first time in the context of a continuous monitoring of a deep-well induction motor (230 HP) operating in a pumping station, where data has been collected every six hours for nearly a year.

5.2 Special features of induction motors in deep-well pumps

The motor and the pump work submerged in the aquifer, with shafts directly coupled and in vertical position; from bottom to top: motor - water inlet - pump - pipe. The motor frame is smooth and without heat sinks. Cooling is achieved in two ways: by pre-filling the motor with a mixture of water and glycol (internal cooling[1]) and by placing a metal cover to force water flow between the cover and the motor surface before entering the pump (external cooling) [3]. Figure 5.2 shows the schematic of the motor-pump assembly.

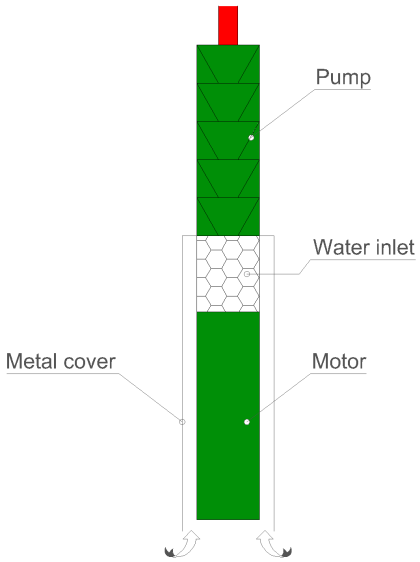

FIGURE 5.2: Schematic of the motor-pump assembly.

As for the motor design and operating characteristics, two poles are used to achieve high power and speed with a small diameter (reducing excavation costs). Usually, an even number of rotor bars is used to avoid the unbalanced magnetic pull. Motors are fed with frequency converters or soft starters, sometimes working continuously for long periods of time and without significant load or speed variations, as water is usually pumped to a tank.

[1]For more information on this mechanism go to Footnote 1 of Chapter 4.

These characteristics make the motors particularly suitable for early detection of inter-turn faults via PSHs through an FFT steady-state analysis. First, because stator windings are subjected to less thermal stress than surface motors (they are doubly water-cooled, with a very constant ambient temperature of around 15°C in the aquifer), which can retard the time between the inter-turn fault occurs and the moment it propagates to a catastrophic failure. Secondly, due to the small diameter of these motors, slots are smaller, and the number of conductors per slot (and phase) is smaller too. Hence, the small number of turns of an early-stage short-circuit represents a higher percentage (with respect to the total number of phase turns) than in conventional motors, thereby becoming a more noticeable fault. Third, due to rotor characteristics (two poles with an even number of rotor bars), motors are PSHs producers [27]. These harmonics are known to be correlated with the stator inter-turn fault [16]. Fourth, because, there are no false positives due to load variations, as this is practically constant, and therefore, PSHs amplitudes do not significantly change under normal operation. Finally, because due to the speed is also practically constant, together with the fact that these motors can run continuously for long periods of time, ideal conditions exist to apply a steady-state analysis using the FFT, and the best results can be obtained from it.

The PSHs frequencies are given by the Rotor Slot Harmonics formula [28] when $k = 1$:

$$f_{RSH} = \left[k\frac{R}{p}(1-s) \pm \nu \right] f_0 \tag{5.1}$$

where $k \in \mathbb{N}$, p is the number of pole pairs, s the slip, ν the order of the time harmonic present in the stator current $1, 3, 5 \ldots$, f_0 the fundamental supply frequency and R the number of rotor bars.

A PSH appears in the line current if the relative order of its associated spatial flux harmonic wave is an odd number non-multiple of three. In a perfectly symmetrical machine, this relative order is given by $h_{rot} = R/p \pm h_{st}$, where h_{st} is the relative order of the spatial harmonic through which the time harmonic νf_0 interacts with the rotor system. Taking this into account, it can be proven that the two PSHs with the lowest $|\nu|$ absent in the line current are (with $n \in \mathbb{N}$):

- For $R/p = 6n - 4$: PSH($\nu = -5, 1$).
- For $R/p = 6n - 2$: PSH($\nu = -1, 5$).
- For $R/p = 6n$: PSH($\nu = -3, 3$).

In real machines, where inherent asymmetries exist, all these harmonics are present in the line current, although with very small amplitudes. Thus, as their existence is directly related to the level of asymmetry, and their amplitudes are practically zero in the healthy machine, they will be the most sensitive PSHs to an inter-turn fault. Therefore, these harmonics are the key to a real solution for the difficult task of detecting intern-turn short-circuits.

5.3 Finite-element analysis

The purpose of this section is to perform a comprehensive analysis on the sensitivity and reliability of PSHs as indicators for inter-turn fault detection. To this end, a FEA approach is used, since the idiosyncrasy of the motors under study does not allow to perform proper tests in an academic laboratory. This is because in order to obtain valid and comparable conclusions, a

deep-well motor should be used, as their special characteristics affect the behavior of the motor under the short-circuit and its diagnosis through PSHs. To replicate industrial conditions, the deep-well motor should be tested under load, for which it would require a well, a pump coupled to the motor, a crane to put the motor inside the well and a system of pipelines and valves to regulate the load: if it is tested surrounded by air, it would over-heat very easily. However, these elements are difficult to be found in an academic laboratory. Therefore, as the laboratory test is not an option with this type of motors, a finite element analysis approach is followed, since it allows to perform very realistic and accurate short-circuit tests, with the motor in load, without compromising the integrity of the motor, while allowing an easy combination of the fault with different asymmetries of different severity.

In this regard, a submersible induction motor (22 kW, $p = 1$, 30 rotor bars, 230 V Δ, 65.6 A, 2900 rpm) has been modeled using a commercial FEA software. To ensure accuracy, complete geometry and B-H characteristic are provided by the manufacturer. The inter-turn fault is created in phase A, following the approach described in [29]. In this approach[2], the coils inside two adjacent stator slots are divided into groups. For example, Fig. 5.3 shows the cross section of the motor for the last of the inter-turn faults considered, where the coils that are placed in slots 1-16 and 2-15 have been divided into three groups (each of the groups is represented by a color and has a certain number of conductors). The short-circuit is then created between the middle groups of the adjacent slots, which consist of a single wire (a one-turn coil), through a contact resistance of 0.1 Ω. The fault severity is handled by modifying the number of conductors in the rest of the groups. Using this approach, the severity of the first four fault states is 1.52 %, 3.03 %, 4.55 % and 6.06 % of shorted turns.

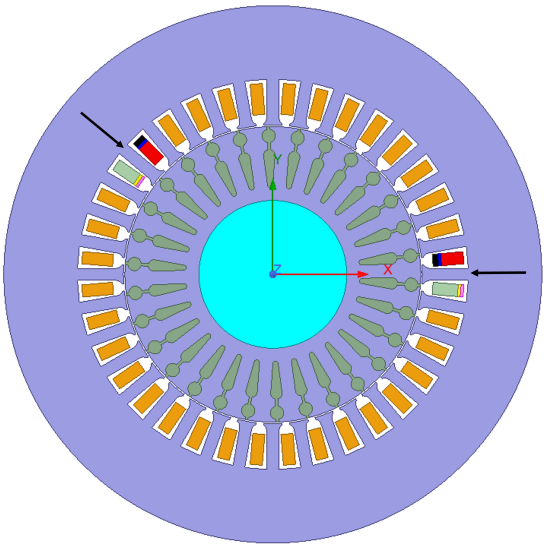

FIGURE 5.3: Cross section of the motor with the coils divided in groups (arrows) to create the inter-turn fault with 6.06% of shorted turns.

Table 5.1 shows, for each fault state (column 1), the line A, phase A, short-circuit and contact resistance currents (columns 2-5); being the last two the currents through the short-circuited coils and the contact resistance respectively. The ratios of these magnitudes with respect to the healthy current (65.57 or 37.87 A) are shown in columns 6-9. Finally, column 10 shows the line Current Unbalance Index (CUI): maximum deviation in RMS value of any of the three line currents with respect to the mean value of their RMS values divided by this mean value.

[2]Expanded information about the short-circuit modeling approach can be found in Appendix A, including the definitions of all of the resulting currents: phase current, short-circuit current and contact-resistance current.

TABLE 5.1: RMS values and fault indexes of the currents in the machine without extra asymmetries.

	$I_{l,A}(A)$	$I_A(A)$	$I_{sc}(A)$	$I_{cr}(A)$	$I_{l,A}/I_{l,A,h}(\%)$	$I_A/I_{A,h}(\%)$	$I_{sc}/I_{A,h}(\%)$	$I_{cr}/I_{A,h}(\%)$	$CUI(\%)$
H	65.57	37.87	-	-	-	-	-	-	-
F1 (1.52%)	65.92	38.39	17.60	35.30	100.52%	101.38%	46.48%	93.22%	0.43%
F2 (3.03%)	66.96	39.81	33.77	66.33	102.12%	105.14%	89.17%	175.18%	1.66%
F3 (4.55%)	68.65	42.07	54.00	92.87	104.69%	111.11%	142.61%	245.25%	3.61%
F4 (6.06%)	71.09	45.26	76.66	120.09	108.41%	119.53%	202.44%	317.14%	6.18%

It can be seen that in this machine the short-circuit currents are less severe than in previous studies for other types of machines and same severity level, where $I_{sc}/I_{A,h}$ ratio is up to two times higher [8], [29]. In fact, the first two fault states originate a short-circuit current that is even lower than the rated phase current (46.48% and 89.17%). This suggests that the fault can be detected at an early stage before it becomes catastrophic. However, the current flowing through the contact resistance is almost equal to the rated phase current in the first fault state and 1.75 times higher in the second. This leads to the formation of a heat source in a very small area that will eventually deteriorate the insulation and propagate the fault to the next stages. Therefore, protective measures should be taken as soon as possible. In this regard, none of the cases considered would activate the overcurrent protections, since the line current in the most severe case only exceeds the rated line current by 8.41%.[3].

Thanks to the theoretical analysis of the previous section, it can be deduced that, for this motor combination of R and p, the PSHs($\pm$3) are absent in the line current spectrum of the healthy machine. When the asymmetry is introduced via the inter-turn fault, these harmonics should become the most sensitive to it, as any change in the amplitudes of the state of the art indicators (PSH(+1) or PSH(-1)) is masked due to their already high amplitude in the healthy state. This is exactly what can be seen in Fig. 5.4, which shows, for each fault state, the amplitudes of the PSHs in the line A current spectrum (in dB with respect to the fundamental component; noise floor around -110 dB; similar conclusions for lines B and C). From the simulations results, it can be concluded that an extremely sensitive indicator for inter-turn faults has been found, even for early stages where other PSHs fail: (PSHs($\pm$3) show an extremely high change of 40 dB from healthy to only 1.52% of shorted turns, and a very high 10 dB change from 1.52% to 3.03%. Next, the reliability of using these PSHs as indicators for inter-turn faults is analyzed under the presence of different asymmetries with different severity levels.

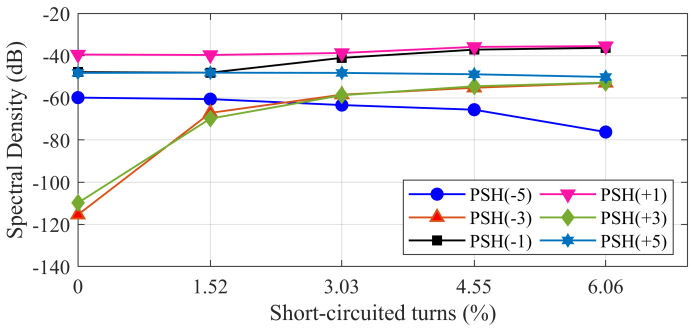

FIGURE 5.4: Amplitude of PSHs for each fault state considered.

5.3.1 Machine with unbalanced supply

Using NEMA MG 1-2016 definition, four levels of Voltage Unbalance Index (VUI) have been considered: 0.25%, 0.5%, 1% and 2.5%. According to this norm, with the first three levels of VUI a motor shall operate successfully, while with the last level it should be derated. Figure 5.5 shows the line voltages for a VUI of 2.5%. Figures 5.6a, 5.6b, 5.6c show, respectively, the amplitudes of the PSH(-3) and PSH(+3) in the line A current spectrum, and the CUI, for each inter-turn fault considered (x-axis), and each level of VUI (different colors).

[3]According to [15], the circuit resulting from the inter-turn fault can be split into two independent circuits: the shorted-loop and the healthy part of the winding. As the number of shorted turns considered is low, the healthy part has practically the same impedance than in the case of no-fault. This means that the main rotating magnetic field would induce almost the same voltage in both cases. Hence, the small effect in the phase/line current.

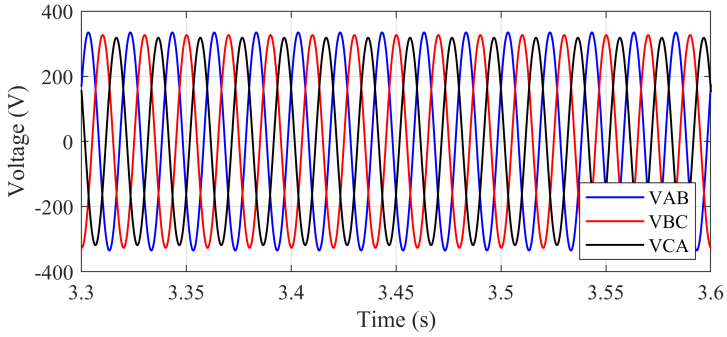

FIGURE 5.5: Line voltages for a voltage unbalance index of 2.5%.

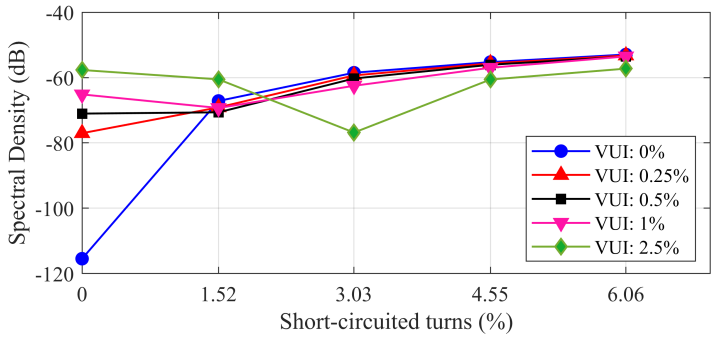

(a)

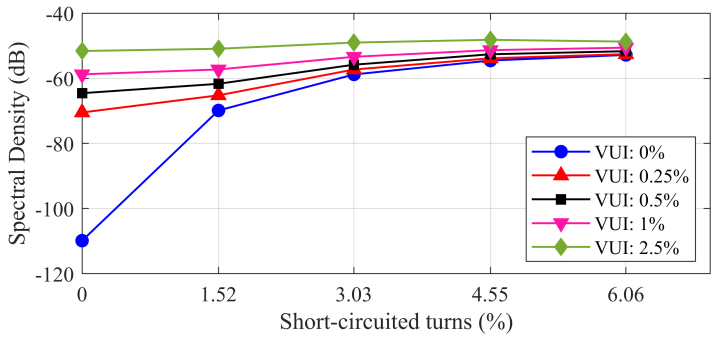

(b)

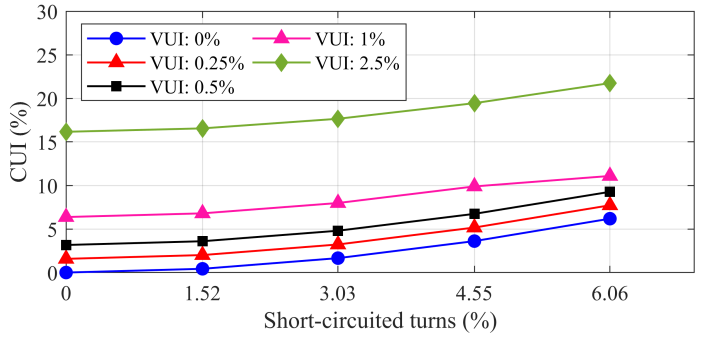

(c)

FIGURE 5.6: Amplitude of PSH(-3) (a) and PSH(+3) (b) in line A spectrum, and CUI (c), for each inter-turn fault and each level of VUI.

PSH(+3) presents a strictly increasing behavior at all levels of VUI. Since the asymmetry introduced by the voltage unbalance gives rise to the PSHs($\pm$3) in the healthy machine (0% of short-circuited turns), amplitude difference with first fault stage (1.52 %) is bigger in the case without voltage unbalance (0 % VUI). Despite this, sensitivity to detect the fault is very high, especially in those stages in which the short-circuit current is still not catastrophic (1.52% and 3.03% shorted turns): at VUI not considered dangerous for the motor (VUI from 0.25 to 1%), from healthy to 1.52%, PSH(+3) amplitude increases between 1.5 dB and 5.3 dB, while from 1.52% to 3.03% increases between 4 dB and 8 dB.

On the other hand, PSH(-3) only presents a strictly increasing behavior for the first level of VUI. In the next two levels of VUI, this behavior starts at the first stage of inter-turn fault, while in the last level of VUI there is no clear trend. Yet, the sensitivity to the fault between the two non-catastrophic inter-turn faults for the three first levels of VUI is higher than in the PSH(+3) (changes going from 7 dB to 10 dB). Similar results are observed in line B. In line C, no strictly increasing behavior is observed for PSH(+3) and only from the first stage onwards for the PSH(-3).

Concluding, depicting the evolutions of the amplitudes of both PSHs(+3,-3) in the three currents, there are two evolutions out of six that maintain a strictly increasing behavior with the fault severity for all levels of VUI (PSH(+3) in lines A and B), enabling the fault detection at an early and non-catastrophic stage. As for the CUI, it strictly increases at all levels of VUI with practically the same change between fault stages.

However, it should be noted that the increase in the VUI for a same inter-turn fault creates significant variations in the PSH($\pm$3). For the healthy machine and the first two levels of intern-turn fault, this increase has a monotonic behavior, and consequently, can lead to a false positive. The same is observed for the CUI, but in this case, for all fault stages. Yet, if the VUI is also monitored it can be easily determined if the changes in these three indicators are due to a voltage unbalance or an inter-turn fault.

5.3.2 Machine with eccentricity

Combining static eccentricity (SE) with dynamic eccentricity (DE), four levels of eccentricity have been considered: SE:5% + DE:5%, SE:10% + DE:10%, SE:20% + DE:20% and SE:30% + DE:30%. According to [30], the first case is within the permissible levels for inherent eccentricity, the second and third cases are considered unacceptable and the last case is a serious problem requiring motor decommissioning. Figure 5.7 shows the amplitude of the Mixed Eccentricity Harmonics (MEH)[4,5] due to each eccentricity level for the machine without inter-turn fault. Figures 5.8a, 5.8b, 5.8c show, respectively, the amplitudes of the PSH(-3) and PSH(+3) in the line A current spectrum, and the CUI, for each inter-turn fault considered (x-axis), and each level of eccentricity (different colors).

[4]Rotational Frequency Sideband Harmonics are also known in literature as Mixed Eccentricity Harmonics. The first nomenclature is used throughout the thesis except in this chapter, Chapter 2, and Chapter 4 where the second one is used instead. This is because a reviewer of the publication of Chapter 3 suggested this change of nomenclature, and as a result, the entire thesis was adapted to it, with the exception of these three chapters, since they must reflect their associated publications as they appear in the accepted version of the manuscripts. Therefore, in this thesis, RFSH is equivalent to MEH, LRFSH to LMEH, URFSH to UMEH, and SRFSHB to SaEHB.

[5]In Fig. 5.7, the RFSH or MEH are pointed with black arrows, marking their vertexes with different geometric symbols according to the eccentricity level.

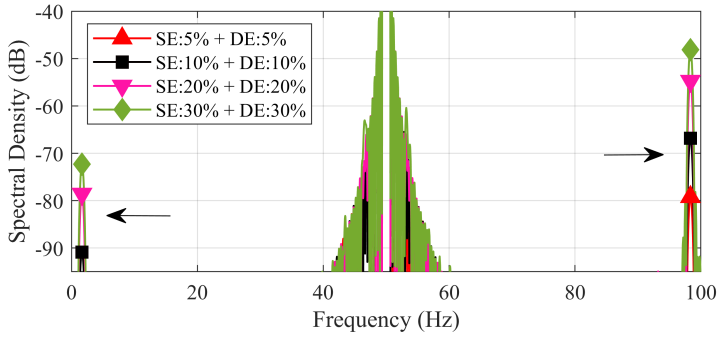

FIGURE 5.7: Mixed Eccentricity Harmonics for each level of eccentricity in the machine without inter-turn fault.

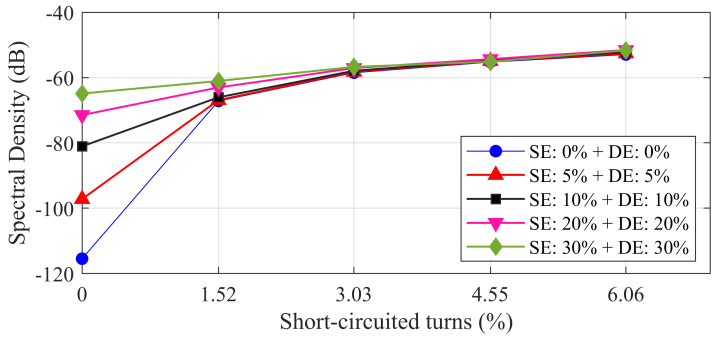

(a)

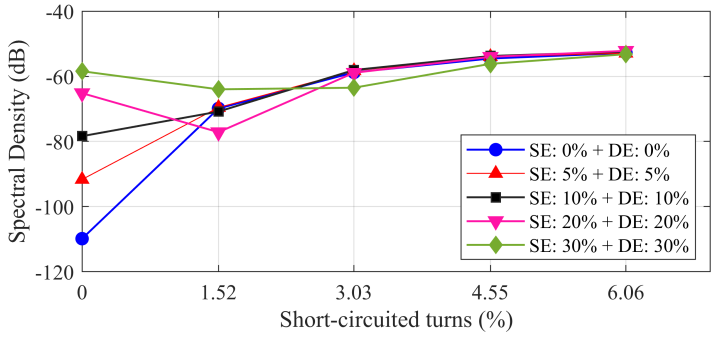

(b)

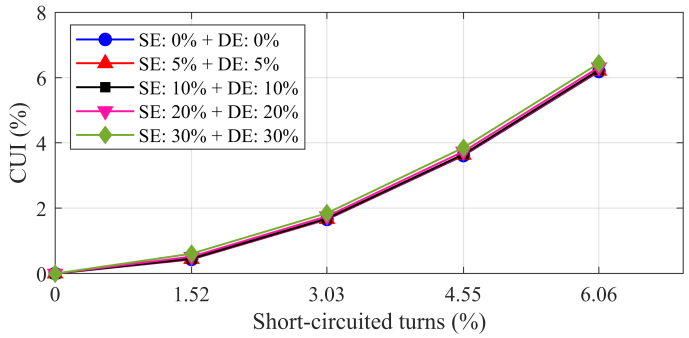

(c)

FIGURE 5.8: Amplitude of PSH(-3) (a) and PSH(+3) (b) in line A spectrum, and CUI (c), for each inter-turn fault and each level of eccentricity.

PSH(-3) presents a strictly increasing behavior with respect to the short-circuit severity, for all levels of eccentricity. From healthy to 1.52%, PSH(-3) amplitude increases between 4 dB and 31 dB, while from 1.52% to 3.03% it increases between 4 dB and 9 dB.

In the case of the PSH(+3), the strictly increasing behavior is lost at the first stages for the two most severe levels of eccentricity, but maintains an overall better sensitivity to the fault severity than the PSH(-3). Similar results can be observed in the line B and C, although in the latter, the strictly increasing behavior of PSH(-3) is already lost for the first fault in the second, third and four level of eccentricity. Thus, in the presence of the asymmetry caused by the eccentricity, it is also important to monitor both harmonics in at least two of the three currents. As for the CUI, it strictly increases in all levels of eccentricity with very small differences between them.

It should be noted that an inter-turn fault monitoring, based solely on tracking PSHs, could lead to a false positive in a healthy motor (and a false increase of the fault severity on the machine with 1.52% shorted turns), as the increase in eccentricity causes a monotonic increase in PSHs($\pm$3). Nevertheless, in this case, the CUI can be used to rapidly discriminate whether the increase in PSHs($\pm$3) is due to an eccentricity fault or an inter-turn fault, as this parameter strictly increases with the shorted-turns, but is insensitive to eccentricity changes (see Fig. 5.8c).

5.3.3 Machine with rotor asymmetries

Analyzing the impact of rotor asymmetries is very important in deep-well motors since, as explained in the introduction, their end-rings wear quite often [3]. By modifying the conductivity of the bars, four levels of rotor asymmetry have been defined: inherent asymmetry (IA), incipient fault (IF), 1 broken bar (1BB) and 2 broken bars (2BB). Figure 5.9 shows the magnetic flux density distribution for the case of 2 broken bars without inter-turn fault. As can be seen, there is an area (ellipse) near the broken bars (arrows) where an increase of the magnetic flux density exists, causing the magnetic asymmetry. This asymmetry is reflected in the line current spectrum through the Lower Sideband Harmonic (LSH), which is normally the harmonic used to diagnose this fault. In the absence of false indications [31], it is well established that amplitudes below -50 dB correspond to inherent asymmetry, between -50 dB and -40 dB to an incipient fault, -40 to -35 dB to a broken bar and above -35 dB to multiple broken bars. Figure 5.10 shows the amplitude of the LSH due to each rotor fault for the machine without inter-turn fault. Figures 5.11a, 5.11b, 5.11c show, respectively, the amplitudes of the PSH(-3) and PSH(+3) in the line A current spectrum, and the CUI, for each inter-turn fault considered (x-axis), and each level of rotor fault (different colors).

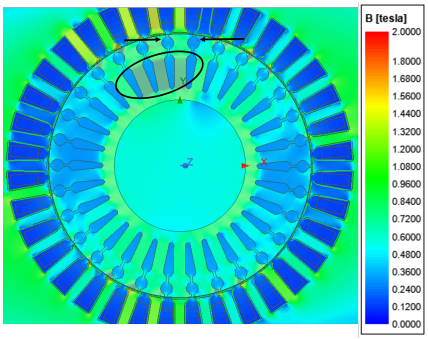

FIGURE 5.9: Magnetic flux density distribution for the case of 2 broken bars (arrows) without inter-turn fault.

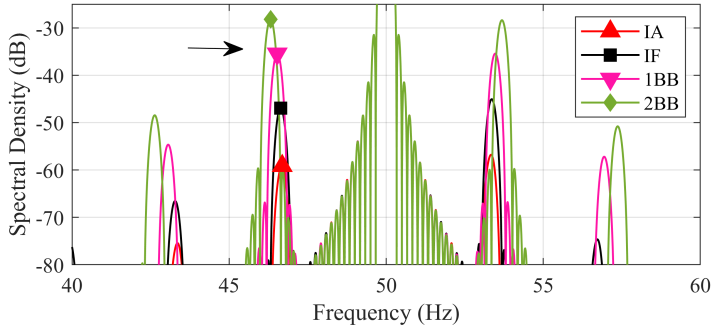

FIGURE 5.10: LSH for each level of rotor asymmetry in the machine without inter-turn fault.

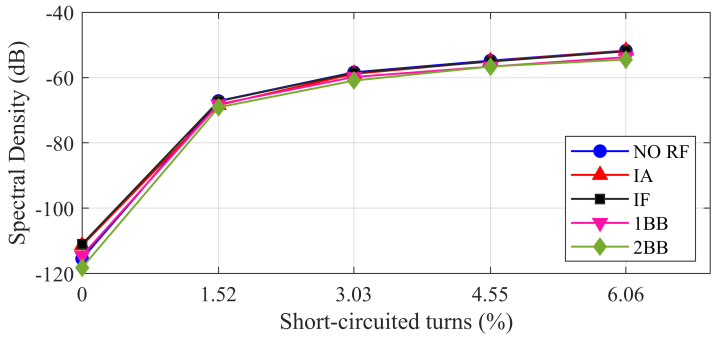

(a)

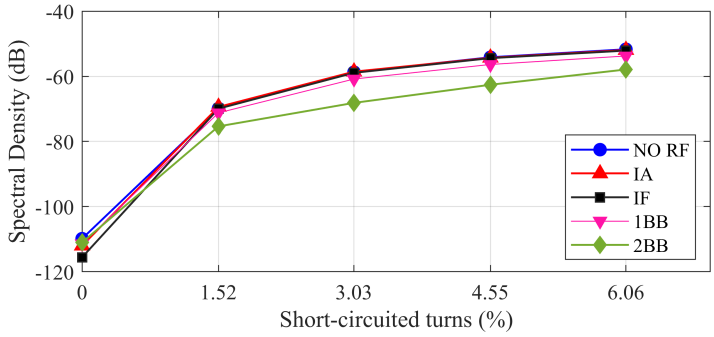

(b)

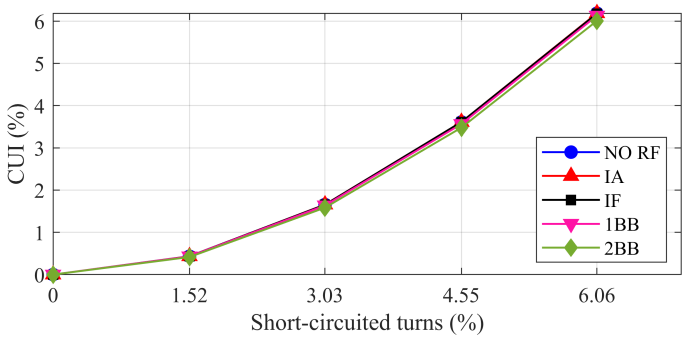

(c)

FIGURE 5.11: Amplitude of PSH(-3) (a) and PSH(+3) (b) in line A spectrum and CUI (c) for each inter-turn fault and each level of rotor fault.

In this case, both harmonics present a strictly increasing behavior for all levels of rotor fault considered. Moreover, PSH(-3) is practically insensitive to the rotor fault severity, while PSH(+3) presents sensitivity only to the most severe case (2 broken bars). The same behavior is observed in line B, while it differs in line C as in the two previous asymmetries. As for the CUI, it is also insensitive to the rotor fault and shows a strictly increasing behavior for all levels considered.

Unlike the other two asymmetries studied, in this case it is not possible to get a false positive since there is one harmonic that is totally insensitive to the fault. Anyway, the CUI can always be used to discriminate, since it changes with short-circuited turns, but is not affected by rotor asymmetry.

5.4 Monitoring method for a reliable detection

Thanks to the theoretical analysis in Section 5.2, and the FEA results in Section 5.3, we can conclude that, for the case of deep-well motors (one pole pairs and an even number of rotor bars), there is always a set of PSHs that are not present in a perfectly symmetrical motor (e.g., PSHs($\pm$3) in the FEA section case, as well as in the field case of the next section). The amplitudes of these PSHs highly increase in the presence of an intern-turn short-circuit; moreover, these amplitudes show a strictly increasing trend with the severity of this fault.

If the supply is unbalanced or an eccentricity takes place, these PSHs amplitudes increase too (under rotor asymmetries, this effect does not take place, or is very light and only for high severity faults). To discriminate inter-turn short-circuits from these asymmetries, two more indexes must be obtained: VUI (increases only under voltage unbalance) and CUI (increases with intern-turn short-circuits, but does not increase under eccentricity and rotor faults). Moreover, it is also observed that the amplitudes of these PSHs behave differently when the inter-turn occurs. For instance, in the case analyzed, PSH(-3) with voltage unbalance shows a similar behavior than PSH(+3) with eccentricity and vice versa. Thus, their behavior also depends on the type of the second asymmetry. This might be due to the fact that they are associated to harmonic flux waves that rotate in different directions with different phases. Despite this, it has been shown that there is always one PSH that presents a strictly increasing behavior under stator fault. Therefore, a monitoring method using PSHs should always include two of the predicted harmonics in Section 5.2, one associated to a clockwise rotating harmonic flux wave and the other a counter-clockwise one. Furthermore, it has also been observed that PSHs are reliable indicators in two of the line currents, therefore, only two of them need to be monitored to assure that at least one of the PSHs amplitude obtained will present a strictly increasing trend under inter-turn short-circuit fault.

Taking into account all this information, three scenarios are possible if the amplitude of one or both of these PSHs increase: if the VUI increases, an unbalance supply problem is taking place; if the VUI is constant, and the CUI is constant too, an eccentricity failure (or a rotor asymmetry in very rare cases), might be taking place (this can be verified monitoring the amplitudes of the MEH and the LSH); if the VUI is constant and the CUI increases, then the increase of the amplitudes in these PSHs is due to an inter-turn short-circuit[6]. This logic is reflected in Fig. 5.12 in the form of a continuous monitoring diagnostic method. In order to account for

[6]It is emphasized that, although an unbalanced voltage system creates an unbalanced current system, an unbalanced current system can appear in spite of having a balanced voltage system, when it appears as a consequence of an inter-turn fault. Therefore, it is necessary to measure both parameters.

error measurements and slight load variations (load is nearly perfectly constant in these applications), a moving average (taking $N+1$ samples), is applied to each indicator: PSHs, VUI and CUI; thresholds are used for each indicator: e_1, e_2 and e_3 (gathering data of machines with different powers is necessary to give precise values to these thresholds); finally the baseline values, from which the increments in the indicators are defined, are obtained by measuring the average values of the indicators during the initial period of monitoring and redefined when the thresholds are surpassed and the indicators stabilize again.

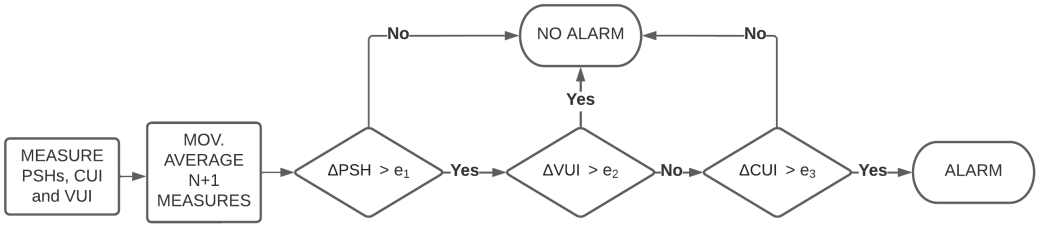

FIGURE 5.12: Flux diagram of the proposed method.

Finally, it should be remarked, that there could be a fourth scenario in which the VUI and PSHs increased simultaneously. In this case, it would not be possible to tell if what has occurred is a voltage unbalance or an inter-turn fault. Nevertheless, this is a very unlikely scenario, as it requires that both happen within the period between measure and measure. As the method is presented in the form of a continuous monitoring (several measures per day), the chances of this scenario to happen are very low. Furthermore, if the inter-turn fault was derived from the voltage unbalance, the voltages should be very high in order to breakdown the insulation. Yet, in this case, it is most likely that the over-voltage protection was triggered. Then, once the cause of the unbalance overvoltage was corrected and the motor put on normal operation (although with an inter-turn short-circuit), the alarms would be triggered since the proposed diagnostic scheme would have detected an increase in the PSHs, a non-increase in the VUI (it is corrected before a new measure), and another increase in the CUI.

5.5 Field case

A deep water well motor from a pumping station was continuously monitored for nearly a year, recording a steady-state of line currents and voltages every six operating hours. The motor is a Caprari M12230 (230 HP, p=1, 30 bars, 380 V Δ, 335 A, 2950 rpm), fed with a frequency converter at 43.97 Hz (model SD7058055 from Power Electronics) and operated at 70% of its rated current. The monitoring equipment consist of: three voltage probes, a three-phase current probe, a high-resolution oscilloscope, and a mini-PC (more details on the DAQ can be found in the Appendix A). Signals are sent via internet to a computer where the diagnostic algorithms are applied. The moving average takes 12 samples, and the thresholds for PSH (e_1), VUI (e_2) and CUI (e_3) are set, respectively, to 4 dB, 0.25 points and 0.25 points (details on how the thresholds are established are found in Appendix B).

Figures 5.13a, 5.13b, 5.13c, 5.13d and 5.13e show, respectively, the amplitude evolution over time (in dB with respect to the fundamental component) of the LSH, the PSH(+1), the PSH(-1), the PSH(+3) and the PSH(-3) from line current A, while Figs. 5.14a and 5.14b show the evolution over time of the CUI and VUI.

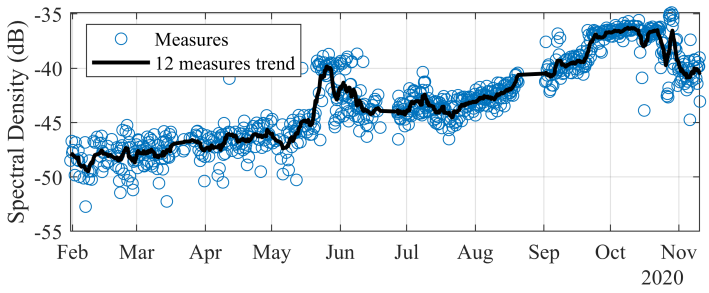

(a)

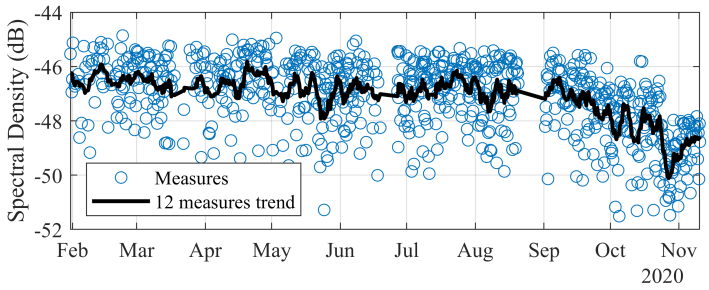

(b)

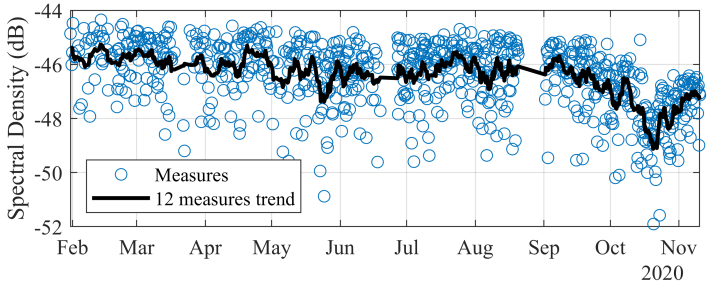

(c)

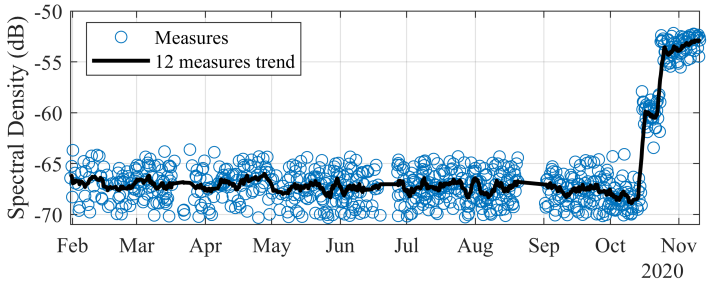

(d)

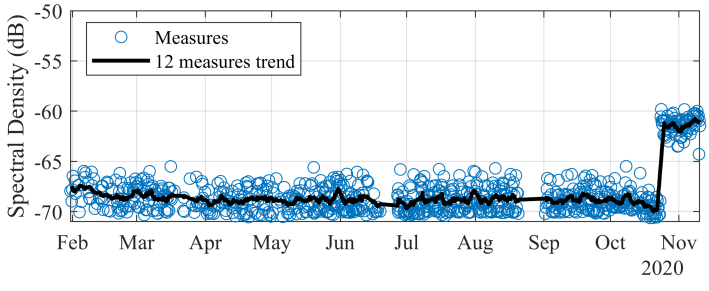

(e)

FIGURE 5.13: Amplitude evolution over time of the LSH (a), the PSH(+1) (b), the PSH(-1) (c), the PSH(+3) (d) and the PSH(-3) (e).

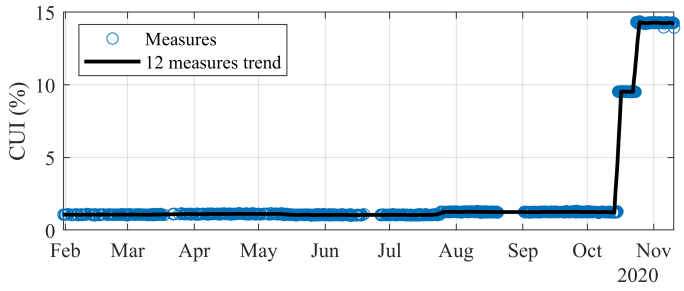

(a)

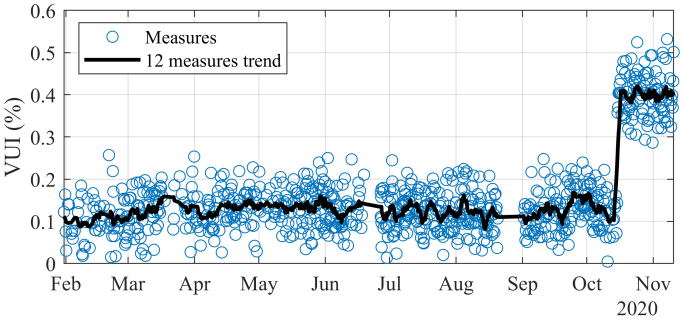

(b)

FIGURE 5.14: Evolution over time of the CUI (a) and VUI (b).

As can be seen in Fig. 5.13a, there is a fault developing in the rotor from the very beginning (more details on the origin of this fault can be found in [3]). Despite this, PSHs and CUI remain insensitive to the fault during the whole period, so no alarm is set for an inter-turn fault. On October 15, a simultaneous increase of 10 dB in the PSH(+3) and 8 points in the CUI, but also of 0.3 points in the VUI is detected, so no alarm is set. Seven days later, another simultaneous increase of 7 dB in the PSH(+3), 8 dB in the PSH(-3) and 5 points in the CUI is detected. Yet, in this case, the VUI does not increase, therefore, the alarm for inter-turn fault is triggered.

After two weeks from the last increase in the indicators, the motor was drawn from the deep-well (Fig. 5.15a) and sent to the motor repair shop for further inspection (Fig. 5.15b). There, it was found that the rotor end-rings were highly worn: this is a common fault in deep-well motors [3], explained in the introduction and detected here through the LSH amplitude increase shown in Fig. 5.13a. Regarding the stator fault, the repair shops of deep-well motors only apply simple tests to determine the state of the stator insulation: very conservative criterions are used, which easily imply rewind of the stator windings, to assure that the components will last longer when the motor is placed in a 100 to 500 m deep well, thus avoiding the high cost of extraction if an early fault takes place. First, the resistance between phases and ground is measured: if the result is under 200 MΩ, the stator is rewound. Second, the resistance between phases is measured to verify continuity. Visual inspection is used to look for a high amount of dirt, which in these motors it is also a reason to rewind. Looking for burn signs is not a standard procedure, and, moreover, it is not conclusive, since due to the small diameter of these motors, coil heads are placed in a very small space and cannot be thoroughly inspected, while the stator inside surface can just be partially seen (even a hand is hardly introduced in a 2 m long stator). Unfortunately, no surge test is applied. In the case of the motor monitored, no signs of burns were identified during the partial visual inspection, but the phase to ground resistance was below 200 MΩ, which confirmed the stator damage, ordering its rewind, and validating the diagnosis made through the indicators proposed in the paper.

(a) (b)

FIGURE 5.15: Motor being removed (a) and sent for inspection (b).

The field results are in total agreement with findings of previous sections. First, because the motor has two poles and 30 bars and the highest increases are observed in PSHs($\pm$3), just as predicted in Section 5.2 and verified in Section 5.3. Second, because the PSHs and the CUI are insensitive to the rotor fault, thus agreeing with simulation results of Section 5.3.3. Third, because the CUI behaves as expected and shows values in the same order of magnitude that the ones observed in Section 5.3.1. Fourth, the PSHs($\pm$3) increase together with the VUI under an unbalanced voltage, and alone when the stator fault found in the motor repair shop takes place. Hence, since there are no load-oscillations, and no eccentricity is taking place, the PSHs increase can only be related to a stator fault.

Since the motor was able to continue operating after two weeks from the last change in the indicators, the results show that, in these motors, it is possible to detect the fault with this diagnostic scheme before it originates an unexpected shutdown, which in the case of the drinking water supply industry is a very sensitive issue. This means that the current flowing through the shorted turns was still too low to create a catastrophic failure. As proved in Table 5.1, an incipient stator fault in this type of motors does not cause a destructive current (it can be even lower than rated current). Moreover, the double water cooling system prevents from a fast insulation degradation. It is not possible to give an accurate estimate of this current for this field case based only on the simulation results, since motors are of different sizes and operate at different speeds and loads. Nevertheless, everything (level of PSHs, CUI and no signs of burns) points in the direction of a short-circuit current not too high.

Finally, it is important to remark that these results are general and applicable to other models of deep-well induction motors since they present very similar characteristics to each other such as rotor construction, length proportionally higher than width and a small number of turns per slot. As for whether all conclusions could also be generalized for conventional induction motors, it is something that it is out of the scope in this study. However, what can be extrapolated for any type of PSHs producer induction motor is that there will always be a set of PSHs that are not present in the spectrum of the perfectly symmetrical healthy machine and will therefore always be more sensitive to the fault.

5.6 Conclusion

This paper has analyzed in detail the use of PSHs as reliable indicators for early inter-turn fault detection in submersible inductions motors of deep-well pumps. The main findings and contributions of this work are listed below:

- Special characteristics of these machines make them suitable for inter-turn fault detection through PSHs, since they are highly water-cooled and they are normally designed with two poles and an even number of rotor bars.
- There is a set of PSHs that are highly sensitive to the fault, especially at early stages. These PSHs can be known beforehand, being only necessary to monitor two of them (one associated to a counter-clockwise rotating harmonic flux wave and the other to a clockwise), in two of the line currents.
- In the presence of other asymmetries, there is always one of these PSHs that maintains a monotonic behavior with the fault severity in one of the line currents.
- False positives due to voltage unbalance and eccentricity can be avoided if the line voltage and current unbalance indexes (VUI and CUI) are also monitored. Rotor cage faults cannot produce false positives.
- A novel diagnostic scheme has been proposed for reliable and early detection of inter-turn faults, which combines the monitoring of the PSHs and the line voltage and current unbalance indexes.
- Finally, and for the first time, the efficacy of a diagnostic scheme is proven by continuously monitoring a 230 HP industrial induction motor from a deep-well pump facility.

Appendix A. DAQ system

- PicoScope 4824A: High-resolution, deep-memory oscilloscope with 80 M/S sampling rate and 12 bits vertical resolution.
- PicoTech TA041: Active differential voltage probe with $\pm$ 2 % DC accuracy and 0 to 25 MHz frequency range.
- PicoTech TA325: 3-phase AC Rogowski current probe with $\pm$ 1 % of reading $\pm$ 0.1 A accuracy and 0.01 to 20 kHz frequency range.

Appendix B. Thresholds

To establish the thresholds of the fault indicators, data gathered from 10 deep-well motors continuously monitored during a year are analyzed. During healthy operation, VUI and CUI are relatively constant. For the field case in Section 5.5: before any fault takes place, 0.04 and 0.13 points respectively are the maximum variations found with respect to the mean taken over 12 measures trend (black lines in Fig. 5.14). In the case of PSHs amplitudes, since the load is

practically constant in this application, only small changes appear. For the field case: before any fault takes place, 1.6 dB for PSH(+3) and 1.32 dB for PSH(-3) are the maximum variations found with respect to the mean taken over the 12 measures trend (black lines in Fig. 5.13d and 5.13e). As observed next, the three thresholds settled are higher than these maximum variations under healthy operation.

To establish the variations that should trigger an alarm, the FEA results are analyzed. With respect to the PSHs, it is observed in Fig. 5.6b that, for a low inherent VU (0.25% similar to that of the case of study), the PSH increases 5.3 dB from healthy to 1.52% shorted turns. Hence, PSH threshold should be a bit lower than this value to have a security margin: $e_1 = 4$ dB. With respect to VUI, it is also observed in this figure that an increase in the VUI from 0.25% to 0.5% (the minimum increase studied) originates an increase in the PSH of 6 dB when the motor is healthy and 3.5 dB for the lowest fault condition (1.52% shorted turns). The VUI threshold e_2 is set to 0.25 points. Finally, with respect to CUI, it is observed in Fig. 5.6c that, for a VUI < 0.5%, the CUI increases 0.4 points from healthy to 1.52% of shorted turns. Hence, threshold should be a bit lower than this value to have a security margin: e_3 is set to 0.25 points.

Bibliography

[1] S. Jasechko and D. Perrone, "Global groundwater wells at risk of running dry," *Science*, vol. 372, no. 6540, pp. 418–421, 2021, doi: 10.1126/science.abc2755

[2] M. J. Brandt, K. M. Johnson, A. J. Elphinston, and D. D. Ratnayaka, "Chapter 19 - pumping, electrical plant, control and instrumentation," in *Twort's Water Supply (Seventh Edition)*, seventh edition ed. Boston: Butterworth-Heinemann, 2017, pp. 777–828, doi: 10.1016/B978-0-08-100025-0.00019-3

[3] J. Bonet-Jara, D. Morinigo-Sotelo, O. Duque-Perez, L. Serrano-Iribarnegaray, and J. Pons-Llinares, "End-ring wear in deep-well submersible motor pumps," *IEEE Transactions on Industry Applications*, vol. 58, no. 4, pp. 4522–4531, 2022, doi: 10.1109/TIA.2022.3166876

[4] H. Henao, C. Demian, and G.-A. Capolino, "A frequency-domain detection of stator winding faults in induction machines using an external flux sensor," *IEEE Transactions on Industry Applications*, vol. 39, no. 5, pp. 1272–1279, 2003, doi: 10.1109/TIA.2003.816531

[5] G. N. Surya, Z. J. Khan, M. S. Ballal, and H. M. Suryawanshi, "A simplified frequency-domain detection of stator turn fault in squirrel-cage induction motors using an observer coil technique," *IEEE Transactions on Industrial Electronics*, vol. 64, no. 2, pp. 1495–1506, 2017, doi: 10.1109/TIE.2016.2611585

[6] M. Irhoumah, R. Pusca, E. Lefevre, D. Mercier, R. Romary, and C. Demian, "Information fusion with belief functions for detection of interturn short-circuit faults in electrical machines using external flux sensors," *IEEE Transactions on Industrial Electronics*, vol. 65, no. 3, pp. 2642–2652, 2018, doi: 10.1109/TIE.2017.2745408

[7] P. C. M. L. Filho, D. C. Santos, F. B. Batista, and L. M. R. Baccarini, "Axial stray flux sensor proposal for three-phase induction motor fault monitoring by means of orbital analysis," *IEEE Sensors Journal*, vol. 20, no. 20, pp. 12 317–12 325, 2020, doi: 10.1109/JSEN.2020.2999547

[8] K. N. Gyftakis and A. J. M. Cardoso, "Reliable detection of stator interturn faults of very low severity level in induction motors," *IEEE Transactions on Industrial Electronics*, vol. 68, no. 4, pp. 3475–3484, 2021, doi: 10.1109/TIE.2020.2978710

[9] J. Seshadrinath, B. Singh, and B. K. Panigrahi, "Vibration analysis based interturn fault diagnosis in induction machines," *IEEE Transactions on Industrial Informatics*, vol. 10, no. 1, pp. 340–350, 2014, doi: 10.1109/TII.2013.2271979

[10] P. Qin, Z. Zhang, Y. Sun, H. Liu, and H. Ren, "Vibration analysis of dfig stator winding inter-turn short circuit fault," in *2018 International Conference on Information Systems and Computer Aided Education (ICISCAE)*, 2018, pp. 436–442, doi: 10.1109/ICISCAE.2018.8666886

[11] P. S. Panigrahy and P. Chattopadhyay, "Tri-axial vibration based collective feature analysis for decent fault classification of vfd fed induction motor," *Measurement*, vol. 168, p. 108460, 2021, doi: 10.1016/j.measurement.2020.108460

[12] K. N. Gyftakis and J. C. Kappatou, "The zero-sequence current as a generalized diagnostic mean in delta-connected three-phase induction motors," *IEEE Transactions on Energy Conversion*, vol. 29, no. 1, pp. 138–148, 2014, doi: 10.1109/TEC.2013.2292505

[13] M. Singh and A. G. Shaik, "Incipient fault detection in stator windings of an induction motor using stockwell transform and svm," *IEEE Transactions on Instrumentation and Measurement*, vol. 69, no. 12, pp. 9496–9504, 2020, doi: 10.1109/TIM.2020.3002444

[14] D. Zheng, G. Lu, and P. Zhang, "A noninvasive interturn insulation condition monitoring method based on the common-mode impedance spectrum of inverter-fed machines," *IEEE Transactions on Industry Applications*, vol. 57, no. 5, pp. 4786–4795, 2021, doi: 10.1109/TIA.2021.3094176

[15] G. Joksimovic and J. Penman, "The detection of inter-turn short circuits in the stator windings of operating motors," *IEEE Transactions on Industrial Electronics*, vol. 47, no. 5, pp. 1078–1084, 2000, doi: 10.1109/41.873216

[16] A. Stavrou, H. Sedding, and J. Penman, "Current monitoring for detecting inter-turn short circuits in induction motors," *IEEE Transactions on Energy Conversion*, vol. 16, no. 1, pp. 32–37, 2001, doi: 10.1109/60.911400

[17] S. Cruz and A. Cardoso, "Diagnosis of stator inter-turn short circuits in dtc induction motor drives," *IEEE Transactions on Industry Applications*, vol. 40, no. 5, pp. 1349–1360, 2004, doi: 10.1109/TIA.2004.834012

[18] M. Wolkiewicz, G. Tarchała, T. Orłowska-Kowalska, and C. T. Kowalski, "Online stator interturn short circuits monitoring in the dfoc induction-motor drive," *IEEE Transactions on Industrial Electronics*, vol. 63, no. 4, pp. 2517–2528, 2016, doi: 10.1109/TIE.2016.2520902

[19] M. Afshar, A. Tabesh, M. Ebrahimi, and S. A. Khajehoddin, "Stator short-circuit fault detection and location methods for brushless dfims using nested-loop rotor slot harmonics," *IEEE Transactions on Power Electronics*, vol. 35, no. 8, pp. 8559–8568, 2020, doi: 10.1109/TPEL.2019.2963295

[20] M. Drif and A. J. M. Cardoso, "Stator fault diagnostics in squirrel cage three-phase induction motor drives using the instantaneous active and reactive power signature analyses," *IEEE Transactions on Industrial Informatics*, vol. 10, no. 2, pp. 1348–1360, 2014, doi: 10.1109/TII.2014.2307013

[21] M. Bouzid and G. Champenois, "Experimental compensation of the negative sequence current for accurate stator fault detection in induction motors," in *IECON 2013 - 39th Annual Conference of the IEEE Industrial Electronics Society*, 2013, pp. 2804–2809, doi: 10.1109/IECON.2013.6699575

[22] X. F. St-Onge, J. Cameron, S. Saleh, and E. J. Scheme, "A symmetrical component feature extraction method for fault detection in induction machines," *IEEE Transactions on Industrial Electronics*, vol. 66, no. 9, pp. 7281–7289, 2019, doi: 10.1109/TIE.2018.2875644

[23] F. Duan and R. Živanović, "Condition monitoring of an induction motor stator windings via global optimization based on the hyperbolic cross points," *IEEE Transactions on Industrial Electronics*, vol. 62, no. 3, pp. 1826–1834, 2015, doi: 10.1109/TIE.2014.2341563

[24] M. Sabouri, M. Ojaghi, J. Faiz, and A. J. Marques Cardoso, "Model-based unified technique for identifying severities of stator inter-turn and rotor broken bar faults in scims," *IET Electric Power Applications*, vol. 14, no. 2, pp. 204–211, 2020, doi: 10.1049/iet-epa.2019.0267

[25] l. Şahin and O. Keysan, "Model predictive controller utilized as an observer for inter-turn short circuit detection in induction motors," *IEEE Transactions on Energy Conversion*, vol. 36, no. 2, pp. 1449–1458, 2021, doi: 10.1109/TEC.2020.3048071

[26] G. H. Bazan, P. R. Scalassara, W. Endo, A. Goedtel, R. H. C. Palácios, and W. F. Godoy, "Stator short-circuit diagnosis in induction motors using mutual information and intelligent systems," *IEEE Transactions on Industrial Electronics*, vol. 66, no. 4, pp. 3237–3246, 2019, doi: 10.1109/TIE.2018.2840983

[27] S. Nandi, S. Ahmed, H. Toliyat, and R. Bharadwaj, "Selection criteria of induction machines for speed-sensorless drive applications," *IEEE Transactions on Industry Applications*, vol. 39, no. 3, pp. 704–712, 2003, doi: 10.1109/TIA.2003.810651

[28] P. Vas, *Parameter Estimation, Condition Monitoring, and Diagnosis of Electrical Machines*. Oxford Science Publications, 1993, [Online]. Available: https://global.oup.com.

[29] K. N. Gyftakis, "A comparative investigation of interturn faults in induction motors suggesting a novel transient diagnostic method based on the goerges phenomenon," *IEEE Transactions on Industry Applications*, vol. 58, no. 1, pp. 304–313, 2022, doi: 10.1109/TIA.2021.3131296

[30] W. Thomson and A. Barbour, "On-line current monitoring and application of a finite element method to predict the level of static airgap eccentricity in three-phase induction motors," *IEEE Transactions on Energy Conversion*, vol. 13, no. 4, pp. 347–357, 1998, doi: 10.1109/60.736320

[31] S. B. Lee, D. Hyun, T.-j. Kang, C. Yang, S. Shin, H. Kim, S. Park, T.-S. Kong, and H.-D. Kim, "Identification of false rotor fault indications produced by online mcsa for medium-voltage induction machines," *IEEE Transactions on Industry Applications*, vol. 52, no. 1, pp. 729–739, 2016, doi: 10.1109/TIA.2015.2464301

Chapter 6

General discussion

In the previous four chapters, the four publications derived from this thesis have been presented. In this chapter, the results obtained are linked and discussed as a whole, all within the general framework of this thesis.

In the first publication, a thorough state-of-the-art review has been conducted in order to see which of the SSE techniques is the most suitable to be used in steady-state MCSA algorithms for the diagnosis of IMs. The study has been complemented with a detailed analysis of the SSE methods used by two of the leading commercial diagnostic devices in their steady-state MCSA algorithms, MCEMAX and EXP4000, highlighting, through real industrial measurements, which are their main drawbacks. The latter has been of utmost importance, as it has allowed to have a deep insight into the problems that industry faces when it comes to estimate speed without a physical sensor. From both studies, it has been determined that the best techniques to use in steady-state MCSA diagnostic applications are those based on Slotting and Rotational Frequency Sideband Harmonics, and more in particular, those based on RSHs. Same conclusions have been drawn from Chapter 1. Introduction for efficiency estimation applications. However, it has also emerged as a result of these analyses that RSH-based techniques, in their past state in the technical literature (prior to this thesis), had the main disadvantage of not having a reliable and non-invasive method to localize the RSHs, assign them their ν index, and operate without the need to know the number of rotor slots, which is the key aspect to have a precise, general, non-invasive and automatic speed estimation method for MCSA steady-state diagnosis and efficiency estimation in the 4.0 Industry. This result has been paramount for the development of the thesis, since it determines the key aspect on which efforts must be focused in order to develop a speed estimation method with such characteristics.

Starting from the results and conclusions obtained in the first publication, a precise, general, non-invasive and automatic speed estimation method for MCSA steady-state diagnosis and efficiency estimation of IMs in the 4.0 Industry has been developed in the second publication. This method is the first SSE method that achieves to automatically localize the family of RSHs, properly assigning their ν indices, without knowing the number of rotor slots, without introducing errors as a preliminary estimate based on rated slip or use of RFSHs, without using invasive tests (e.g., no-load test), not restricting to PSHs, and not wrongly assuming that the highest amplitude corresponds to $\nu = 1$. To this end, a new formula for the RSHs frequencies has been deducted, allowing to characterize a RSH through two parameters, $[O_\nu, \nu]$, thus eliminating the need to know the number of rotor bars. Based on the properties of said formula, a smart RSH search method has been built, allowing to localize and classify the RSHs by families. Then, based also on the properties of the formula, a method has been given to calculate parameters $[O_\nu, \nu]$. O_ν is directly calculated as $f_{RSH}|_{s=0}/f_0$, being f_0 the frequency of the fundamental component, and $f_{RSH}|_{s=0}$ the frequency of the located RSH at no-load ($s = 0$), which in turn coincides with the nearest odd multiple of f_0 to the right (left in generator mode) of the said harmonic when ($s \neq 0$). The other parameter, ν, is calculated using a novel iterative method, whose convergence criteria is based on matching the information provided by 16 different speed-dependent harmonics. This last step ensures that the slip estimated is in concordance with position of all the speed dependent harmonics present in the stator current.

First, the algorithm has been proved to work with different number of rotor bars theoretically and by simulation. In these simulations, the rotor of a two pole pair ($p = 2$) motor has been configured under three different number of bars: 26 (odd R/p), 27 (non-integer R/p) and 28 (even R/p). Then, each configuration has been tested under 85% and 55% of the rated load with four typical skewing angles: straight bars, half rotor slot pitch, one stator slot pitch and one rotor slot pitch. From the 24 simulations obtained, in 23 of them, the algorithm has correctly located and characterized from 2 to 9 RSHs per study case. This is a differential feature with respect to other works in the technical literature, where the methods presented are commonly designed for motors that are PSHs producers (even R/p), ignoring the rest of motors (odd and non-integer R/p), where the detection tends to be more difficult. Therefore, this deep analysis shows the general applicability of the method.

Next, the algorithm has been tested using signals from a test-rig, assessing its capabilities in localizing the RSHs, determining their pairs $[O_\nu, \nu]$ and obtaining the speed/slip, using a 1000-line incremental encoder for comparison. The motor from which the signals have been acquired has been tested under three different supply frequencies (20 Hz, 35 Hz and 50 Hz-line-fed) and with three different slips at each of these frequencies (0.046, 0.02 and 0.0067). For testing the ability to locate and characterize RSHs, signals of 200 s have been used, while for testing the speed estimation accuracy, 50 signals of 50 s per case have been taken to obtain the average errors in speed and slip. The test shows that the algorithm is able to correctly characterize the RSH family for all cases, locating from 5 to 6 RSHs per case and detecting from 5 to 8 fault harmonics with the estimated speed. These results put in value the general applicability and robustness of the algorithm, since it proves to work under different load and feeding conditions, without losing performance. The test also shows that the speed error and the relative slip error between the 1000-line encoder and the algorithm are extremely low: below 0.05 rpm and 0.5% (if the slip is 1% and the slip relative error is 0.5%, the measured slip is either 1.005% or 0.995%). These results show the high accuracy of the method, proving that the designed speed estimation method can replace a 1000-line encoder in a MCSA steady-state diagnostic or efficiency estimation application.

Finally, the algorithm has been industrially validated using an own database of real measurements belonging to 105 different IMs with a wide range of nameplate characteristics: from a few kW to 2 MW, 0.67% to 8% slip, 400 V to 6.6 kV and from 1 to 5 pole pairs. This database includes measurements of motors with low rated-slips (21 motors with slip lower than 1%) and converter-fed at low frequencies, which are the most challenging conditions for algorithms based on harmonics detection. The algorithm has been successful at estimating speed in 100 out of 105 cases (the 5 remaining cases are under extremely no load condition or improperly measured), giving a mean value of 7.3 RSHs and 7.6 fault harmonics localized per motor. These results not only demonstrate the general applicability of the method, since it works with 100 different IMs, but also its robustness, as the slips estimated through the RSHs localized and their assigned pairs $[O_\nu, \nu]$ allow locating a high number of speed-dependent fault harmonics, thus verifying the coherence between the RSHs (plus their estimated $[O_\nu, \nu]$) and the information available in the spectrum.

As seen above, the algorithm results with laboratory or industrial measurements are better than in simulation, despite the higher noise. This is because a real motor has an iron core with a non-linear characteristic and inherent asymmetries. These features create extra RSHs in the spectrum that are not present in ideal conditions, and enhances the amplitude of the harmonics related to motor imperfections, such as rotor defects or eccentricity, which are precisely the ones that the algorithm tracks.

Once the algorithm has been developed and its accuracy, automaticity and general applicability proved, the next step has been to implement it in a continuous monitoring system. In this regard, a continuous condition monitoring system based on steady-state MCSA has been designed to autonomously operate in ten deep-well pumping stations. The system has been automated to take steady-state measures every six operating hours, sending the signals via internet to a computer where a steady-state MCSA algorithm that uses the designed speed estimation method has been implemented. This MCSA algorithm has been periodically reporting the evolution of different fault harmonics. At a given point of the monitoring in one of the facilities, it was observed the LSH, associated to rotor faults, described strange patterns with ups and downs. This opened a new line within the present thesis that led to the third publication, where a previously unreported failure that takes place in deep-well submersible motors is described: the wear of the rotor end-rings. In this publication, the peculiarities of

these IMs, and especially, of their unusual rotor manufacturing process have been analyzed, explaining how they intervene in the failure mechanism of the end-ring. Moreover, the difficulties of diagnosing this fault through conventional rotor asymmetry indicators have been addressed too, coming up with a new paradigm when diagnosing rotor faults through rotor asymmetry harmonics: the ratio of change in the LSH amplitude must be used as an indicator of end-ring wear, even if classic LSH alarm thresholds are not reached. Conclusions have been supported by simulation, laboratory tests and the continuous monitoring of two field motors working in deep boreholes during nearly a year. It is important to remark that in this discovery the speed estimation algorithm has played a key role. First because it is not possible to observe the patterns without a high-accurate and automatic method to localize the fault harmonics, or in other words, without a precise method to estimate speed, since there are many other harmonics around due to the frequency converter. Second because these motors are submerged at depths of up to 500 m, and therefore, it is not possible to test the motor to determine the number of rotor bars, as other methods based on RSHs do.

After proving the accuracy, automaticity and generality of the method (second publication) and its capability to be implemented in a continuous condition monitoring system (third publication), the last step has been to study whether the same harmonics used to estimate the speed (RSHs) can also be used to diagnose. This line of investigation has led to the fourth publication: a comprehensive study of PSHs (a particular case of RSHs) to assess their reliability as indicators for early detection of inter-turn faults in deep-well submersible motors. In this study, the operating and constructional characteristics of these motors have been theoretically analyzed, concluding that they can act as game changers in terms of inter-turn fault detection through PSHs, and that, it is possible to predict the most fault sensitive PSHs as a function of the number of rotor bars and pole pairs of the machine.

These findings have been validated using FEA by building the model of a 22 kW deep-well submersible motor with four levels of inter-turn fault severity (the four least severe). The results show that the most sensitive PSHs are precisely those predicted by the theoretical analysis, showing extremely high changes of 40 dB from healthy to only 1.52% shorted turns, and a very high change of 10 dB from 1.52% to 3.03%. Moreover, it is also observed that, in this motor, for the first two fault states, the short-circuit current is even lower than the rated phase current (44.48% and 89.17%), thus suggesting that the fault can be detected at an early stage before becoming catastrophic.

As a part of the FEA, the reliability of these harmonics to detect inter-turn fault in the presence of other asymmetries (voltage unbalance, eccentricity and rotor fault) with different degree of severity has also been assessed. This analysis shows that by monitoring two of the most fault sensitive PSHs, associated to harmonic flux waves with opposite rotating direction, and in two of the line currents, it is possible to reliably detect the inter-turn fault. In the case of a voltage unbalance between 0.25% and 1%, increases ranging from 1.5 dB to 5.3 dB are observed when going from healthy state to 1.52% of shorted-turns, while when going from 1.52% to 3.03% of shorted-turns the increases are in the range of 4 dB to 8 dB. In the case of eccentricity, increases ranging from 4 dB to 31 dB are observed when going from healthy state to 1.52% of shorted-turns, while when going from 1.52% to 3.03% of shorted-turns the increases are between 4 dB to 9 dB. In the presence of rotor asymmetries, the same behavior is observed that in the case of only inter-turn fault, which means that rotor asymmetries do not affect this indicator. Furthermore, from this analysis, it is also observed that two extra indexes are needed to discriminate an increase in the PSHs due to a voltage unbalance or eccentricity from an increase due to inter-turn fault. These indexes are the VUI and the CUI.

Finally, taking into account all the findings obtained from the theoretical analysis and FEA

results, a diagnostic scheme has been developed to reliably detect inter-turn faults through the use of the most fault sensitive PSHs, the VUI and the CUI. This scheme has been applied during the continuous monitoring of a 230 HP deep-well submersible motor during nearly a year, achieving early detection of an inter-turn fault (corroborated by a motor repair store). Moreover, this case study allows to conclude and confirm that the rotor asymmetries do not affect the PSHs, that the use of the VUI and CUI successfully prevent from false positives, and that the PSHs selected as the most fault sensitive are indeed the most sensitive to the fault (changes of 8 dB are observed in the analysis for these PSHs, while of 2 dB for other PSHs).

Therefore, all this proves that the method solves the challenging problems of RSH-based state of the art techniques (first publication and Chapter 1. Introduction), being not only capable of providing accurate and automatic speed estimation for almost any IM (second publication), as well as being implemented in a continuous condition monitoring system that helps to solve real problems in industry (third publication), but also to possess a second direct application for diagnostics through the exploitation of the same harmonics that are used to estimate speed (fourth publication).

Chapter 7

Contributions and conclusions

In the previous chapter, a general discussion about the results obtained in this thesis has been made. In this chapter, the contributions made to scientific knowledge through this work are listed and the conclusions drawn from it are presented. As the thesis is presented in the form of *Collection of Articles* the contributions and conclusions are listed by publication. Finally, the fulfillment of the objectives is discussed.

7.1 Contributions

In this section, the original and novel contributions of this thesis are presented.

7.1.1 First publication and state-of-the-art review

- An identification of the requirements that a SSE method should meet in order to be implemented in a MCSA steady-state diagnosis or efficiency estimation application for IMs in the context of 4.0 Industry.
- A thorough state-of-the-art review on SSE techniques focused on determining which family of techniques meets the requirements to be implemented on a MCSA steady-state diagnosis or efficiency estimation application in the context of 4.0 Industry, identifying their current weaknesses and which are the lines of investigation that could lead to overcome such problems.
- A detailed analysis of the SSE techniques implemented in two of the leading diagnostic commercial devices, MCEMAX and EXP4000, identifying the problems of such techniques and confronting them to other SRFSHB techniques using a database of 79 industrial IMs.

7.1.2 Second publication

- A formula that allows to calculate slip/speed in a RSH-based technique without the need to know the number of rotor slots, only requiring the fundamental frequency (easily identified as the maximum peak in the spectrum), the number of poles (available in the nameplate), a new parameter called O_ν (easily calculated as the frequency of the odd multiple of the fundamental nearest to the right of a RSH divided by the fundamental frequency) and ν (calculated through a sophisticated iterative method that takes into account the speed information contained in up to 16 different speed-dependent harmonics).
- A method based on the properties of said formula that allows to locate and classify RSHs into families in a very reliable, autonomous, and robust way.
- The definition of the parameter O_v, of easy calculation and direct assignation to each detected RSHs, which avoids the need to know the number of rotor slots.
- An iterative method to correctly assign to each of the detected RSHs its corresponding parameter ν, which ensures the coherency between the estimate speed through the RSHs and the speed information contained in up to 16 different speed-dependent harmonics.
- A detailed study showing which families of RSHs appear in the stator-line current spectrum for each combination of rotor bars and pole pairs, identifying the most critical cases for the algorithm and how the algorithm can deal with them, all supported by theoretical analysis and a statistical study of a database of 3474 IMs containing information on their number of rotor bars and pole pairs.
- A new, precise, general, non-invasive and automatic speed estimation method for MCSA steady-state diagnosis and efficiency estimation of IMs in the 4.0 Industry, developed through the conjunction of the previous contributions.

- An extensive validation of the speed estimation algorithm using simulations, laboratory tests and a database of industrial measurements of 105 IMs, covering a wide range of nameplate characteristics: from a few kW to 2 MW, 0.67% to 8% slip, 400 V to 6.6 kV and from 1 to 5 pole pairs.

7.1.3 Third publication

- The design and automation of a steady-state MCSA health condition system based on the developed speed estimation technique, showing during nearly a year, and for the first time in the technical literature, the continuous monitoring of two inductions motors (the industry application is a deep-well pumping station).
- The discovery and characterization of a failure that very frequently takes place in deep-well submersible motors: the wear of the rotor end-rings.
- A detailed description of the design and operating characteristics of deep-well submersible motors.
- A detailed description of the failure mechanism that leads to the wear of the end-rings and how this failure may be the trigger of additional failures in this type of motors.
- A thorough analysis on the problematic of detecting this failure through traditional rotor fault indicators, using signals obtained by simulation and from an experimental test-rig.
- The definition of a new diagnosis paradigm that must be considered in order to detect the wear of the end-ring in deep-well submersible motors.

7.1.4 Fourth publication

- An investigation on how the special constructional and operating characteristics of deep-well IMs act as game changers in terms of inter-turn fault detection through PSHs.
- A rule to determine which PSHs are the most sensitive to the inter-turn fault as a function of the number of rotor slots and pole pairs.
- A comprehensive finite element analysis on the sensitivity and reliability of PSHs as indicators for early detection of inter-turn faults, considering different fault severities, both alone and coexisting with other asymmetries such as unbalanced voltages, eccentricities or rotor faults.
- A diagnostic scheme, based on the results obtained through finite element analysis and industrial data, to reliably detect inter-turn faults at early stages using the most sensitive PSHs, the VUI, and the CUI.
- The first application of an inter-turn fault diagnostic scheme in the context of a continuous monitoring of a deep-well IM operating in a pumping station, where data has been collected every six hours for nearly a year.

7.2 Conclusions

In this section, the conclusions drawn from this thesis are presented.

7.2.1 First publication and state-of-the-art review

- SRFSHB methods are the most suitable techniques to be applied in MCSA steady-state diagnosis or efficiency estimation applications in a 4.0 Industry context, since they are the only ones that can potentially meet the four requirements of: accuracy, general applicability, non-invasiveness and automaticity. However, up to the completion of this thesis, high accuracy was only characteristic of RSH-based methods, while general applicability only of RFSH-based methods.
- SRFSHB methods used in commercial devices are not reliable in a considerable amount of cases. On the one hand, EXP4000 has the main problem of using RFSHs, which do not provide enough accuracy due to its narrow bandwidth and are difficult to be detected, particularly in two-pole machines. On the other hand, MCEMAX uses the BBH and the RFSH of the demodulated current. In this case, the major drawback is that, in order to locate these harmonics, the algorithm uses a preliminary speed estimation whose accuracy depends on the magnitude of the no-load current and the consistency between nameplate data and actual values. Nevertheless, detection difficulties also arise in these two harmonics, and besides, their different speed estimation errors may generate inconsistencies, leading the device to ask for a human check. Therefore, there is a clear need to provide an accurate and reliable speed estimation method for the industry.
- The best SSE solution for steady-state MCSA or efficiency estimation in 4.0 Industry is a RSH-based technique (high-accuracy). However, in order to ensure non-invasiveness, this technique should eliminate the need to know the number of rotor slots. Moreover, in order to be automatic, it should be able to detect the RSHs and assign their ν indexes autonomously. Finally, the algorithm should be able to work for any IM, reaching general applicability.

7.2.2 Second publication

- The SSE algorithm developed is highly accurate: absolute speed errors and relative slip errors below 0.05 rpm and 0.5% respectively, when compared to a 1000-line encoder.
- The SSE method developed is completely general: it works with different skewing angles, with odd, even or not integer R/p (given that it also detects RSHs with $k > 1$), with grid or frequency-converter supply, with high or low load, and with high or low slip. Moreover, it has been successfully tested in 105 industrial motors of different characteristics (specifically under the most challenging conditions: low fundamental frequency and low slip).
- The SSE method developed is completely non-invasive: it only uses as starting point the stator line-current (which can be captured with a current clamp) and the number of pole pairs (which is available on the nameplate).
- The SSE method developed is completely automatic: it can autonomously localize the RSHs, calculate their parameters O_ν, determine their indexes ν, and finally calculate speed/slip.

- The Speed Estimation method developed is easily implementable in field monitoring systems: it has a low computational burden (it takes less than 2 s to be executed in a PC with an Intel Core i7-8700 processor for a 200 s signal at 10 kHz), and a simple signal processing (FFT and hilbert transform).

7.2.3 Third publication

- Deep-well submersible motors have a specific rotor end-ring manufacturing process not found in conventional copper fabricated or die-cast aluminum rotors. End-rings are made of copper laminations with punching holes where the bars are placed. The end of these bars are glued to the end-ring laminations using a copper liquid soldering.
- The internal cooling water used in these motors, which is propelled by the rotor and moves at high speed, erodes the liquid soldering, thereby producing the wear of the end-rings.
- The wear starts at some point of the end-ring (e.g., a segment between two bars), and progressively spreads over the whole end-ring, but in a random and non-uniform way.
- The wear of the end-ring causes the same electro-magnetic asymmetry effects that broken bars, and therefore, is correlated to the amplitude of the traditional BBHs, being the most significant of them, the LSH.
- At the beginning, the fault can be too subtle to be detected. Later, as it spreads to non-adjacent segments, the electro-magnetic asymmetry effects can be canceled out, leading to false negatives.
- Traditional approach of LSH monitoring with long periods between measurements (e.g., biannual) is insufficient for end-ring wear reliable detection. First, in a single amplitude measurement, the wear might not be enough to rise the LSH amplitude to a level considered faulty, according to traditional rotor fault indicators. Second, once the wear spreads, rotor asymmetry might even be canceled due to multiple segments wear, lowering the LSH amplitude.
- A new paradigm must be considered in deep-well IMs: condition monitoring must be conducted continuously using the ratio of change in the LSH amplitud as an indicator of end-ring wear, even if classic LSH fault related thresholds are not reached (-45 dB). Changes in the secondary rotor asymmetry harmonics, properly chosen, are a very useful complement in the LSH monitoring.
- Stopping the motor at an early stage of end-ring wear may prevent this fault from contaminating the water. The suspended particles might be impelled by the centrifugal force, and impact into the stator winding, causing serious damage to the insulation.
- The SSE algorithm developed can be implemented in an industrial continuous condition monitoring system, providing reliable speed information, and therefore, reliable harmonic positioning, thereby enabling fault detection, as the end-ring wear.

7.2.4 Fourth publication

- Deep-well submersible motors characteristics make them particularly suitable for early detection of inter-turn faults via PSHs through an FFT steady-state analysis, since:

  - An incipient stator fault in this type of motors does not cause a destructive current; it can be even lower than the rated current.
  - Stator windings of deep-well submersible motors are subjected to less thermal stress than conventional motors since they are doubly water-cooled and operate with a very constant ambient temperature of around 15ºC. This acts as a retarding factor in the propagation of the inter-turn fault to a catastrophic failure, and therefore, enables an early detection of the fault.
  - These motors are built with two poles to achieve high power and speed with a reduced diameter (to also reduce excavation costs), and with an even number of rotor bars to avoid unbalanced magnetic pull. Therefore, as the number of rotor bars per pole pair is an even number, they are Principal Slot Harmonics producers.
  - As a consequence of the reduced size of its diameter, the slots are small, and therefore, so is the number of conductors per slot. Hence, the small number of turns of an early-stage short-circuit represents a higher percentage, with respect to the total number of phase turns, than in conventional motors, thereby becoming more noticeable for the fault indicator.
  - These motors work continuously for long periods of time and without significant load or speed variations, as water is usually pumped to a tank. This highly reduces the possibilities of false positives due to changes in the Principal Slot Harmonics amplitude originated by changes in the load. Moreover, it also makes the steady-state FFT analysis ideal to be applied.
  - In these motors, there is always a set of PSHs that are nearly absent in the healthy machine, and highly increase when the inter-turn short-circuit takes place, especially at early stages (this can be extrapolated to any motor that is PSHs producer). These PSHs can be known beforehand.

- In the presence of other asymmetries, by selecting from this set two PSHs where one of them is associated to a counter-clockwise rotating harmonic flux wave and the other to a clockwise one (PSHs associated to the same $|\nu|$ but with different sign), it is observed that always one of them maintains a constant amplitude increase with the fault severity in one of the line currents. Hence, it is only necessary to monitor these two Principal Slot Harmonics, in two of the line currents.

  - These PSHs can be determined thanks to the use of the SSE algorithm, which not only localizes the PSHs and calculates their O_ν parameters, but also determines their associated ν.

- Short-circuit false positives due to voltage unbalance and eccentricity can be avoided if the VUI and CUI are also monitored.

- Rotor cage faults cannot produce short-circuit false positives.

- Repair shops of deep-well motors only apply simple tests (usually phase-to-phase, phase-to-ground resistance and visual inspection looking for dirt) to determine the state of the stator insulation, using very conservative criteria, which easily imply rewind of the stator windings to assure that the components will last longer when the motor is placed in a 100 to 500 m deep well, thus avoiding the high cost of extraction if an early fault takes place.

7.3 Fulfillment of the objectives

The specific objectives of this thesis are:

- To conduct an exhaustive state-of-the-art review of the families of sensorless speed estimation techniques, also including commercial devices that make use of them in their efficiency estimation and diagnosis algorithms, with the aim of identifying: which of the families is the best suited to be implemented in steady-state MCSA diagnosis and efficiency estimation algorithms for IMs, which are the main drawbacks of said family, and how these weaknesses might be overcome.
- To develop a theoretical formula to obtain the frequency of the RSHs without knowing the number of rotor bars, thus overcoming the non-applicability of these type of techniques in IMs of unknown parameters.
- To build an algorithm to locate the RSHs, among the numerous harmonics of the current spectrum, as well as to determine their parameters (e.g., ν index), all in an automatic and reliable way, thus allowing to determine the speed with accuracy, as well as the position of the fault harmonics.
- To test the algorithm with a set of motors covering different designs, driving different loads and fed with different power supplies, achieving this by using signals from simulation, lab tests and 105 industrial motors.
- To implement the algorithm in a plug and play device that conducts the continuous condition monitoring of an IM in an automatic and online way, so that it can detect those faults present in IMs that generate speed-dependent harmonics in the stator current spectrum.
- To study the RSHs as potential indicators for early detection of inter-turn short-circuits (especially in deep-well motors).

The first of the objectives was achieved with the publication of Chapter 2 and complemented by the state-of-the-art review conducted in Chapter 1. Second to fourth objectives were fulfilled by the development and testing of the speed estimation method presented in Chapter 3. Fifth objective was achieved by implementing the method in a continuous monitoring system as shown in the publication associated to Chapter 4. Finally, the last of the objectives was achieved with the study conducted in the publication of Chapter 5.

Therefore, it can be concluded, that all the objectives proposed for this thesis have been successfully fulfilled.

Chapter 8

Future works

The work conducted during this thesis has led to a precise, general, non-invasive and automatic speed estimation method that has been successfully tested to reliably provide the speed required by MCSA diagnostic and efficiency estimation algorithms for induction motors. In addition, it has also laid the groundwork for new lines of research, which are presented in this chapter.

8.1 Extension of algorithm capabilities to estimate speed in transient conditions

The algorithm presented in this thesis has been successfully tested to provide accurate speed information using steady-state currents, since this is the condition in which MCSA diagnosis and efficiency estimation are usually applied. However, certain MCSA diagnostic techniques for transient conditions have emerged that also require precise knowledge of the speed [1]. In addition, efficiency estimation techniques have also been recently proposed, in which the parameters necessary for their application (such as equivalent circuit parameters) are obtained through transient signals (such as start-up) and in which it is also necessary to know the speed during the transient [2]. In this regard, it would be interesting to extend the capabilities of the algorithm to provide speed in such transient conditions, so it could be used by these new diagnostic and efficiency estimation techniques for induction motors.

8.2 Development of a low-cost commercial system for MCSA diagnosis and efficiency estimation in induction motors

The sensorless speed estimation algorithm has been implemented using an academical license for MATLAB in a PC with an Intel Core i7-8700 processor, while the signals have been obtained using commercial equipment from PicoTech. This results in an expensive and non-commercially exploitable system. Therefore, if the work conducted in this thesis, along with its future extension to transient conditions, are to have a real and feasible applicability to the industry, it is of utmost importance to design a low-cost hardware where the diagnostic and efficiency estimation methods are implemented using a non-proprietary programming language (e.g., Python).

Bibliography

[1] V. Fernandez-Cavero, J. Pons-Llinares, O. Duque-Perez, and D. Morinigo-Sotelo, "Detection of broken rotor bars in nonlinear startups of inverter-fed induction motors," *IEEE Transactions on Industry Applications*, vol. 57, no. 3, pp. 2559–2568, 2021, doi: 10.1109/TIA.2021.3066317

[2] J. W. Rengifo and J. M. Aller, "An efficiency estimation method for inverter fed induction motors," in *2021 IEEE Workshop on Electrical Machines Design, Control and Diagnosis (WEMDCD)*, 2021, pp. 22–27, doi: 10.1109/WEMDCD51469.2021.9425682

Appendix A

Short-circuit modeling

This appendix expands the information found in Chapter 5 regarding the method used to model the inter-turn fault.

A.1 Model

The approach used to model the inter-turn fault is depicted in Fig. A.1.

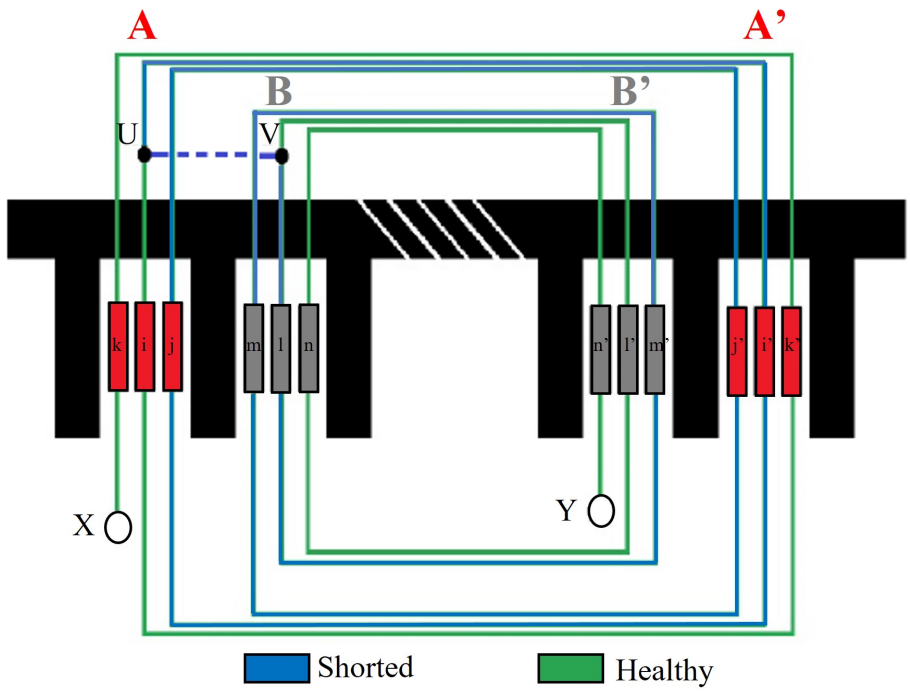

FIGURE A.1: Scheme of the approach used to create the inter-turn fault.

In this approach, a certain coil is designated as coil AA'. Then, another coil of the same phase which has at least one of its sides located in a slot adjacent to where one of the sides of coil AA' is located is designated as coil BB'. Next, each of these coils is divided into three groups of coils (kk', ii', jj', mm', ll', and nn'), with the middle groups (ii' and ll') consisting of a one-turn coil , so that:

$$\begin{aligned} Z_{slot} &= Z_A = Z_{A'} = Z_k + Z_i + Z_j = Z_{k'} + Z_{i'} + Z_{j'} \\ Z_{slot} &= Z_B = Z_{B'} = Z_m + Z_l + Z_n = Z_{m'} + Z_{l'} + Z_{n'} \end{aligned} \tag{A.1}$$

where Z_{slot} is the number of conductors in series per slot or the number of conductors in series per slot divided by two when its a double layer winding, and Z_x the number of conductors in the side x of the coil group xx'.

The short-circuit is then created between the middle groups of the coil sides located in adjacent slots through a contact resistance of 0.1 Ω between points U-V (where the blue dashed line is). The conductors in the healthy part of the winding (green path) are the ones in the coil sides k, k', n, n', i and l', while the conductors in the shorted loop (light blue path) are the ones in the coil sides j, j', m, m', i' and l. As the number of conductors in the middle groups is fixed (one turn coil), the fault severity can be handled by modifying the number of conductors in the rest of the groups (always satisfying (A.1)), being the fault severity or % of shorted-turns:

$$\%\ of\ shorted\ turns\ = \frac{Z_j + Z_{j'} + Z_m + Z_{m'} + Z_{i'} + Z_l}{Z_T} \cdot 100 \tag{A.2}$$

where Z_T is the total number of conductors in series of one phase.

A.2 Currents

With this approach three circulating currents appear:

- **Short-circuit current**: is the current circulating through the shorted-loop (light blue path).
- **Phase current**: is the current circulating through the healthy part of the phase winding (green path).
- **Contact-resistance current**: is the current circulating through the contact resistance (dashed blue path).

Appendix B

Publications

This appendix lists those contributions derived from the present thesis that have been published, up to the date of submission, in the form of journal/conference articles and patents.

B.1 Journals

1. J. Bonet-Jara, A. Quijano-Lopez, D. Morinigo-Sotelo, and J. Pons-Llinares, “Sensorless Speed Estimation for the Diagnosis of Induction Motors via MCSA. Review and Commercial Devices Analysis,” *Sensors*, vol. 21, no. 15, p. 5037, Jul. 2021, doi: 10.3390/s21155037.

2. J. Bonet-Jara, D. Morinigo-Sotelo, O. Duque-Perez, L. Serrano-Iribarnegaray and J. Pons-Llinares, "End-Ring Wear in Deep-Well Submersible Motor Pumps," in *IEEE Transactions on Industry Applications*, vol. 58, no. 4, pp. 4522-4531, July-Aug. 2022, doi: 10.1109/TIA.2022.3166876.

3. J. Bonet-Jara and J. Pons-Llinares, "A Precise, General, Non-Invasive and Automatic Speed Estimation Method for MCSA Diagnosis and Efficiency Estimation of Induction Motors," in *IEEE Transactions on Energy Conversion*, 2022, doi: 10.1109/TEC.2022.3220853.

4. J. Bonet-Jara, J. Pons-Llinares and Konstantinos N. Gyftakis, "Comprehensive Analysis of Principal Slot Harmonics as Reliable Indicators for Early Detection of Inter-turn Faults in Induction Motors of Deep-Well Submersible Pumps," in *IEEE Transactions on Industrial Electronics*, 2022, doi: 10.1109/TIE.2022.3231333.

B.2 Conferences

1. J. Bonet-Jara and J. Pons-Llinares, "Sensorlees Speed Estimation. A Review," *2019 IEEE 12th International Symposium on Diagnostics for Electrical Machines, Power Electronics and Drives (SDEMPED)*, 2019, pp. 283-289, doi: 10.1109/DEMPED.2019.8864878.

2. J. Bonet-Jara et al., "End-ring wear in deep well submersible motor pumps," *2021 IEEE 13th International Symposium on Diagnostics for Electrical Machines, Power Electronics and Drives (SDEMPED)*, 2021, pp. 79-85, doi: 10.1109/SDEMPED51010.2021.9605520.

3. J. Bonet-Jara, V. Fernandez-Cavero, F. Vedreno-Santos and J. Pons-Llinares, "Very Accurate Time-Frequency Representation of Induction Motors Harmonics for Fault Diagnosis Under Arbitrary Load Variations," *2022 International Conference on Electrical Machines (ICEM)*, 2022, pp. 1517-1523, doi: 10.1109/ICEM51905.2022.9910768.

B.3 Patents

1. J. Bonet-Jara and J. Pons–Llinares. Método y dispositivo para medición de velocidad y diagnóstico de una máquina asíncrona. *UNIVERSIDAD POLITECNICA DE VALENCIA*, P202230400. Fecha de depósito: 02 May 2022.